**République Algérienne Démocratique et Populaire**
**Ministère de l'Enseignement Supérieur et de la Recherche Scientifique**
**Université 8 Mai 1945 Guelma**

**Faculté de Science et de Technologie**
**Département de Génie Civil et Hydraulique**
**Laboratoire de de Génie Civil et Hydraulique LGCH**

# THÈSE

## EN VUE DE L'OBTENTION DU DIPLOME DE DOCTORAT EN 3ème CYCLE

Domaine : Sciences et Technologie Filière : Hydraulique
Spécialité : Hydraulique

**Présentée par**
**Kadri Ismahen**

***Intitulée***

**Simulation des ruissellements dans les bassins non jaugés avec la prise en considération des surfaces imperméables**

Soutenue le : 06/10/2022 Devant le Jury composé de :

| Nom et Prénom | Grade | Université | |
|---|---|---|---|
| **Mr MAOUI Ammar** | Professeur | Univ. 8 Mai 1945 Guelma | Président |
| **Mr MANSOURI Rachid** | Professeur | Univ. 8 Mai 1945 Guelma | Encadreur |
| **Mr ZEGHADNIA Lotfi** | Professeur | Univ.Mohamed Cherif Messaadia Souk Ahras | Examinateur |
| **Mr KHROUF Mazouz** | MCA | Univ. 8 Mai 1945 Guelma | Examinateur |

**Année Universitaire: 2021/2022.**

I Dedicate this Thesis to my Parents, my Family, and my cats.

# Acknowledgment

I would like to thank God, for letting me through all the difficulties. I have shown your guidance day by day. You are the one who let me finish my degree. I will keep on trusting you. الحمد لله

I would like to acknowledge and give my warmest thanks to my supervisor *Pr. Rachid Mansouri* made this work possible. Her guidance and advice carried me through all the stages of writing my project. I would also like to thank my laboratory members for letting my defense be an enjoyable moment, and for your brilliant comments and suggestions, thanks to you.

I would like to offer my sincere thanks to the Jury members, Pr. Zghadnia Lotfi, Pr. MAOUI Ammar, and Pr. Kherouf Mazouz For their acceptance to judge my thesis and honor me with their presence.

# Content Table

## Figure list

## Table list

# Abstract

The existed hydrological models that were used to describe the hydrological processes varied between the pure mathematics analysis and equations to relations that describe the process empirically based on the physics of the watershed. An oscillation exists between the model's performance and robustness but it was approved that such a hydrological model is chosen according to the study objective and perspectives. The models that are based on purely physical or conceptual, face the problem of calibrating the large number of parameters that contain. Furthermore, the major watershed measurement is scarce, especially in developing countries. To further understand and excavate this concept, we engaged in this study and went deeper into the hydrological models. We choose different models from both conceptual and Data-driven to analyze. The study area was selected in order to verify the applicability of the NARX-NN model in small drainage areas, containing the conditions of the Semi-urbanism and the low intensity of rainfall, and then it will be compared to the conceptual HEC-HMS model. We investigate the NARX-NN model to simulate the basin response to real storm events of a small urban watershed. The NARX-NN steps are described in detail, from data representation and insertion, and then calibration and testing. To reach the target hydrograph by the conceptual HEC-HMS, we must pass through several stages. Conceptually, the hole R-R process is a combination of several sub-processes; we need to treat each one separately. We proposed a new method to carry out the best parameters of calibration using the weighted average function of HEC-HMS models and that gave the best performance. The steps involved in each model to reaching the hydrograph are dramatically different; the significance is to present an analytical comparison step by step of each model. The two models are extremely different in terms of data requirements. The conceptual and black box models are compared statistically and graphically. The statistical assessment shows that during calibration, the two models are closely the same in terms of NSE and MAE with a slight superiority of NARX-NN. Except for the PEP benchmark which indicates the supremacy of the NARX-NN over HEC-HMS in mapping the peak of the hydrograph, which is agreed as one of the most important elements in the short storm events. In the testing phase, statistical parameters indicate that the NARX-NN outperforms modeling the basin response

The findings drawn from the results demonstrate the high capability of the NARX-NN model to capture the R-R process, although the short time-series data is used in the training and testing phases. Moreover, the result of the testing is more accurate than that of the training phase, which

demonstrates the strength of the generalization feature of NARX-NN. It has more strength to produce the shape bending of the hydrograph; in contrast, the rising and falling limb in the HEC-HMS model presents straight curvature. Consequently, the NARX-NN model is better to highlight the curvatures resulting from the local peaks of rainfall.

**Keywords**: hydrological Models, Conceptual Models, Data-Driven Models, Watershed, NARX-NN, HEC-HMS, Rainfall-Runoff, Hydrograph

# Résumé

Les modèles hydrologiques utilisés pour décrire les processus hydrologiques variaient entre l'analyse mathématique pure et les relations décrivant le processus de manière empirique basées sur de la physique du bassin versant. Il existe une oscillation entre la performance et la robustesse du modèle, cependant, il a été montré que le choix du modèle dépend des objectifs et des perspectives de l'étude. Les modèles reposant sur des données de nature physique ou conceptuelle, sont confrontés au problème du calibrage, et ce suit au grand nombre de paramètres qu'ils contiennent, et a la rareté des données de mesures, en particulier dans les pays en développement. Pour mieux appréhender ce concept, nous nous sommes engagés dans de la cadre de cette thèse à l'usage de la modélisation hydrologique. Deux différents modèles ont été sectionnés, à savoir un modèle conceptuel, et un autre dit model numérique. Pour vérifier l'applicabilité de ces modèles dans les petits bassins versant, une zone d'études a été sectionnée. Cette zone est de type semi-urbain et caractérisée par une faible intensité des précipitations.

Pour réaliser l'étude, nous avons fait appel au modèle NARX-NN, et ce pour simuler la réponse du bassin sollicité par des événements pluvieux réels. Les étapes NARX-NN sont décrites en détail, depuis la représentation et l'insertion des données, jusqu'au calibrage et aux tests correspondants. Pour obtenir l'hydrogramme cible simulé par le modèle HEC-HMS, un certain nombre d'étapes est indispensable. Conceptuellement, l'ensemble du processus Pluie-débit est une combinaison de plusieurs sous-processus, dont chacun doit être traité séparément. Une nouvelle méthode, pour l'obtention des meilleurs paramètres de calage, a été proposée. Cette méthode utilise la fonction moyenne pondérée des modèles HEC-HMS, et a donné les meilleures performances. Les étapes de simulation incluses dans chaque modèle pour la production de l'hydrogramme de ruissellement sont radicalement distinctes. L'intérêt est de présenter une comparaison analytique étape par étape de chaque modèle. Les deux modèles sont extrêmement distincts en termes d'exigences en matière de données. La comparaison entre les deux modèles est réalisée de manière statistique et aussi graphique. L'évaluation statistique des deux modèles montre que lors du calage, les résultats montrent que les valeurs du NSE et du MAE sont approximativement très proches. Cependant termes une légère supériorité de NARX-NN a été constatée. À l'exception du benchmark PEP qui indique la suprématie du NARX-NN sur le HEC-HMS dans l'estimation du pic de l'hydrogramme. Ce dernier s'avère comme une des caractéristiques les plus importantes dans les événements de pluvieux de courte durée. Dans la

phase de test, les paramètres statistiques indiquent que le NARX-NN reproduit mieux la réponse du bassin

Les conclusions tirées des résultats démontrent l'efficacité du modèle NARX-NN dans la simulation du processus pluie-débit, nonobstant le fait que les données de séries chronologiques courtes soient utilisées dans la phase apprentissage et la phase test. En outre, les résultats des tests sont plus précis que ceux de la phase d'apprentissage, montrant, par conséquent, la nécessité de généraliser l'usage du modèle NARX-NN. Ce dernier est meilleur dans la reproduction de la phase de récession de l'hydrogramme, au moment où, la courbe de concentration et la courbe de décrue obtenues par le modèle HEC-HMS présentent une allure droite. Par conséquent, le modèle NARX-NN met mieux en évidence les courbures résultant des pointes des événements pluvieux locaux.

**Mots Clés** : Model hydrologique, Model conceptuelle, Model Numérique, Bassin versant, NARX-NN, HEC-HMS, Pluie-Débit, Hydrogramme.

# الملخص

اختلفت النماذج الهيدرولوجية المستخدمة لوصف العمليات الهيدرولوجية بين التحليل الرياضي البحت والعلاقات التي تصف العملية بناءً على فيزياء مستجمعات المياه. هناك تذبذب بين الأداء وقوة النموذج، ومع ذلك، فقد تبين أن اختيار النموذج يعتمد على أهداف ووجهات نظر الدراسة. تواجه النماذج المبنية على بيانات ذات طبيعة مادية أو مفاهيمية مشكلة المعايرة، وهذا ناتج عن العدد الكبير من المعلمات التي تحتويها، وندرة بيانات القياس، لا سيما في البلدان قيد التطوير. لفهم هذا المفهوم بشكل أفضل، نحن ملتزمون في سياق هذه الأطروحة باستخدام النمذجة الهيدرولوجية. تم تقسيم نموذجين مختلفين، وهما النموذج المفاهيمي، والآخر يسمى النموذج المستند إلى البيانات. للتحقق من قابلية تطبيق هذه النماذج في مستجمعات المياه الصغيرة، تم تقسيم منطقة الدراسة. هذه المنطقة شبه حضرية وتتميز بانخفاض كثافة هطول الأمطار.

لإجراء الدراسة، استخدمنا نموذج. NARX-NN لمحاكاة استجابة الحوض التي تطلبها أحداث هطول الأمطار الحقيقية. يتم وصف خطواتNARX-NN بالتفصيل، من تمثيل البيانات وإدخالها، إلى المعايرة والاختبارات المقابلة. للحصول على مخطط هيدروغرافي مستهدف محاكى بواسطة نموذج HEC-HMS هناك عدد من الخطوات ضرورية. من الناحية المفاهيمية، فإن عملية هطول الأمطار بالكامل هي مزيج من عدة عمليات فرعية، يجب معالجة كل منها على حدة. تم اقتراح طريقة جديدة للحصول على أفضل معايير المعايرة. تستخدم هذه الطريقة دالة المتوسط المرجح لنموذج HEC-HMS ، وقدمت أفضل أداء. خطوات المحاكاة المضمنة في كل نموذج لإنتاج هيدروغراف الجريان السطحي متميزة اختلافًا جذريًا. الاهتمام هو تقديم مقارنة تحليلية خطوة بخطوة لكل نموذج. النموذجان متميزان للغاية من حيث متطلبات البيانات. يتم إجراء المقارنة بين النموذجين إحصائيًا وأيضًا بيانياً. يُظهر التقييم الإحصائي للنموذجين أنه أثناء المعايرة، تُظهر النتائج أن قيم NSE و MAE قريبة جدًا تقريبًا. ومع ذلك، لوحظ تفوق طفيف في نموذج -NARX NN باستثناء معيارPEP الذي يشير إلى تفوق NARX-NNعلىHEC-HMS في تقدير ذروة الهيدروغراف. تبين أن الأخير هو أحد أهم الخصائص في أحداث هطول الأمطار على المدى القصير. في مرحلة الاختبار، تشير المعلمات الإحصائية إلى أن NARX-NN يعيد إنتاج استجابة الحوض بشكل أفضل.

توضح الاستنتاجات المستخلصة من النتائج فعالية نموذج NARX-NN في محاكاة عملية جريان الأمطار، على الرغم من حقيقة أن بيانات السلاسل الزمنية القصيرة تُستخدم في مرحلة التعلم ومرحلة الاختبار. بالإضافة إلى ذلك، تكون نتائج الاختبارات أكثر دقة من نتائج مرحلة التعلم، مما يدل على الحاجة إلى تعميم استخدام نموذج NARX-NN . هذا الأخير أفضل في استنساخ مرحلة الركود في الهيدروغراف، عندما يمثل منحنى التركيز ومنحنى الركود الذي تم الحصول عليه بواسطة نموذج HEC-HMS اتجاهًا مستقيمًا.

لذلك، فإن نموذج NARX-NN يبرز بشكل أفضل الانحناءات الناتجة عن قمم أحداث هطول الأمطار المحلية.

**كلمات مفتاحية:** النماذج الهيدرولوجية، النماذج المفاهيمية، النماذج الرقمية، حوض مائي، NARX-NN, HEC-HMS، أمطار-سيول، هيدروغراف

# Research entrance

Problems related to water oscillate between scarcity and flood, Freshwater is increasingly becoming a scarce resource in many regions of the world due to both natural and man-made causes (Amisigo, 2005). The degree of water scarcity and its political, economic, and social implications are felt much more severely in regions like the Mediterranean. Water resources are unevenly distributed in the Mediterranean region with 72 percent of resources in the north, 23 percent in the east, and five percent in the south. Thus, the shortage of water is mainly focused on the southern and eastern Mediterranean countries. However, the severe droughts experienced between 1990 and 2005 have marked the vulnerability of the water supply even in the industrialized northern Mediterranean countries (Burak & Margat, 2016; Kibaroğlu, 2017).

Flooding is one of the most manageable natural disasters if flood-prone areas are identified and suitable flood mitigation strategies are implemented. The most practical way of identifying flood-prone areas, and the effectiveness of flood mitigation strategies is by the application of mathematical models, which consider the complex hydrological processes of these areas. The hydrologic models compute peak flows and/or flood hydrographs, which are required to design the system components of drainage systems to minimize flood damage (Freire Diogo & Antunes do Carmo, 2019). If there are errors in peak flows and/or flood hydrographs, the drainage system will be either undersized or oversized. The former results in flooding of the urban areas and causes inconvenience to the residents in the flood-affected area. The latter produces an uneconomical design, which is equally undesirable (Dayaratne, 2001).

During the past half-century, urbanization has been the dominant demographic trend, not only in Algeria but also in the entire world. Increased impervious surfaces are a common cause of increased peak-runoff volumes. Urban floods have remained a key challenge to various socio-economic activities of the cities, threatening the sustainability of urban areas in many countries around the world (Dube et al., 2021). Urban development makes drainage systems unable to keep up with that pace of growth (Ridwansyah, 2010). Urbanization has led to a massive increase in infrastructure, areas that used to be bare land of free-grown trees, are now replaced by houses, tall buildings, or concrete streets. The increase of impervious surfaces increases the amount of water discharge, exceeds the drainage capacity, and leads to flooding (Feng et al., 2021). The predominance of highly impermeable surfaces and lack of water storage in typical urban districts makes them more vulnerable to heavy rainfall. The situation could worsen when

pluvial flooding is combined with fluvial flooding. Throughout the entire history of mankind, intense human utilization of land resources has resulted in significant changes in land use and land cover. Since the area of industrialization and rapid population growth, land-use change phenomena have strongly accelerated in many regions of the world. Land-use changes are frequently indicated to be one of the main human-induced factors influencing the hydrological system (Feng et al., 2021).

The prior knowledge and the good prediction can significantly help in the development of scientific plans that can contribute to the creation of suitable infrastructure to serve communities. Forecasting the hydrological response introduces valuable information to the planners and engineers to put forward appropriate strategies for hydrological solutions. With the fast improvement of computer technologies and remotely sensed technologies, numerical models show great potential to be an effective and economical tool to study this urban flood issue. An accurate representation of the terrain and a comprehensive understanding of the rainfall-runoff process is required to mimic the flow propagation in urban areas realistically. Previously, conventional analyses based on empirical methods were inadequate to simulate hydraulic variables

River basin management poses big challenges especially in developing countries because of the lack of continuous data, particularly data that require automatic recording instruments to acquire. As an alternative to observed data, rainfall-runoff models can be used, such models are distributed, semi-distributed, or lumped. The distributed models have more parameters and therefore they are used in catchments with good data records. The less complex lumped models have fewer parameters and are commonly used in catchments with poor data. The rainfall-runoff models used in simulating runoff data are made of physical and conceptual parameters, which need to be estimated before the models can be used to improve data in gauged catchments or be extrapolated in ungauged catchments. Simulation of streamflow data in ungauged catchments is complicated by the lack of observed data for model calibration.

Remote sensing technology can increase the conventional methods to a great extent in rainfall-runoff studies. The role of remote sensing in runoff calculation is generally to provide a source of input data or it is used as an aid for estimating equation coefficients and model parameters. One of the first applications of remote sensing data in hydrologic models used satellite data to determine both urban and rural land use for estimating runoff coefficients. The runoff coefficient, which is influenced by not only climatic effects but also human impacts, is a fundamental indicator used in flood control (Dhawale, 2013).

Studying the impacts of land cover change on flood behavior is considered a complex and time-consuming process because the factors that determine river flow and flood intensity, e.g., land cover, vary both spatially and temporally. However, such problems have been overcome through the application of Remote Sensing (RS) and Geographic Information System (GIS) technologies together with hydrologic and hydraulic models. RS provides the most fundamental information describing the nature and extent of land cover, especially over large areas in an accurate and timely manner, together with GIS as an efficient tool for spatial data analysis, have been proven to be effective in characterizing the patterns, intensity, and dynamics of land cover change. On the other hand, hydrologic models (also called rainfall-runoff models) can be used to simulate the hydrology of the river basins using rainfall and land-cover information as important inputs. Using this model, a watershed's response to rainfall in the form of surface runoff and peak flows can be estimated based on different land cover conditions, and the model outputs (e.g., flow hydrographs) are compared to determine the impact of land cover change.

The association of Algeria with the international project DMC (Digital Monitoring Constellation) which implies 8 observation satellites shows that the identification of the causes and the forecast of flood formation in several Algerian cities became one of the dominating concerns of public authorities (Sandau, 2006). The interest of Algerians is to supervise the phenomena called «dynamic changes », as the disaster, which occurred in Bab El – Oued (Algiers) in November 2001, when a 24 hours flood (110 mm of rain) had caused a national disaster. Today the modeling in hydrology has reached a mature stage. The benefits that remote sensing holds for hydrology are always apparent and the use of the distributed models became more convenient. Remote sensing can be incorporated into the system in a variety of ways: as a measure of land use and for impervious surfaces, for providing initial conditions for flood forecasting, and for monitoring flooded areas.

Catchment modeling requires a clear understanding of the hydrologic cycle at the catchment scale. The cycle has no beginning or end, and its processes occur continuously. Many hydrologists investigated this cycle in a number of studies. The hydrologic cycle may be treated as a system whose components are precipitation, evaporation, infiltration, runoff, and other processes like in the hydrologic cycle. The different components can be grouped together into subsystems or broken down into new subprocesses, depending on the level of details in the analysis and the purpose of the analysis.

The rainfall-runoff relationship is an important issue in hydrology and a common challenge for hydrologists. Due to the tremendous spatial and temporal variability of basin characteristics such as Land use/ land cover, soil moisture, hydraulic conductivity, and topography (relief), the impact of rainfall on runoff becomes more intensive and their proper estimate is essential for flood management.

The rainfall-runoff relationship is one of the most complex hydrologic phenomena to comprehend due to the tremendous spatial and temporal variability of watershed characteristics and precipitation patterns, and the number of variables involved in the modeling of the physical processes. The reason for modeling the relation between precipitation on a catchment and the runoff from it is that runoff information is needed for hydrologic engineering design and management purposes; however, the relationship between rainfall and runoff is one of the most complex hydrologic phenomena to comprehend. This is due to the tremendous spatial and temporal variability of watershed characteristics and precipitation patterns, and the number of variables involved in the modeling of the physical processes. The highly non-linear and complex nature of R-R relations is a reason for empiricism being an important approach to R-R modeling. Empirical R-R models simulate catchment behavior by transforming input to output based on certain parameter values, which are determined by a calibration process. A calibration algorithm is often used to determine the optimal parameter values that, based on input data samples, produce an output that as close as possible resembles a target data sample. Another R-R modeling approach, which opposes empirical modeling, is physically based modeling. This approach is based on the idea of recreating the fundamental laws and characteristics of the real world as closely as possible. Physically-based modeling requires large amounts of data, since spatially distributed data is used, and is characterized by long calculation times.

The behavior of the rainfall-runoff process is completely non-linear and not easy to predict. This arises the need to use a sophisticated methodology that can introduce accurate forecasting. Since the middle of the 19th century, different methods have been demonstrated by hydrologists to assess the impact of rainfall on runoff whereupon many models have attempted to describe the physical processes involved in it. These rainfall-runoff models generally fall into a black box or system of theoretical models, conceptual models, and physically-based models.

Black box models normally contain no physically based input and output transfer functions and therefore, are considered to be purely empirical models. Conceptual rainfall-runoff models usually incorporate interconnected physical elements with simplified forms, and each element is

used to represent a significant or dominant constituent hydrologic process of the rainfall-runoff transformation. Physically-based models are distributed models consists a large number of parameters as input to the model. According to Refsgaard (1997), the hydrological models classified to physical or conceptual, based on the manner through which the description of the relationship between the inputs and the outputs is presented. The black-box models express the relationship between inputs and outputs of a given hydro-system. It provides quantification of adjusting parameters, excluding physical properties or any hydro-system description. This latter includes the linear or the nonlinear patterns, such as the AR-X and the N-AR-X models, (AR : AutoRegressive, : Nonlinear, X : eXogenous.) (Samarasinghe, 2007; Suykens et al., 1996) The term nonlinear refers to the mapping function of the Artificial Neural Networks ANN models. Results from earlier studies demonstrate the ANN capabilities in R-R modeling over physically-based or conceptual models (Bhadra et al., 2010; Hsu et al., 1995; Rezaeianzadeh et al., 2013). Over the last decades or so, artificial neural networks (ANNs) have become one of the most promising tools for modeling hydrological processes such as rainfall-runoff processes. In most studies, ANNs have been demonstrated to show superior results compared to the traditional modeling approaches. They are able to map underlying relationships between input and output data without detailed knowledge of the processes under investigation, by finding an optimum set of network parameters through the learning or training process. The static feedforward neural networks require special input drivers' configuration. Selecting predictors is an essential task to get the best performance (Christian W, 2004; Luk et al., 2000; Luk et al., 2001; Maier & Dandy, 2000; Maier et al., 2010; Senthil Kumar et al., 2005) . In the static network the input data must be lagged to provide a consistent and robust resilience against the highly non-linear behavior of the hydrological system. In such studies the modelers looking for a causal relationship between a set of input data and lagged time and network response (Christian W, 2004), they attained this goal through the use of analytical technics or selecting appropriate inputs based on modelers' expertise (Ali, 2009; Dawson & Wilby, 1998; Dehghani et al., 2014; Maier & Dandy, 2000; Roadknight et al., 1997; Talei et al., 2010). The choice of optimal rainfall lag is a crucial task in static NN modeling. as it can affect the outflow's prediction accuracy. The short lag conductive to insufficient information available to the network in order to cover the whole process. In contrast, too long rainfall lag provides a rainfall that did not actually participate in surface flow (Anthony W & Michael J, 2004). According to Maier et al. (2010), the selection of data input configuration based upon the hydrologist's skill leads to the loss of certain elements that might be needed for the network to capture the dynamism. In contrast, dynamic models have the advantage as it can commensurate with the non-stationary behavior of

different hydrological systems (Bhattacharjee & Tollner, 2016; F.-J. Chang et al., 2014; Chang et al., 2015; Coulibaly et al., 2001; Coulibaly & Baldwin, 2005; Ghose et al., 2018; Wang et al., 2020) and R-R transformation modeling (L.-C. Chang et al., 2014; Sahoo et al., 2019) This work suggests solving this problem by using a Nonlinear Auto-Regressive recurrent with exogenous input neural network (NARX). The dynamic NARX Neural Network model classified under this category, it was applied massively in the hydrology field with rousing success, such as sediment concentration estimation (Singh & Chakrapani, 2015), groundwater level forecasting (Guzman et al., 2017; Hasda et al., 2020; Izady et al., 2013; Wunsch et al., 2018; Yang et al., 2019) , and river flow forecasting (Faruq et al., 2019; Nanda et al., 2016; Remesan et al., 2008; Shamseldin, 2009; Shamseldin & O'Connor, 2001; Shen & Chang, 2013) . The continuous storm events have the focus of most of the previous studies mentioned above. The use of single storm events to design the R-R process in urban areas is very few in the literature. Shen and Chang (2013) used single storm events to investigate three NARX network configurations to simulate online flood inundation depth, the conclusion is the great ability of NARX-NN to inhibit error growth even though the use of outputs from the model instead of real data, but only if consistent input-output data is used in both training and testing.

Hydrologists are often confronted with problems of prediction and estimation of runoff, precipitation, water stages, and so on. Although many watersheds have been gauged to provide continuous records of streamflow, hydrologists are often faced with situations where little or no information is available for calibration and validation. In such instances, simulation models are often used to generate synthetic flows. The available rainfall-runoff models are HEC-HMS, MIKE-11, SWMM, etc. These models are useful for hydrologic and hydraulic engineering planning and design as well as water resources management; e.g., hydropower generation, flood protection, and irrigation. The existing popular model is considered not flexible and they require many parameters. Obviously, the models have their own weaknesses. Therefore, in view of the importance of the relationship between rainfall-runoff, the present study was undertaken in order to use a rainfall-runoff model that can be used to provide reliable and accurate estimates of runoff, namely the HEC-HMS Model. The Hydrologic Modelling System (HEC-HMS) is designed to simulate the precipitation-runoff processes of dendritic watershed systems.

# *Study Objectives*

The present study aims to represent an analytical comparison between different hydrological models and investigate their applicability to an urban watershed. we investigate the NARX-NN model to simulate the basin response to real storm events of a small urban watershed. The NARX-NN steps are described in detail, from data representation and insertion, and then calibration and testing. Therefore, the black box NARX-NN compared by the famous conceptual HEC-HMS model in the hydrological modeling community. This basin was selected in order to verify the applicability of the NARX-NN model in small drainage areas, containing the conditions of the Semi-urbanism and the low intensity of rainfall. To reach the target hydrograph by the conceptual HEC-HMS, we must pass through several stages. Conceptually, the hole R-R process is a combination of several sub-processes; we need to treat each one separately We proposed a new method to carried out the best parameters of calibration using the weighted average function of HEC-HMS models and that gave a best performance. The steps involved in each model to reach the hydrograph are dramatically different; the significance is to present an analytical comparison_step by step of each model. The two models are extremely different in terms of data requirements. The conceptual and black box models are compared statistically and graphically and the results are discussed.

# *Thesis Outline*

The thesis is consisting of Seven chapters, chapter **1**, providing the general information on watershed models and their categories classification based of several criteria. The hydrological model building and implementation are also presented. Previous research on the applications of hydraulic models and hydrologic models in flood simulations is reviewed. In chapter **2** the Hydrological processes are described, and the runoff generation is presented. This chapter discusses these runoff components and the flow processes that underlie them, the watershed hydrograph is explicated, and the factors that affect it. Chapter **3** highlighted the urban storm hydrograph and how they differ from that of natural watershed. We discuss the urbanization growth and their impact of natural drainage system. We define based on literature the urban watershed. And process of discharge in urban areas, we demonstrate the difference between the Total and Effective impervious area. And how they are estimated. In chapter **4** we debate the importance and effectiveness of the new technologies regarding the Remote sensing and Geographical information system, which facilitate gathering of information about the studied

system. After what we presented regarding the literature that directly related to our research proposition, we present in chapter **5** a detailed description of the study area, its geographic location, we justified why we choose this area for this study, and we demonstrate their wadis and watercourses and their climatological characteristics. In the penultimate chapter we show the data used, their acquisition, preparation for insertion in the models, and analysis. The last chapter introduces the methods and the materials used to conduct the simulation of the study area, we demonstrate the research processes and the discussed the results obtained from the use of the two models. The benefits and forfeits of hydrologic models in the rainfall-runoff simulation are also discussed in this chapter. Moreover, a conclusion presents along with suggestions for future research.

# Watershed models

# I Watershed Models

## I.1 Introduction

The tool that can be used to understand the natural phenomenon with a simplified approach is called a model (Wheater et al., 2007). It is used to characterize a wide range of environmental processes with respect to time and space. Hydrological models are tools used to represent a catchment's response to land-use variability in order to assess the flow hydrograph. It is a mathematical representation of hydrologic processes which divide precipitation into two main parts, namely losses and runoff. The hydrologic system includes physical processes (interception, depressions, infiltration, evaporation, and transpiration) that are involved in the conversion to streamflow. Hydrological modeling has become a very vital part of decision-making processes for water engineers and managers. they are useful in understanding hydrological responses of a catchment and how certain changes in the catchment can influence those responses.

The main factors behind runoff are rainfall, soil and land use/land covers which are vary spatially and temporally. Because of spatial and temporal heterogeneity of factors, the runoff also varies with respect to space and time. So, the modelling approaches based on space and time to explore the process behind the runoff generation is important. Also, the study of effects of catchment properties on runoff is needed. This can be achieved by the runoff model. The use of computer models to simulate the hydrologic system is of a major significance in the performance of such flood-runoff analysis.

In the late 17th century, a French scholar called Pierre Perrault estimated the flow of water in a tributary of the Seine River and compared it to rainfall across the river's catchment area. In doing so, he demonstrated for the first time that rainfall was all you needed to account for the flow of water in large rivers. His revolutionary work "De l'origine des fontaines" (On the Origin of Springs) was published in 1674. This link between rainfall and river flow in Paris was confirmed in 1686 by the French physicist Edme Mariotte, who quantitatively measured the velocity in the Seine near the Pont Royal by observing the passage of boats and debris on the current. The study on rainfall-runoff modeling realized by Perreault (1674) was the first report published on quantitative measurements in hydrology. In this report, Perreault developed the relationship between rainfall and stream flow of Seine River in Paris by using the relation of rainfall which was equal to six times of the runoff. This relation was the foundation for many developments in modern hydrology. The concept of rainfall-runoff modelling used for various developmental

activities started in the first half of the 20th century. From 1950 onwards, the research on inter-related process of runoff had been increasing by using variety of innovative techniques (Džubáková, 2010). The Sherman's unit hydrograph concept (1932) and the Hortons infiltration theory (1933) were the examples of the improvements in hydrological study. The entry of digital revolution in the field of rainfall runoff modelling was started in 1960's. This revolution effectively changed the modelling approaches from event based models to continuous simulation models (Wheater et al., 2007).

Actually, tanks de evolutions of the informatics and the increase in available computing power have provided an important contribution in the development of models. While event-based models were developed in the 1930s, the first hydrological models for continuous simulation of rainfall-runoff processes emerged in the 1960s, when computing power was sufficient to represent the relevant land phase processes in a simplified "conceptual" manner. Later, in the 1970s and 1980s, it was possible to develop "physically based" hydrological models through solving a coupled set of partial differential equations to represent overland and subsurface flows. Now a day, a countless number of rainfall-runoff models have been dedicated to handle the complex problems that exist in the watershed and these can be applied specifically for particular watershed conditions with respect to space and time. Recently, various hydrologic models have been used to simulate the quantitative dimensions of the rainfall-runoff process. Based on previous research, the hydrologic modelling system (HEC-HMS) has had effective results in this regard. Hellweger and Maidment (1999) combined a geographic information system (GIS) directly with HEC-HMS to access a rainfall runoff model. Their results were favorable and desirable because of the high speed and capacity of the resultant model in simulation of a flood hydrograph and also in the estimation of flood quantitative characteristics such as runoff volume and peak discharge. Also based on the research results of Dibike et al. (2001) the HEC-HMS model has sufficient reliability in the estimation of the infiltration parameters and for simulating daily streamflow. Today, the use of the artificial neural network (ANN) method in simulating processes has increased. This method has been inspired by the human brain and nervous system patterns (Varvani & Khaleghi, 2019; Varvani et al., 2019). Using this method has had very appropriate results. ANN has a high potential and ability to establish the relationship between different factors and also in the simulation of a parameter. The use of ANN causes a reliable and flexible learning ability in creating models and due to this property, converts the ANN to an attractive inductive approach in hydrological response forecasting (Sahour et al., 2020). Some of the researchers such as Jain et al. (2004) emphasized the effectiveness of ANN

in the simulation of rainfall-runoff process. Therefore, based on recent reviews, one can say that ANN has a high ability and potential in hydrological process modelling. Therefore, the incorporation of HEC-HMS model (optimizing a simulated hydrograph) and ANN (the high performance in the simulation) will result in much more effective results. For example, Verma et al. (2010) used remote sensing (RS) and GIS to investigate the performance of HEC-HMS and WEPP[1] models in simulating the runoff generation in watersheds. Peters et al. (2006) incorporated the HEC-RAS[2] capacities and ANN to perform flood routing in a stream. One of the features of this method is that if there is no observational data, synthetic precipitation can be used repeatedly (Moretti & Montanari, 2008).

A variety of definitions of rainfall runoff model was given by Singh and Beven and Cloke (2012); Singh et al. (2006); Wheater et al. (2007). According to them, the rainfall runoff model could be defined as a tool that has components of interrelated runoff process and can explore their properties influencing runoff production with real world situation. They also reported that in reality this could make the best model for a particular problem with least parameters and simplicity. Hydrological processes at the catchment scale are no longer stationary when the changes taking place in the catchment are highly variable in nature(Cornelissen et al., 2013)Various models are available to solve the hydrological problems. Rainfall–Runoff (RR) prediction is one of the most complicated processes in environmental modeling. This is due to the spatial and temporal variability of topographical characteristics, rainfall patterns, and the number of parameters to be derived during the calibration.

Song and James (1992) reviewed several models and described five scales (laboratory, hill slope, catchment, basin, and continental/global scale) used in hydrologic simulation. The catchment scale models add topography in simulation of surface runoff and geology in simulation of base flow, and often divide larger catchments into smaller homogeneous parts. Basin scale

[1] The Water Erosion Prediction Project (WEPP), is a physically-based soil erosion prediction technology. WEPP has a number of customized interfaces developed for common applications such as roads, managed forests, forests following wildfire, and rangelands. It also has a large database of cropland soils and vegetation scenarios. The WEPP model is a distributed parameter, continuous simulation model, and is able to describe a given erosion concern in great detail for an experienced user.

[2] HEC-RAS is a computer program that models the hydraulics of water flow through natural rivers and other channels. Prior to the 2016 update to Version 5.0, the program was one-dimensional, meaning that there is no direct modeling of the hydraulic effect of cross section shape changes, bends, and other two- and three-dimensional aspects of flow. The release of Version 5.0 introduced two-dimensional modeling of flow as well as sediment transfer modeling capabilities. The program was developed by the United States Army Corps of Engineers in order to manage the rivers, harbors, and other public works under their jurisdiction; it has found wide acceptance by many others since its public release in 1995.

models employ storage and translatory routing schemes in combining runoff. Singh (1995) also classified hydrological models based on the basis of their intended use: planning models, management models and prediction models. Hydrologic models are also grouped as field scale models, event-based watershed scale and continuous watershed scale models. Nowadays, various hydrologic and hydraulic models have been used to predict floods and the required actions to reduce their effects. Many of these models are site specific containing assumptions and simplifications, which exclude their universal use. So, it is very important to understand the candidate model clearly in order to use it appropriately. Some of the models use physically based governing equations having computationally intensive numerical solutions, while others are based on simple empirical relations having strong algorithms. Sometimes, the simple models are insufficient in giving appropriately detailed results, and the detailed models are inefficient and prohibitive for the large catchment. Therefore, it is quite a challenging task to find an appropriate model for a certain watershed.

## I.2 Classifications of hydrological models

Many hydrological models have been developed and refined during the past four decades and it is required to fully understand their characteristics to effortlessly employ them. Therefore, hydrologists need to familiarize themselves with the classification of hydrological models and understand the theoretical definition behind them. However, in regard to this issue, only a few discrete studies had been done. Classification of hydrological models is not exact and different hydrologist may give different definitions. The reason is that the nature of models is often the same but many models have overlapping characteristics. Thus, this section was aimed at showing the dominant classifications for hydrological models alongside the different views from past to present but generally, they have common meaning even though they may be classified under different categories. In addition, although there are overlapping features in different hydrological models, their nature is not that hard to understand.

Hydrological models are usually characterized or classified to help describe and discuss their capabilities, strengths, and limitations. Hydrological models can be divided into three distinct classes using the classification proposed by Wheater et al. (1993), namely mechanistic (i.e. physically-based models), parametric (known as grey box or conceptual models) and metric (called empirical, black box, or data-driven models). In **Fig.I.1**, a representation of these classes is given. Hydrological models can also be classified according to the spatial discretization of the model itself as distributed, semi-distributed or lumped (Solomatine & Wagener, 2011).

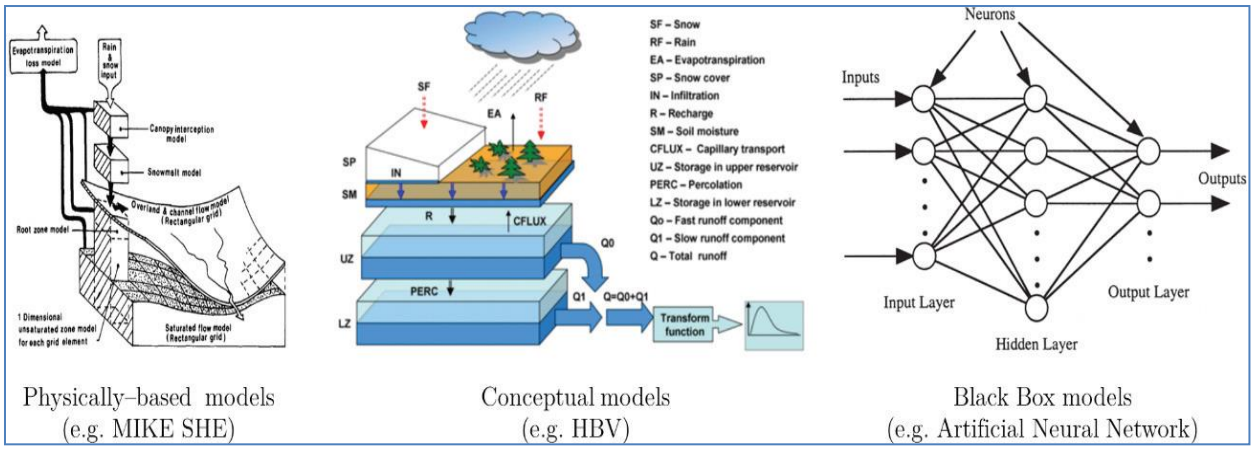


Figure I-1 Hydrological models classification (Solomatine & Wagener, 2011)

### *I.2.1 Model Structure*

A model's structure determines how runoff is calculated. The three structural categories of run-off models, with strengths and weaknesses for each are displayed in **Table.I.1**. Models are listed below in order of increasing complexity, with empirical models being the simplest and physical mechanistic models the most complicated. Physical and conceptual models need thorough understanding of the physics involved in the movement of surface water in the hydrological cycle.

Table I-1 Comparison of the basic structure for rainfall-runoff models

| | Empirical | Conceptual | Physical |
|---|---|---|---|
| Method | Non-linear relationship between inputs and outputs, black box concept | Simplified equations that represent water storage in catchment | Physical laws and equations based on real hydrologic responses |
| Strengths | Small number of parameters needed, can be more accurate, fast run time | Easy to calibrate, simple model structure | Incorporates spatial and temporal variability, very fine scale |
| Weaknesses | No connection between physical catchment, input data distortion | Does not consider spatial variability within catchment | Large number of parameters and calibration needed, site specific |
| Best Use | In ungauged watersheds, runoff is the only output needed | When computational time or data are limited. | Have great data availability on a small scale |
| Examples | Curve Number, Artificial Neural Networks[a] | HSPF, TOPMODEL, HBV, Stanford | MIKE-SHE, KINEROS, VIC, PRMS |

### *I.2.2 Empirical models*

Wagener et al. (2004) reported that the empirical models simplify the reality with the available time series data for the basin and did not consider the information about the basin properties and flow process and so it is called black box model. Also, it considered watershed as a single unit. Empirical models, sometimes called data-driven models, use non-linear statistical relationships between inputs and outputs. Empirical runoff models are best used when other outputs

are not needed; for example: the distribution of runoff values between upstream and downstream areas cannot be calculated with this model type. Very few parameters are needed, making data-driven models easy to use but they have no physical connection to the catchment. Simplicity of implementation, faster computational times, and cost effectiveness are reasons for empirical models to be chosen for modeling. Simple regression model, ANN, fuzzy logic, and Genetic Algorithm are examples of the empirical models. Empirical models contain no physical transformation function to relate input to output; such models usually build a relationship between input and output based on hydro-meteorological data. ANN models are capable of modeling non-linear relationships between inputs and outputs.

The popular curve number method is often considered a semi-empirical model because it assumes the ratio of actual runoff to potential runoff is equal to the ratio of actual to potential retention, but there is no physical justification for this assumption.

The major limitation of empirical models is due to the absence of explicit consideration of physical processes such as subsurface flow, surface runoff, and infiltration in the catchment. Also, these numerical models are not capable of modeling the influence of change in vegetation on various hydrological components

### *I.2.3 Conceptual models*

Conceptual models interpret runoff processes by connecting simplified components in the overall hydrological process. They are based on reservoir storages and simplified equations of the physical hydrological process, which provide a conceptual idea of the behaviors in a catchment. These models need a range of parameters and meteorological input data. The approximation is the key concept of Conceptual Rainfall Runoff model (CRR), and it can be used to explain the mechanisms of hydrologic cycle. CRR models are used to forecast runoff and other hydrological variables for shorter as well as longer duration. Since the accuracy of CRR model is based on the calibration of parameter, the hydrologist should have a clear understating of calibration techniques. In the past decades, manual calibration was done by using trial and error procedure of data adjustments. In this process, eye judgment played an important role to determine the accuracy of the calibrated CRR model (Sitterson et al., 2018).

Nowadays, the automatic calibration with computer technology has replaced the manual calibration which is time consuming and inaccurate approximation. Conceptual models have gained popularity in the modeling community because they are easy to use and calibrate. Lack

of physical meaning in governing equations and parameters is also a limitation. Conceptual models are best used when computation time is limited and catchment characteristics are not analyzed in detail.

### *I.2.4 Physical models*

Modelling approach based on the knowledge of topographical characteristics related with run-off process and having equations with physics concepts is called physically based runoff model. In this modelling the spatial variability of the basin is taken into account for hydrological process analysis. The greatest strength of a physical model is the connection between model parameters and physical catchment characteristics which make it more realistic. Spatial and temporal variations within the catchment are incorporated into physical models.

### *I.2.5 Watershed-scale models*

The rainfall-runoff model can also be classified as lumped, semi distributed and distributed model based on spatial discrimination.

The spatial structure of catchment processes in rainfall-runoff models can be categorized as lumped, semi-distributed, and fully distributed (see **Table.I.2**).

Table I-2 Comparison of the spatial structures in rainfall-runoff models

| | Lumped | Semi-Distributed | Distributed |
|---|---|---|---|
| Method | Spatial variability is disregarded; entire catchment is modelled as one unit | Series of lumped and distributed parameters | Spatial variability is accounted for |
| Inputs | All averaged data by catchment | Both averaged and specific data by sub-catchment | All specific data by cell |
| Strengths | Fast computational time, good at simulating average conditions | Represents important features in catchment | Physically related to hydrological processes |
| Weaknesses | A lot of assumptions, loss of spatial resolution, not ideal for large areas | Averages data into sub-catchment areas, loss of spatial resolution | Data intense, long computational time |
| Examples | Empirical and conceptual models, machine learning | Conceptual and some physical models, TOPMODEL, SWAT | Physically distributed models, MIKESHE, VELMA |

Lumped models do not consider spatial variability within the catchment; semi-distributed models reflect some spatial variability; and fully distributed models process spatial variability by grid cells. Semi-distributed models take spatial variability into consideration at smaller scales

than lumped models, but do not calculate runoff at every grid cell. Spatial interpretation in a lumped model, a semi-distributed model, and a distributed model are shown in **Fig.I.2**.

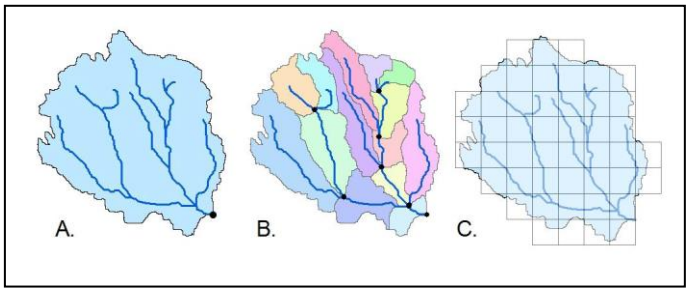


Figure I-2 Visualization of the spatial structure in runoff models. A: Lumped model, B: Semi-Distributed model by sub-catchment, C: Distributed model by grid cell.

Runoff is calculated for each sub-catchment at the pour point represented by the black dots in **Fig I.2 B**. Distributed models calculate runoff for each grid cell, while lumped models calculate one runoff value for the entire catchment at the river outlet point represented by the black dot in **Fig.I.2A**.

Lumped models treat the catchment area as a single homogenous unit. By assuming homogeneity over the catchment, lumped models lose spatial resolution of the input data; for example, using the mean soil storage and uniform precipitation amounts. A lumped model is designed to simulate total runoff and streamflow at the outlet point, not specific flows within a catchment (shown in **Fig.I.2A**). For this reason, lumped models adequately simulate average runoff conditions with fast computational times.

Semi-distributed models are variations of lumped models, with features of distributed models. They can consist of a series of lumped parameters applied in a quasi-spatially distributed manner. For example, semi-distributed models can have data that are separated within a catchment but homogenous within a sub-area (**Fig I.2 B**) (Beven & Cloke, 2012)

Distributed runoff models are the most complex because they account for spatial heterogeneity in inputs and parameters. Fully distributed models separate the model process by small elements or grid cells. Each small element (or cell) has a distinct hydrological response and is calculated separately, but incorporates interactions with bordering cells (Rinsema, 2014). By calculating runoff for every grid cell, the model provides detailed runoff information at various points within the catchment (see **Fig I.2C**). Distributed models are data-intensive, with all input data distributed spatially and temporally. Inputs needed for a typical distributed model are Digital Elevation Models (DEM); land use imagery from satellites; gridded precipitation; soil

characteristics and how they change over time; topography; and watershed characteristics such as dimensions and boundaries.

### *I.2.6 Model functionality and complexity*

While choosing a model for specific application, it is important to consider its applicability to simulate the impact of land use change and also prediction performance. The model functionality and complexity can become major criteria in model selection. The model functionality differs in terms of hydrologic process representation, the equations adopted to simulate these processes and model discretization. In addition, model complexity can be defined by the estimated data, resources, time, and cost that are required to parameterize and calibrate a model, as well as the professional judgment and experience required to operate these models. The description of several widely-used hydrological models is provided in **Table.I.3**

## I.3 Building and implementing a hydrological model

Building and implementing a hydrological model is a complex process. In the following, we present the hydrological modelling process using the five steps described by Refsgaard and Henriksen (2004), and Scholten et al. (2007)

### *I.3.1 Model Study Plan*

A hydrological model is designed to answer a specific water-related question. For example, it can be built to predict in high-flow or low-flow periods. Therefore, modeling objectives may strongly influence the way the model is developed. The relevance of the model may also depend on climatic and physical conditions of applications. Last, the development of the hydrological models may be limited by external factors such as the availability of recorded data and the observation of the physical processes at stake. These aspects must be accounted for at the very beginning of the modelling process, as they may play a key role on model efficiency.

Table I-3 Description of hydrologic models related to model functionality and complexity

| Model | Main component | Evapotranspiration | Overland Flow | Subsurface Flow | Spatial Scale |
|---|---|---|---|---|---|
| **HEC-HMS (Verma et al., 2010)** | Precipitation, losses, baseflow, runoff transformation, and routing | Priestley-Taylor | CN, Kinematic wave, Soil moisture accounting model | Linear reservoir, volume accounting model, exponential recession model | Semi distributed |
| **MIKE SHE (Wijesekara & Marceau, 2012)** | Interception, overland/channel flow, unsaturated/saturated zone, snowmelt; aquifer/rivers exchange, advection/dispersion of solutes, plant growth, soil erosion, and irrigation | Based on canopy storage and soil evaporation | 2-D diffusive wave equations (St.Venant equations) | 3-D groundwater flow (green Ampt infiltration method) | Distributed |
| **SWAT (Wu & Johnston, 2007)** | Hydrology, weather, sedimentation, soil temperature and properties, crop growth nutrient, pesticides, agricultural management, and channel and reservoir routing | Penman-Monteith, Hargreaves, Priestley-Taylor | CN Method | Lateral subsurface flow/ground flow (Green and Ampt equation) | Semi-Distributed |
| **WaSIM (Bormann & Elfert, 2010)** | Evapotranspiration, soil module, infiltration, overland flow, interflow, baseflow routing) | Penman-Monteith | Hortan overland flow | Green and Ampt equation | Distributed |
| **DHSVM (Thanapakpawin et al., 2007)** | Surface and subsurface flow, soil moisture, Snow cover, runoff, and evapotranspiration | Penman-Monteith equation | Saturation excess and infiltration excess mechanisms | Saturated subsurface flow | Distributed |
| **VIC Model (Mao & Cherkauer, 2009)** | Infiltration, runoff, baseflow process, and evapotranspiration | Penman-Monteith equation | Saturation excess and infiltration excess mechanisms | Saturated subsurface flow | Distributed |
| **PAWS (Shen & Phanikumar, 2010)** | Overland flow, snowpack, soil moisture, groundwater flow, and stream flow | Penman-Monteith + root extraction | Manning's formula + kinematic wave formulation+ coupled to Richards equation | Green and Ampt equation | Distributed |

### *I.3.2 Data and conceptualization*

A hydrological model transforms input meteorological variables (mainly precipitations and potential evapotranspiration) into an output hydrological variable (mainly flow) over a time period (see **Fig.I.3**). A hydrological model is made of mathematical representations of the key processes like evapotranspiration, infiltration and transfer in streams. The model technically consists in a set of hydrological parameters describing the catchment properties, and algorithms describing the physical processes. There are many ways to build hydrological models. As mentioned above, the choice of the modelling approach (or of an existing model) may depend on the objectives, available data and user experience. In this modelling step, the way the natural system should be represented is defined

### *I.3.3 Model set-up*

The structure of the model is then implemented. The typical structure of a hydrological model is composed of two parts (see **Fig.I.3**):

- A production module assesses the portion of precipitation that feeds runoff at the catchment outlet (effective rainfall). The remaining part either is stored, infiltrates to deep aquifers or returns to the atmosphere through evapotranspiration,
- A transfer module routes effective rainfall to the catchment outlet, depending on the water pathways (surface, sub-surface or groundwater flow).

### *I.3.4 Calibration and validation*

The values for the parameters included in process equations cannot always be determined from field measurements. Therefore, numerical optimization is often necessary to obtain a set of parameters suitable for the studied catchment. Optimization requires observed output data on a given time period. A variety of optimization approaches were developed. The simplest ones start from an initial set of parameters that is iteratively changed to improve the quality of an objective function (a criterion defining the quality of the fit between observed and simulated flow values) until an optimum value is reached. The calibration step should be systematically associated with a validation test, in which one assesses the results of the model on an independent data set. It should be noted that uncertainty always remains due to errors in models' structure, parameters, data, etc. This uncertainty should be properly assessed for a more informed model application.

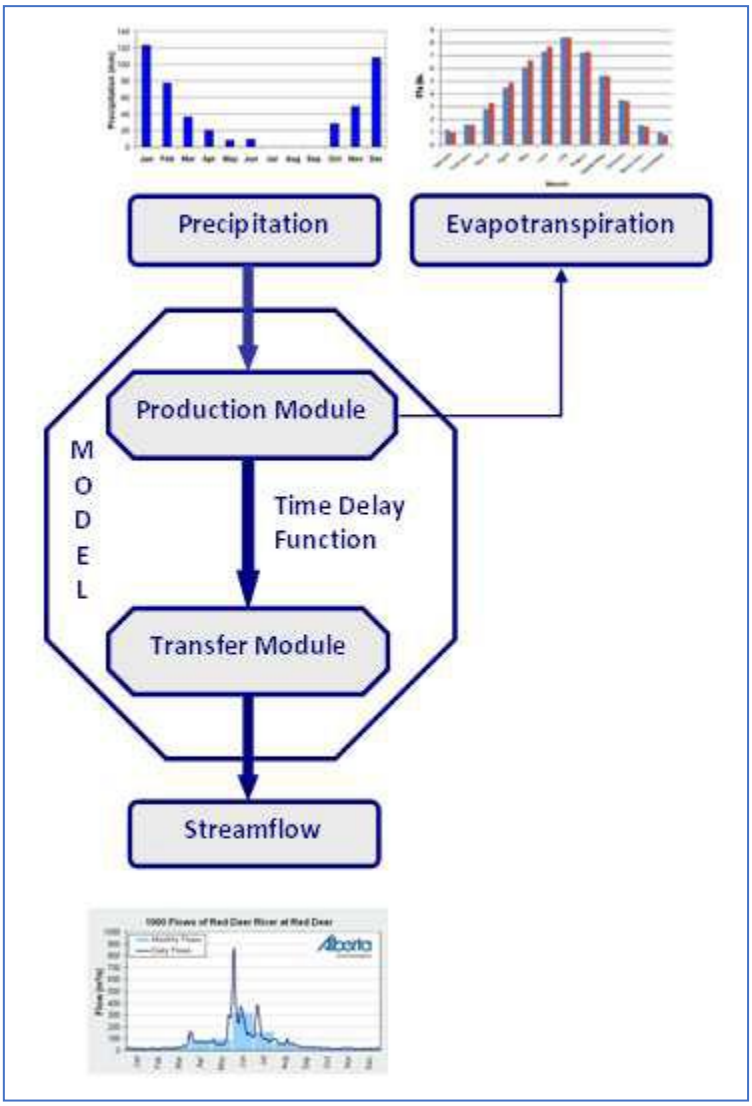


Figure I-3 Example structure of a hydrological model

### *I.3.5 Simulation and evaluation*

Once the model has been set up, calibrated and validated, it can be run for the target application. Examples of applications requiring hydrological models include the design and management of water control facilities such as dams, and the anticipation of flood or low flow periods. The uncertainty in results has to be analyzed in order to assess the reliability of the simulated variable and support the decision-making process.

Finally, the results of the model have to be evaluated, either by visually comparing observed and simulated plots or by applying a mathematical criterion to calculate the distance between observed and simulated data. Visual and mathematical evaluations may differ and generate different diagnosis on model quality and efficiency.

### *I.3.6 Evaluation criteria*

Since the early stages of hydrological modelling, there was a need to evaluate the results of models and to quantify their efficiency for flow prediction. It is very important to quantify the residuals of their models. This can be obtained simply by plotting observed and simulated hydrographs or by calculating the percent difference between observed and simulated flows. A large variety of evaluation criteria and tools were introduced in the literature, corresponding to various modelling objectives or target variables. This led researchers from various environmental disciplines to recommend the following criteria:

### *I.3.7 Visual criteria*

The most straightforward possibility to evaluate models is to use graphical means and compare observed and simulated values. This evaluation method is often considered approximate or qualitative since model fit is evaluated by eye. Typical graphical representations of results from hydrological models include plotting:

- observed and simulated flow hydrographs over time simulated flows against the observed flow (Q-Q plots),
- the cumulative distribution function of observed and simulated flows (known as flow duration curves).

Visual inspection benefits from the expert comprehension, interpretation and experience, which can be of real help in finely judging of model accuracy.

Nevertheless, this advantage can also be seen as a drawback as the dependence on the expert's own experience and references may make the evaluation subjective and quite different from one person to another. Moreover, depending on the kind of graphs that is used for the evaluation, the characteristics of model fit that are assessed will not be the same.

### *I.3.8 Mathematical criteria*

Another possibility for evaluating and comparing models is to compute a mathematical criterion which evaluates a distance between the measured and simulated flow values over a chosen time period. It usually takes the form of a norm that quantifies the distance between the observed and simulated series. These criteria are often considered more objective and are described as quantitative.

The existence of qualitative and quantitative criteria may put the hydrologist in a tricky situation, with potentially disagreeing diagnostics on model efficiency depending on the type of criteria used. Nevertheless, visual inspection is acknowledged to be a full-fledged evaluation technique as essential as evaluation by mathematical criteria.

### *I.3.9 Model selection*

The correct choice of a model for use in a specific project should lead to better results .Choosing a rainfall-runoff model is based on the modeling purpose such as understanding and answering specific questions about the hydrological process; assessing the frequency of runoff events; or estimating runoff yield for management purposes (Vaze et al., 2011). Identifying the priorities of modeling and the limitations of data availability, time, and budget for models help to narrow the choices and ensure that the model is the best for the intended purpose.

In their study Ghonchepour et al. (2021) proposed three stages for hydrological model selection process, namely

1) Initial selection based on modeling purpose;
2) Selection of the model based on intercomparison; and
3) Final selection of the model based on influencing criteria.

To find appropriate model(s) to use and execute in a specific project, model screening is undertaken based on the presented process. The three stages of the presented process are explained below. **Fig.I.4** also shows the methodological framework used for selecting a suitable hydrological Model.

#### *I.3.9.A First stage: Initial selection based on modeling purpose*

In the first stage of the choice of a hydrological model, defining the purpose of the modeling is critical and the initial choice is made based on the different classification of models. As shown in **Fig.I.4**, if the modeling purpose is only to predict flow discharge and the calibration data are available, then simple lumped models can provide predictions that are as good, if not better, than complex physically based models. Some explanations about different classes of hydrological models are available below in the sections above.

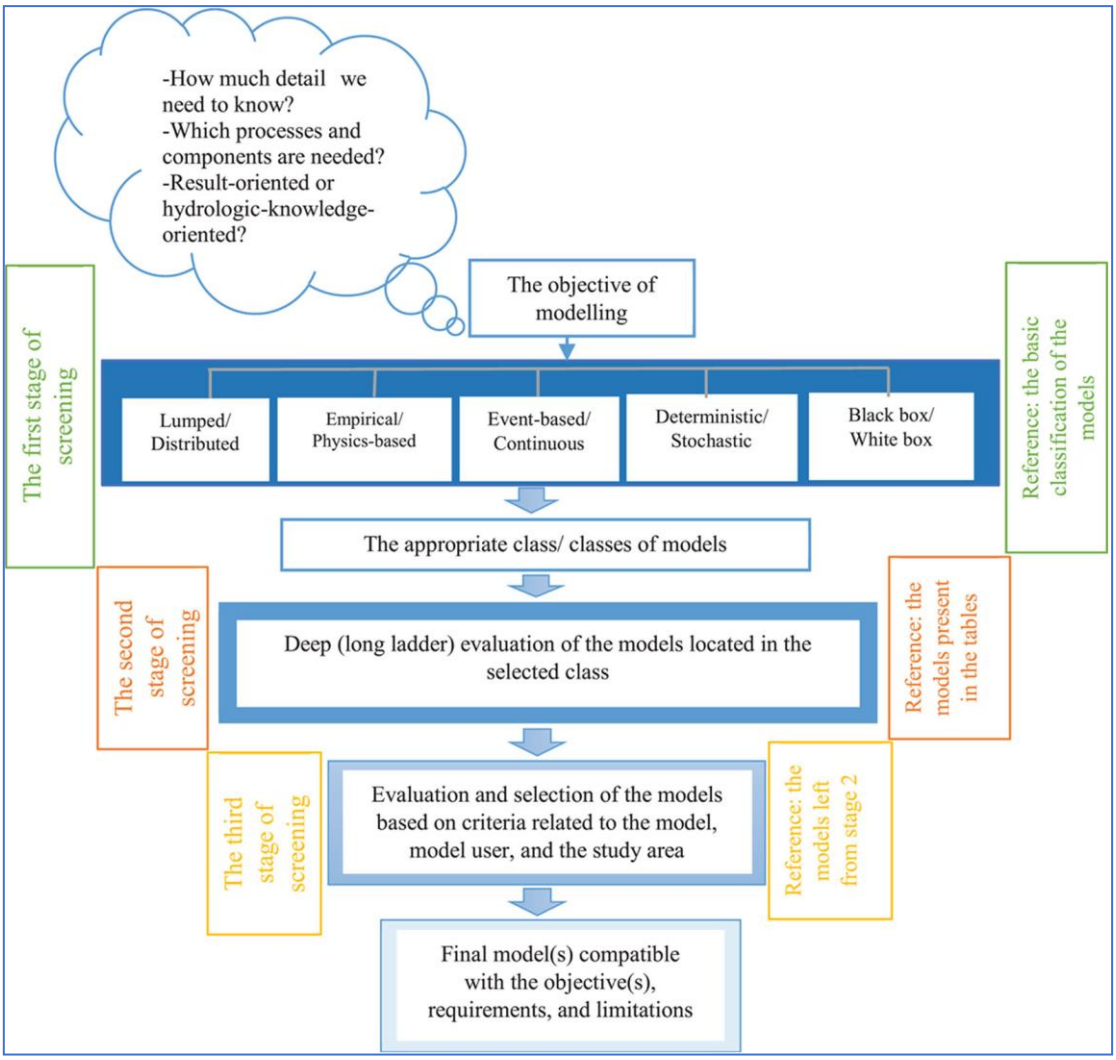


Figure I-4 Schematic diagram of the methodological framework for hydrological model selection (source (Ghonchepour et al., 2021)

### *I.3.9.B Second stage: Selection of the model based on intercomparison*

Intercomparison can reveal the strengths and weaknesses of each model which can be achieved using the short ladder (shallow evaluation) and long ladder (deep evaluation) approaches. In the short ladder approach, the performance of the models is compared based on the simulated hydrographs generated by each model being considered, and the observed data. In the long ladder approach, evaluation enables us to know which hydrological processes are represented in the model and how they are interlinked. So, in this type of assessment, it is not reasonable to compare an ANN black-box model with a fully distributed physically based model. To reach the final choice of model, the candidate models are compared with each other using the long ladder approach. In this regard, the procedure adapted from Beven (2011) can be helpful by listing:

- the models of interest;
- the variables simulated and predicted by each model;
- assumptions considered in each model;
- the inputs of each model; and then
- weighing the conditions/limitations, and
- determining if any model satisfies all conditions.

#### *I.3.9.C Third stage: Final selection of the model based on influencing criteria*

Furthermore, issues that can be effective in the final choice of a hydrological model for a specific project can include the availability of time and financial supply for the model user (Beven, 2011); the availability of the model, code, and documentation for public use; the temporal and spatial scale of the model; the existence of multiple applications of the model in different regions; the climatic conditions for which a specific model has been developed; and the quantity and quality of the available climatic and hydrologic data.

# Hydrological processes

# II Hydrological Processes

## II.1 Introduction

As stated in Maidment (1993) "Hydrology is concerned with the circulation of water and its constituents through the hydrologic cycle. It deals with precipitation, evapotranspiration, infiltration, groundwater flow, runoff, streamflow, and the transport of substances dissolved or suspended in flowing water". Hydrology is primarily concerned on water on or near the land surface. Therefore, at a particular point on a channel the streamflow is generated by a contribution area. Their boundaries are mainly delimitated by topography and it can be distinguished between surface and subsurface catchments. Thus, catchments are Hydrological cycle can be defined as the sequence of cyclic events which correlates the movement of water from the atmosphere to the earth's surface and then to the large water bodies through surface and subsurface routes and finally going back to the atmosphere.

According to (Chow Ven Te & Larry), hydrologic processes convert the distribution in space and time of water during the hydrological cycle. Physical properties as the shape and size of a stream influence the motion of water in the hydrologic system.

The study of hydrological cycle and hydrological response of a catchment have become very complex due to complicated inter-relationship between various hydrological components such as precipitation, evaporation, transpiration, infiltration, and runoff. This means that when one process is affected the others are also affected (Dwarakish & Ganasri, 2015).

The hydrologic system embodies all of the physical processes that are involved in the conversion of precipitation to runoff as well as physical characteristics of the watershed and atmosphere that influence runoff generation.

Precipitation is viewed as an input to a hydrologic system. The precipitation might be associated with a historical storm, a design storm, or may result from a stochastic generation procedure. Generally, precipitation is averaged spatially over a sub-basin, which affects the shape of the outlet hydrograph. Likewise, precipitation intensity is averaged over a time interval which is significant on a small watershed. Thus, precipitation input to the hydrologic system is commonly represented by hyetographs of spatially and temporally averaged precipitation. By returning excess precipitation and controlling how much water flows into stream systems, runoff is important in balancing the hydrological cycle.

Flooding events have been known to be related to meteorological, hydrological and anthropogenic factors (Erena & Worku, 2018). An anthropogenic factor that may be a strong indicator of flood risk is urban growth (Erena & Worku, 2018; Hemmati et al., 2020). There are trends that are well covered in the literature related to flooding and urban development. For example, when there is more urban development there is an increase in flooding that occurs downstream. Hemmati et al. (2020) fount that the rapid population growth and development puts an increased strain on the likelihood of flood related risks This result was shown through 42 different inundation scenarios that were evaluated, in each one increased flooding happened when the urban, economic and population growth increased.

The direct involvement of rainfall in runoff generation and runoff in streams, rivers, and even floods, makes it one of the most focused hydrological phenomena. Therefore, precise and accurate rainfall–runoff modeling is important for effective management of water resources and prediction and prevention of natural disasters (Khan et al., 2021).

Runoff is the portion of the rainfall draining from a catchment area through drainage lines by the gravitational force and fed into the common point called watershed. It is generated after satisfying both surface and subsurface losses such as evaporation, interception and infiltration. It is also called as rainfall excess expressed as volume per unit time. Runoff volume in a particular catchment largely depends on the intensity of rainfall in the catchment.

The watershed management plans are based on the quantity of runoff generated in the basin from the rainfall. It explores the wealth of the watershed and developmental activities related to flora and fauna. Hydrologists explain the process behind the runoff generation to identify the area where the runoff is generated. Runoff generation process mainly depends on flow conditions such as surface flow that accelerates the infiltration. Spatially the runoff processes vary within the watershed due to non-uniformity of geological and geo-hydrological environment. It is very important to identify the main mechanism behind runoff generation which may be either infiltration excess or saturation excess. This identification will help to delineate the runoff zones in the catchment.

## II.2 Runoff Mechanisms

The rainfall-runoff model simulates the processes from precipitation reaching the surface to the outflow from the watershed. The model includes the single processes runoff generation, runoff concentration and runoff routing. These components may appear in different guises and levels

of complexity but should always be embedded in a rainfall-runoff model (Mays, 2012). defines the processes to determine the runoff hydrograph from the rainfall input. See **Fig.II.1**.

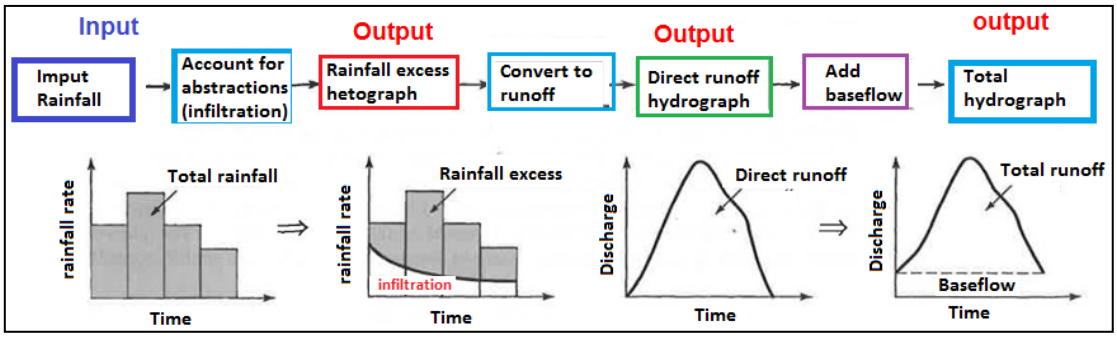


Figure II-1 Steps to define a storm runoff hydrograph (Mays, 2012)

### *II.2.1 Runoff Generation*

The runoff generation determines how much rainfall becomes part of the storm hydrograph. In this phase the discharge is separated in general or into individual components. The acquisition of the single components is the most essential part for the determination of the storm hydrograph of the effective precipitation. Prior to the transformation from discontinuous rainfall to continuous runoff, the losses caused by interception, depression storage and infiltration have to be covered. The infiltration describes the movement of water draining into the soil. Infiltration is influenced by the soil structure, the hydraulic conductivity and the initial soil moisture content. The hydraulic conductivity decreases considerably as soil becomes unsaturated since less pore space is filled with water, the flow paths become increasingly tortuous and therefore drag forces between the fluid and the solid phase increase. Just when rainfall intensity exceeds infiltration capacity, water will accumulate at the surface and eventually in depression storages, before starting to contribute to surface runoff as overland flow. Hence, the comparison of rainfall rates with infiltration capacities leads to an ability to estimate the effective rainfall for a storm (Beven & Cloke, 2012).

This approach is based on Horton, 1933, where he used an empirical function to describe the decline of infiltration capacity with time that he found in his experiments. At element (a) of **Fig.II.2** the rainfall intensity is higher than the initial infiltration capacity of the soil. At element (b) in **Fig.II.2**, the rainfall intensity is lower than the initial infiltration capacity so that the infiltration rate is similar to the rainfall rate until time to ponding $t_p$. $F_c$ represents the final infiltration capacity of the soil.

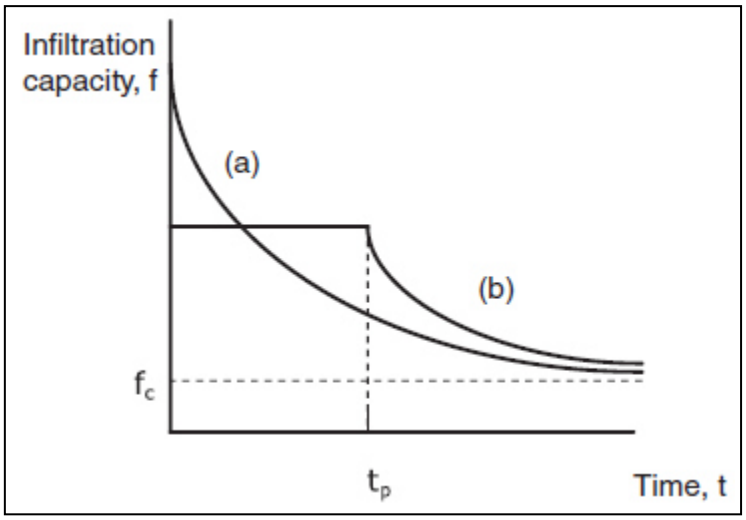


Figure II-2 Decline of infiltration capacity with time (Beven & Cloke, 2012)

There are different methods available in order to estimate the effective rainfall from a storm. The infiltration excess model is widely applied and shown in **Fig.II.3.a** Simplified concepts to generate effective rainfall in rainfall- runoff modelling are also in use, by assuming a constant loss rate (the Φ- index method) (**Fig.II.3.b)** or by setting a percentage of the total rainfall to become effective rainfall (**Fig.II.3.c**).(Beven & Cloke, 2012)

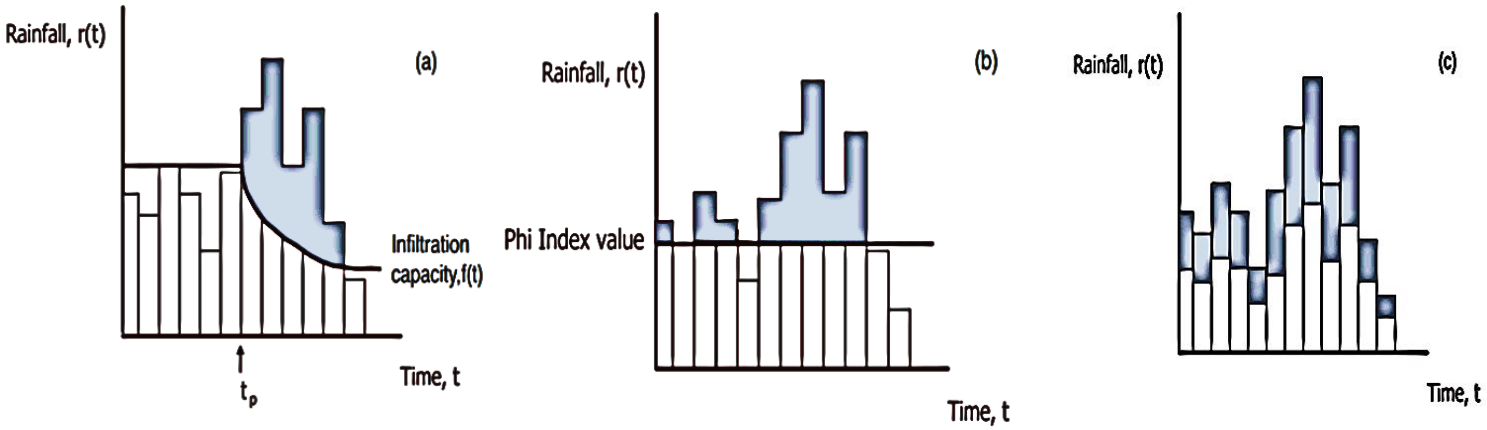


Figure II-3 Methods for calculating effective rainfall: (a) infiltration excess model, (b) constant loss rate, (c) constant proportion (Beven & Cloke, 2012)

Surface flow is represented as precipitation which falls on the ground and flows directly on the surface to the main channel. Surface flow may occur as sheet flow, shallow concentrated flow or channel flow. Surface flow with transmission losses includes surface runoff and additionally the infiltration into the ground surface. The amount of transmission losses depends on the amount of runoff, moisture characteristics of the soil, topography and hydraulic features of the

flow. This type of flow mainly occurs in arid, semiarid and sub-humid climate zones. Interflow or quick return flow is described as infiltration and rapidly movement of the water in the underground. The water may return to the surface and continue as surface flow to the main channel. This type of flow is faster than baseflow and occurs mainly in humid climates or in areas with high infiltration rates and steep slopes. Baseflow is represented as direct infiltration into the ground where water enters the groundwater table. From there, it can flow slowly to the channel. The objective of the runoff concentration is to develop the runoff hydrograph with the rainfall hyetograph as an input. One of the most popular methods of describing the runoff concentration of a catchment is the unit hydrograph approach. When observed rainfall- runoff data are not available for the unit hydrograph development, a synthetic unit hydrograph can be created. In contrast to the synthetic hydrograph, the unit hydrograph is only applicable in that watershed where rainfall and streamflow data were obtained to create it, and at the point on the rainfall event where the streamflow data were measured. The synthetic hydrograph procedures have the ability to develop unit hydrographs for different locations in the same or a similar watershed (Mays, 2012)

When rain and reach the surface of the ground, they encounter a filter that is of great importance in determining the path by which hillslope (The 'hillslope' is defined as the morphological unit of the catchment that does not include perennial flows. As such, it is the portion of the catchment where runoff is generated.) runoff will reach the stream channel. The paths taken by the water (see **Fig.II.4**) determine many of the characteristics of the landscape, the uses to which land can be put, and the strategies required for wise land management. If the rate of rainfall is greater than the capacity of the soil to absorb water, the unabsorbed excess becomes overland flow, referred to often as Horton overland flow (Path n. 1 in the **Fig.II.4** below)

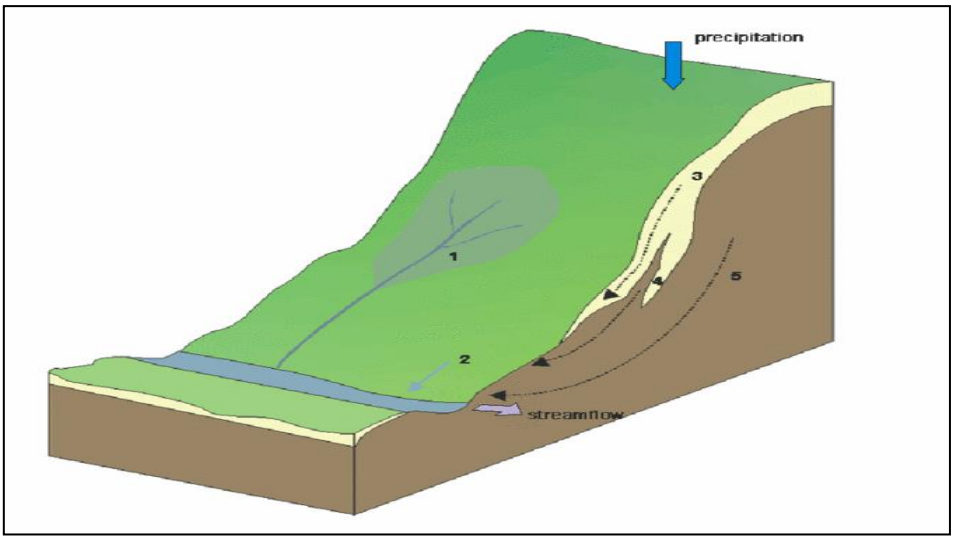


Figure II-4 Mechanisms of runoff generation (1 infiltration-excess overland flow, 2 saturation overland flow, 3 rapids through flow in macropores, 4 displacement flow in saturated macropores, 5 ground water flow)

If the precipitation is first absorbed by the soil, it may be stored there, or may move toward stream channels by a variety of routes. If the soil or rock is deep and of uniform permeability, the subsurface water moves vertically to the zone of saturation, and thence follows a curving path to the nearest stream channel (groundwater flow) (**Fig.II.5**).

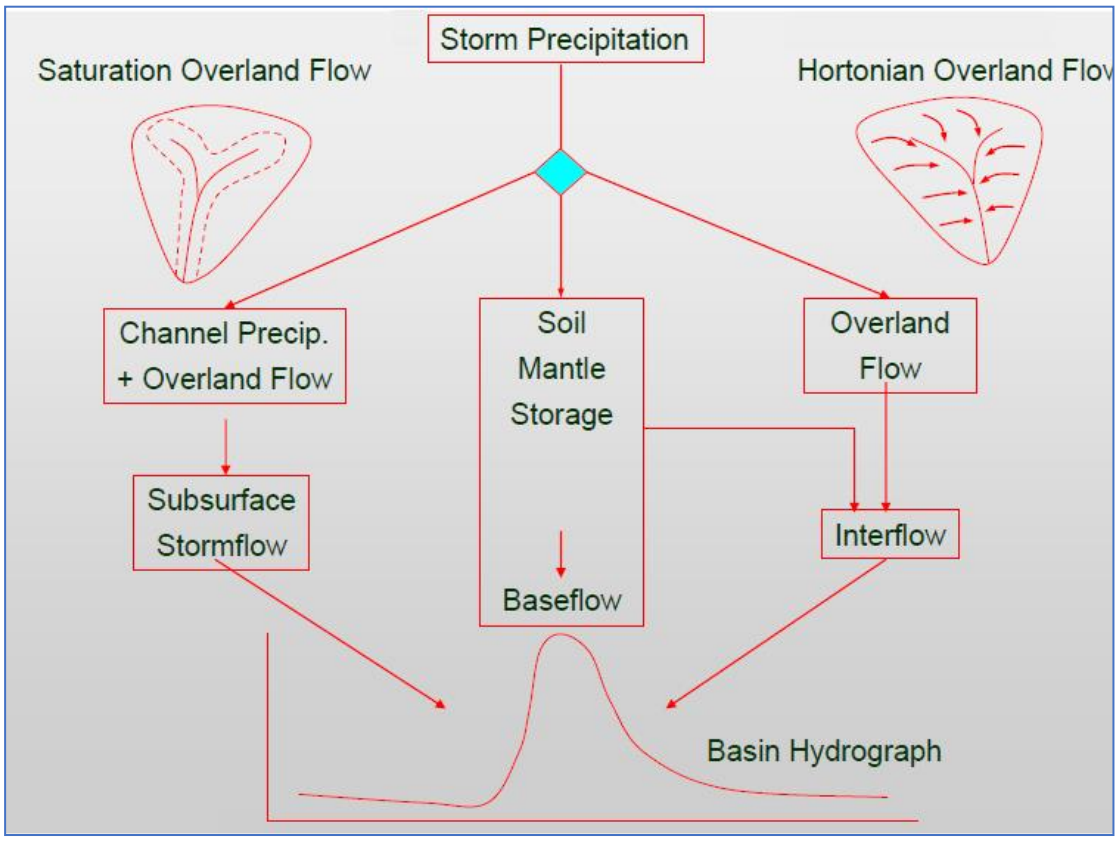


Figure II-5 Schematic summary of controls on runoff pathways

The location of runoff production in a watershed depend on the mechanism by which runoff is generated. Infiltration excess/ Hortonian/ unsaturated flow occur when the rainfall intensities exceed to the soil infiltration rate or any depression storage has been already filled. Soil infiltration rates are controlled by soil characteristics, vegetation cover and land use practice This type of flow mostly occurs in arid and semi-arid conditions.

In contrast, there is another phenomenon behind runoff generation, Saturation excess, which occurs when the rain encounters soils, fully or nearly saturated due to perched water table that forms when the infiltration front reaches a zone of low transmission. The location of areas generating saturation-excess runoff, typically called Variable Source Areas (VSAs), depends on the topographic position in the landscape and soil transmissivity. This type of flow mostly occurs in humid, well vegetated regions, especially those with permeable soils underlain by shallow restricting layer. The **Table.II.1** depicts the effect of environmental factors on response mechanism.

Table II-1 Environmental factors affecting event-response mechanism, Source: (www.ees.nmt.edu/vivoni/are/runLectures/Lecture2.pdf)

| **Mechanism** | **Soil** | **Water table** | **Topography** | **Vegetation** | **Water-input Rate** |
|---|---|---|---|---|---|
| **Hortonian flow** | Low surface *saturated hydraulic conductivity* | Deep | Steep Slopes | Absent to spare | High |
| **Saturation flow** | High *saturated hydraulic conductivity* | Near surface | Concave, convergent Slopes, wide Valleys | Absent to abundant | Low to high |

When precipitation exceeds losses such as infiltration, surface storage, interception, and evaporation, runoff is generated to become concentrated flow in valleys and stream channel. Two mechanisms are included in runoff generation, which are Hortonian overland flow and saturation overland flow. A severe storm will lead to runoff generation when the soil is saturated, while Hortonian overland flow depends on the relationship between infiltration capacity versus rainfall intensity. This means that runoff is generated when rainfall intensity exceeds infiltration capacity.

Infiltration excess is most commonly observed with short-duration intense rainfall. It also occurs in areas with high clay content or where the surface has been altered by soil compaction,

or urbanization, in fact, the soil can be quite dry, but soil properties or land cover do not allow for infiltration to keep up with high rainfall rates. Infiltration excess overland flow is sometimes called *Hortonian* flow.

In **Fig.II.6.a** the infiltration excess overland flow mechanism is illustrated. There is a maximum limiting rate at which a soil in a given condition can absorb surface water input. This was referred to as the infiltration capacity of the soil by Robert E. Horton (1933), one of the founding fathers of quantitative hydrology, and hence this mechanism is also called Horton overland flow. When surface water input exceeds infiltration capacity the excess water becomes infiltration excess runoff. Note that infiltration capacity typically declines during a storm due to the pores in the soil being filled with water, which reduces the capillary forces drawing water into pores.

Due to spatial variability of the soil properties affecting infiltration capacity and spatial variability of surface water inputs, infiltration excess runoff does not necessarily occur over a whole drainage basin during a storm or surface water input event. This idea has become known as the partial-area concept of infiltration excess overland flow and is illustrated in **Fig.II.6. b**. In most humid regions, infiltration capacities are high because vegetation protects the soil from rain-packing (compaction of the crust of the soil) and dispersal and also because the supply of humus and activity of micro fauna create an open soil structure. Under such conditions surface water input intensities generally do not exceed infiltration capacities and infiltration excess runoff is rare. Overland flow can occur due to surface water input on areas that are already saturated. This is referred to as saturation excess overland flow, illustrated in **Fig.II.6. c.** Saturation excess overland flow also occurs in locations not initially saturated, but where infiltrating water completely saturates the soil profile until there is no space for any further water to infiltrate. This expansion of the saturated area results in what is referred to as a variable source area for the generation of saturation excess overland flow. The complete saturation of a soil profile resulting in the water table rising to the surface is referred to as saturation from below. Once saturation from below occurs at a location, all further surface water input at that location becomes saturation excess overland flow.

Geometrical considerations dictate that near stream saturated zones will be most extensive in locations with concave hillslope profiles and wide flat valleys. However, saturated overland flow is not restricted to near-stream areas. Saturation from below can also occur:

- where subsurface flow lines converge in slope concavities (hillslope hollows) and water arrives faster than it can be transmitted down slope as subsurface flow (**Fig.II.6.c**);
- at concave slope breaks where the hydraulic gradient inducing subsurface flow from upslope is greater than that inducing down slope transmission;
- where soil layers conducting subsurface flow are locally thin; and
- where hydraulic conductivity decreases abruptly or gradually with depth and percolating water accumulates above the low-conductivity layers to form perched zones of saturation that reach the surface (**Fig.II.6. e**).
- Layering in soils can also result in the occurrence of a perched water table with subsurface flow above an impeding layer contributing to storm flow (**Fig.II.6. e)**
- In areas with high infiltration capacities and steep slopes, the water table is far from the surface and there is little opportunity for either infiltration excess or saturation excess overland flow. In these settings, interflow or subsurface storm flow is usually the dominant contributor to streamflow (**Fig.II.6. d**). Subsurface flow may be rapid in cases where there are preferential pathways such as macropores for rapid subsurface downslope movement of water.

As evident from many studies, antecedent wetness conditions of the catchment, limited storm extent in space and time and pattern of rainfall intensities add to the complexity and non-linearity of runoff generation processes (Beven, 2000) . Runoff is often only generated above a certain runoff threshold and fast surface runoff components with a short time lag to the triggering rainfalls are dominant. The relevant spatial infiltration patterns are determined by surface properties and vegetation as well (Beven, 2000).

Factors that encourage infiltration, percolation, and higher evapotranspiration (ET) will decrease surface runoff, while factors associated with anthropogenic activities like urbanization and logging will increase surface runoff.

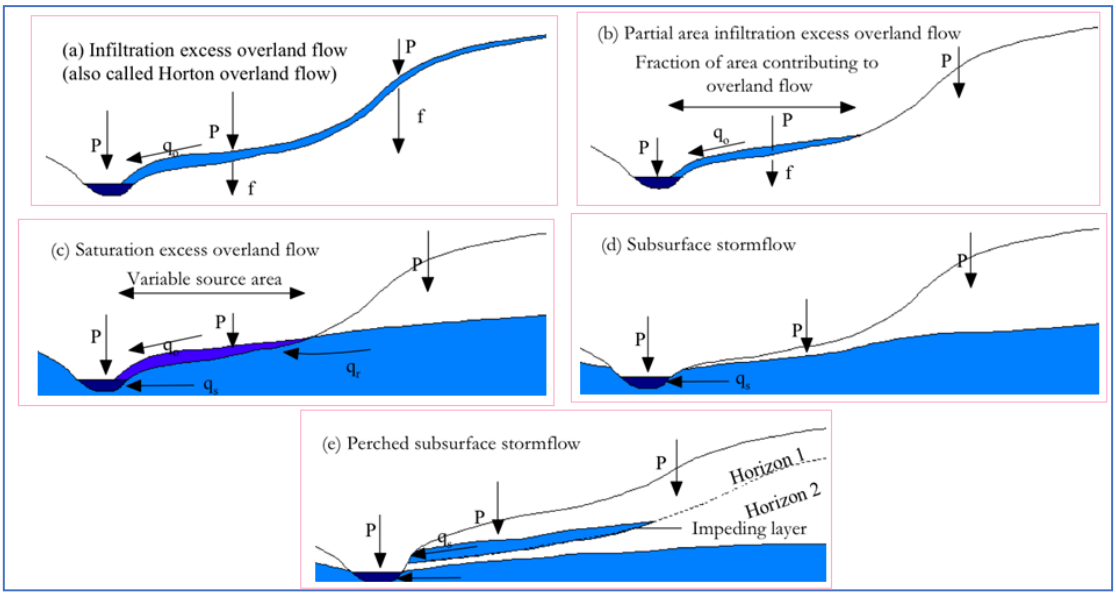


Figure II-6 Classification of runoff generation mechanisms following where P = precipitation, f = infiltration, and q = surface flow. (Beven, 2000)

- Overland flow is influenced by a wide range of features like:
- Geomorphology of the catchment's landscape;
- Spatially distributed watershed's soil characteristics;
- Land use land cover change throughout the catchment;
- Catchment's geologic characteristics.

Most of the physiographic features may be changed with anthropogenic effect on the catchments' landscape, and it therefore very essential to understand not only the associations between catchments' landscape characteristics and surface runoff in a mountainous region but also how direct anthropogenic watershed impacts and climate change affects these physiographic characteristics.

## II.3 Flood Hydrograph

A plot of the discharge in a stream plotted chronologically against time is called a Hydrograph. Hydrograph is the graphical representation of the response of the watershed for a given storm as input. A hydrograph of a catchment produced by a storm is a graphical representation of discharge rate of a stream with respect to the time from the commencement of storm. It is an inverted U-shaped diagram. When a concentrated storm producing a uniform rainfall over a subbasin for duration of hours, the excess rainfall reaches the stream through overland and channel flows after the initial and infiltration losses are met. In the process of translation, a certain amount of storage is built up in the first phase of flows and gradually depletes after the

rainfall has ceased. The runoff measured at the stream gauging station gives a typical hydrograph, due to an isolated storm, which is known as the runoff hydrograph or storm hydrograph. **Fig.II.7**shows the hydrograph portraying the relationship between flow and the time. A hydrograph is very important to study flow characteristics and to determine peak flow and its time

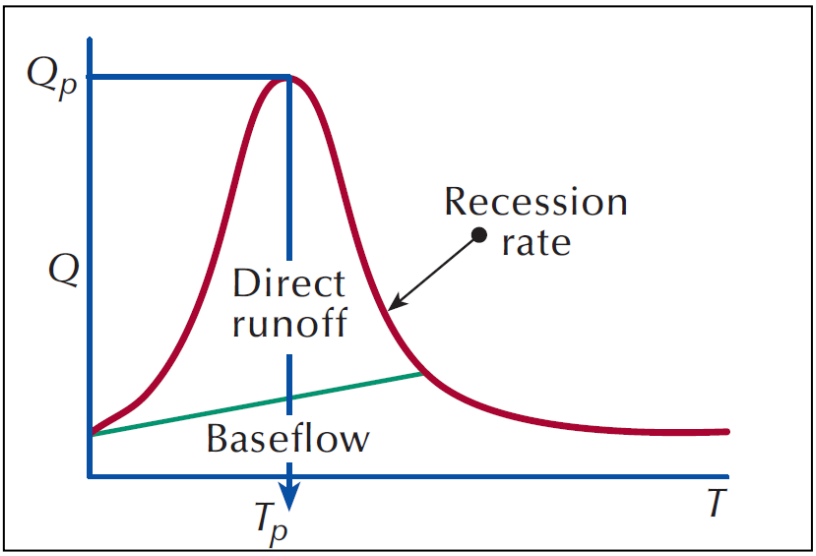


Figure II-7 Strom Hydrograph. ($Qp$: Peak flow. $Tp$: Peak flow time.)

- **Direct runoff:** is the rapid runoff and includes: channel precipitation, overland flow, and interflow.
- **Base flow:** is a slow and longer flow and includes: groundwater flow, dry weather flow, and the release of water stored in reservoirs and lakes.

Basically, a hydrograph shows you the ways in which a river is affected by a storm. This helps us to understand discharge patterns of a particular drainage basin and helps to predict flooding and plan flood prevention measures. Chow (1964) stated that hydrograph can be regarded as an integral expression of physiographic and climatic characteristics that govern the relation between the rainfall and runoff of a particular drainage basin. It shows the time distribution of runoff at the point of measurement, defining the complexities of the basin characteristics by a single empirical curve. Hydrograph generally contains the following three parts **Fig.II.8.**

- The rising limb gives an indication of how fast water is reaching the channel and represents the level of water rising in the channel. is the ascending curved portion of the hydrograph. The rising limb rises slowly in the early stage of the flood but more rapidly toward the end portion. The shape of rising limb depends on duration

and intensity distribution of rainfall. This is because in early stages the losses are more and water reaches to the stream faster the steeper the rising limb the more likely a flood is to occur; this is vital knowledge for flood forecasters.

- The falling limb shows the river as its level falls. Recession Limb represents the withdrawal of water from the storage built up during the early phase of hydrograph. It extends from the point of inflection at the end of the crest to the beginning of the natural groundwater flow. The shape of recession limb depends upon basin characteristics only and independent of the storm.

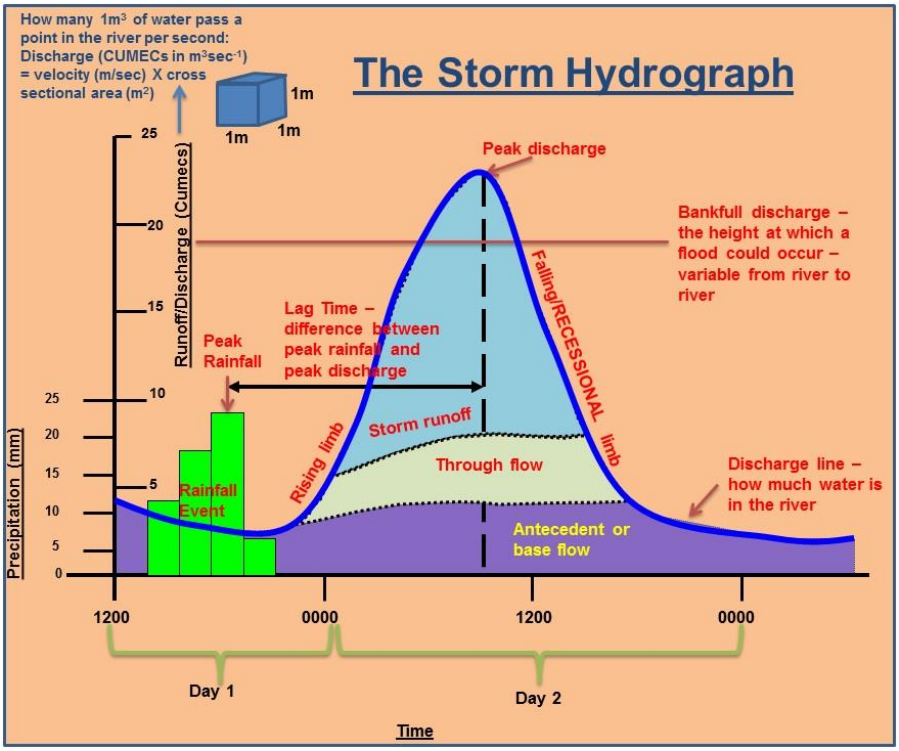


Figure II-8 parts of Hydrograph

- Peak discharge is the maximum amount of water in a river after a rainfall event; if this level surpasses the bank full discharge, then a flood will occur where the river overtops its banks.

- Peak segment **or Crest Segment** is shown by inverted U in the hydrograph. This is the part which is taken as matter of interest by hydrologists. Peak of hydrograph occurs when all parts of basins contribute at the outlet simultaneously at the maximum rate. Depending upon the rainfall-basin characteristics, the peak may be sharp, flat or may have several well-defined peaks. The last item indicated on the hydrograph is the lag time **Fig.II.9;** this is the amount of time between the peak

amount of rainfall and the peak discharge in the river. Generally, the less the lag time the quicker the river rises, the flashier the graph and the more likely a flood.

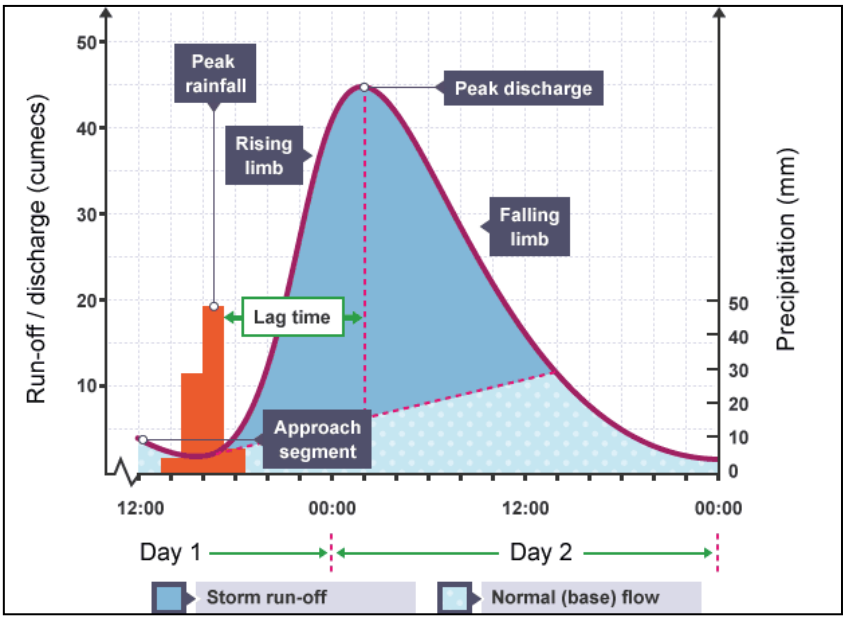


Figure II-9 Lag-time

Generally, a stage recorder is installed in the channel to obtain the hydrograph of the stream flow. When a rainstorm occurs, a part of it remains on the land surface after accounting for the initial abstraction and infiltration losses. This reaches the drainage channels or the stream through overland and channel flow of rainfall excess. The process of overland and channel flows of rainfall excess is known as translation. During the process of translation, storage is built up both in the overland and channel flow phases, and the storage gradually depletes after the rainfall stops. Thus, there is a time lag between the time of initiation of rainfall and the time when the rainfall excess reaches the outlet of the watershed, where the runoff is measured by a stage level recorder or by manually noting the stage of flow at different times.

Hydrographs depict changes in water flow or elevation as a function of time. They typically begin when flow levels increase above baseflow and end when the flow level returns to baseflow; baseflow is the regular streamflow, without contributions from rainfall events. Rainfall events are illustrated using hyetographs, which show precipitation depth as a function of time. **Fig.II.10** contains a generic hyetograph (plotted along a reversed y-axis) and hydrograph, broadly illustrating the relationship between precipitation and streamflow. Precipitation that falls within a watershed becomes infiltration and runoff, runoff travels downstream and

eventually arrive a stream, causing water levels to increase. The time interval between the start of the rising limb and the peak level is called the time to peak.

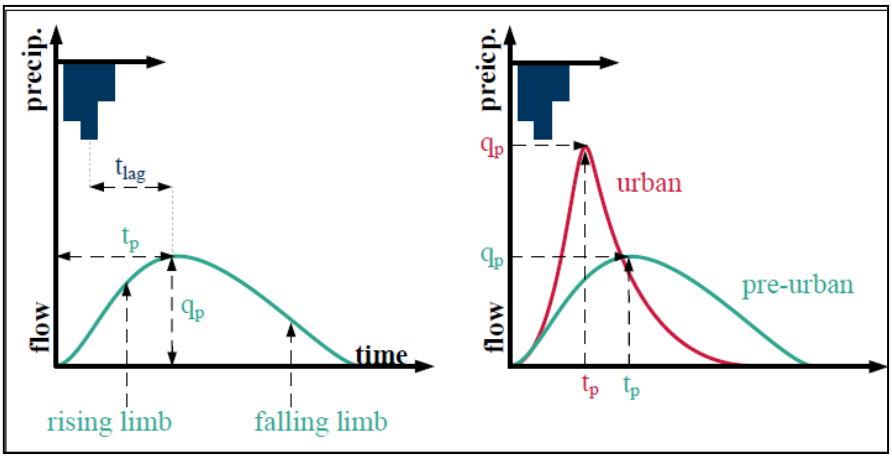


Figure II-10 Left: example of time lag (tlag), time to peak (tp), rising and falling limbs; right: comparison of hydrographs for urban and pre-urban watersheds.

The intensity of rainfall, the time of concentration of the watershed, the succession of storms, the groundwater recession pattern and similar other factors determine the peak of a hydrograph. A concentrated storm of rainfall over an isolated duration produces a single-peaked skewed-distributed hydrograph. In other cases when storm rainfalls are separated by short time intervals or when rain storms of varying intensities occur over an extended time period, multiple peaked hydrographs are likely to occur. A multiple peaked hydrograph **Fig.II.11**can be separated into a number of single peaked hydrograph, when required for analysis.

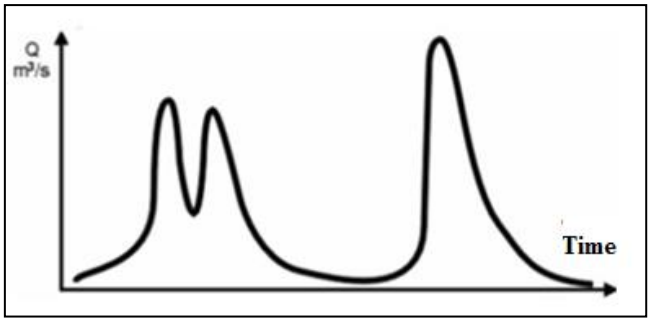


Figure II-11 A multiple peaked hydrograph

Depending upon the unit of time involved, the hydrographs are classified as:

- Annual hydrograph represents the variation of daily or weekly or daily mean flow over a year.

- Monthly Hydrograph Monthly hydrograph represents the variation of daily mean flows over a month.
- Seasonal Hydrograph Seasonal hydrograph represents the variation of the discharge in a particular season such as the monsoon season or dry season.
- Flood Hydrograph Flood hydrograph or simply hydrograph represents stream flow due to a storm over a catchment.

Each of these types has specific applications. Annual or seasonal hydrograph is used in calculating the surface water potential of stream, reservoir studies and drought studies. Whereas, flood hydrographs are essential in analyzing stream characteristics associated with floods. Many factors affect the rainfall-runoff process and also the runoff phenomenon

### *II.3.1 Factors Affecting the Storm Hydrograph*

The factors that affect the runoff are precipitation characteristics, antecedent moisture content, shape and size of the catchment, topography, geological characteristics, meteorological characteristics and the catchment surface and storage conditions. The rainfall is the most important factor that influences the runoff. Its characteristics such as intensity, duration and distribution according to time and space, and high intensity with long duration produce more runoff. Low intensity with light showers of rainfall lost through the process of evaporation and infiltration will lead to less runoff or no runoff.

The presence of moisture content of soil at the time of rainfall will also affect the runoff from the catchment. The soil pores completely filled with water produce high runoff than the dry soil. In the arid and semi-arid regions, moisture content in the soil pores is very less and has less impact on runoff.

The shape of the catchment controls the peak of runoff with travel time of water from the distant parts to its outlet. The fan shaped basin which has less drainage density and travel time produce high peaked low volume runoff compared to broad basin with high drainage density. Size of basin also affects the runoff. In small basin the travel time and exposure of water to atmosphere is very less and hence high runoff is produced. In large basin the channel flow is predominant over overland flow and hence it produces low runoff.

Slope of the catchment controls the velocity of flow and time of concentration of water. Steep slope influences the high velocity of flow and less time of concentration will produce more runoff than the gentle slope. High runoff rate in steep slope can be influenced by low infiltration rate and reduction in initial abstraction. Soil is the main component of watershed affecting the runoff. Among the various characteristics of soil, infiltration capacity plays an important role. Based on the type of soil the infiltration and runoff have a negative relationship with respect to time. A fine textured soil has low infiltration and high runoff compared to a coarse textured soil because of compact arrangement of soil particles. Also, the pore space between the particles is very less in fine textured soil. The coarse textured soil has granular structures and influence high infiltration and low runoff.

The type of land cover and land use on a particular location seriously affect the runoff of watershed. Among the several factors, this is a very causative factor due to its exhibited properties such as surface cover, type of crop, cropping pattern. Barren land produces more runoff than thick vegetation and dense forest cover. Improper usage of fallow land will produce surface sealing and reduce the storm water entering into the soil pores. Dense forest and thick vegetation will produce more foliage and organic matter in which the lives of the micro-organisms get increased. The presence of microorganisms can make the soil particles to have more pore space. In such a land the storm water can easily enter into the soil and produce less runoff. Thick vegetation can produce more transpiration loss through leaves and makes deficiency in the soil moisture. This process can influence more infiltration to replace the moisture deficiency. It also makes more barriers in the path of waterway over the surface of the land and slows down the water flow. Land covering with impervious material and the water body can prevent entering of storm water into the soil and produce more runoff.

### *II.3.2 Climatic Factors*

Heavy, sudden bursts of rainfalls leads to steep rising limbs and short lag times. Water is not given time to infiltrate thoroughly. This is why in deserts dried up rivers quickly replenish after a heavy storm (flash floods). Conversely, light rains favor gradual and thorough infiltration, hence less water reaches the river. This results in long lag times. But if rainfall continues for a long period, the ground may become completely saturated and water can flow as saturation overland flow, this is typical of tropical areas.

Among the climatic factors the intensity, duration and direction of storm movement are the three important ones affecting the shape of flood hydrograph. Intensity For a given duration, the peak and volume of the surface runoff are essentially proportional to the intensity of rainfall. The duration of storm for a given intensity also has a direct proportional effect on the volume of runoff. The effect of duration is reflected in the rising limb of the peak flow. If the storm moves from upstream of the catchment to the downstream end, there will be a quicker concentration of flow at the basin outlet. This results in a peaked hydrograph. Conversely, if the storm movement is up the catchment, the resulting hydrograph will be a lower peak and longer time base. The intensity of rainfall has a predominant effect on the shape of the hydrograph. If other conditions remain the same, a higher intensity storm will produce a rapid rise in the hydrograph and a higher peak than that in case of a low intensity rainfall. Such floods give little warning time and so are dangerous. In **Fig.II.12** the variation in intensity of rainfall changes the shape of hydrographs.

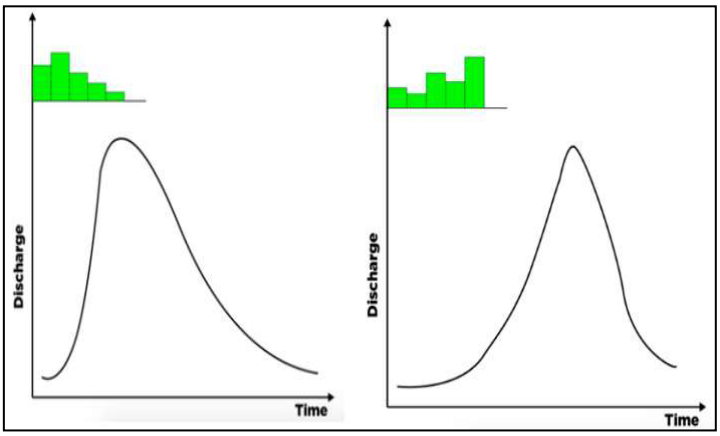


Figure II-12 Intensity of Rainfall

For larger storm the rainfall is distributed over a larger area due to which most of tributaries contribute to the stream discharge which results in the hydrograph with larger peak and vice versa. As we can see in **Fig.II.13** Storm A is smaller storm that's why it covered less area in graph while Storm B have relatively bigger Storm size then Storm A so it has cover large area.

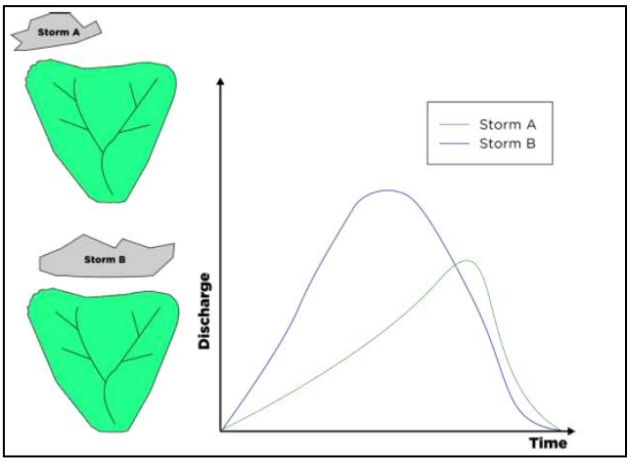


Figure II-13 storm size on surface runoff

### *II.3.3 Land Use*

Vegetation and forests increase the infiltration and storage capacities of the soils. Further they cause considerable retardance to the overland flow. Thus, vegetal cover reduces the peak flow. In general, for two catchments of equal area, other factors being identical, the peak discharge is higher for a catchment that has a lower density of forests cover. The effect of land use on hydrograph is shows in **Fig.II.14** Ice covered surfaces hinders infiltration and encourage high run-off rates leading to higher discharges and short lag times. Baked surfaces in arid regions prevent infiltration and encourage more runoff. The results are high peak discharges and short lag times. Vegetation can absorb and hinder surface runoff from reaching the river. In addition, densely vegetated areas in tropical regions can intercept rainwater and less water reaches the surface as runoff.

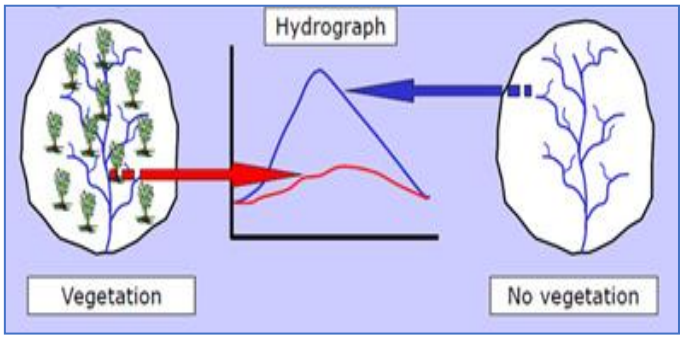


Figure II-14 Effect of land use on hydrograph (Source: http://www.lanarkgrammargeography.pbworks.com)

### *II.3.4 Slope*

Overland flow (run-off) is highest on steep slopes because infiltration is reduced, therefore water reaches the river fast (short lag time) and discharge is high. The slope of the main stream controls the velocity of flow in the channel. As the recession limb of the hydrograph represents the depletion of storage, the stream channel slope will have a pronounced effect on this part of the hydrograph. Large stream slopes give rise to quicker depletion of storage and hence result in steeper recession limb of hydrograph and smaller time base. The effect of channel slope is illustrated in **Fig.II.15**.

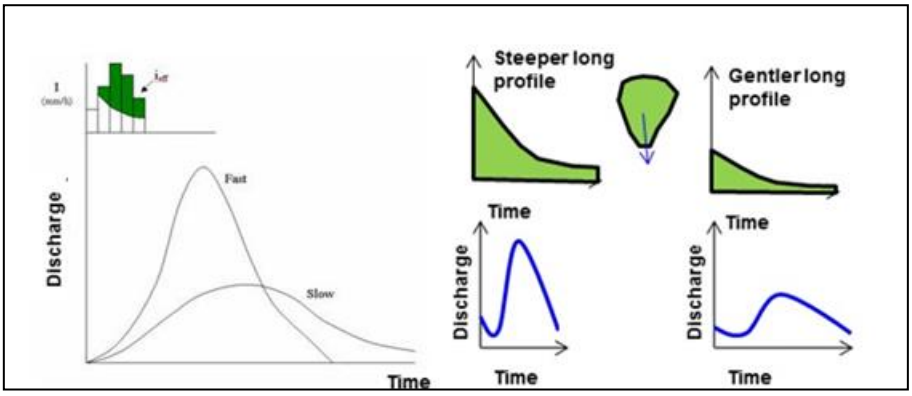


Figure II-15 The effect of channel slope on hydrograph (Source: https://www.daad.wb.tuharburg.de)

### *II.3.5 Basin Morphology, size and shape of the Basin*

Small circular catchments will have short lag times as runoff water quickly reaches the river. High elevated basins result in high runoff rates which shortens the lag time.

The effect of catchment shape on hydrograph is illustrated in **Fig.II.16.**

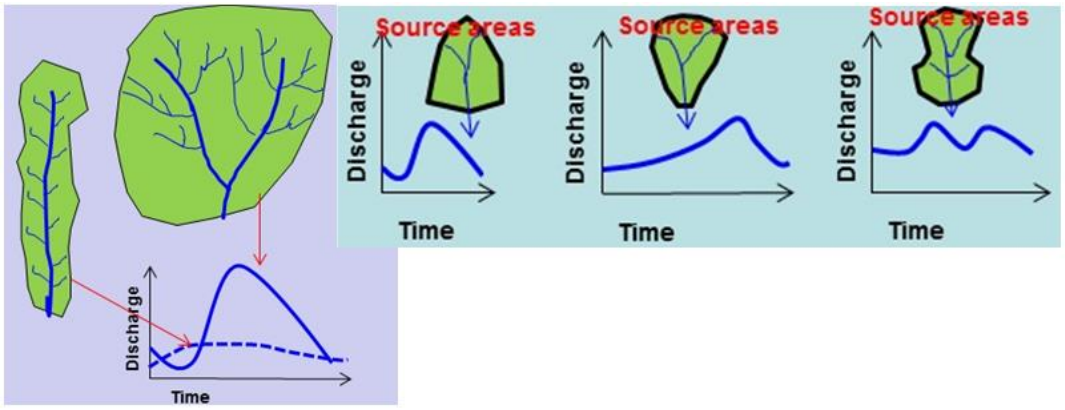


Figure II-16 Effect of catchment shape on hydrograph. Sources (Subramanya, 2008)

Small basins behave differently from large ones in terms of the relative importance of various phases of runoff phenomenon. Effect of basin size is illustrated in **Fig.II.17.**

In small basins the overland flow phase is predominant over the channel flow, whereas; in large basins channel flow is predominant. The peak is high in a large basin than in a small basin as peak discharge is found to vary as An, where A is the catchment area and n is an exponent, whose value is less than unity, being about 0.5. The base of hydrograph from larger basins will be larger than those of corresponding hydrographs from smaller basins.

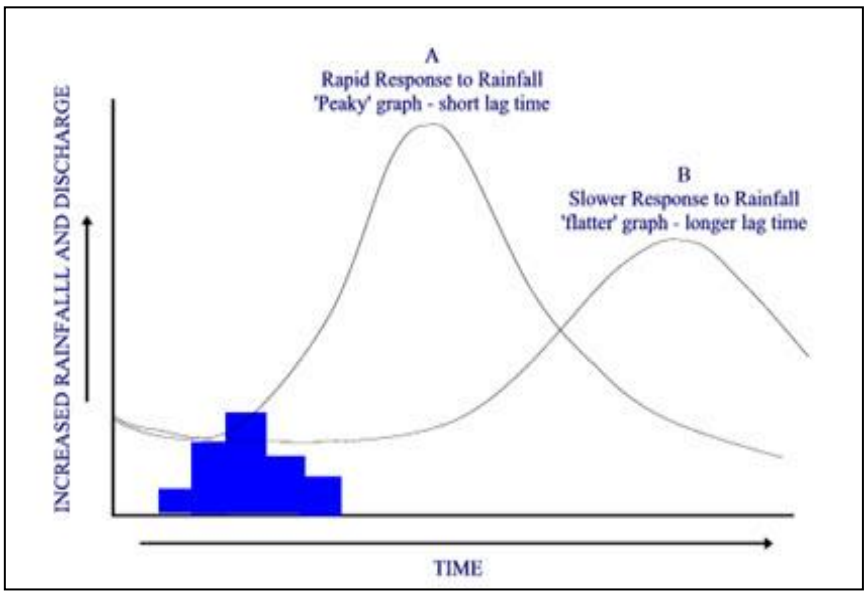


Figure II-17 Effect of basin size on hydrograph. (Sources: https://www.cgz.e2bn.net)

### *II.3.6 Drainage Density*

The drainage density is a measure of the total length of well-defined channels that drain the catchment (sometimes measured as the blue lines representing the streams on a topographic map). Drainage density is defined as the sum of the lengths of all of the channels (km) divided by the total catchment area (km2). This ratio can be determined from topographical maps. The effect of drainage density on hydrograph is illustrated in **Fig.II.18.** Drainage density affects the response of the catchment to rainfall. High densities usually allow fast runoff removal. Therefore, hydrographs having greater peaks and with shorter durations are expected for catchments with higher drainage densities. In catchment with smaller drainage densities, the overland flow is predominant and the resulting hydrograph is squat with a slowly rising limb. predominant and the resulting hydrograph is squat with a slowly rising limb.

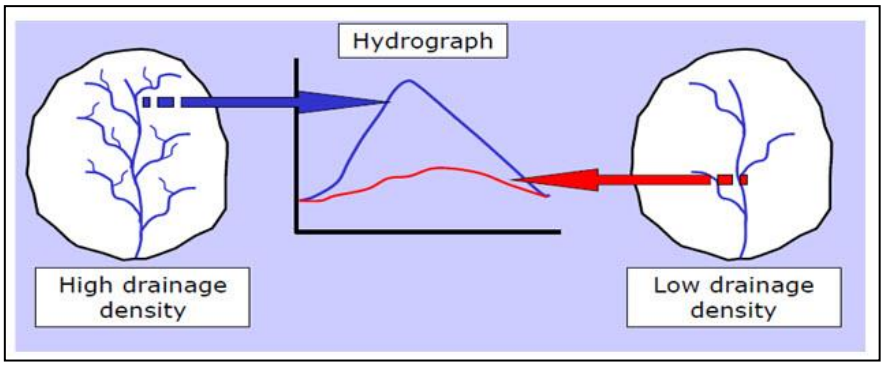


Figure II-18 Effect of drainage densities on hydrograph (Source: http://www.lanarkgrammargeography.pbworks.com )

### *II.3.7 The anthropogenic effects*

Human activities significantly influence runoff generation in urban catchments. As a result, they have gained a great deal of attention in the past few years (Wang et al., 2015). Urbanization is the most significant aspect of anthropogenic impacts in urban areas, affecting surface runoff. Field data has also been used by some studies to investigate the hydrological effects of urbanization (Boggs & Sun, 2011; Meierdiercks et al., 2017; Katherine L. Meierdiercks et al., 2010; Katherine L Meierdiercks et al., 2010) The large population growth in urban areas and their potential activities has brought about significant alterations in the natural hydrological processes in urban areas. The urban runoff can severely be affected by urbanization and land use change. The more the surface cover is sealed, the more runoff will be generated. The impermeable surface cover leads to both higher peaks and larger volume of runoff in urban catchments. In addition, more surface runoff and higher peak discharge is generated by urbanization in a shorter course of time because when impervious surface increases, the infiltration and the time of concentration will decrease (Cuo et al., 2008) This excess runoff from urban areas is widely considered as a threat to both human and aquatic ecosystems.

Rezaei et al. (2019) reviewed and investigated various and the most effective factors influencing urban runoff generation. They reported that the main reason for many alterations in the natural hydrological processes in urban areas is population growth and the pertinent human activities, changing the natural features of urban catchments. This population growth, along with the migration of people from rural areas to mega cities, has led to the vast development of urban areas. As a result, natural pervious surfaces have been modified into a wide range of sealed surfaces, such as paved roads, parking lots and roofs that typically clear the vegetation and compact the soil. This process is broadly known as urbanization which greatly affects urban catchments. Therefore, urbanization usually results in the modification of natural

landscapes; and eventually vegetated surfaces are replaced with impermeable surfaces. The main results of urbanization are:

- increase of road surface areas;
- reduction of drainage capacity;
- channelization and engineered water exchanges, especially among major surface waters; as land modification for agriculture.

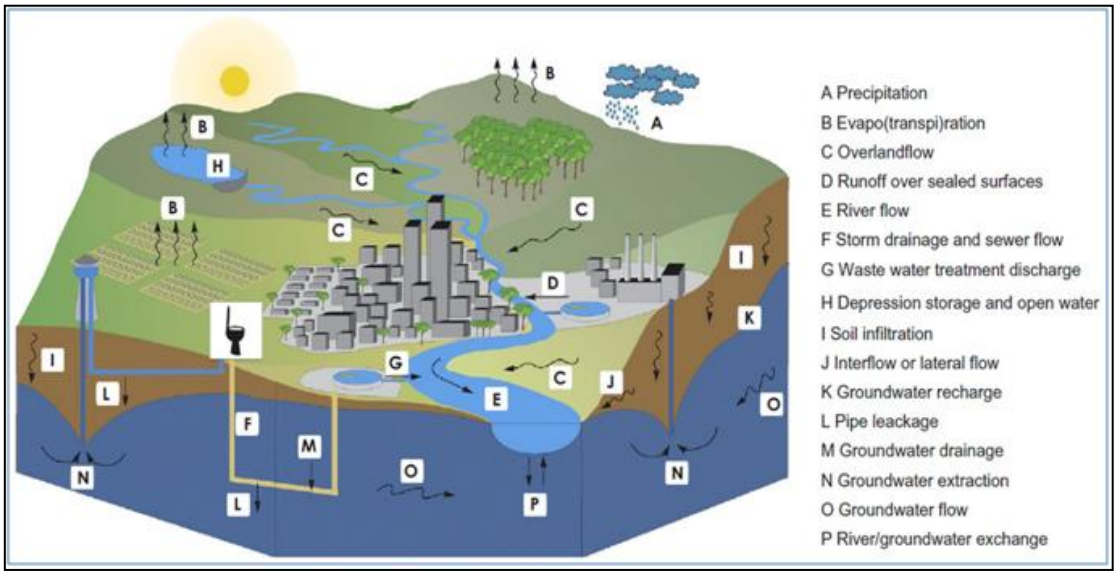


Figure II-19 Water cycle in an urban catchment which is not typically homogeneous and undergoes different physical phenomenon and interactions (Salvadore et al., 2015)

The most significant difference between urban and non-urban catchments is related to sealed surfaces versus vegetated areas. An urban catchment consists of a heterogeneous mixture of natural and artificial surface coverage. It should also be noted that the natural and artificial processes interact with each other in urban catchments **Fig.II.19.**

So far, land use/ land cover, urbanization, soil characteristics, slope, topography, and precipitation characteristics have been the focus of a great deal of research, investigating urban runoff. One main factor influencing the surface runoff and hydrological processes in urban catchments is urbanization. The main factor leading to hydrological changes in urban areas is the catchment imperviousness which directly affects the runoff. Urbanization decreases the natural temporal and spatial scale of runoff process because urban surfaces are usually spatially heterogeneous and also because urbanization reduces the catchment response time to precipitation (Salvadore et al., 2015).

# Urban Runoff process

# III Urban Runoff Process

## III.1 Introduction

The population growth and their displacement from the rural or countryside encouraged the increasing of urbanization. It is envisaged that urban areas will receive the total growth of future world population. The global population is expected to reach 8.5 billion in 2030, 9.7 billion in 2050 and 10.9 billion in 2100, see **Fig.III.1**, Rapid urban growth poses a huge challenge for implementing a smart urban development agenda that strive for make cities and human settlements inclusive, safe, resilient and sustainable (DESA, 2019). In the other, side the concept of natural water cycle which is defined as estimation of water quantity storage and circulation between the biosphere, atmosphere, lithosphere and hydrosphere. This water can be stored in the atmosphere, oceans, lakes, rivers, streams, soils, glaciers, snowfields and groundwater aquifers.

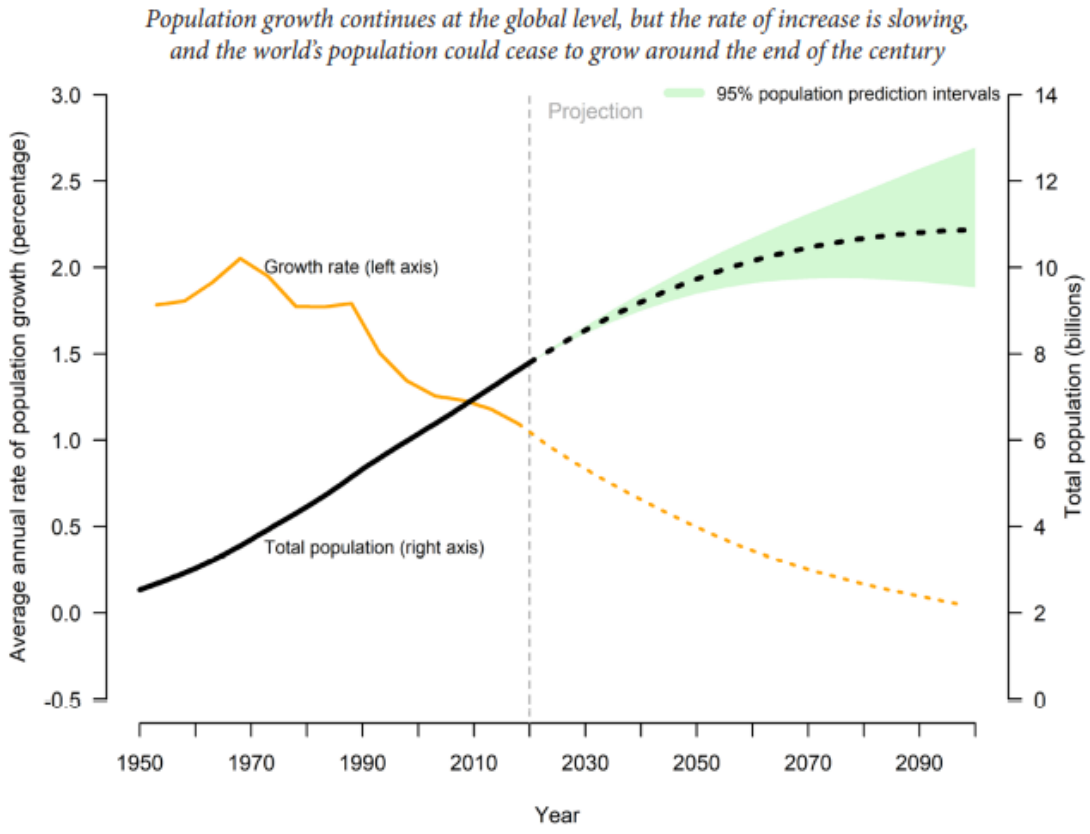


Figure III-1 Population size and annual growth rate for the world: estimates, 1950-2020, and medium-variant projection with 95 percent prediction intervals, 2020-2100. *source (DESA, 2019)*

Its circulation among these storage compartments is caused by such processes as evapotranspiration[3], condensation, precipitation, infiltration, percolation, snowmelt and runoff, which are also referred to as the water cycle components **Fig.III.2**. The Population growth, industry evolution, and the apparent urbanism affect the natural landscape cover, and thus the response of watershed (Marsalek et al., 2008). The urban catchment is the one in which the impervious surface cover a considerable areas (SCS, 1986). Impervious surfaces include the roads, sidewalks, parking lots, and buildings. Therefore, the natural watercourse can be deviated or replaced by the artificial channels. The process of rapid urbanization has a dramatic effect on catchment hydrology leading to increased runoff rates and volumes, decreased of infiltration process and subsurface flow, and speeding up the concentration time. Urbanization can have severe implications for the hydrologic functioning, or magnitude, and frequency of floods(Lazaro, 1990), and floodplains, see **Fig.III.3.**

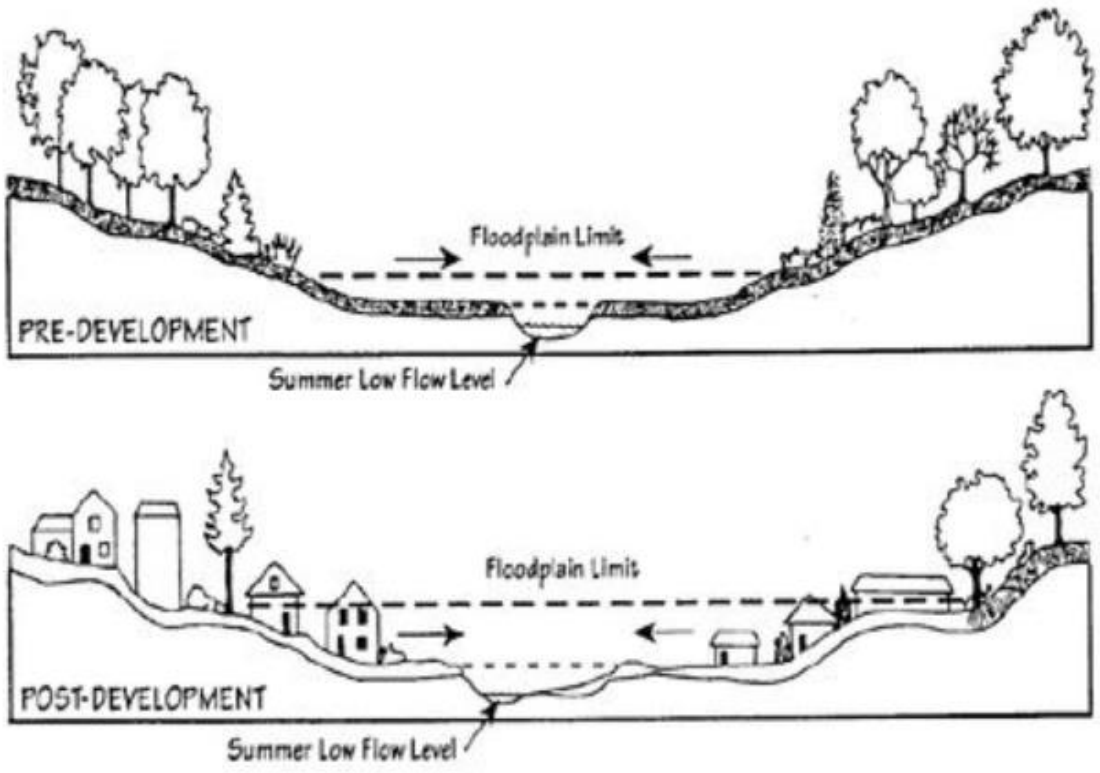


Figure III-2 Floodplains limits in pre-development (the natural status and post development), and post-development, *Source (Ramachandra & Mujumdar, 2009)*

[3] Some prefer to retain use of the term evapotranspiration which combines evaporation from free water and transpiration from plants. Transpiration is a physiologic process involving the activity of plant stomata mediating the release of plant water as vapor. The end point of transpiration is still evaporation Oke, T. R., Mills, G., Christen, A., & Voogt, J. A. (2017). *Urban climates*. Cambridge University Press. .

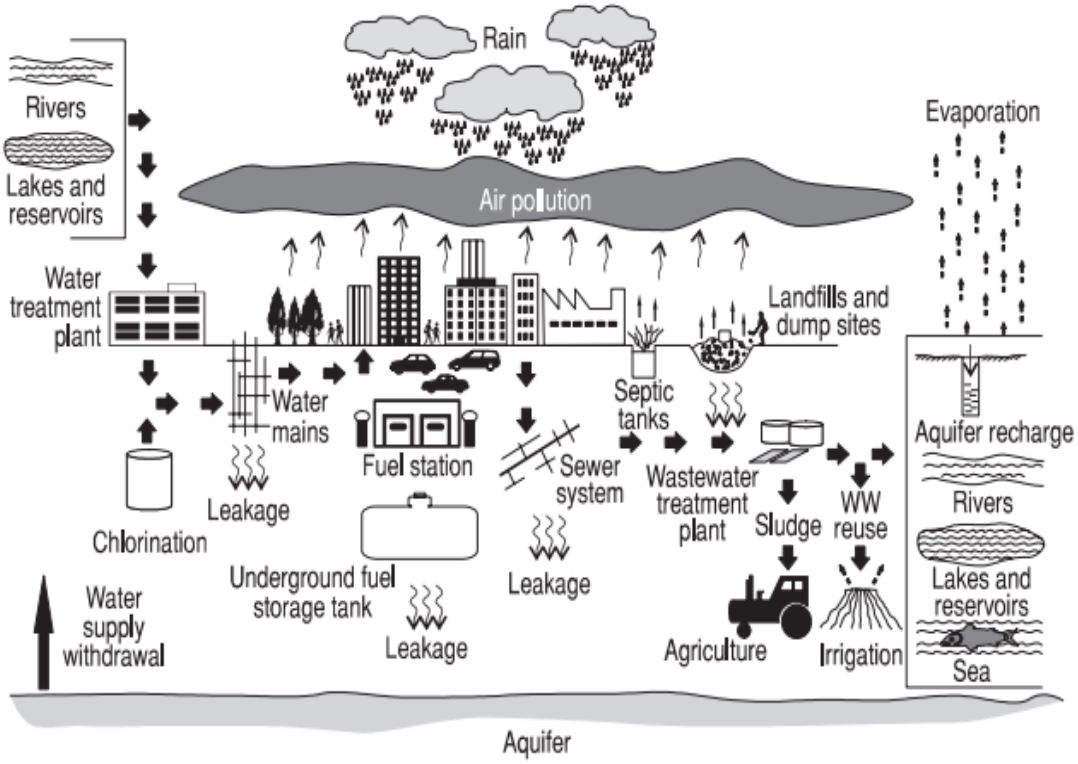


Figure III-3 Urban water cycle, source (Marsalek et al., 2008)

## III.2 Urbanization Growth

In recent decades, the world has been urbanizing rapidly. In 1950, only 30 per cent of the world's population lived in urban areas, a proportion that grew to 55 per cent by 2018. The global urbanization rate masks important differences in urbanization levels across geographic regions. Northern America is the most urbanized region, with 82 per cent of its population residing in urban areas, whereas Asia is approximately 50 per cent urban, and Africa remains mostly rural with 43 per cent of its population living in urban areas in 2018 (United Nations, 2019). A regional variation in levels of urbanization raises the question of whether some regions urbanize faster or slower. To address this question, the following analysis compares the increase in the percentage urban in several less developed regions between 1950 and 2015 with historical trends of urbanization in the more developed regions. Since pace and level of urbanization are related, the analysis across regions compares the speed of urbanization at equal levels of the percentage urban.

**Fig.III.4** presents changes in the percentage urban across several regions or subregions of the world. The black line refers to urbanization in the more developed regions between 1800 and 2015 and serves as a base line for the comparison. The black line shows an S-shaped profile,

indicating that the rise in the percentage urban was relatively slow at low levels of urbanization, before accelerating at medium levels and then falling again at elevated levels of urbanization.

For the sake of comparison, trends in urbanization for less developed regions start in each case with the percentage urban in 1950, which is plotted at the point along the black line when the more developed regions experienced the same percentage of population living in urban areas. In cases where the subsequent trajectory of a region lies above the black line, the pace of urbanization, starting from an equal level of urbanization, was relatively more rapid in that region, albeit at later date. Conversely, if the trajectory of a region lies below the black line, the speed of urbanization was lower in that region compared to the historical experience of the more developed regions. The speed of urbanization in sub-Saharan Africa between 1950 and 2015, for example, represented by the blue line, was higher than for the more developed regions between 1850 and 1915, represented by the black line. In 1950, the percentage urban in sub-Saharan Africa was about 11 per cent, equal to the urbanization level of the more developed regions in 1850. Over the following 65 years, the percentage urban rose more rapidly in sub-Saharan Africa, reaching 39 per cent in 2015, while the more developed regions reached a percentage urban of only 34 per cent in 1915. The pace of urbanization in other less developed regions can be compared with that of the more developed regions in similar terms (**Fig.III.5).**

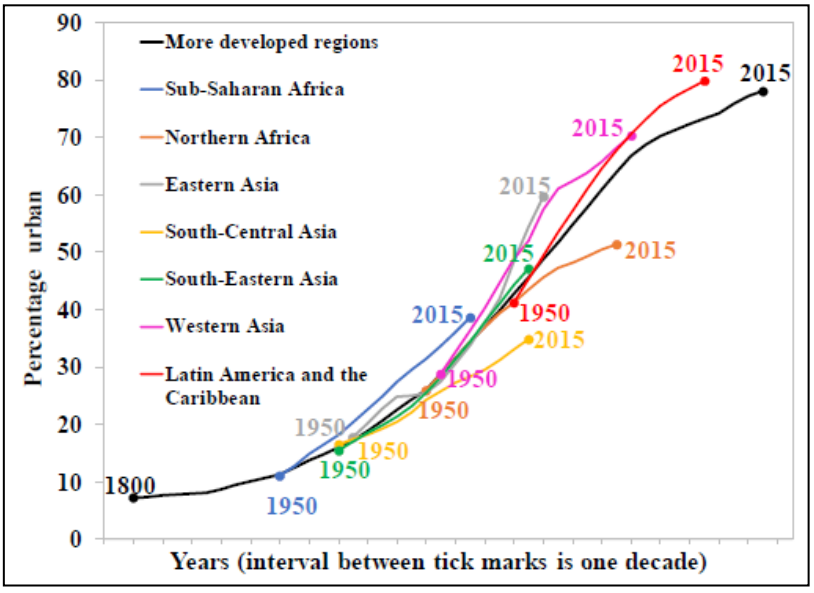


Figure III-4 Levels and trends of urbanization in selected regions (United Nations, 2019)

The speed of urbanization also varies substantially across countries. **Fig.III.5** illustrates the diversity in the pace of urbanization for some populous countries located in the regions

considered here. Starting at almost identical levels in 1950, trajectories of urbanization have been very similar for China and Indonesia. In contrast, despite having comparable levels in 1950, Brazil and Egypt followed very different trajectories thereafter, with Brazil experiencing rapid urbanization while the trend in Egypt has been flat since the 1970s, a reflection of the official definition of cities not accounting for the recent urbanization of rural settlements.

Due to a slow process of reclassification of rural areas as urban, urbanization in India has progressed more slowly compared to other countries at similar levels of the percentage urban. In contrast, starting from a very low level of urbanization in 1950, Ethiopia has undergone relatively rapid urbanization compared both to the historical experience of the more developed regions and to other developing countries at similar levels of urbanization

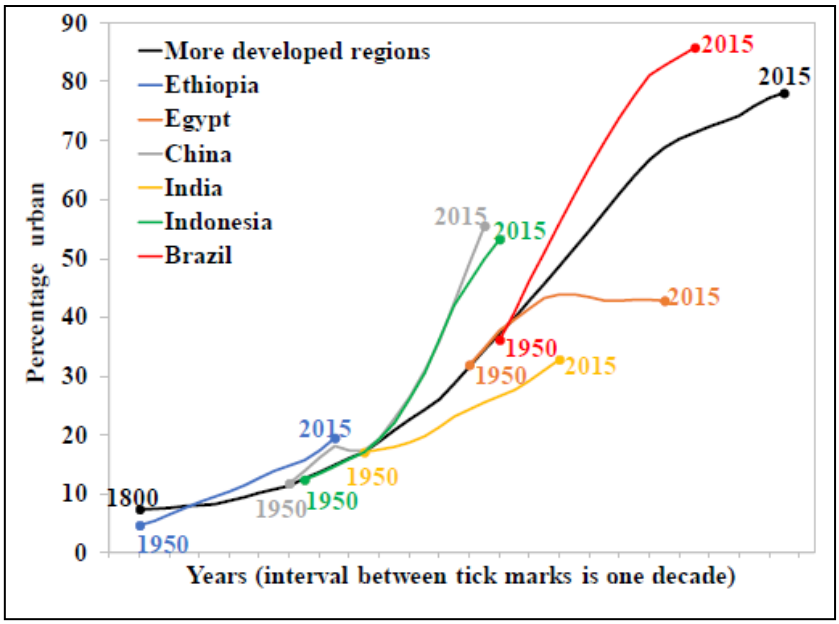


Figure III-5 Levels and trends of urbanization in selected countries

The Algerian population expanded from about 11.3 million in 1960 to almost 43 million in 2019, quadrupling in 50 years. This statistic (**Fig.III.6**) shows the degree of urbanization in Algeria from 2010 to 2020. Urbanization means the share of urban population in the total population of a country. In 2020, 73.73 percent of Algeria's total population lived in urban areas and cities.

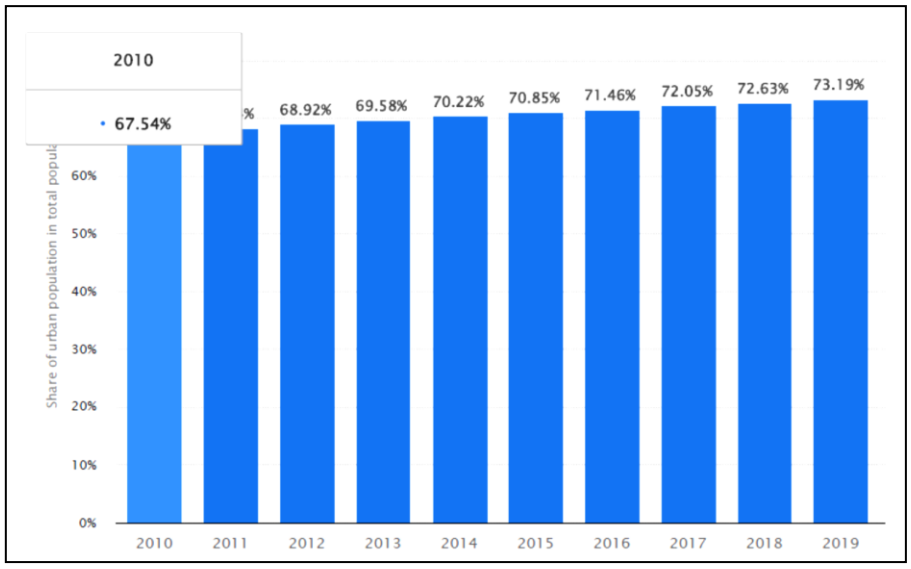


Figure III-6 degree of urbanization in Algeria from 2010 to 2019

As presented in **Table.III.1** the current population of Algeria is **45,099,898** based on projections of the latest United Nations data. The UN estimates the July 1, 2022 population at **45,350,148**. Algeria is currently growing at a rate of 1.85% per year, a rate that adds over 800,000 people to the population every year. This rate will gradually slow down towards the end of the century.

Table III-1 Population and Density growth in Algeria from 1955 to 2022

| Year | Population | Density (km²) | Year | Population | Density (km²) |
|---|---|---|---|---|---|
| **2022** | 45,350,148 | 19.04 | **2000** | 31,042,235 | 13.03 |
| **2021** | 44,616,624 | 18.73 | **1995** | 28,757,785 | 12.07 |
| **2020** | 43,851,044 | 18.41 | **1990** | 25,758,869 | 10.82 |
| **2019** | 43,053,054 | 18.08 | **1985** | 22,431,502 | 9.42 |
| **2018** | 42,228,408 | 17.73 | **1980** | 19,221,665 | 8.07 |
| **2017** | 41,389,189 | 17.38 | **1975** | 16,607,707 | 6.97 |
| **2015** | 39,728,025 | 16.68 | **1970** | 14,464,985 | 6.07 |
| **2010** | 35,977,455 | 15.11 | **1965** | 12,550,885 | 5.27 |
| **2005** | 33,149,724 | 13.92 | **1960** | 11,057,863 | 4.64 |

A disproportionate spatial redistribution has resulted in this demographic development. The population of the coastal areas and valleys is focused on the cities. In 2018, 90% of the population is located on 13% of the country's area. The urbanization rate went from 30.5% in 1960 to 72% in 2019 (**Fig.III.7).**

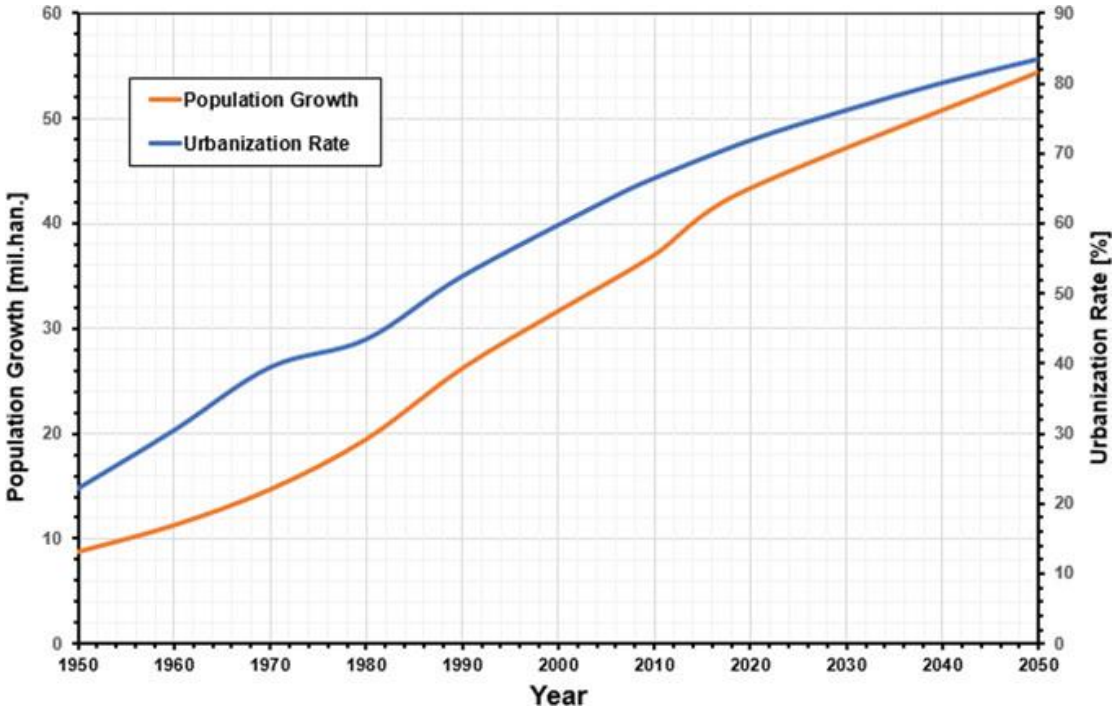


Figure III-7 Population growth and changes in urbanization rate (source (Boutaghane et al., 2022)

## III.3 What is an Urban Watershed UW?

In the literature there is no agreed definition of the term "urban watershed (UW)", this term is come out in the context of description of the existence of totally or partially impervious covers that result in general from urban expansion. To start with, there is some question that come to mind. For example, how large does the degree of human agglomerations inside a catchment must be? Should an urban catchment be defined on the basis of the percentage of buildings areas and industries that cover their surface, or there is another criterion must be taken into consideration? (Salvadore et al., 2015). Many authors have used in their studies a drainage basin with a certain percentage of impervious cover as a threshold for watershed classification. However, the rate of Impervious area differs from case to case, some researchers described their studied basins by an UW as they contain a little percentage of Impervious surface. Zhou et al. (2010) considered that two studied watersheds are an UWs because it contains only 5% and 10% respectively of those areas that are urbanized. In another study of four catchment, the percentage of Imperviousness reached the 97.9% (Tsihrintzis & Hamid, 1998). Even it was highly urbanized, there are some considerations that need to be taken into account, the first one is errors that result from misclassification of the land cover, and the used methodologies, the source of the used map, the resolution of the satellite, and the algorithms of classification. In other hand distribution form the impervious cover over the catchment, the building and the density of population over the catchment, the integration of trees and greenness around the

urban areas, the position of this area relative to the total surface of catchment, etc., to better understanding the catchment inherent, a preliminary and detailed assessment must be performed.

## III.4 Urban Runoff Process

Since the natural drainage basin differ from those that cover the urban areas, nevertheless the drainage in both is totally different. The urban hydrology is not much different from natural hydrology except for the interaction with the new water components in the urban system, which makes the significance and complications, especially for the developed and undeveloped agriculture land that crossing the urban watershed boundaries (Fletcher et al., 2013). Although the fact that the surface runoff become more severe within the surfaces that are experiencing increasing of impervious rates i.e., in urban areas; therefore, the relationship between surface runoff and impervious surface is variable and depends on the manner in which the impermeable areas is distributed over the watershed, particularly how the urbanization pattern is designed along the main channel (Dow & DeWalle, 2000; Grove et al., 1998; Sheeder et al., 2002).

### *III.4.1 Precipitation*

Precipitation is affected by the regional weather and climate; it has been suggested that urban areas modify the processes of cloud development, atmospheric electricity and precipitation (Oke et al., 2017). The condensation nuclei[4], which is responsible to water vapor into droplets, whose occurrence is related to air pollution. The large urban areas affect the local rainfall, as a consequence of change in energy regime, air pollution and air circulation patterns, which are caused by buildings, land transformations and release of greenhouse gases. These factors contributes modification in radiation balance and therefore the evaporation and precipitation amounts (Marsalek et al., 2008). It had been proven by Geiger et al. (1987) cited in (Marsalek et al., 2008) that precipitation in urban and large industrialized areas is much higher by 5 to 10% that in the adjacent areas , and particularly for the big storms precipitation can rising 30% in large urban cities, improving that the precipitation in the direction of wind. Temperature also is a phenomenon of interest, as it controlled the precipitation form (solid, or liquid), It is

[4] **Condensation nucleus/nuclei**, tiny suspended particle, either solid or liquid, upon which water vapor condensation begins in the atmosphere. Most condensation nuclei are produced by natural and man-made fires over land and by wave action over the oceans. When mixed with the more hygroscopic material, dust and soil particles blown into the atmosphere also are sources of nuclei. Britannica. (1 May 2017). *condensation nucleus*. Encyclopedia Britannica. https://www.britannica.com/science/condensation-nucleus

known that temperatures of urban cities is superior than that of natural places by approximately 4 to 6°C (Geiger et al., 1987; Marsalek et al., 2008).

### *III.4.2 Infiltration*

Imperviousness affect considerably the infiltration capacity and hydraulic efficiency. The rate of infiltration affected by a set of drivers (Jacobson, 2011). Soil compaction in urban development and construction activities decreases the infiltration rate 70 to 99% (Gregory et al., 2006). The slope angle had little or no effect on the characteristics of the surface seal[5], and the influence of the slope angle on the infiltration rate occurred primarily through its influence on the depth of surface flow (Fox et al., 1997). The infiltration rate influenced also by rainfall intensity, vegetation cover, soil saturation, soil type and porosity (Dunne et al., 1991). As illustrated in **Fig.III.4**, the infiltration rate is 50%, 40% evaporates and/or transpired (Evapotranspiration[1]) from the plants, and only 10 % is flow over surface land. Rising of buildings and construction in developed areas prevent water to hack these surfaces. instead, it is forced to runoff as overland flow and evaporates. The amount of impermeable surface within the catchment determines the extent of the change in runoff. For 10 to 20% of imperviousness (medium residential area) runoff is twice and infiltration is reduced. For 35 to 50% (high-density residential) impervious cover runoff is threefold, in industrial and commercial areas the imperviousness reaching 75 to 100% and runoff up to beyond 50%. The majority of rainfall become runoff. Evaporation becomes third of what it was prior to development (Federal Interagency Stream Restoration Working, 1998).

### *III.4.3 Depression Storage*

Paved roads and large areas definitely eliminate the storage in depressions, and restrict the ability of surface land to store and retain water, this water which is stored in cracks, grooves and pits, that is an important quantity that does not involved in surface runoff (Barnes et al., 2001). A study conducted in American Chicago (case study) indicated that the storage in depressions in impervious areas is four times greater than that in natural or pervious regions (Vladimir & Gordon, 1981). The water stored in natural areas penetrate to first layers of the earth's land while in impervious area the little stored water in irregularities evaporate quickly

[5] **Surface sealing** is a physical and physico-chemical process of aggregate breakdown and/or coalescence and subsequent compaction and/or deposition under conditions of rapid wetting or raindrop impact Fox, D., Bryan, R., & Price, A. (1997). The influence of slope angle on final infiltration rate for interrill conditions. *Geoderma*, *80*(1-2), 181-194.

(Barnes et al., 2001; Douglas, 1983), given that paved and urban lands is much warmer, and city temperatures that are ty1pically a few degrees higher than in the surrounding countryside (Ward & Grimmond, 2017).

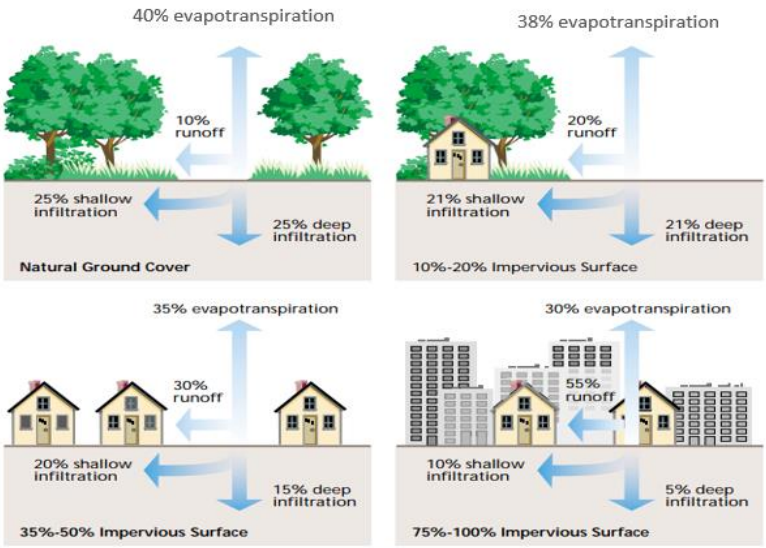


Figure III-8 Influence of urbanization on different water components, for natural ground cover the runoff is only 10%, for 50% of imperviousness, 30% of water runs and 20 infiltrates. *Source (Federal Interagency Stream Restoration Working, 1998)*

### *III.4.4 Urban Drainage system*

Cities seek a reliable supply of water of sufficient quality to meet consumption requirements; They also seek to remove excess water and wastes to reduce the possibility of flooding and reduce water pollution. There is a need to prompt construction of urban drainage system to avoid flooding and relocate quickly to natural stream network or wadis and other suitable detention storage. Therefore, the natural watercourses are modified by amplifying and straightening to face dash that followed a rainstorm or a sudden snowmelt (Oke et al., 2017). Several attempts have been made to demonstrate changes that occurred in natural stream (Hammer, 1972). Urbanization changes fluvial morphology and processes, and it pass through three stages, each of them influences the natural stream, ass follow:

- Pre-urbanization, where the land surface is naturally vegetated and cultivated, instinct with forests and herbaceous areas.
- A period of construction and building, that generate erosion, the high amount of erosion disequilibrate the channels status.

- New urban landscape, that consists of an important rate of imperviousness, sediment yielding is decrease, the channels remain in their disequilibrium status that either respond to the new changed environment or not.

Ladson et al. (2006) assumed that the directly connected impermeable surfaces to urban stream has a damaging effect on stream health, they indicated that the less direct connection of impervious surfaces to stream may be mitigated the damage to its health, thus, they are suggested some alternative solutions to reduce the quantity of rainfall, include collecting water in a tank that used later in water supply for residentials, penetrable asphalts that diminish overflow from streets; and swale channels and bioretention frameworks along streets, rather than channeled waste direct to streams. Gupta (1982) summarized the changes that occurred in the nature and behavior of natural stream as a result of urbanization process in their catchments, that are shown in **Table.III.2**.

Table III-2 changes in nature and behavior of natural streams by virtue of urbanizing prosses of watershed, *adopted by (Gupta, 1982)*

| A. Hydrological changes | B. Sedimentological changes | C. Morphological changes |
|---|---|---|
| • **Changes in flow-duration**<br>• modification of flow-duration curve-lower baseflows, larger and quicker floods<br>• **Changes in flood frequency**<br>• increase in the frequency of floods of a given size<br>• increase in the size of a given flood,e.g. mean annual flood<br>• **Modification of runoff from individual storms**<br>• decrease in lag-time between rainfall and stream flow<br>• increase in the size of flood peaks<br>• increase in peak velocity<br>• **Changes in water quality** | • Deposition of relatively coarse textured sediment in the channel in the early stages of urbanization followed by a reduction in the amount of sediment arriving. Creation of bars, sand dunes and tributary-mouth fans. | • Changes in channel size, width, depth and associated depositional forms |

There are two commonly used urban drainage system, the first uses a separated drainage network for drinking water, a storm sewer for surface runoff, and sanitary sewers for wastewater. The alternative is cities that have a combined sewer system that collect both stormwater and wastewater in a single network. This latter is capable to route the little quantities of rain, but during the heavy rainstorms the water passes into the natural channels without treatment. Even

for some cities in undeveloped areas, there is no relief channels, therefore the stormwater overflowing, deteriorates the infrastructures, and thrusting solid and

suspended soils. We may also mention that an important quantity of water lost through leaks from channels of water transportation that increases soil moisture, and some water may penetrate to deeper layers. Pizzuto et al. (2000) speculated that the sediment supply from hillslopes to urban drainage streams and channels erosion is significant and it cannot be neglected even that the watershed urban uplands is covered by nonerodable materials.

### *III.4.5 Urban hydrograph*

It is mentioned that the urban development's affect directly the streamflow. The volume of runoff generated in urban areas after a storm event is much greater, decrease of time before water join gutters, drains, canals, and streams. Furthermore, the water infiltrate in surface and subsurface is diminished thereby the subsurface runoff is declining. All of those clearly appear in the engendered storm hydrograph. The rising and falling limbs of the storm hydrograph is steeper in the urban hydrograph **Fig.III.5,6** this is most likely due to the accelerated overland flow in the impermeable areas that characterized by a relatively smoother surface e.g., roofs, roads, paved areas, surface roughness is lowered that exhibits a quick response of the watershed. To the contrary of rural areas where the flow crossing the natural land and pass through the vegetation, herbaceous, and grassy land (Oke et al., 2017).

Several attempts have been made to addressing the increase of runoff volume, and peak by effect of urbanization. As illustrated in **Fig.III.5,6**. Shanableh et al. (2018) found that, the minimum precipitation required to generate runoff decreased by around 30% (from about 15 mm in 1976 to about 10 mm in 2016) in built areas, in their study conducted to Sharjah United Arab Emirates. Recent research implemented by Pabi et al. (2021) simulates peak runoff and water flow rate to land use/land cover, and scenarios of rainfall intensity of different durations and return periods in an urban flood-prone Odaw River catchment of Accra, Ghana. In this study the peak flow estimated per unit area of each land cover type, they were concluded that because of urbanization which extended from 40% in 2000 to 65% in 2020, the peak flow increases 3.6 times for built-up areas.

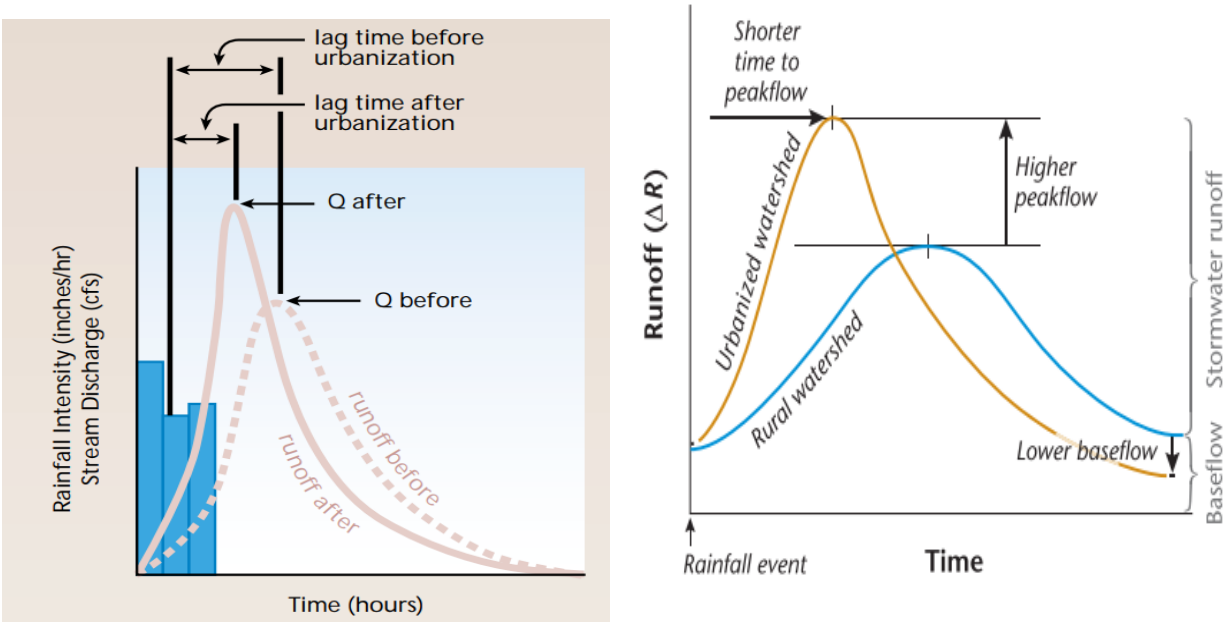


Figure III-9 Comparison of hydrographs before and after urbanization. The discharge curve is higher and steeper for urban streams than for natural streams. *Source (Federal Interagency Stream Restoration Working, 1998)*

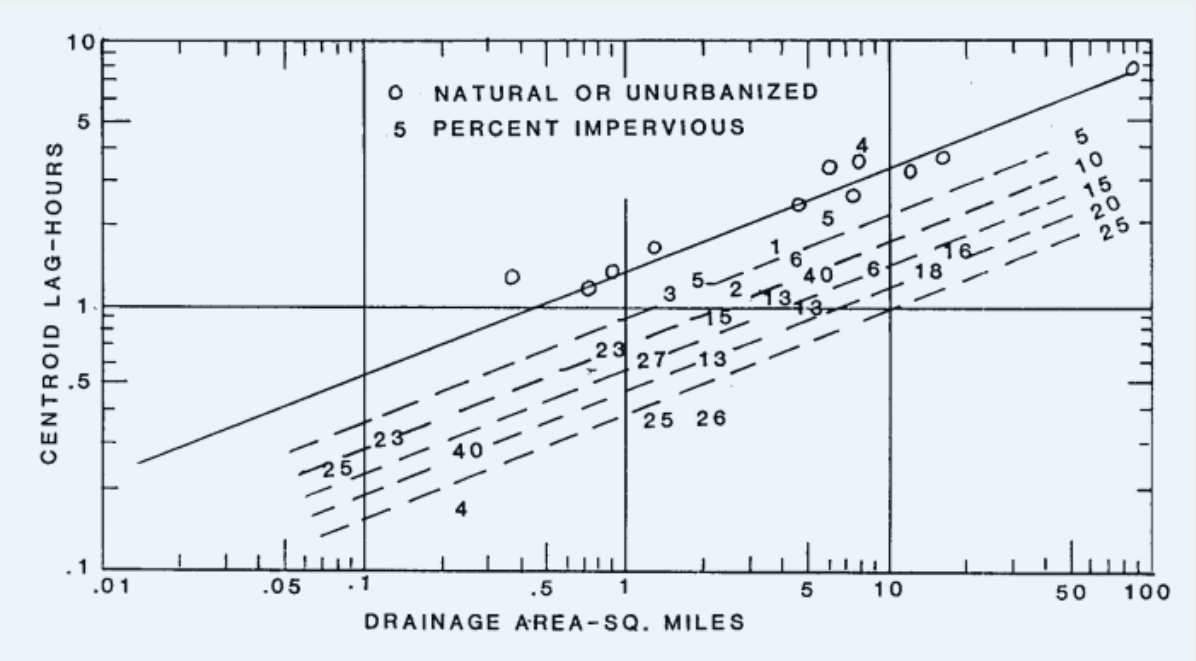


Figure III-10 lag time in hours in function of drainage area. The position of each plotted point is designated by the estimated percentage impervious area. A series of parallel lines on the graph represent various values of percent impervious are, *source (Leopold, 1991). The data is collected by Leopold (1991)*

The **Fig.III.5**,and **Fig.III.6** demonstrate that the lag time[6] is likely to altered by urbanization, lag time is an comprehensive measure of the celerity of rainfall to appear downstream as a runoff hydrograph, in that context lag time is a mirror that reflect the velocity and shortage of rainwater on its way over the watershed towards the downstream (Leopold, 1991). It is found that the relationship between the lag time and the urbanized catchment is constant and simple, even introducing of slope and length, that did not affect this relationship (Richards, 1980). Leopold (1991) developed a method to compute the effect of urbanization on storm hydrograph by using a synthetic unit hydrograph computed from lag time of the basin, the idea is to develop a synthetic hydrograph for existing conditions that checks or agrees with an observed hydrograph. Then using the same volume of runoff and a different lag time to compute another synthetic hydrograph that representing the changed condition.

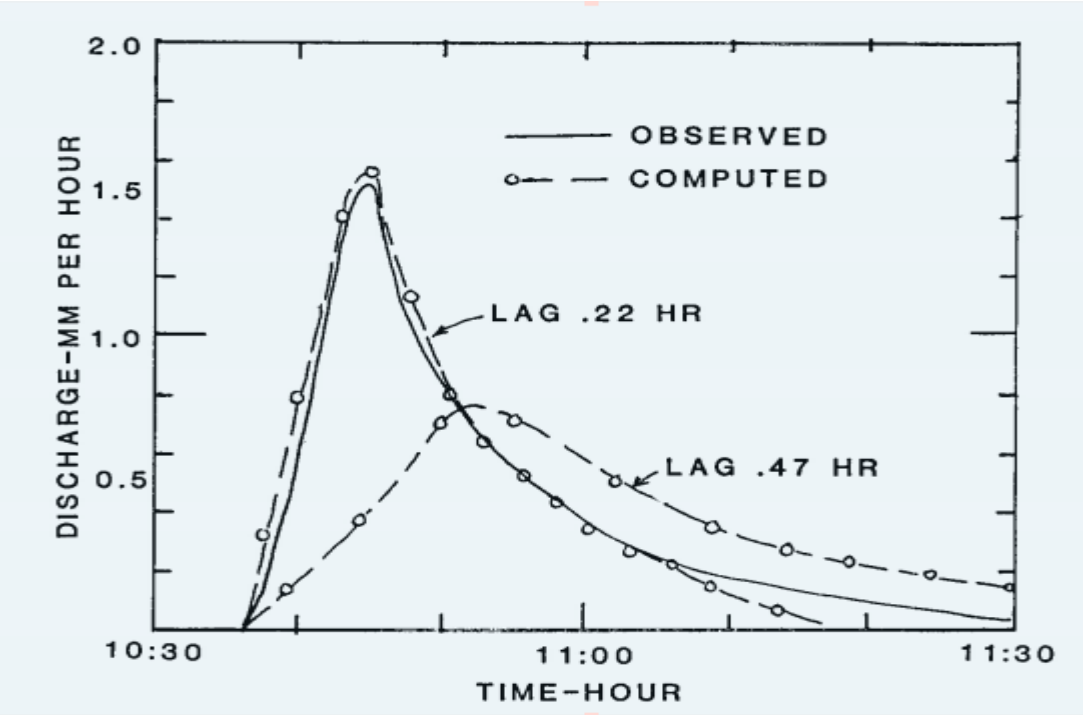


Figure III-11 Observed and synthetic hydrograph computed from the observed lag time of 0.22 hours. Another computed hydrograph computed with a lag time of 0.47 hours represents the discharge from the same storm before urbanization or under natural conditions. (Study area: Cerrito Creek, storm of February 15, 1984), *source (Leopold, 1991)*

[6] In hydrology , The lag time expressed as time between center of mass of rainfall and center of mass of runoff, is a specific measure of some basin characteristics including the effect of urbanization e.g., lag time refers to the hours or minutes elapsing between a burst of rainfall and the resulting hydrograph downstream Leopold, L. B. (1991). Lag times for small drainage basins. *Catena*, *18*(2), 157-171. https://doi.org/https://doi.org/10.1016/0341-8162(91)90014-O .

The first step is to synthesize a hydrograph under observed conditions as a demonstration that the synthesis agrees with observation. Therefore, if the basin is urbanized, a longer lag time is used to construct the hydrograph pattern of the natural condition. Alternatively, if the basin is natural, we need to know the effect of urbanization to it, accordingly a pattern hydrograph is constructed to represent the new condition of urbanization on the same runoff. This is illustrated in **Fig.III.7**, where the continuous line presents the observed hydrograph for a given region and storm event, 0.22 hour is the lag time of this storm event, used to compute the hydrograph patten that presented in dashed line, herein the basin of the corresponding hydrograph is 20 % urbanized their lag corresponds to 0.22 hour, if the basin is unurbanized or natural, it would have a lag of 0.47 hours, that used to compute hydrograph for the same storm but with different lag of 0.47 hour. This computation showed the effect of urbanization on lag time and hydrograph shape, where the hydrograph peak decreased from 0.76mm/hour to 1.55mm/hour.

In addition to increased runoff volume, and lag time that addressed by several studies over the world (Christopher & Derek, 2002; Christopher et al., 2005; Dale & Richard, 1982; Desmond et al., 1970; Harris & Rantz, 1964; In Shik et al., 1998; Kenneth et al., 1992; Maria & Moshe, 1992; Rafael & Frank, 1975; Yao et al., 2016), urbanization also led to changes of all elements of the hydrograph. Existing research recognizes the critical role of urbanization on time to peak (Almousawi et al., 2020; Huang et al., 2012; Nigussie & Altunkaynak, 2016), hydrograph peak discharge (H.-j. Huang et al., 2008; S.-y. Huang et al., 2008) and runoff volume (Arnell, 1982), runoff depth and runoff coefficient (Wei et al., 2020), and baseflow (Simmons & Reynolds, 1982).

### III.5 Total and Effective Impervious Area

Impervious surface is an indicator of the existence of urbanization on water management and practices. In the urban watershed, almost impervious area is connected to artificial hydraulic drainage system but not all the impervious cover. In most studies, researchers considered the entire rate of impervious cover whether water travels over an entirely impervious pathway to a stormwater drainage system inlet or not. That's what we call the Total Impervious Area TIA, which is a lumped metric describing the total fraction of impervious area, comprising those impervious surfaces that drain to permeable ground for example a roof that drains onto a lawn. The TIA is more precisely capture the watershed developments by indicating directly the amount of total runoff produced from the impermeable areas (Finkenbine et al., 2000; Yao et al., 2016). recent studies suggest that a better indicator of urban runoff is the “effective”

impervious area (EIA), or the portion of total impervious area that is hydraulically connected (i.e., piped) to the storm sewer system. The **Fig.III.9** show an example of EIA (B), and TIA(A).

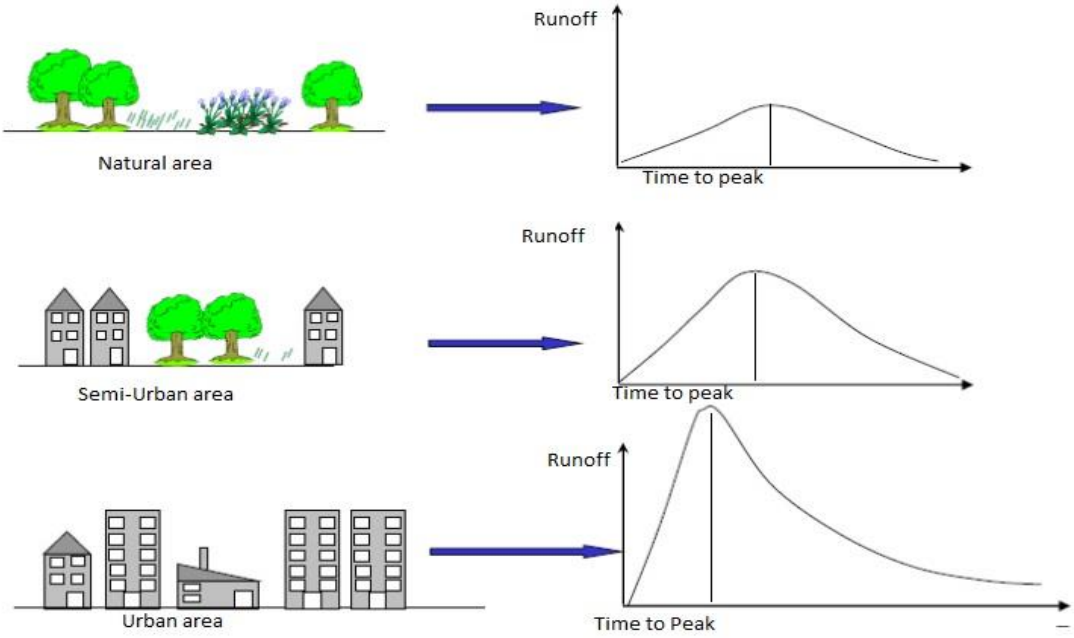


Figure III-12 Evolution of runoff peak and Time to Peak in function of changes in Land use and urbanization growth

Runoff generated from TIA is different from the resulted from EIA in their pathway, therefore their contribution to the outlet hydrograph is different (Han & Burian, 2009). Most of the studies in urban watershed used the methodologies that estimate the TEA inasmuch as estimating EIA is difficult task (Derek B Booth & C Rhett Jackson, 1997). However, the studies that used the TIA as predictor, result in a overestimation of the amount of runoff (Alley & Veenhuis, 1983; Yao et al., 2016). Derek B. Booth and C. Rhett Jackson (1997) explained the limitations of using TIA in urban hydrology. They suggested using EIA to characterize urban development, but noted that its direct measurement is complicated. Whereas the use of EIA is better for studies of hydrologic change by act of urbanization. EIA further qualifies how imperviousness affect each hydrologic component. some water transported from impervious to pervious surfaces, for example a water drained from a roof with downspouts onto either a grassed area; or routed into bio-detention facilities (raingardens), herein the overland flow is afterwards infiltrated. Which indicate that EIA is most marked effect on runoff watershed (Shuster et al., 2005).

A

B


Figure III-13 Example of TIA (A), and EIA (B)

### *III.5.1 Estimation of Imperviousness*

Practitioners, policy makers and engineers responsible for Urban drainage design and storm-water management need an accurate estimate of percentage of impervious area. Imperviousness is the most important parameter in the urban catchment. The oldest method that considers the imperviousness is the Rational method (Kuichling, 1889; Lloyd-Davies, 1906; Mulvaney, 1851). This method is the simplest and have been raised several criticisms, but it remains the most used in the nineties because of its simplicity. The runoff coefficient of the Rational Method is presumed to be directly proportional to the total imperviousness which relating the Peak discharge by the rainfall intensity. Runoff coefficient is depending on several parameters and its proper selection requires judgment and experience on the part of the hydrologist. Lloyd-Davies (1906) assumed that all area that must be drained is EIA, thus it considers 100% of runoff drained from the considered basin $Q = i \times A_{EIA}$ , where $A_{EIA}$ is the drainage area. knowing that the original formula is $Q = i \times A \times C$ , where C is the runoff coefficient, that depend on the nature of each sub-area, which therefore multiplied by their corresponding runoff coefficient (Lee & Heaney, 2003; Te Chow, 2010).

#### *III.5.1.A Empirical estimate*

Imperviousness estimation is not an obvious task; its determination is relatively difficult. Common methods to estimate TIA for small urban watershed modeling applications include direct measurement by field survey and visual inspection of aerial photos.

Heaney et al. (1976) proposed a relationship relates the population density with imperviousness. Boyd et al. (1993) investigate storm rainfall and runoff depths from 380 events on nine

Australian basins plus a further 383 events on 17 basins from other countries to empirically estimate previous and impervious surfaces. Plots of runoff depth against rainfall depth have been used; therefore, the slope of each segment gives the fraction of the basin which is contributing to runoff. Thus, a least squares linear regression of the form $Q = a + bP = (P - I_{L_i})F_i$ was fitted to the data, where: Q is total depth of runoff for the storm; P is total depth of rainfall; $I_{L_i}$is the initial loss for the impervious surf aces; and $F_i$ is the effective impervious fraction, estimated from storm data.

An empirical relationship between EIA and TIA was determined by Livingston and Veenhuis (unpublished report, 1981) for 14 of the Denver basins in Colorado as $EIA = 0.15\,TIA^{1.41}$ ($R^2$=0.98) (Alley & Veenhuis, 1983). The used data represent a small sample of basins in a single metropolitan area. Thus, their utility is limited. Only similar investigations in other urban areas can confirm the transferability of these values. For example Miller (1979) reported similar estimates of TIA and EIA for two watersheds in southern Florida consisting of multi-family residential and commercial developments. However, he found the ratio EIA/TIA was only 0.14 for a watershed consisting of single-family residential development. This is because drainage in this watershed is by swales in the lawns along the streets rather than by curb and gutter. All the streets in the Denver watersheds had curbs and gutters.

Wenger et al. (2008) developed a percent EIA for the Etowah River basin north of Atlanta, Georgia. For their study, TIA data were generated from the National Land Cover Database (NLCD)[7] imperviousness layer and EIA data were determined based on interpretation of high-resolution aerial photographs for 15 sites that ranged in size from 25 to 70 ha. The best fit model was ($R^2$ = 0.98):

$$EIA = (1.046 \times TIA) - 6.23\% \qquad (1)$$

Where EIA is 0 for areas where TIA values are less than 6.23%.

[7] NLCD: The USGS (United States Geological Survey) in partnership with several federal agencies, has developed and released five National Land Cover Database products over the past two decades: These products provide spatially explicit and reliable information on the Nation's land cover and land cover change ***(Only for United states)***. To continue the legacy of NLCD and further establish a long-term monitoring capability for the Nation's land resources, the USGS designed a new generation of NLCD products released in 2016. This design continues in 2019 and aims to provide innovative, consistent, and robust methodologies for production of a multi-temporal land cover and land cover change database from 2001 to 2019 at 2–3-year intervals.

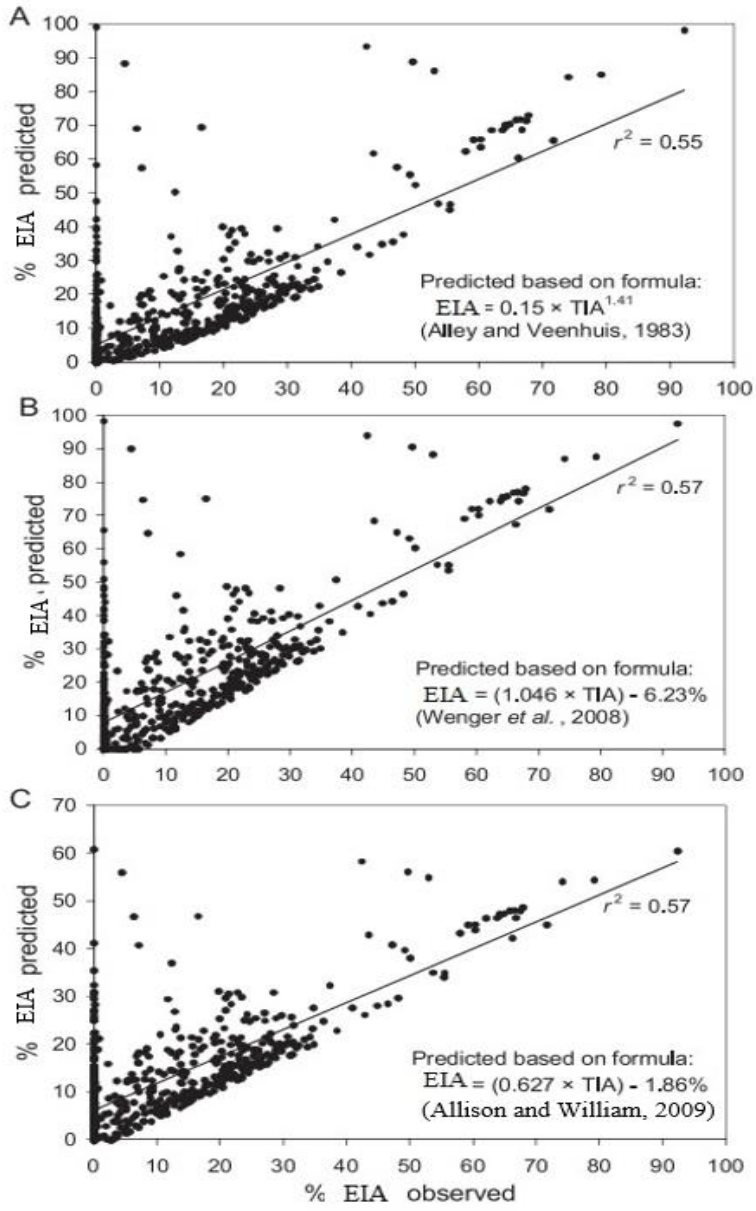


Figure III-14 Relationship Between Effective Impervious Area (EIA) Observed from Field Assessments and EIA Predicted from Empirical Formulas. EIA was predicted from parcel scale % total impervious area (TIA) at 521 parcels with impervious surfaces based on formulas (A) published by Alley and Veenhuis (1983), (B) published by Wenger et al. (2008),and (C) developed based on a linear regression relationship between % TIA and % EIA within parcels for this study. Best fit linear regressions and corresponding $R^2$ values are reported. *Source (Allison & William, 2009).*

Allison and William (2009) used the two above mentioned formulas provides by (Alley & Veenhuis, 1983), and (Wenger et al., 2008) for the Shepherd Creek catchment located in Hamilton County, Ohio, United States (1.85 $km^2$) to estimate EIA, and then compared the results by a directly field assessment and publicly available geographic information system (GIS) data. The authors developed their own formula based on a linear regression relationship between % TIA and % EIA within parcels for this study as follow ($R^2$ = 0.57):

$$EIA = (0.627 \times TIA) - 1.86\% \quad (2)$$

which indicates that EIA is 0 where TIA was less than 1.86%.

The authors concluded that predicted % EIA based on this model and the two published models were all similarly ineffective at predicting observed % EIA ($R^2$ ranged from 0.55 to 0.57) see **Fig.III.10**

*III.5.1.B Remote sensing RS and Geographical Information system GIS Estimates*

Alternative solution to produce more refined TIA is through land cover estimation. Differencing each land cover allow to identify its permeability, since that every Land cover type is characterized by a certain amount of penetration, and usually the urban areas considered as impervious cover. Hence a different technic of classifying and digitizing the imagery and photos of land surface is used (Fankhauser, 1999; Ragan & Jackson, 1975). Interpretation of land use information from satellite imagery or aerial photography is another means of obtaining land use and land cover data .Numerous methods have been exploits satellite imagery to estimate percent impervious surfaces for hydrologic modeling, resources management, ecosystem assessment, and urban planning (Ali et al., 2011; Anne, 2006; Antonius, 1983; Derek et al., 2002; Fola, 1989; Ravagnani et al., 2009; Richard, 1979).

Access to satellite data in the 1970s promoted the use of satellite imagery to classify impervious surfaces for urban hydrologic modeling (Ragan & Jackson, 1975). The Landsat 30 m resolution satellite data is a yet widely available, despite their coarse resolution. Imperviousness was estimated using a variety of approaches, but in general they relied on relationships between impervious surfaces and spectral derivatives.

Several studies addressed that the use of Remotely sensed data enhanced greatly the hydrology research field, given the fact that hydrological modelling field is data required, and it would never be conducting a hydrological study without collecting sufficient data. It can also be expected, that in many other fields of hydrological modeling the existing or expected availability of remote sensing information will lead to the development of much more efficient hydrological models (Schultz & Engman, 2012). RS sensors never measure hydrological data. They can

measure only electromagnetic signals[8] in certain spectral bands[9] emitted from bodies on the earth or in the atmosphere (passive RS[10]) or reflected from such bodies (active RS[11]).

Remote sensing technology has been widely applied in urban land use, land cover classification, and change detection. A conceptual model proposed by Ridd (1995) for remote sensing analysis of urban landscapes, i.e., vegetation-impervious surface-soil (V-I-S) model. It assumes that land cover in urban environments is a linear combination of these three components. The author believed that this model can be applied to spatiotemporal analyses of urban morphology, biophysical, and human systems. While urban land use information may be more useful in socioeconomic and planning applications, biophysical information that can be directly derived from satellite data is more suitable for describing and quantifying urban structures and processes.

There are a large number of published studies that uses the thematic classification approach of the obtained satellite images, this is based on translating spectral information into thermal classes. Thematic classification referred to transformation of reflection measurements from remote sensing images into discrete objects, which are distinguished from each other by separate thematic classification. Within different objects of a single class, and even within a single object, different reflections may occur. Conversely, different thematic classes cannot always be distinguished in a satellite image because they show (almost) the same reflection (Schultz & Engman, 2012). The task of classification is to assign a class label to each feature vector, which means

[8] electromagnetic signals: Electromagnetic waves or EM waves are waves that are created as a result of vibrations between an electric field and a magnetic field. In other words, EM waves are composed of oscillating magnetic and electric fields (https://economictimes.indiatimes.com/definition/electromagnetic-waves)

[9] spectral bands: Whenever any sensor can make filter a specific wavelength induced energy/light then it called spectral band Example, 0.4–0.5 micrometer called blue, 0.5–0.6 micrometer called as green and 0.6–0.7 called as red. Apart from that 0.7 to 1 micrometer is called as infrared. Those are spectral bands. An image is a form of overlaying of different bands. (https://www.quora.com/What-are-spectral-bands-in-remote-sensing)

[10] passive RS: Remote sensing systems which measure energy that is naturally available are called passive sensors.

[11] active RS: Sensor provides their own energy source for illumination. By emits radiation which is directed toward the target to be investigated. The radiation reflected from that target is detected and measured by it.

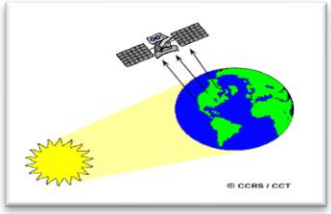

*Passive RS*

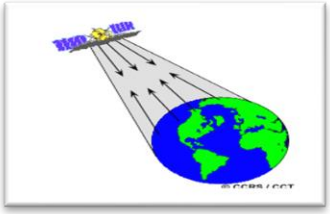

*Active RS*

to subdivide the feature space into partitions that correspond to classes. This task can be achieved by pattern recognition (Ripley, 2007). Rezaul et al. (2010) used Multi-temporal and multi-spectral satellite images were used to generate historical land use/land cover Digital land use maps were generated to estimate the impact of land use changes on the hydrologic evaluation. Image pre-processed using GIS from *Idrisi selva 17.0* software. The satellite images were processed by carrying out radiometric calibration, geometric rectification, and projection to the Universal Transverse Mercator (UTM, 38N) system. The boundary of the sub-basin was used to extract by mask the satellite images for the study area. The supervised classification method, with *maximum likelihood clustering*[12], was applied to classify the images and generate land use maps. Land use categories were identified as impervious surfaces (built up area), farm land, vegetation and barren soil .On the same way and using the *maximum likelihood clustering Du et al. (2012)* used two different sensors *Landsat Thematic Mapper (TM)* images from 1988, 1994, 2006, *Enhanced Thematic Mapper Plus (ETM+)* images from 2001, 2003 (all with 30 m resolution), and 20 m resolution *China Brazil Earth Resources Satellite (CBERS)* image from 2009. image pre-processing was carried out in *ERDAS Imagine 9.3*. The satellite images were generated by applying coefficients for radiometric calibration[13] geometric rectification[14] and projected to the Universal Transverse Mercator (UTM) ground coordinates with a spatial resampling of 30 m. Geometric rectification was carried out on Landsat images from 1988, 1994, 2003, 2006 and CBERS image from 2009 using the ETM+ from 2001 as a base-map, and nearest neighbor resampling algorithm[15], with root mean square (RMS) error of less than 0.5 pixels via image-to-image registration. Radiometric calibration and atmospheric correction[16]

[12] maximum likelihood clustering: The maximum likelihood classifier is one of the most popular methods of classification in remote sensing, in which a pixel with the maximum likelihood is classified into the corresponding class (http://sar.kangwon.ac.kr/etc/rs_note/rsnote/cp11/cp11-7.htm).

[13] Radiometric calibration is the process of converting image brightness values in a remotely sensed image to spectral radiance values https://www2.geog.soton.ac.uk/users/trevesr/obs/rseo/radiometric_calibration.html

[14] Geometric correction corrects systemic and nonsystematic errors in the remote sensing system and during image acquisition (Weng, 2009)

[15] Nearest neighbor is a resampling method used in remote sensing. The approach assigns a value to each "corrected" pixel from the nearest "uncorrected" pixel. The advantages of nearest neighbor include simplicity and the ability to preserve original values in the unaltered scene https://mapasyst.extension.org/remote-sensing-resampling-methods/

[16] atmospheric correction: removes the scattering and absorption effects from the atmosphere to obtain the surface reflectance characterizing (surface properties) https://gisgeography.com/atmospheric-correction/.

were carried out to correct for sensor drift, differences due to variation in the solar angle, and atmospheric effects.

*III.5.1.C Field assessment estimates*

Field investigation is another method to identify impervious cover and the degree of their effectiveness. Studies that have used this method confirmed how difficult it is. Even that it was very efficacious for an accurate assessment of EIA to identify and verify where pipes are draining (Allison & William, 2009; Lee & Heaney, 2003; Walsh et al., 2002) field campaigns to determine EIA may be necessary so as to understand its extent and design optimal approaches to stormwater management. Allison and William (2009) used a field assessment of Shepherd Creek catchment of an area about 1.85 Km2, in addition to GIS that used for digitizing aerial photos, NLCD database, and empirical estimation. They concluded that, the aerial photos digitizing provides a good estimate of TIA, whereas the Classified satellite imagery (NLCD imperviousness layer) underestimates actual TIA. Moreover, Imperviousness connectivity can only be accurately assessed via field assessments. And finally, the EIA was not accurately predicted from empirical relationships with TIA.

# RS and GIS for Extracting land information for Hydrological Modelling

# IV RS and GIS for Extracting land information for Hydrological Modelling

## IV.1 Introduction

Land cover as defined by Barnsley et al. (2000) is "the physical materials on the surface of a given parcel of land (e.g. grass, concrete, tarmac, water)," and land use as "the human activity that takes place on, or makes use of that land (e.g. residential, commercial, industrial)". Land use can consist of varied land covers, (i.e., a mosaic of bio-geophysical materials found on the land surface). For instance, a single-family residential area consists of a pattern of land-cover materials (e.g., grass, pavement, shingled rooftops, trees, etc.). Land cover and land use terms are often used together. Therefore, it is important to define them clearly. A definition from the INSPIRE (2013) explains that land cover represents the physical and biological cover of the Earth's surface including classes as build-up areas, forests, agricultural areas, wetlands, (semi-) natural areas, water bodies. On the other hand, the land use represents the actual and future planned human activities on a territory, characterized as residential, industrial, commercial, agricultural, forestry and leisure. It is the expression of the human activity developed for social, economic, cultural and political purposes. This means that land cover includes the land use features and they should be represented on different maps (Kleemann et al., 2017).

Land-use is an abstract concept, constituting a mix of social, cultural, economic and policy factors, which have little physical importance with respect to reflectance properties, and hence has a limited relationship to remote sensing (Treitz & Rogan, 2004). Remote sensing data record the spectral properties of surface materials, and hence, are more closely related to land-cover. In short, land use cannot be measured directly by remote sensing, but rather requires visual interpretation or sophisticated image processing and spatial pattern analyses to derive land use from aggregate land-cover information and other ancillary data (Treitz & Rogan, 2004). Integrated analyses within a spatial database framework (i.e., GIS) are often required to assign land cover to appropriate land-use designations.

This human modification of land use and land cover (LULC) can significantly influence the watershed hydrological conditions. Hydrologic modeling is regarded as an effective way to deal with the impacts of land use and land cover change (Öztürk et al., 2013) for a watershed in regard to flood monitoring. Over the last decades, using computer-based hydrological model to quantify the hydrologic impact of LULC change garnered considerable attention and was applied in many areas around the world (Ngigi et al., 2007; Nie et al., 2011).

Remote sensing aids acquiring information about a phenomenon/object or surface while at a distance from it. Remote sensing technology collects the data of the earth's surface at spatial, spectral and temporal scales. The spatial data includes land use, vegetation cover, soil, topography, etc. In most of the cases, remote sensing data is directly used for hydrological modelling by extracting input variables such as LULC. through digital image processing.

A geographic information system (GIS) is a tool, which helps to manage, integrate, analyze and manipulate the spatial information including remote sensing data according to the user needs. Nowadays, GIS platforms have become increasingly dynamic, narrowing the gap between historical data and recent hydrologic reality (Naidu, 2015). GIS has become a useful and essential tool in hydrology for scientific study and management of water resources. Remote sensing and GIS provides observation of changes in hydrological states, which vary over both time and space that can be used to monitor hydrological conditions and changes (Ritchie & Rango, 1996).

Recently hydrological modeling has been improved with the development of remote sensing, geographic information systems (GIS), and fine-resolution geospatial data, including satellite imagery, digital elevation models (DEM), and radar rainfall data (Preetha & Al-Hamdan, 2022). The integration of remote sensing (RS) and geographic information systems (GIS) has been widely applied and has been recognized as a powerful and effective tool in detecting urban growth. Remote sensing collects multispectral, multi-resolution, and multi-temporal data, and turns them into information valuable for understanding and monitoring urban land processes and for building urban land-cover data sets (Weng, 2019). GIS technology provides a flexible environment for entering, analyzing, and displaying digital data from various sources necessary for urban feature identification, change detection, and database development (Al-Hashimi & Mohsin, 2008). In hydrological and watershed modelling, remotely sensed data are found to be valuable for providing cost-effective data input and for estimating model parameters. The introduction of GIS to the field makes it possible for computer systems to handle the spatial nature of hydrological parameters (Weng, 2019). The hydrological community now increasingly adopts GIS-based distributed modelling approaches.

Integration of modern modelling techniques and GIS data has made the study of watershed more efficient. Use of satellite observed data with finer resolution, increased computational capacity and improved GIS database management has improved spatial modelling and simulation for flood monitoring and forecasting. Surface runoff amount and distribution is closely linked with land use considering parameters, such as the types of soil, surface roughness and

infiltration capacity of the soil. These parameters are inputs for generation of information from a hydrologic model.

### IV.2 Role of Remote Sensing in Hydrological Modelling

Remote sensing is defined as the science of obtaining information about an object, area, or phenomenon through the analysis of data acquired by a device that is not in contact with the object, area, or phenomenon under investigation (Lillesand et al., 2015). Since the launch of Landsat-1 – the first Earth resource satellite in 1972, remote sensing has become an increasingly important tool for the inventory, monitoring, and management of earth resources. The increasing availability of information products generated from satellite imagery data has added greatly to our ability to understand the patterns and dynamics of the earth resource systems at all scales of inquiry (Bawahidi, 2005).

The increasing availability of satellite imagery with significantly improved spectral and spatial resolution has offered greater potential for more detailed land-use mapping. At the same time, rapid advances in the computer science as well as other information technology fields have offered more powerful tools for satellite image processing and analysis. Image processing software and hardware are becoming more efficient and less expensive. Access to faster and more capable computer platforms has aided our ability to store and process larger and more detailed image and attributes data sets. Digital image processing involves manipulation and interpretation digital images with the aid of computer technology. Recently, digital image processing is central to efficient use of satellite imagery in land-use studies (Bawahidi, 2005).

A major problem in the hydrology is the inadequate field measured data to describe the hydrologic process. Remote Sensing has been identified as a tool to produce information in spatial and temporal domain, instead of point measurement, in digital form, with high resolution. This spatial information can be used as input data for hydrological models and are extremely relevant as a means of estimating a number of key variables specifically in situation where distributed hydrological models are used (Gupta et al., 1999).

The use of remote sensing data, in combination with distributed hydrological model, provides new possibilities for deriving spatially distributed time series of input variables, as well as new means for calibration and validation of the hydrological model. With the development of remote sensing and satellite technology, the satellite data can be used to derive a variety of surface

parameters. One of the important hydrologic model inputs such as land use and land cover can be obtained from Landsat satellite images.

Remote sensing techniques are a powerful tool in data capturing and analysis in the process of quantifying the nature of urbanization and rapid growth. An image resolution temporally and spatially is now an important method of challenging urban problems by creating a thematic mapping for the general environment within the study periods by producing outcomes from the study and guides to policy makers.

Baig et al. (2022) conducted a study in order to assess the LULC changes and predict future trends in Selangor, Malaysia. The satellite images from 1991–2021 were classified to develop LULC maps using support vector machine (SVM) classification in ArcGIS. The image classification was based on six different LULC classes, i.e., water, developed areas, barren, forest, agriculture, and Wetlands.

The resulting LULC maps illustrated the area changes from 1991 to 2021 in different classes, where developed, barren, and water lands increased by 15.54%, 1.95%, and 0.53%, respectively. However, agricultural, forest, and wetlands decreased by 3.07%, 14.01%, and 0.94%, respectively. The cellular automata-artificial neural network (CA-ANN) technique was used to predict the LULC changes from 2031–2051. The Landsat images for the years 1991, 2001, 2011, and 2021 were used for image classification to identify land use patterns and create LULC maps. Landsat-5 satellite images were obtained for 1991 and 2001. Similarly, Landsat-8 satellite images were acquired for 2011 and 2021. The Landsat images had the spatial resolution for 30 m. The flow chart illustrating the process for land use classification to create LULC maps is shown in **Fig.IV.1**.

For urban hydrological modeling, as a focus in the study conducted by Elaji and Ji (2020) several related research questions are raised:

- How sensitive are runoff simulation to land use and land cover change patterning?
- How will input data quality impact the simulation outcome?
- How effective is integrating and synthesizing various forms of geospatial data for runoff modeling?

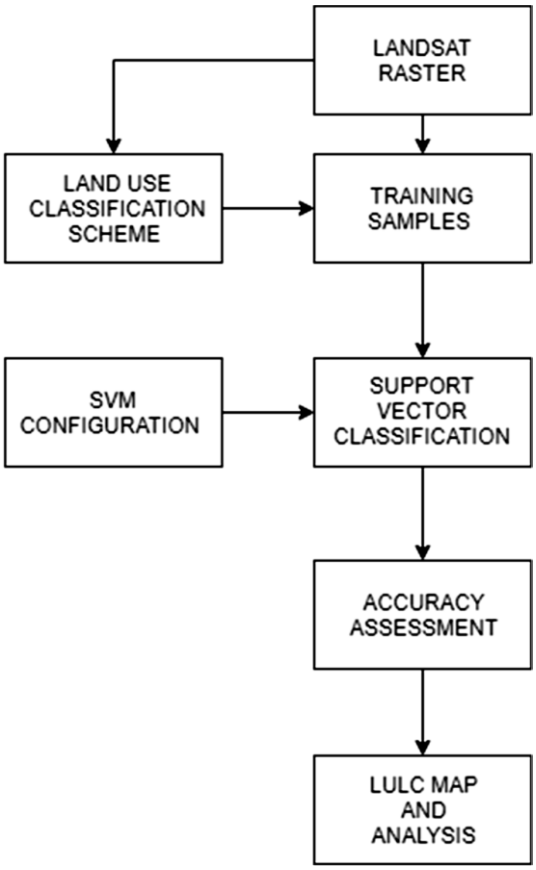


Figure IV-1 Flow chart for creating LULC maps using SVM image classification (Baig et al., 2022)

With the aim of answering these questions as research objectives, they conducted a spatial land use and land cover (LULC) change analysis and an urban runoff simulation in the Blue River watershed in the Kansas City metropolitan area between 2003 and 2017. In this study, approaches were developed to incorporate the Hydrologic Engineering Center Hydrologic Modeling System (HEC-HMS) model with remote sensing, geographic information systems (GIS), and radar rainfall data. The method in their study can be described in several major stages (**Fig.IV.2**).

Four satellite images with various resolutions were used to derive the LULC maps of 2003 and 2017 and to monitor the land use/cover change over time. It first derives the LULC maps with 6, 20, and 30 m spatial resolution using the Maximum Likelihood classification (MLC) and performs a change detection analysis, which is followed by delineating the drainage networks with 3 and 30 m spatial resolution DEMs. The process then prepares the soil data in order to derive the Soil Conservation Service (SCS) curve number (CN) values and then prepares the rainfall data. The final step includes the model setup and simulation run.

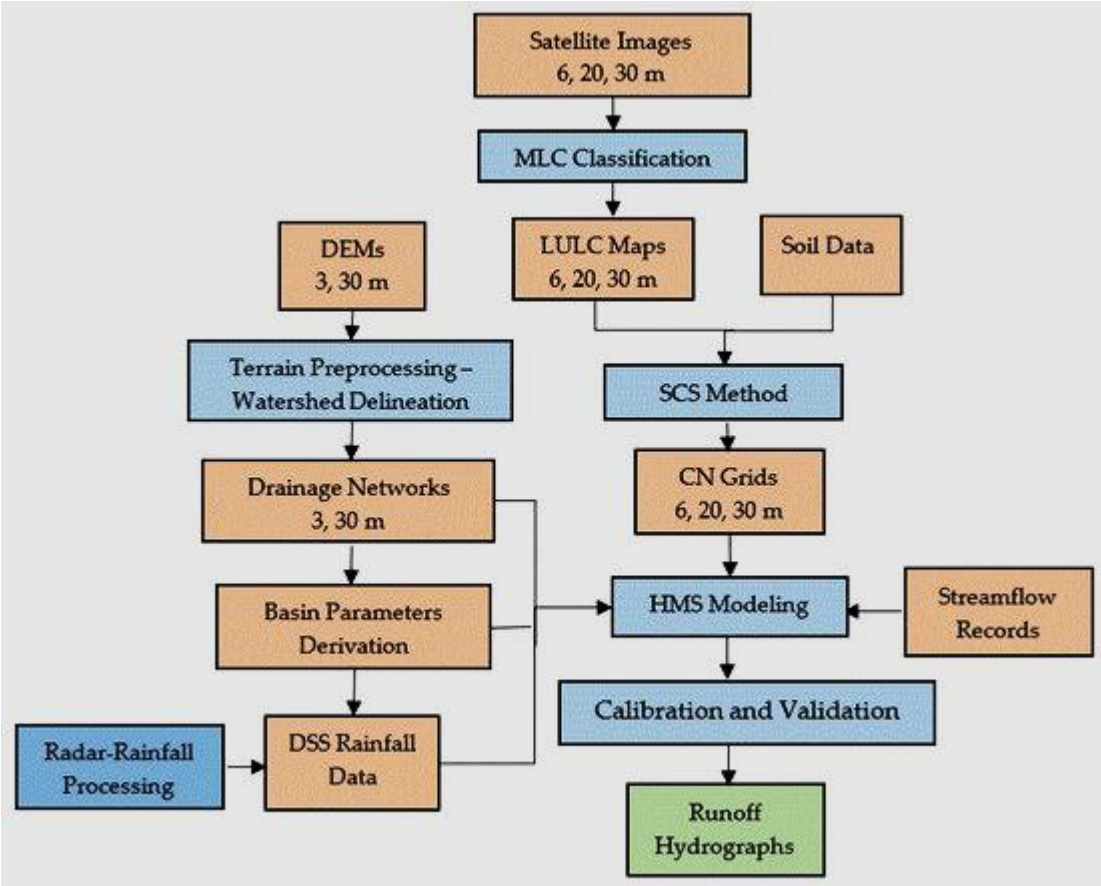


Figure IV-2 Data processing and modeling procedures: orange boxes indicate data inputs with different spatial resolutions, blue indicates processing, and green indicates final simulation outputs (Elaji & Ji, 2020)

Many researchers have developed various methods to estimate both human influence on changes in surface runoff, especially storm runoff, and consequent effects on downstream activities. Among these models, the SCS-CN is one of the most enduring methods for estimating the volume of direct surface runoff in ungauged rural catchments. It is also noted that several complex models such as Soil and Water Assessment Tool (SWAT), Hydrologic Modeling System (HEC-HMS), have been developed based on SCS-CN method.

The SCS-CN model has a key parameter, Curve Number (CN), which is developed from an empirical study of runoff in small catchments. The CN method expresses runoff volume as a function of rainfall volume, hydrologic storage, and initial abstraction. The CN value depends on land surface characteristics and hydro-soil conditions. The higher the CN value, the higher the volume of direct surface runoff. Many researchers developed CN calculation methods by incorporating land cover information. Apparently, most previous studies showed that impervious surface played an important role in computing the CN, because it affected the infiltration of the surface water.

Based on the considerations of urban landscape complexity and the characteristics of medium-resolution satellite imagery. Fan et al. proposed a method to calculate the composite CN with the vegetation-impervious surface-soil (V-I-S) model, NDVI[17] and soil types. First, soil types and NDVI are classified into several classes, second, each class of soil type and NDVI are given an initial CNs (initial CN of soil) and CNv (initial CN of vegetation), respectively. Lastly, the CN is calculated by computing the percentages of impervious surface, NDVI class, and soil class. Impervious surface is the land surface through which water cannot infiltrate. Impervious anthropogenic features include roads, driveways, highways, sidewalks, parking lots and roof-tops.

In their work a procedure is designed (**Fig.IV.3**) to calculate composite CN, which includes four steps:

- Obtaining NDVI values and classifying vegetation types. The NDVI values are grouped into four categories and each is assigned an initial CN value in reference to the TR-55 table[18];
- Extracting V-I-S fraction images using the linear spectral mixture analysis (LSMA model. Vegetation, impervious surface and soil fractions are extracted from the satellite image;
- Soil classification. Each type of soil is given an initial CN value in reference to the TR-55 based on its characteristics; and
- Calculating composite CN.

The composite CN is calculated as the weighted average of the initial CN values of vegetation, impervious surface and soil fractions.

[17] The Normalized Difference Vegetation Index (NDVI) is a standardized index allowing you to generate an image displaying greenness (relative biomass). This index takes advantage of the contrast of the characteristics of two bands from a multispectral raster dataset—the chlorophyll pigment absorptions in the red band and the high reflectivity of plant materials in the near-infrared (NIR) band.

[18] Technical Release 55 (TR-55) presents simplified procedures to calculate storm runoff volume, peak rate of discharge, hydrographs, and storage volumes required for floodwater reservoirs. These procedures are applicable in small watersheds, especially urbanizing watersheds, in the United States. First issued by the Soil Conservation Service (SCS) in January 1975, TR-55 incorporates current SCS procedures. This revision includes results of recent research and other changes based on experience with use of the original edition.

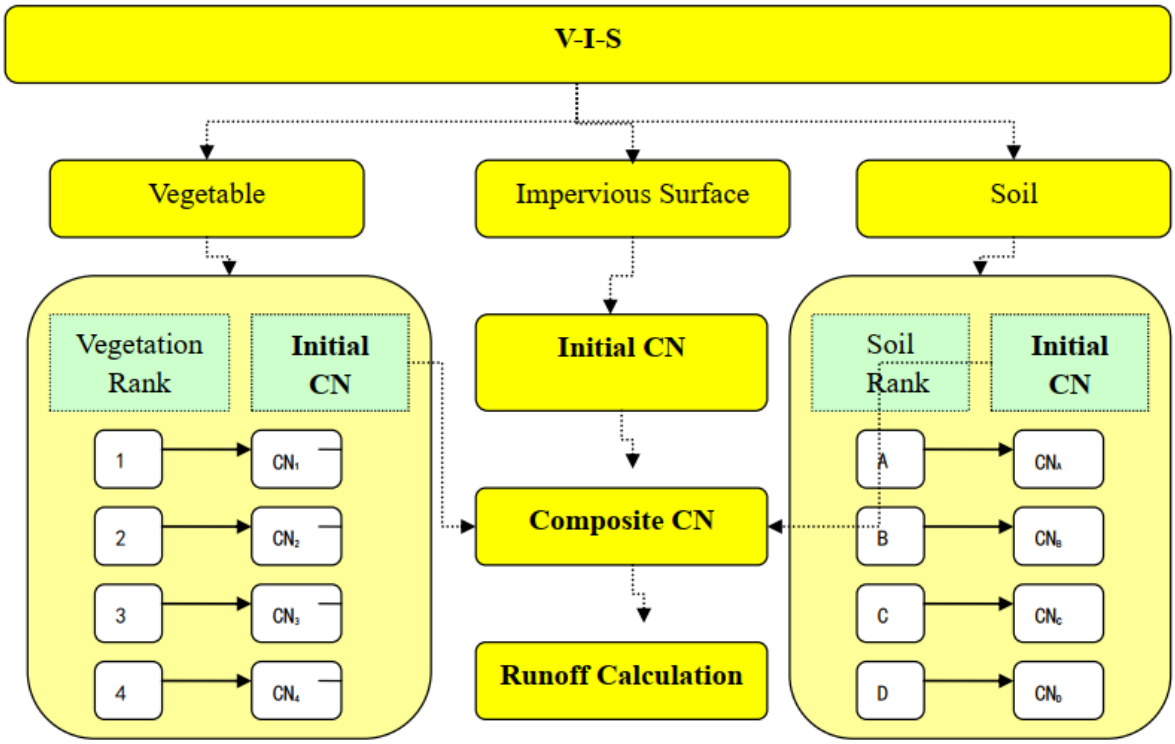


Figure IV-3 Procedure for computing composite CN (Fan et al.).

## IV.3 Role of GIS in Hydrological Modelling

The use of remote sensing technology involves large amount of spatial data management and requires an efficient system to handle such data. Hence GIS makes it possible to store, analyze and retrieve data for large and complex problems. GIS is a computer-based system designed tool applied to geographical data for integration, collection, storing, retrieving, transforming and displaying spatial data for solving complex planning and management problems (Ali, 2020). When historical map of the study area was collected during the data collection at the study area, the collected data was processed in GIS techniques as a source data in line with the objectives of the study of identifying the land use and land cover changes in the study area. This GIS application has important advantage of using powerful function with good example of ArcGIS software that has good tools for multi-source data processing of the change detection studies of the GIS

The possibility of rapidly combining data of different types in a GIS has led to significant increase its use in hydrological applications. It also provides the opportunities to combine a data from different sources and different types. One of the typical applications is use of a digital terrain model (DTM) for extraction of hydrologic catchment properties such as elevation

matrix, flow direction matrix, ranked elevation matrix, and flow accumulation matrix. It also provides the ability to analyze spatial and non-spatial data simultaneously.

Remote Sensing provides a large amount of data about the earth surface for detailed analysis and change detection with the help of sensors. Some of the application of remote sensing technology in mapping and studying of the land use and land cover changes are; mapping and classifying the land use and land cover, assessing the spatial arrangement of land use and land cover, allowing analysis of time-series images used to analyze landscape history, report and analyzing results of inventories including inputs to Geographic Information System (GIS), provide a basis for model building.

The importance of land cover mapping is to show the land cover changes in the watershed area and to divide the land use and land cover in different classes. For this purpose, remotely sensed imagery play a great role to obtain information not only temporal trends and spatial distribution of watershed areas and changes over the time dimension for projecting land cover changes but also to support change impact assessment (Atasoy et al., 2006).

# Study area description

# V Study Area Description

## V.1 Geographic location

The study area is a sub-watershed included in the large basin among the 17 existing in Algeria, which is "***Algerian coastal 02b***", the study basin is located between meridians 4° 58' 4' 'and 5° 5' 4 " t the parallels of 36° 46' 49" and 36° 43' 35" the basin covers an area of 42 square kilometers. It is located in the province of Bejaia. It is characterized by a very uneven and flat terrain which corresponds to the outlet of wadi "Sommam" and wadi "Segir" which crosses an urban area, the study basin is of temperate (subhumid) climate, according to the ANRH (national water resources agency) the average annual rainfall varies between 800 and 1500 mm, and the average annual temperature is 18 ° C. The study region is essentially made up of intermittent runoff streams, with a most often dry regime in summer and sometimes intense floods in winter. The most notable is Oued Sommam which is the most important in terms of length; it does not cross urban areas. However, its outlet is located on the south side of the study area. Oued Srir passes from the south of the area to join Oued Sommam and Oued Sghir, which it separates from Oued Srir and directly joins the sea. The basin covers a large urban area from the bottom side near the outlet and the dense forests in the back thrust of the basin (**Fig.V.1**).

## V.2 Study area selection

Despite the lack of hydrological measurements in the Wadi Sghir basin, it is a suitable research environment considered as ungauged basin. In addition to their geographical location, since it inflowing directly into the Mediterranean Sea. A very ragged relief characterizes the Wadi Sghir basin, the basin's upper boundaries are covered totally with forests while the lower boundaries near the basin outlet are covered with an extensive urban area, knowing that this area is entirely flat see **Fig.V.2**. This would cause disaster flooding due to acceleration of runoff after a short period of rain (short time of concentration). The geographical location of Wadi Sghir is between the Highlands in the East and the Sommam Valley in the West; this location and the proximity of the urban areas to the basin outlet make the area of particular interest and fertile for research and exploration. In particular, this area was the subject of a previous public contract conducted by the National office of Sanitation (ONA). Therefore, the hydrological and meteorological measures were obtained. This data is used for calibration and validation purposes.

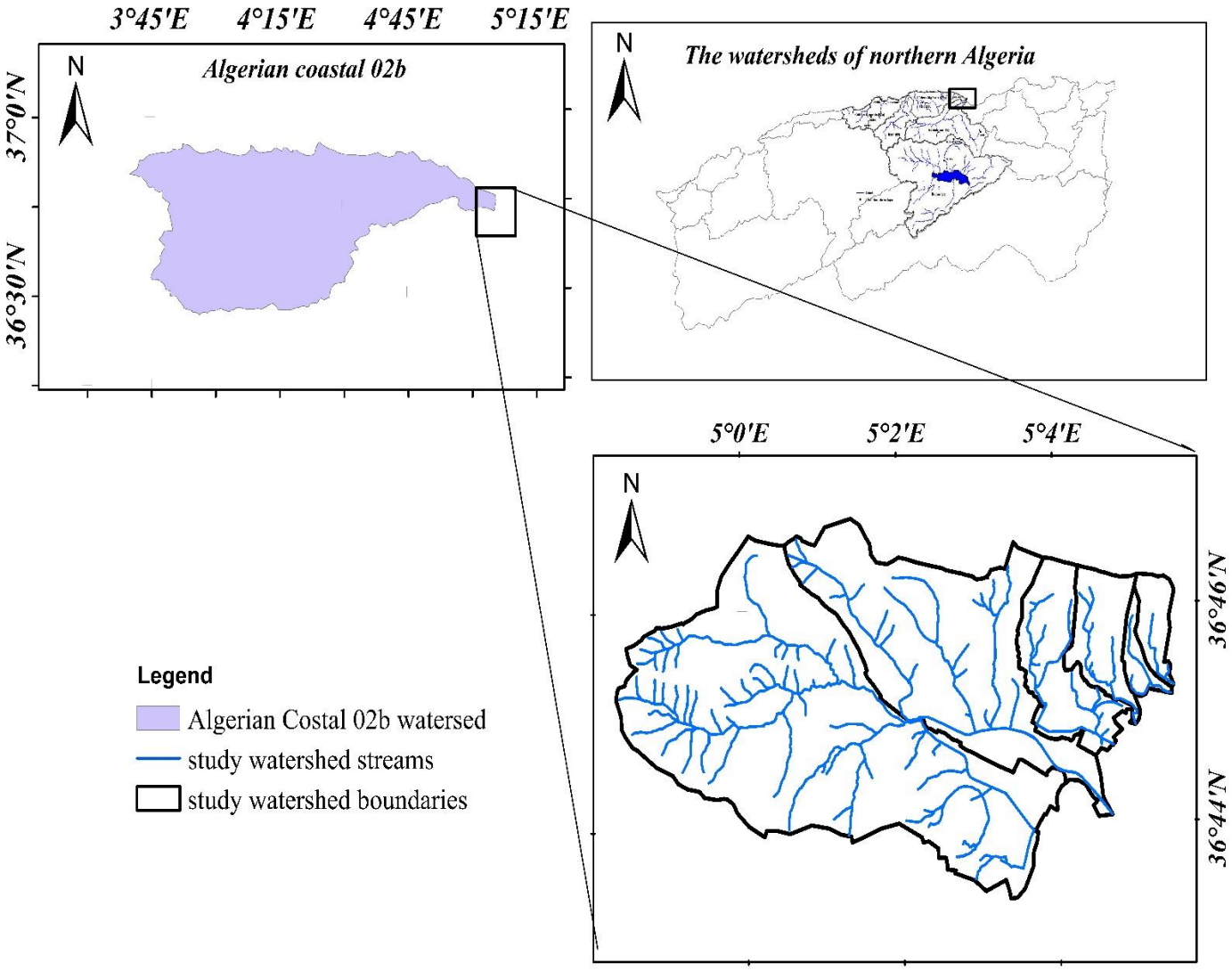


Figure V-1 Geographical location of the basin study.

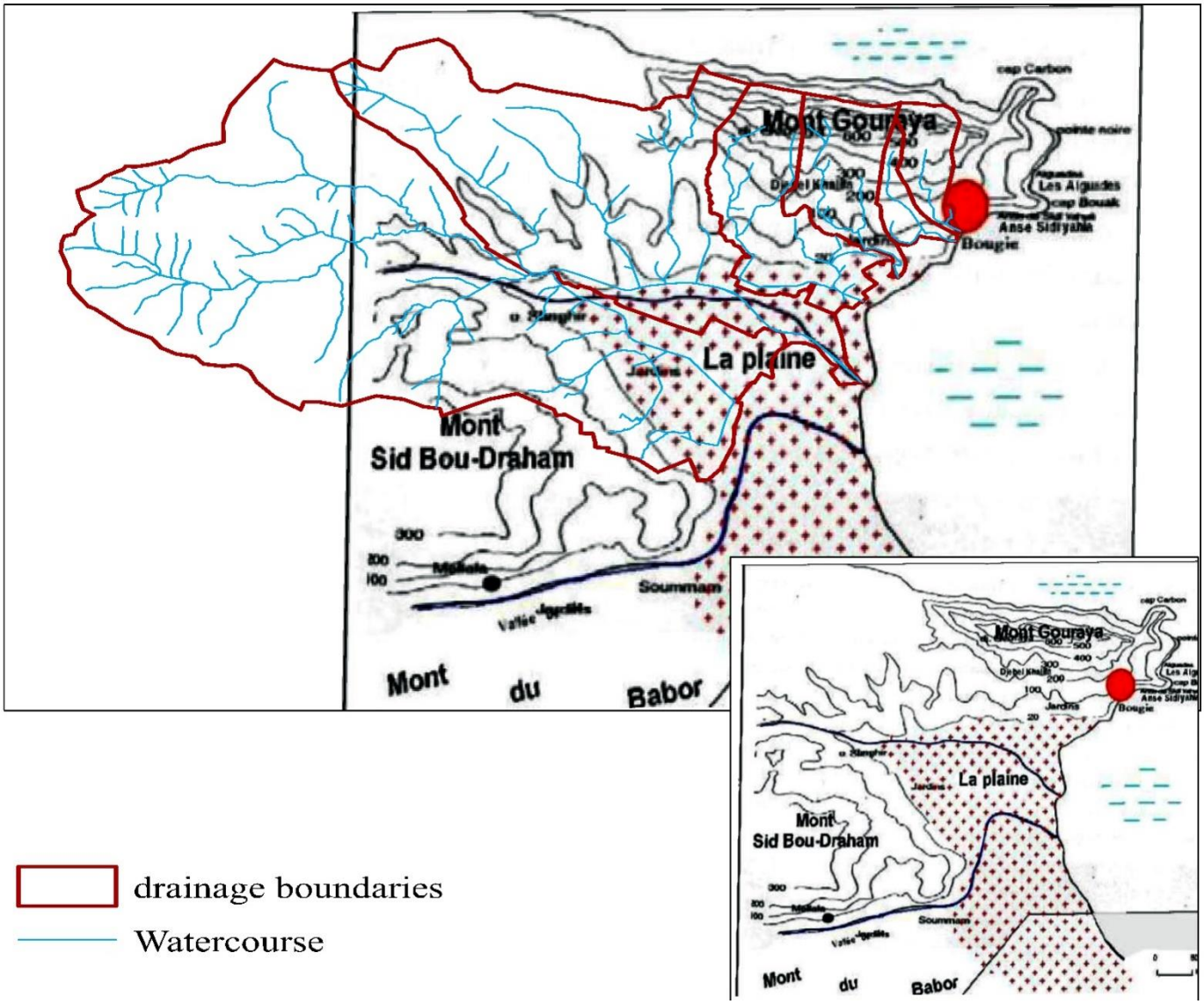


Figure V-2 map shows the relief of the study area

## V.3 Geomorphology and territory of the region

This region is characterized by a wooded mountainous relief occupying about 2/3 of its total surface. It is widely available on the Cliffs, steep areas, escarpments. There is also a flat area that stretches along the Gulf. It characterizes the coastal plain whose soil is as favorable for agricultural production as for the enjoyment of their beautiful beaches, which sometimes constitute a single peace. It is very suitable land for agriculture as well as for tourism. Neither one nor the other constitutes his exclusive activity, Tourism without one or the other being its exclusive activity. This regional context was formed on the one hand by the Tillian bend and the Sommam Valley, and on the other hand by the sea strip and the coastal plain, which, combined

with the rich historical context, witnessed the birth and then the development of the city of Bejaia. **Fig.V.7**.

The city reclines on the south side of Guraya Mount and has an extensive morphology on the floors, like an amphitheater. It is located from the Foothills of Guraya Mount in the North (150 m altitude above 672 m of the mountain) to its sea gulf in the south (Mediterranean Sea). It extends from East to West and southwest over the northern part of the Gulf in a semi-elliptical shape, at an average length and width of about 5 kilometers. This part of the territory lies between Cape Carbon in the East and Ighzer N'Themelaht (airport location) in the West, and it represents a flat strip section between the sea and relief of high and steep mountains. The site thus provides natural protection and defensive opportunity that justifies the construction of this large-scale city.

Because of its heterogeneous topography and Mediterranean climate, it has maintained a variety of terrestrial and aquatic environments. There are permanent and temporary rivers, the most important of which is Wadi Al Sommam. There are temporary pools such as Lake Tamilhat located near the Bejaia airport and about one kilometer east of the Wadi Sommam outlet.

The landscape of plants in the middle of a low-rise slope is shaped by traditional agricultural practices based on the maintenance of orchids (mainly olive trees) and small plots of family subsistence markets developed on the outskirts of populated areas. High mountain environments are generally covered with natural vegetation. There are shrub formations of mangrove oak (Quercus coccifera), holm oak (Quercus ilex), cork oak (Quercus suber), or Aleppo pine (Pinus halepensis). The plains form a mosaic of environments with a fertile sedimentary substrate; Intensively maintained gardening and fruit crops are natural coastal plant formations on the banks of rivers, especially along the Sommam Valley.

## V.4 Geology and structural geology of the region

On the geological level, the Bejaia region, belonging to the Tellian domain, presents a complex and diversified structure because of the overlaps recorded between the different formations. The various sedimentary formations have undergone tectonic deformations due to the alpine orogenic movements of the end of the Tertiary era and the beginning of the Quaternary. Overall, this region corresponds to the following major geological groups:

A. The geological formations of the Oligocene group: These formations are found mainly at the level of the slope which overhangs to the North, the Sommam wadi (High reliefs of Akfadou, Adekar, Tifra, Chemini, and low foothills overhanging the valley), and to a lesser degree in the coastal mountains of Beni Ksila, Toudja and Bejaia

   a) In Lithological terms, these formations consist exclusively of:
      - ✓ The sandstone, for the territories located on the slope which dominates to the North the Sommam wadi as well as the slope which dominates Cape Sigli (Adekar, Taourit Ighil, and Beni Ksila)
      - ✓ The flysch for the territories corresponding to Toudja and Bejaia.
   b) From an agroecological point of view, sandstone and flysch are moderately stable substrates and very favorable to the development of hardy arboreal and forest species.

B. The formations of the Cretaceous: These formations are concentrated mainly on the slope which succeeds to the south the alluvial deposits of the Sommam wadi

   a) Found also:
      - ✓ in the western coastal mountains: Beni Ksila, north Taourit Ighil, Toudja, and South of Bejaia
      - ✓ on the western end of Djurdjura: Beni Mellikech, Ighram and partially Chelata, Ouzellague.
   b) At the Babors level, these formations alternate with those of the Jurassic
   c) In Lithological terms, these formations are made up of:
      - ✓ Flysch and schists on the slope located to the south of the Sommam wadi
      - ✓ Flysch and soft limestones at Toudja and Bejaia
      - ✓ Conglomerates, on the western end of Djurdjura
      - ✓ Marls, hard limestones (dolomites), and conglomerates in the Nabors
   d) It should be noted that the marly substrates, which are widespread in the South of the Babors, combined with the slope of the land and the absence of perennial plant cover, give land susceptible to erosion and landslides.

C. Jurassic formations: These predominantly complex limestone formations correspond mainly to the Babors range

D. Miocene and Quaternary formations: These formations generally occupy the alluvial terraces and the low foothills which overhang them. They are mainly found in the Sommam valley, where Quaternary alluvial deposits rest on a tertiary substratum of Eocene marls. From an agricultural point of view, these formations correspond to land of agronomic value.

The following maps (**Fig.V.3,4**) are based on "SCE L'aménagement & l'environnement" www.SCE.fr, which focus on Bejaia municipality and the study area in geological and lithological terms. Eleven geological surveys were identified. They correspond to excavation made during the construction of public buildings. The **Table.V.1** summarizes the data collected at the different horizons. The limit of the last horizon surveyed indicates the starting depth of the hard rock.

Analysis of these maps and study area surveys provides the following insights:

1) The northern and northwestern part is dominated by marine chalk formations on a solid bed of hard limestone, resulting in permeable rocks with many possibilities of emanation and emergence from a permanent or temporary source. In other words, degraded valleys and pipes in this area can drain a large amount of groundwater and the water source.
2) The Quaternary continental formations dominate the southern and southeastern part. These are silts and sands resulting from the deterioration of rocks formed in the marine sedimentation ages mentioned above. This type of formation is often characterized by a weak backfill layer with a wetland formation on the surface as in the swampy area of Sidi Ali Aorta. These substances are quickly saturated with water and are not very stable, which leads to practical consequences for sewer pipes laid at this level, Permanent danger for surface water drainage, and hazards of earth movement that puts pressure on the pipes, which could lead to their deterioration (cracking) or even breakage.
3) The soundings indicate zero or low aggressiveness of the subsoil: there is little or no risk of chemical degradation of the pipes from the outside.
4) Surveys n°2 confirm the analysis of the southeastern part, with the risk of clear water leaking into the pipes and the risk of breakage or cracks in the pipes.
5) The Third, and the Eleventh surveys, located in the upstream part of Wadi Seghir, indicate that the pipes are most often positioned in backfills (horizon 2.5 - 3.0 m) and for the deepest in layers clayey sands and gravels leading to the risk of temporary intrusion of clear water and constraints leading to the risk of breakage or cracks.
6) The surveys n°1,4,5,6, and seven located at the level of the Salomon wadi indicate that the pipes are most often positioned in backfills (horizon 0.5 - 2.5 m) and for the deepest in clayey layers saturated with water, hence the risk of permanent intrusion of clear water and stresses leading to the risk of breakage or cracks.
7) The surveys n°8,9, and ten located at the level of the wadis Romaine and Bois Sacré indicate that the pipes are most often positioned in backfills (horizon 4.5 m) and for very deep in

layers of schist from where risks of temporary intrusion of clear water. However, the complicated nature of the rocks entails a slight risk of breakage or cracks.

## V.5 Hydrogeology

A study carried out by the Directorate and Means of Alluvial Resources (DMRA) revealed the existence of a water table extending from Cheurfa (Wilaya de Bouira) to Oued Ghir (Wilaya de Béjaia) (AGEP, 1999). This water table is divided into two parts by a geological threshold at Sidi Aich, constituting a hydraulic barrier. The static volume of this water table is estimated at 1,600 billion m3. The study of fluctuations in the piezometric levels of the alluvial aquifer showed that the Sommam wadi drains the aquifer and that the tributaries influence the aquifer's recharge. The surface flow of the wadi and the direct precipitation on the alluvium ensure the infiltration towards the water table. Thus, the system formed by the Sommam wadi and its tributaries plays a vital hydrological role (recharge of the underground aquifer, regulation of flows, and mitigation of downstream flood risks).

In the region, we can distinguish among the aquifers:

1. Alluvium at the bottom of the valley;
2. The filling of alluvial cones in the foothills of the left bank (on the right bank, they are reduced or absent and are formed of fine particles of clay and silt);
3. The formations in place include the karst limestones of the Jurassic, the conglomerates of the Miocene, and the sandstones of the Secondary and Tertiary.

The Valley of the Oued Sommam has geomorphology that has the shape of an elongated "gutter" and is inclined transversely (North-South) and longitudinally (West-East). Under the alluvium, of the continental conglomerate Miocene which outcrops on the southern flank of the Djurdjura. This Miocene presents coarse levels (pebbles and gravels) alternating with sandy or gravelly clays.

The lateral facies variations seem to be very rapid there. It would therefore seem that the Miocene-Cretaceous contact plunges rapidly going north. The calcaneo-marly Cretaceous, which outcrops on the right bank of the Oued Sahel, can be considered the impermeable limit or substratum of aquifer formations. Note that the distinction between alluvium and conglomerate Miocene is difficult to make, the lithology of its two formations being identical.

The alluvium forms a continuous band from the village of Chorfa (in the West) to Sidi Aich (in the East), having an area of about 120 km², a length of 45 km, and variable width. It is maximum in the vicinity of Tazmalt and Akbou: 4.5 km, and minimum in Takrietz and Sidi Aich: 150 to 200 m. Between Sidi Aich and Oued Ghir at the limit of the deposits of the Bejaia delta, the area is 75 km² for a length of 28 km and a variable width ranging from 1 km to 3 km. The downstream part of Oued Ghir and the Bejaia delta has an area of 40 km² with a length of 10 km and a width ranging from 2 to 4 km. It is formed by a filling of practically impermeable fine sediments. The entire band of alluvium of Chorfa, passing through Akbou, Sidi Aich, downstream of the Oued Ghir and even up to the mouth, has an area of approximately 235 km² for a total length of 83 km, and variable width. The limits of the aquifer system are formed by the natural course of the cones of excreta and alluvial terraces

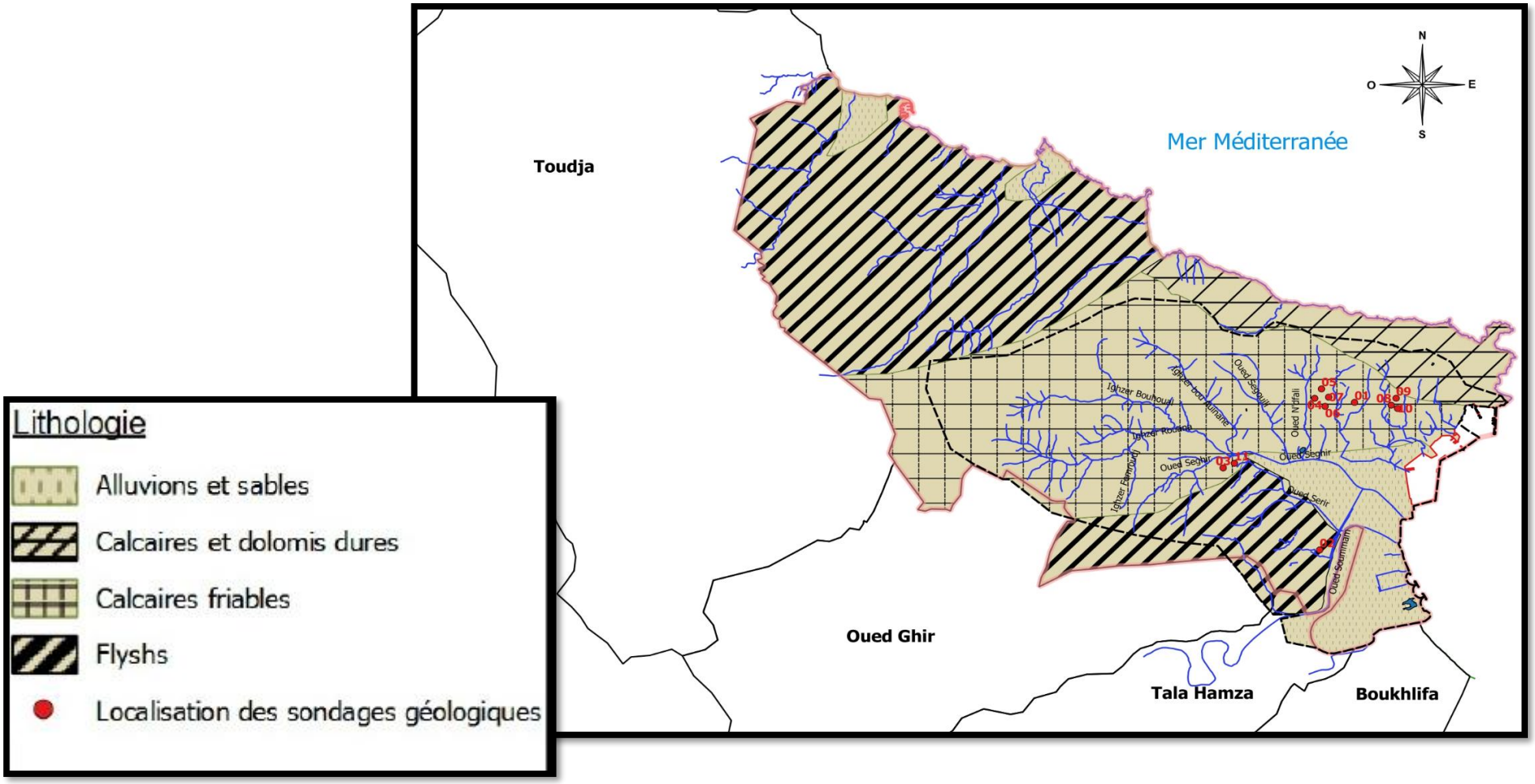


Figure V-3 Soil map of the study region

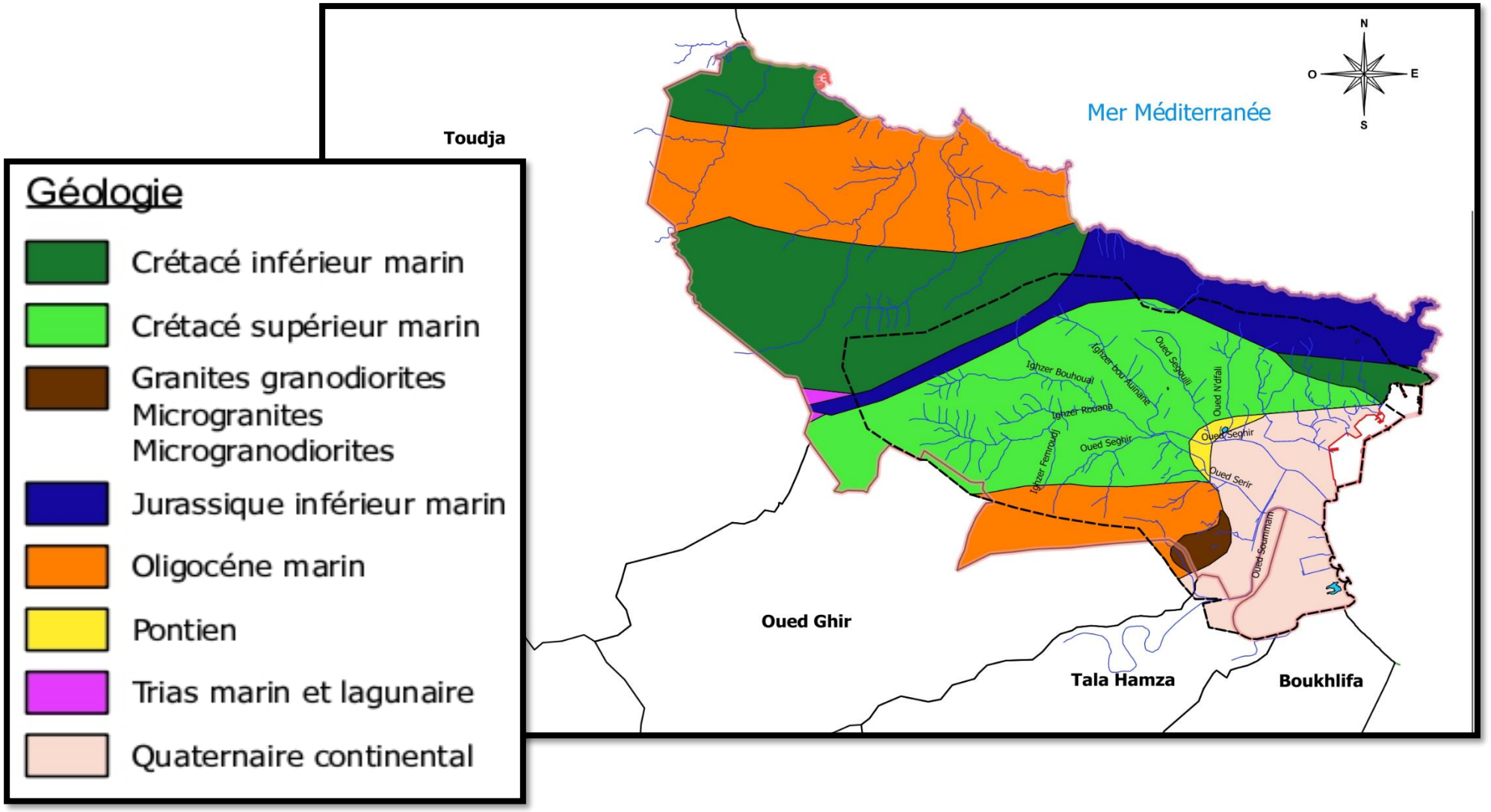


Figure V-4 Geological map of the study region

Table V-1 Inventory and description of geological surveys (SCE)

| Code | Nom de station | Horizon1 | | Horizon2 | | Horizon 3 | | Horizon4 | | Comments | Soil capacity |
|---|---|---|---|---|---|---|---|---|---|---|---|
| | | Depth (m) | Description | Depth (m) | Description | Depth (m) | Description | Depth (m) | Description | | |
| 1 | Ain Harar Library | 0,4 | backfills | 2,5 | Micaschists and schists superficially altered in clay | - | - | - | - | le sol est très plastique, de faible teneur en eau, d'agressivité nulle | 3 bars |
| 2 | "Chouhada Hammoum school canteen" | 2,8 | gravelly sand, all-terrain, alluvium | 4,2 | "Plastic clay" | 9,0 | Clayey marl, marly clay | - | - | sol avec une plasticité variable et d'agressivité nulle | 1 bars |
| 3 | TAKHRIBTH school canteen | 2,8 | backfills | 6,0 | "sandy gravelly marly loam" | 9,0 | pebble sand gravel of dolomitic sandstone origin associated with gray friable silts | - | - | un sol peu plastique saturé d'une agressivité nulle | "0.5 bars of 0-4 m, 1.0 bars over 4 m " |
| 4 | Sidi Ahmed S01 Mosque | 2,0 | backfills | 6,0 | "Marly silt" | 10,0 | Silty marne | 12,0 | Marne with calcite | le sol est: très plastique, sol saturé, agressivité nulle | 1.5 bars |
| 5 | Sidi Ahmed S02 mosque | 3,5 | backfills | 15,0 | "Marly silt" | - | - | - | - | le sol est: très plastique, sol saturé, agressivité nulle | 1.5bars |
| 6 | Local market Sidi Ahmed S01 | 2,5 | backfills | 3,2 | Slope scree (clay, silt, boulders) | - | - | - | - | agressivité nulle | 1.5 bars |
| 7 | Local market Sidi Ahmed S02 | 2,2 | backfills | 3,0 | Slope scree (clay, silt, boulders) | - | - | - | - | agressivité nulle | 1.5 bars |
| 8 | Sidi Oali S01 Mosque | 4,5 | backfills | 7,0 | Marly schist of brown color | 8,0 | Marly schist of dark brown to gray color | 9,0 | Gray marl schist | un sol peu plastique, partiellement saturé d'une agressivité faible | - |
| 9 | Sidi Oali S02 Mosque | 4,5 | backfills | 7,0 | Marly schist of brown color | 8,0 | Marly schist of dark brown to gray color | 9,0 | Gray marl schist | un sol peu plastique, partiellement saturé d'une agressivité faible | - |
| 10 | Sidi Oali S03 Mosque | 4,5 | backfills | 7,0 | Marly schist of brown color | 8,0 | Marly schist of dark brown to gray color | 9,0 | Gray marl schist | un sol peu plastique, partiellement saturé d'une agressivité faible | - |
| 11 | TAKHRIBTH Gateway | 2,5 | backfills | 5,0 | marly silt | 9,0 | compact marl and small pebbles of a beige dolomitic nature | - | - | un sol peux plastique, saturé d'une agressivité faible | 1.2 bars |

The distribution of the piezometric wells shows two main directions of groundwater flow from the alluvial infill. In the longitudinal direction, the water table flow is from southwest to north-east, per the direction of the flow of surface water. This flow characterizes the hydrogeological

basin's central circulation of the alluvial filling, from upstream to downstream. This circulation reflects a flow that takes place from the water table towards the sea. According to the transverse direction to the valley axis, the water table's flow is from the edges towards the center of the plain, following two directions of circulation, NS and SN. These two directions of circulation reflect the lateral contributions from the slopes, which border the alluvial infill layer. In general, the main water table flow converges from upstream to downstream and becomes divergent in the coastal plain of Bejaia. The **FigV.5,6** Show the upper and lower Sommam valley.

## V.6 hydrography and watersheds

Before reaching the Mediterranean, the most critical wadis and rivers cross an alluvial plain varying from 100 m to 1000 m in some places. For the other Wadis, the downstream part of their watercourse is almost non-existent, with a minor riverbed roughly significant in the hillsides dominating the alluvial plains. These small streams were being lost in their natural state in multiple small ditches before even reaching the alluvial plain, thus promoting the deposition of terrigenous materials. These small gullies are now more or less channeled.

Many wadis and chaabat across the study region. This large number of streams results from the natural topography, together with an abundance of rainfall.

- The watercourses originating from the Gouraya mountains from the northern side which are: *Oued ouchaalal, Oued romaine, Oued danous, oued Salomon.*

### *V.6.1 Oued ouchaalal*

Oued Ouchaalal originates from the heights of Djebel Guouraya and flows into the first undeveloped Retention Basin located at the level of the Guouraya gateway. The wadi continues its path until the retention basin. Its path continues to the collector of *Sidi-Abd-el-kader*. That watercourse has experienced the same overflow problems in urban areas during the dry seasons. This has been successfully eliminated by the effect of cleaning and flushing of all the waterways by the services of the municipality of Bejaia

### *V.6.2 Oued Romaine*

Oued Romaine takes its origins from the heights of Jebel Guouraya. The tributary is quite essential; it flows into the DANOUS wadi. The wadi crosses the road in culverts; the flow continues in a rectangular channel Broken in places by steep waterfalls that accentuate the flow, causing inconvenience to the downstream at the Covered Market (slightly above). There is also

the presence of city containers on the river and slums on the wadi banks. Then he continued his journey buried in the ground.

### *V.6.3 Oued Danous*

The Oued DANOUS originates from the heights of the city MOULLA. The Upstream is in its natural state; it becomes channeled from la Liberté City to boulevard MOULAY EL NACER City, where it returns to its natural state. The DANOUS wadi meets downstream with the SAL-LOMON wadi to form a single wadi (outlet) and emerges towards the sea.

### *V.6.4 Oued Salomon*

Oued SALOMON takes its origins from the heights of the GOURAYA mountains; it is also located on the right side of wadi Romaine and contributes to the direction of the flow of Wadi Romaine. Twelve (12) crossings from Dar Nacer on Boulevard des Martyrs to the outlet (the sea). This wadi runs along with the place Ahraroub. With a zig-zag shape. It is full of scrub in its Natural State. The first sections of the wadi are in their natural state, but the rest is a trapezoidal canal. Then the wadi is laid out in the form of (U) with slabs near the polyclinic. The canal follows its path to the Retention Basin located at the Naceria traffic circle. From there, the canal continues towards the Aures route. It continues as a canal built throughout the barracks. At the end of the barracks, it returns to an artificial open channel until it meets the Danous wadi and enters under the port.

- Wadi Seghir is the main watercourse of the municipal territory. The morphology in this region is characterized by an average hillside inclined from the East towards the sea. A hydrographic network chisels these slopes with a generally sub-equatorial orientation. Wadi Seghir takes origins from the Bouzegua mountains western, and it is the most significant urban wadi that crosses the urban areas and flows into the sea directly. It separates from the Wadi Serir just before the most urbanized areas of Bejaia then directly joins the sea bypassing the central industrial zone to the North. Five rivers are connected to this wadi which originates from Tazeboujt. The watercourse is then channeled with a succession of overhead or covered (buried) passages. Overflows are possible during special rainy episodes, especially when hurdles accumulate on the gates. In the downstream part, the concomitance of extreme rain events and exceptional tides can generate overflows. In the upstream part of the watershed and to the right of the confluence of three small wadis, earthworks barring the entire valley bottom have been carried

out without the existence of a drain. This area has been classified as a high hazard. At mid-height of the watershed, an exceptional flood and/or the formation of alluvial deposits can generate overflows on the roadway and then flood neighboring dwellings. In the downstream part, overflows may occur at the confluence of the plain channels with the Seghir wadi. Oued Seghir is the first wadi that takes the name of the wadi Serir and runs along with the city of Bejaia; after the development of the wadi Serir, it has taken as an overfull service for the wadi Serir as one of their functions.

- Oued Serir is the best developed compared to the other existing wadis in Bejaia; it originates from the sand trap and flows into the Sommam wadi. Along this wadi, several tributaries apart from those which discharge, at the junction of Oued Boukhiama and Oued Taghzouit, such as (wadi Ihadaden, wadi N'savone, wadi Bir Sellam) and several discharges from factories (factory of manufacture of concrete products).

## V.7 Urban Framework Revolution

The diversity of architectural styles and urban forms of Bejaia is explained by the wide variety of urban cultures that have successively shaped its historic landscapes. For some civilizations, the intervention was partially part of the continuity (the medieval period from the 11$^{th}$ to the 16th century), unlike the interventions with a colonialist tendency, the impact of which was radical. The period of the Spanish invasion was marked by the destruction of almost the entire urban surface (around 2/3), followed by that of the Turks who had delivered what remained to abandonment and ruin. At the same time, the French intervention adopted a development plan with straight axes, in total contrast to the existing network of winding streets and alleys forming a labyrinth.

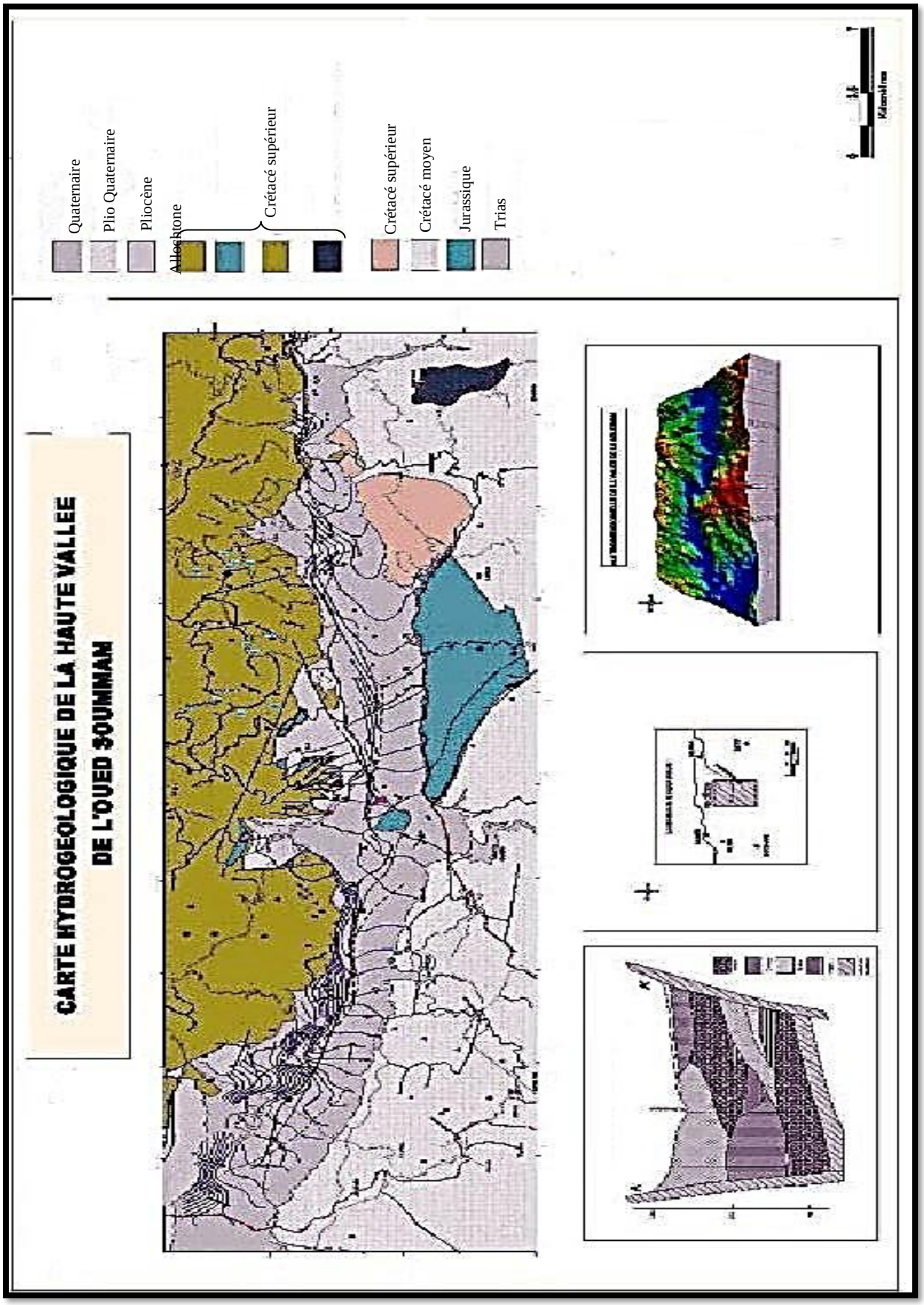


Figure V-5 Hydrogeological map of the upper valley of the Sommam wadi

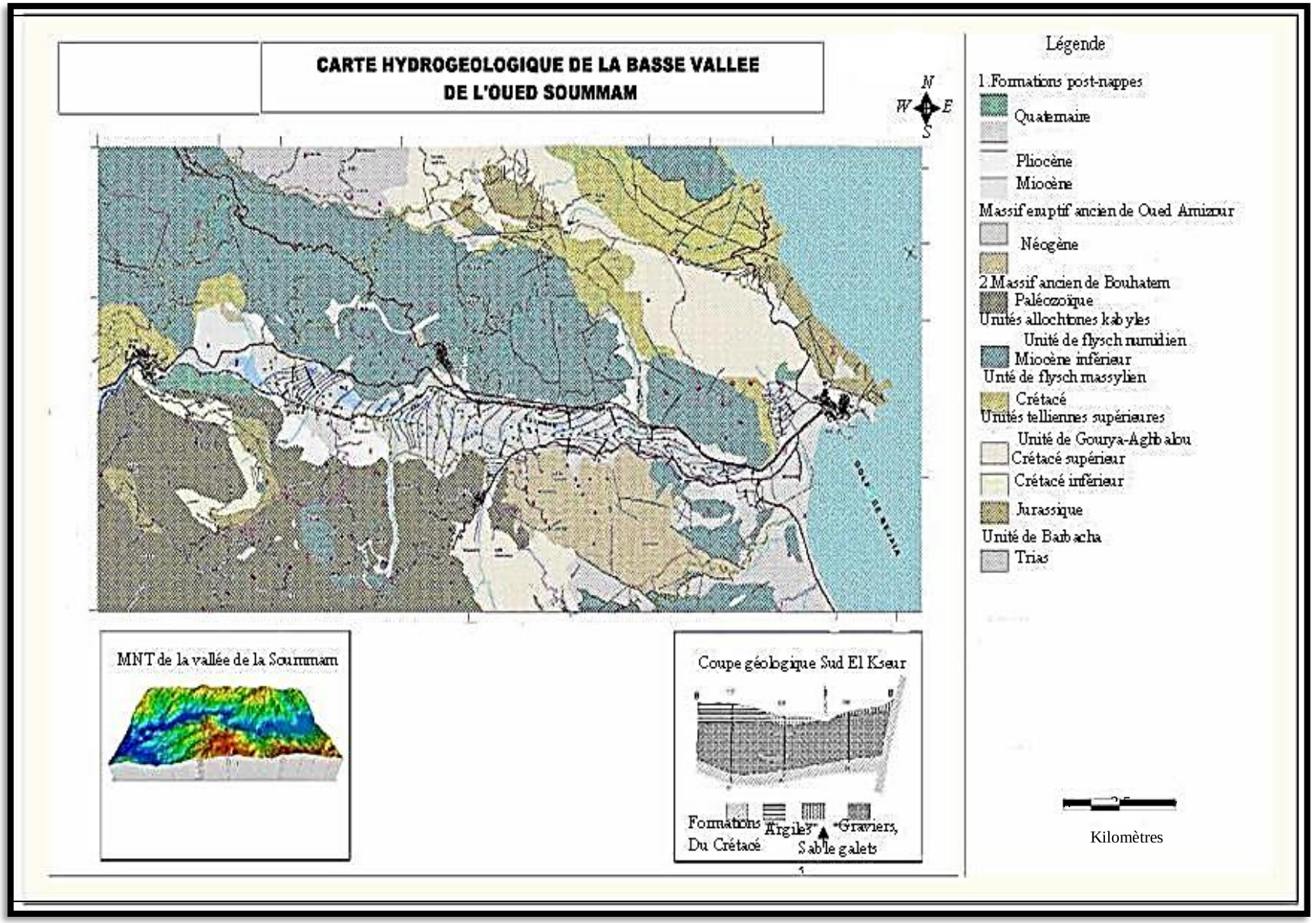


Figure V-6 Hydrogeological map of the lower valley of the Oued Sommam

➢

Figure V-7 Alignment plan of French military engineers in 1854

The new structure established in 1846, like the urban forms newly produced in Europe, particularly in France, would produce a radical upheaval in the urban landscape of Bejaia, partly replacing the old layout with medieval connotations. It was not a question of operations of rehabilitation or restoration via the existing profile, but actions of redefinition of the urban

landscape according to the European colonial model, through operations of destruction and reconstruction, transformation, reallocation, and urban renewal.

The geometrical rigor adopted for the alignment plan of 1854, as shown in **Fig.V.7**, resulted in a network of straight and more or less orthogonal axes materialized by the drilling of vast well-aligned paths through the medieval fabric.

Western-style town planning brought upheaval as well as the image that the city partly retains today. Following radical restructuring operations, the city was endowed with a central space clearly defined by establishing administrative and socio-cultural entities. The properly central space has grown in size and has entered the interior of a renewed urban structure. The port would resume its determining character after its role was reduced by the Turks, accentuated by the presence of a strong connection with the hinterland represented by the plain. The urbanization of the post-independent city was marked by the urgency of alleviating a need for reconstruction and response to the needs of the local population and those resulting from the rural exodus in terms of infrastructure, housing, and services. Accelerated urbanization was followed by various urban planning instruments (Master Plan, PDAU, POS), which focused on quantifying needs and planning actions and spaces necessary for their satisfaction. We are witnessing the emergence of fragmented urban complexes with unique functions.

The administrative axis that materializes the Liberty City, relieved the original core of its functions of control and power by capturing most of the administrative equipment (the seat of the Wilaya, the post office, the seat of the assembly communal popular, and various services). It is this axis that functionally constitutes a centrality that characterizes the administration. However, their juxtaposed form is relatively poor in composition and takes the form of ghettos devoid of any architectural significance and urban animation **Fig.V.9.** The development of the city by extension towards the western sector of the plain was carried out mainly through housing. Its current surface is multiplied by almost seven in a quantitative spread, without a coherent urban structure, a dominant function, and a spatial reference mark. To this extension model, we must add the informal growth, which has produced extensive areas of illegal housing (50% urbanization in some areas), in total lack of aesthetics, meaning and are never completed.

The development and extension of Bejaia city from the medieval period to the present state are shown in **Fig.V.9.**

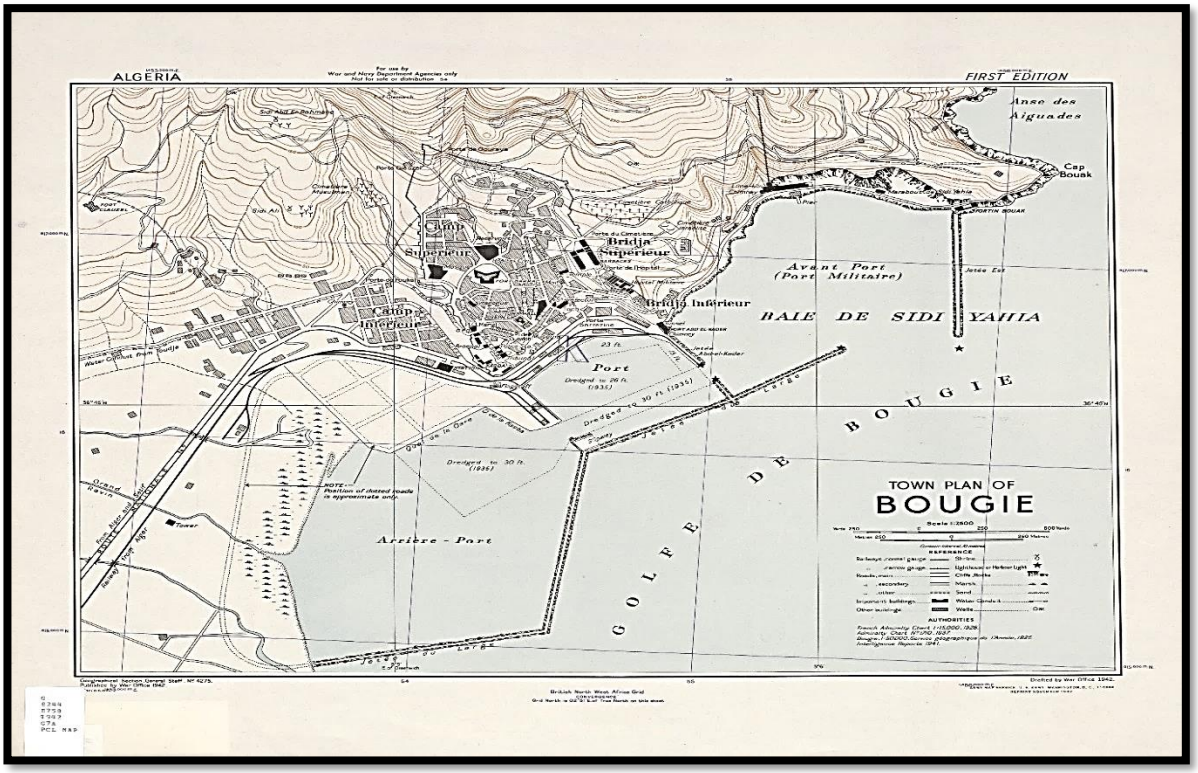


Figure V-8 Plan of Bejaia City in 1942, source (Northern African encyclopedia 1830-1962)

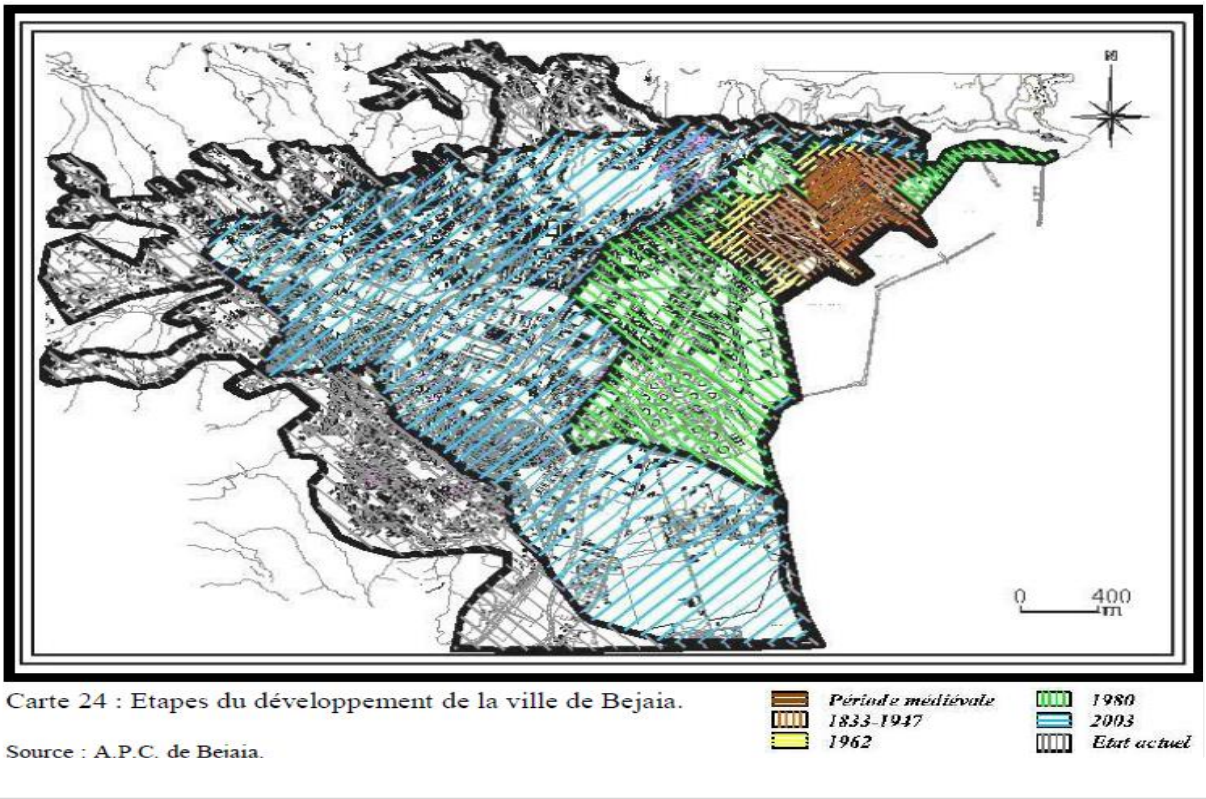


Figure V-9 The successive addition of urban zones towards the north-west

## V.8 Economy And Equipment

Due to its geographical location, the city of Bejaia represents the most crucial industrial pole in the region, concentrating many industries due to the presence of one of the largest oil and commercial ports in the Mediterranean. Indeed, the city of Bejaïa has an international trade port. Today the main activity of the port is the export of hydrocarbons. However, the city of Bejaia serves as a local market, particularly in local craft products and agricultural products, which are sometimes exported. The port of Bejaia is the most important in the country in terms of volume of activity behind that of Algiers. The city of Bejaïa also benefits from a peach port activity. It is one of the sectors set to develop in the future. The city of Bejaia also benefits from the agricultural production of the Kabylie region by having the role of local market or even export of products, with olive growing, fig production, and beekeeping. At the national level, it is the headquarters of certain agri-food companies such as Ifri and groups such as Cevital that have settled there. In terms of craftsmanship, the city mainly benefits from the local production of pottery. The city of Bejaïa also tries to exploit its magnificent Mediterranean coast and its historical heritage to develop a tourist activity. However, the majority of tourists are Algerians or immigrants from the region.

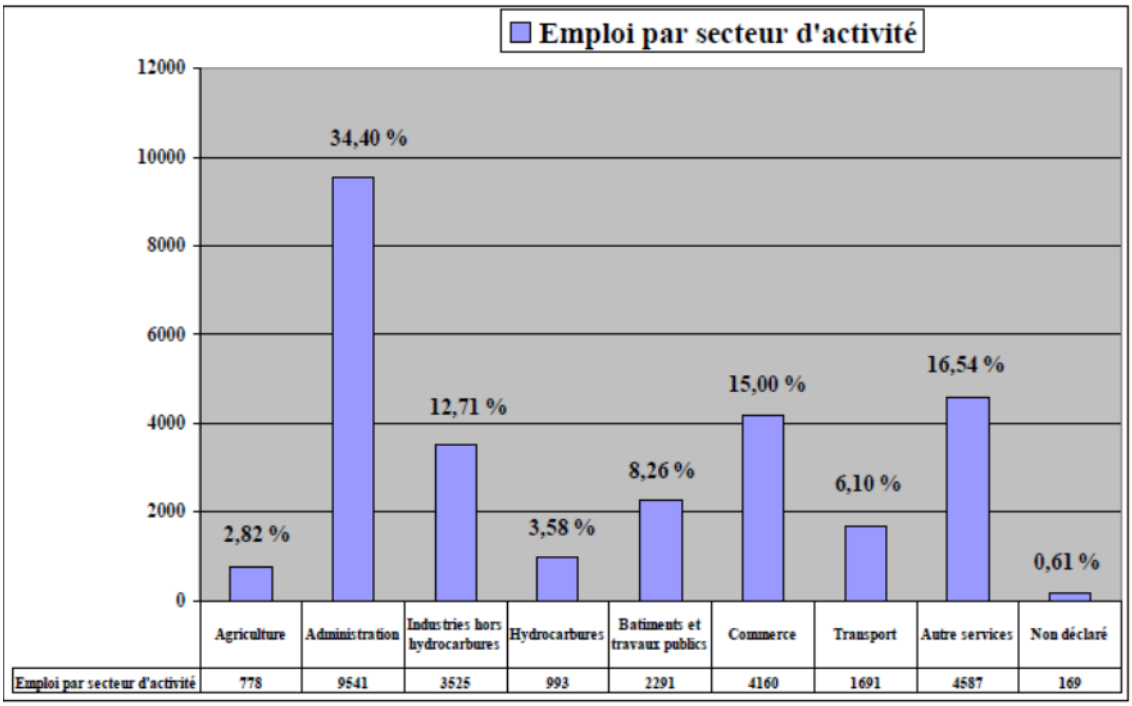


Figure V-10 Employment by sector of activity

Bejaïa has a university named after Abderrahmane Mira (an Algerian war martyr). The establishment has a staff of 698 teachers for 22,792 students (2006). Following its promotion as the capital of a Wilaya in the administrative division of 1984, the city of Bejaia was endowed with all the representative institutions and services of the state (a seat of the Wilaya, a court, new seats of daïra and town hall, etc.). It becomes an administrative center for 700,812 individuals, and the evolution of needs since, by an annual growth rate always positive (2% on average), gradually increased the share of the administrative function which occupies today the top of all other activities. **Fig.V.10.** shows that 35% of the working population is in administrative work, 25% of which is in the service sector. This situation can reinforce a tertiary vocation in support of the promotion of its tourist vocation. These two potentialities should constitute the strategic support for the city's development, especially as an observation on the site shows that an essential part of the services is that of the central administration. Nevertheless, the spatial materialization of this sector is marked by a very dispersed distribution for certain service activities and too concentrated for sure others, accentuating the spatial imbalance by that of the functional.

## V.9 Climatological characteristics of the study area

The control of water in a particular area is linked to the phenomena which govern surface and groundwater and the climatic conditions that play a determining role in stream water regime. The study area is characterized by a Mediterranean-type climate. Its climatic depends on meteoric precipitation and temperature. The significant changes in topographical elevation over short horizontal distances give rise to a large variety of local climatic conditions of the study area. It is well known that the amount of precipitation and available energy are the actual controller of the evapotranspiration rate and therefore surface runoff for the annual scale (Arora, 2002; Budyko, 1974; Zhang et al., 2004; Zhang et al., 2008). Precipitation is a fundamental component in hydrology. Their measurements and exhaustive studies are essential for understanding the wadis regime, the state of soil water reserves, and groundwater recharge. Runoff is one of the most important variables in hydrological processes, both in space and time (at annual, monthly, and daily scales).

Rainfall remains the most crucial factor in this regard. It intervenes by:

- The total annual height, which determines the river abundance.
- The monthly and seasonal distribution, which has a direct influence on the hydrological regime.

In addition to precipitation, we mentioned other climatic factors, which are the temperature and evapotranspiration, necessary for developing the water balance. Air temperature is a major climatic factor in estimating evapotranspiration; it represents a variable allowing the description of the climate of a given region. The study of temperatures is necessary as they affect a large number of factors. They have a powerful influence on the distribution of vegetation.

### *V.9.1 Temperature*

The Maximum temperature degree is raged between 22 and 45 °C, the heigh temperatures occurred in summer season May, Jun, July, and August. Where the temperatures reach their maximum degrees in these months. the mean temperature is about 18 °C, and the minimum temperatures occurred in Mars by -7 °C, the maximum minimum values is 10 °C which occurred in July.

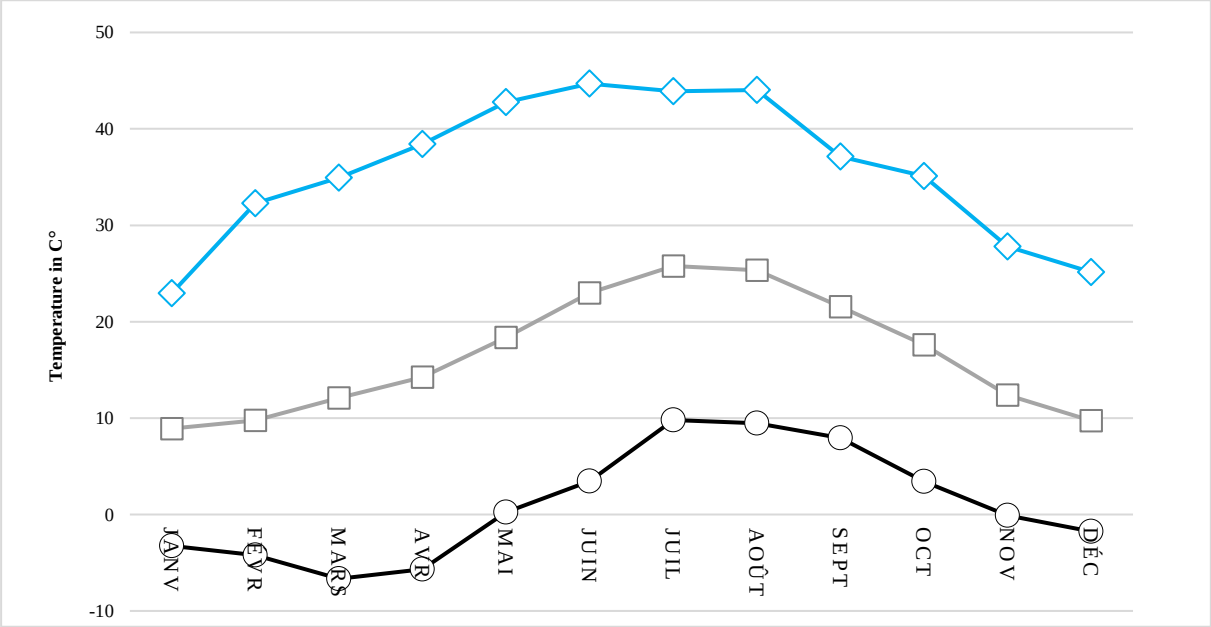


Figure V-11 Minimum, Maximum, and Average temperature (C°) for the study region (x=5°, y= 37°) for the period (1979-2014)

### *V.9.2 Wind*

Wind is an important feature of climate. Its action is accompanied by more or less accentuated evaporation on the surface of the soil and the drying out of the plant cover.

The maximum values of wind that reached between 2.4 and 2.8 m/s is occurred in the winter season such as November, December, January, and February. While the minimum values occurred in May, September, and October.

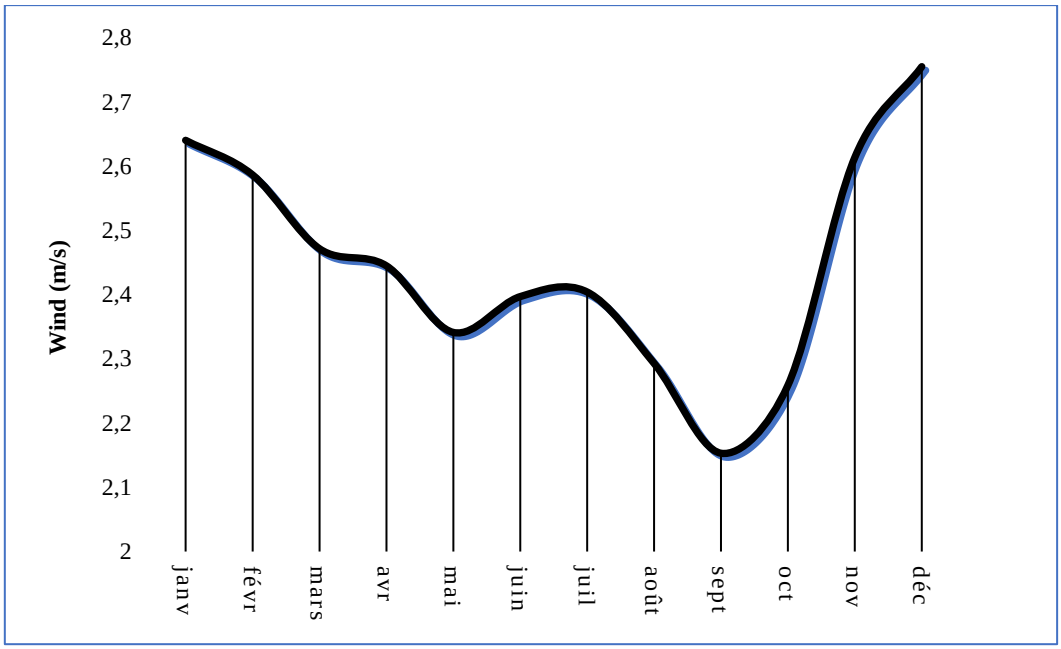


Figure V-12 Average of wind speed (m/s) for the study region (x=5°, y= 37°) period of (199-2014)

### *V.9.3 Rainfall characteristics and variability*

Rainfall is one of the key components of the hydrological cycle and is severely affected by the globe changing climate. Climate change altered the spatial and temporal variability of mean annual and seasonal rainfall (Deng et al., 2018). The Mediterranean region is considered the most affected by the globe warming. Giorgi (2006) classified the Mediterranean climate region as a hot-spot point since it is the most responsive to future globe warming. For the majority of Mediterranean regions, these variations have resulted in significant precipitation decreases, with an augmentation of exceptional phenomena such as severe droughts, and flash floods.

### *V.9.4 Annual rainfall, Mean of Annual Rainfall, and Monthly Extreme Rainfall*

Annual rainfall is the sum of total rainfall within a hydrological year. Average annual precipitation – the climatic normal – is the average annual depth of precipitation that falls at a given point, measured over several years.

The annual rainfall is an important indicator for many hydrological phenomena and is used to estimate several climatological and hydrological indices. It is an important indicator for the hydrological and hydrogeological water balance models as they are considered the main component the of water balance equation. It is used also for the classification of bioclimate floors.

It is important to predict annual, seasonal and other scales in the water resources management. Thus, we analyze the Annual Rainfall AR, Mean Monthly Rainfall MMR, Mean Annual Rainfall MAR, and Finally Monthly extreme rainfall MER. A single rain gauge was chosen for the study area, as the study watershed is a small basin (11.84km$^2$). for that, we decide that one single rain gauge is largely sufficient. A scattergram and boxplots curve were chosen to represent the mean annual rainfall of the wadi Sghir watershed between the period 1979-2014 as shown in **Fig.V.14**

$$AR = \sum_{i=1}^{12} MR \qquad (3)$$

$$MAR = \sum_{i=1}^{12} \frac{AR}{12} \qquad (4)$$

$$MER = max(MR_{i=1,12}^{j=1,m}) \qquad (5)$$

$$MMR_{i(1,12)} = \frac{\sum_{j=1}^{m} MR_j}{M} \qquad (6)$$

AR: Annual Rainfall;

MR: Monthly Rainfall;

MMR: Mean of Annual Rainfall;

MER: Monthly Extreme Rainfall;

MMR: Monthly Mean Rainfall;

M is the total number of record years, j corresponding to value of each year for one month

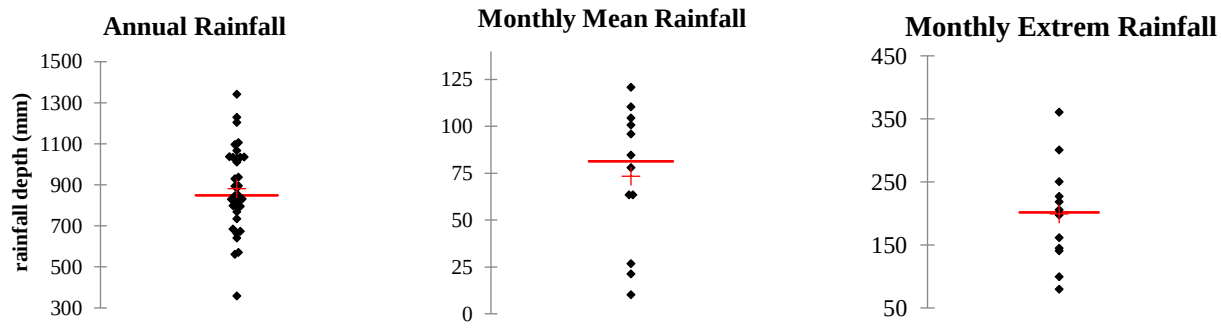


Figure V-13 . A scattergram of AR, MMR, and MER for the study region (1979-2014)

The **Table.V.2** shows the statistical description of the total annual rainfall AR and Mean annual rainfall MAR and the Monthly Extreme Rainfall MER, and Mean Monthly Rainfall MMR. The equation (3), (4), (5) and (6) are used to calculate these parameters. The minimum value of rainfall is recorded in July which indicates that almost no rainfall in the summer, the mean value is 10.26 and the maximum value is 79.72 This is explained by all the rain falling in a short period or almost in a few days. The *Cv* which equals 1.53 (The biggest of all months) is supported that interpretation, indicate necessarily the high temporal variability of rainy days in the summer season. By effect of very high temperatures the convective uplift is occurring.

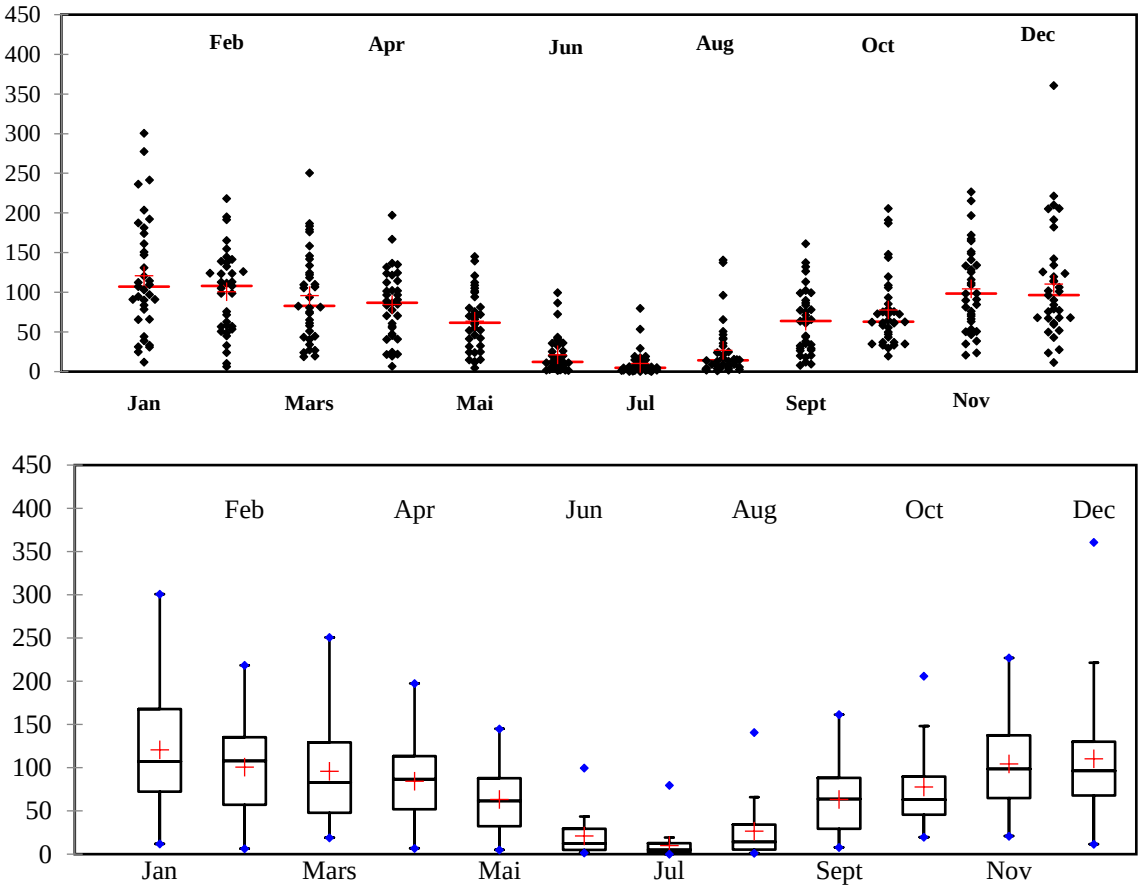


Figure V-14 scattergram (above), and boxplots (bottom) of mean annual precipitation of wadi sghir catchment for the period between 1979 and 2014. The measure point located in ***(long=5, lat=36.69, elev=117)***

### *V.9.5 Monthly rainfall variability*

The mean monthly rainfall of 36 years of the rain gauge located within the wadi Sghir watershed is analyzed. The monthly variation of mean monthly rainfall and temperature is presented by the Ombro-thermic curve that summarize trends in temperature and precipitation for the last 36 years, they also allow to establish a relationship between temperature and rainfall and to determine the length of dry, wet, and extremely wet periods. When the temperature curve runs above

the precipitation there is dry season, whereas, when the temperature curve runs below the precipitation histograms there is wet season. The dry season is occurred in May to October, and the wet season occurred from January to April, November, and December. The mean annual rainfall reached the 100 mm January, November and December. We can say that there is no rainfall in the dry season and the temperature exceed than 25°C.

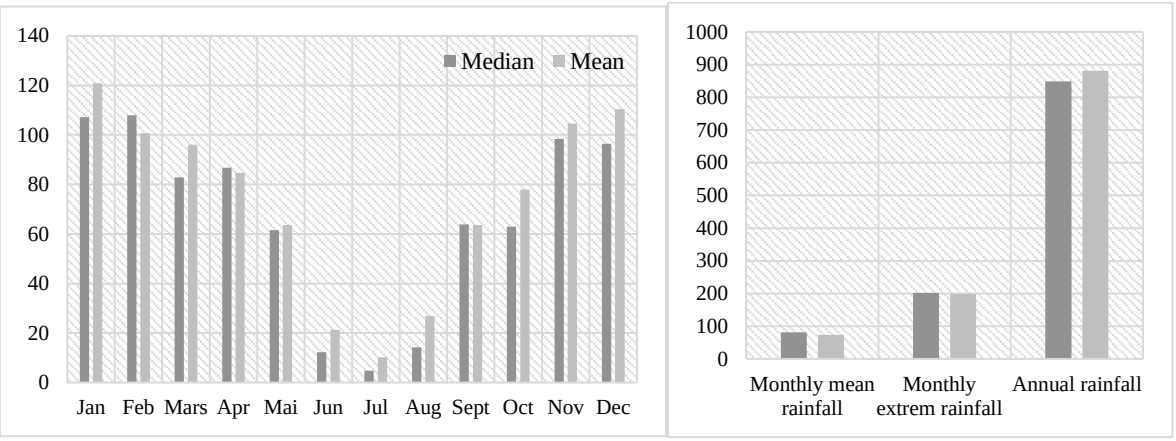


Figure V-15 Median and Mean of mean annual precipitation (Left), and MMR, MER, and AR (Right)

Table V-2 Statistic description of the rain gauge point measurement (1979-2014)

| ***Statistic*** | ***Min*** | ***Max*** | ***1st Q*** | ***Med*** | ***3rd Q*** | ***Sum*** | ***Mean*** | ***Variance*** | ***Sdr. Devi*** | ***CV*** |
|---|---|---|---|---|---|---|---|---|---|---|
| ***Jan*** | 11.88 | 300.75 | 72.41 | 107.15 | 167.96 | 4231.69 | 120.91 | 5211.12 | 72.19 | 0.60 |
| ***Feb*** | 6.36 | 218.42 | 57.03 | 108.00 | 135.20 | 3523.96 | 100.68 | 2710.24 | 52.06 | 0.52 |
| ***Mars*** | 18.99 | 250.68 | 47.85 | 82.86 | 129.25 | 3360.15 | 96.00 | 3185.32 | 56.44 | 0.59 |
| ***Apr*** | 6.88 | 197.47 | 51.76 | 86.79 | 113.36 | 2963.27 | 84.66 | 1870.41 | 43.25 | 0.51 |
| ***Mai*** | 4.99 | 145.04 | 32.19 | 61.59 | 88.02 | 2224.98 | 63.57 | 1374.42 | 37.07 | 0.58 |
| ***Jun*** | 1.65 | 99.71 | 4.81 | 12.22 | 29.40 | 744.68 | 21.28 | 563.87 | 23.75 | 1.12 |
| ***Jul*** | 0.17 | 79.72 | 1.77 | 4.80 | 12.64 | 359.06 | 10.26 | 247.76 | 15.74 | 1.53 |
| ***Aug*** | 1.26 | 140.74 | 5.13 | 14.26 | 34.14 | 940.34 | 26.87 | 1184.96 | 34.42 | 1.28 |
| ***Sept*** | 7.91 | 161.39 | 29.29 | 63.82 | 88.27 | 2224.35 | 63.55 | 1600.03 | 40.00 | 0.63 |
| ***Oct*** | 19.64 | 205.76 | 45.47 | 62.92 | 89.52 | 2729.86 | 78.00 | 2177.32 | 46.66 | 0.60 |
| ***Nov*** | 20.97 | 226.94 | 64.94 | 98.40 | 137.61 | 3658.31 | 104.52 | 2813.16 | 53.04 | 0.51 |
| ***Dec*** | 11.60 | 360.54 | 67.71 | 96.47 | 130.05 | 3866.15 | 110.46 | 4840.45 | 69.57 | 0.63 |
| ***MMR*** | 10 | 121 | 54 | 81 | 102 | 881 | 73 | 1255 | 35 | 0.483 |
| ***MER*** | 80 | 361 | 144 | 202 | 233 | 2387 | 199 | 6011 | 78 | 0.390 |
| ***AR*** | 359.13 | 1341.39 | 781.17 | 848.63 | 1034.25 | 30826.81 | 880.77 | 41033.03 | 202.57 | 0.230 |

**The Fig.V.15 (the left one)** Is a histogram compare the median and the mean of the MAR data, we observe that these two statistics are closely equal, therefore, data excluding random fluctuations, and it is invariant with respect to time the same as **fig.V.15 (the right one).** It is argued that systems for management of water throughout the developed world have been designed and operated under the paradigm of hydrologic stationarity. The stationarity assumption suggests that hydrologic variables have time-invariant probability density functions whose properties can be estimated from the instrumental record. Given the magnitude and time lags of climate change associated with the buildup of greenhouse gases, stationarity may indeed be dead (Teegavarapu, 2019). The **Fig.V.13** also indicates the stationarity of time series data as they not contain a significant outlier, in the major of data the outlier is replicate the third quartile.

One can observed from the table that the high coefficient of variation occurred significantly in the dry months (Jun, July, and august), which indicate the high temporal variability distribution over the one month. All precipitation can occur in one day or over separated few days, and characterized by high intensity over short period of few minutes to one hour. This variability explained by the thermal contrast land surface- Mediterranean Sea.

### *V.9.6 Aridity indices*

Aridity is the degree to which a climate lacks effective, life promoting moisture; the opposite of humidity, in the climate sense of the term (Chahine et al., 2006) An aridity index is defined as the numerical indicator of the degree of dryness of the climate at a given location and it classifies the type of climate in relation to water availability. The higher the aridity indices of a region, the greater water resources variability. The increasing aridity represents a higher frequency of dry years over an area (Deniz et al., 2011).

#### *V.9.6.A De Martonne Index IDM*

De Martone Index (De Martonne, 1926) is a climatological function, used for determining the evaporating power of the air from the temperature. Evaporation being considered as a linear function of temperature. De Martone classify the climate stages according to water availability and temperature degree. their equation defined as:

$$IDM = \frac{P}{(Ta + 10)} \qquad (7)$$

where P is the annual amount of rainfall (in millimeters) and Ta is the mean annual air temperature (in degrees Celsius).

Table V-3 Climate aridity according to De Martone index

| ***Climate type*** | ***IDM values*** |
|---|---|
| Arid | IDM < 10 |
| Semi-arid | 10 ≤ IDM < 20 |
| Mediterranean | 20 ≤ IDM < 24 |
| Semi-humid | 24 ≤ IDM < 28 |
| Humid | 28 ≤ IDM < 35 |
| Very humid | 35 ≤ IDM < 55 |
| Extremely humid | IDM > 55 |

*V.9.6.B Difference from the mean*

The Difference from the mean Pc is a simple measure for determine the precipitation of a given year compared with a long period of observation of the same rain gauge that allow differencing the wet and dry years. Defined by

$$Pc = \frac{P}{pi} \qquad (8)$$

P is the mean on annual precipitation for a given period; and pi is the precipitation of i year.

This measure allows to identify the wet and dry periods, when Pc is less than 1, therefore the precipitation is less than the mean annual.

The **Fig.V.16** shows the curves that represents the IDM values and the histograms of the difference from the annual mean. The results show a periodic change of annual rainfall variability between dry and wet. The rainfall was driven by an abrupt shift from wet years to successive dry years between 1992 and 2002.

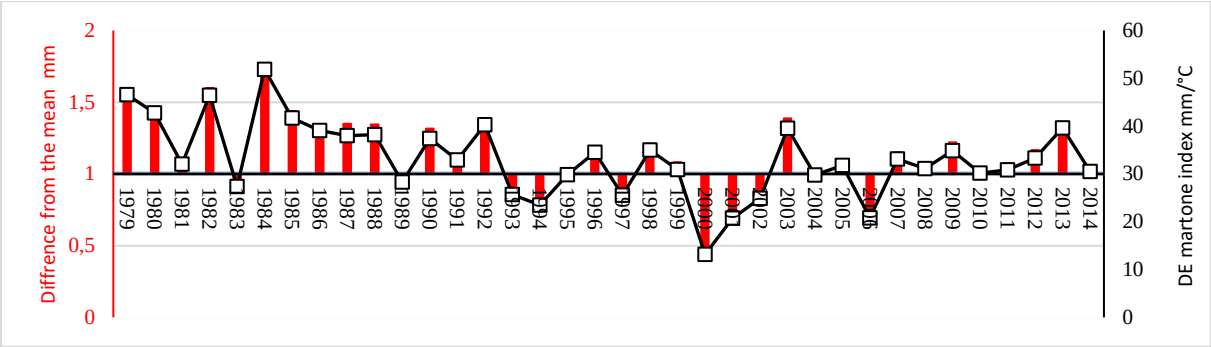


Figure V-16 Difference from the mean, and the De Martonne Index Of the study basin from 1979 to 2014

### *V.9.6.C Precipitation concentration index PCI*

The Precipitation Concentration Index PCI is a straightforward indicator to evaluate the precipitation concentration that can be used to provide information on its variability and to analyses and understand hydrological processes. PCI is used to measure the annual, and seasonally precipitation distribution. The Precipitation concentration index considered as a powerful indicator to control temporal precipitation distribution, it is recommended, as it provides information on long-term total variability in the amount of rainfall received, it was proposed by Oliver (1980). This index is also very useful for the assessment of annual and seasonal precipitation change, which noted by PCI and SPCI, given by Equations (9) and (10), respectively

$$PCI = \frac{\sum_{i=1}^{12} P_i^2}{(\sum_{i=1}^{12} P_i)^2} \times 100 \qquad (9)$$

$$SPCI = \frac{\sum_{i=1}^{3} P_i^2}{(\sum_{i=1}^{3} P_i)^2} \times 25 \qquad (10)$$

where pi represents the monthly precipitation in month i, that is calculated for each year of the study.

According to this classification, Oliver (1980) suggested that PCI values of less than 10 represent a uniform precipitation distribution (i.e., low precipitation concentration); PCI values from 11 to 15 denote a moderate precipitation concentration; values from 16 to 20 denote irregular distribution and values above 20 represent a strong irregularity (i.e., high precipitation concentration) of precipitation distribution.

*V.9.6.C.1 Annual PCI*

The precipitation concentration index (PCI) calculated on an annual scale for the wadi Seghir catchment for a period of 35 years. PCI values from 1979 to 1993 except for one value of 1980 represents a moderate precipitation concentration, therefore the distribution of precipitation presents a moderate variability. However, we detected a general increase in PCI values in the most recent period from 1994 to 2014, thus the significant value is occurred in 2001 by 18.6 we considered that the temporal distribution of precipitation in this year is irregular.

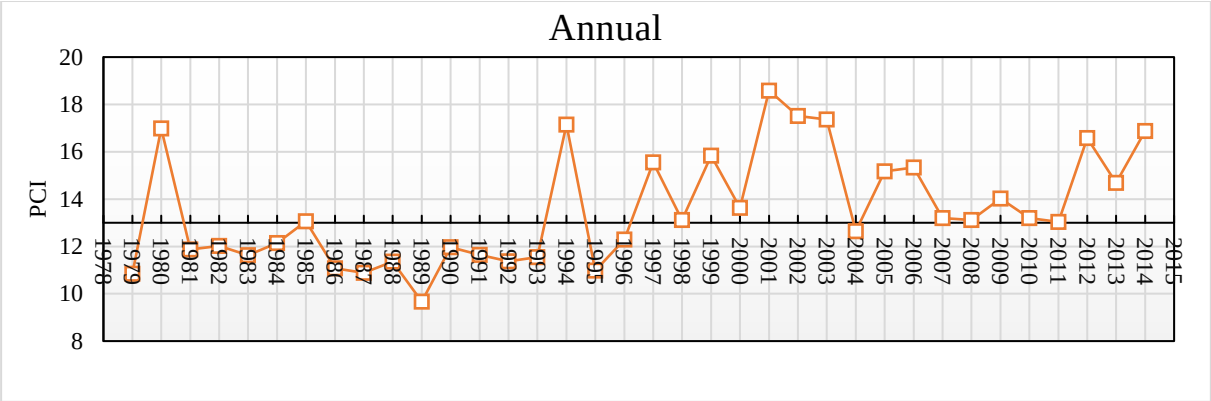


Figure V-17 Annual PCI of the study area between 1979 and 2014

*V.9.6.C.2 seasonal PCI*

The precipitation concentration index calculated on a seasonal scale shows complex spatial patterns of precipitation. Generally, an irregular distribution of PCI over the summer season is observed, where the PCI is oscillates between high, medium and low values. The winter season presents a moderate precipitation concentration in all year's exception for 1990. Over the spring season the precipitation is almost uniformly distributed to moderately distributed from 2001 to 2007. Autumn presents a uniform pattern of rainfall distribution while the major values present a small PCI.

From the **Fig.V.17** (annual PCI) and the **Fig.V.18** (seasonal PCI) we found a significant irregularity and a high variability distribution of rainfall pattern. In other side the dry season witnessed a great temporal variability distribution.

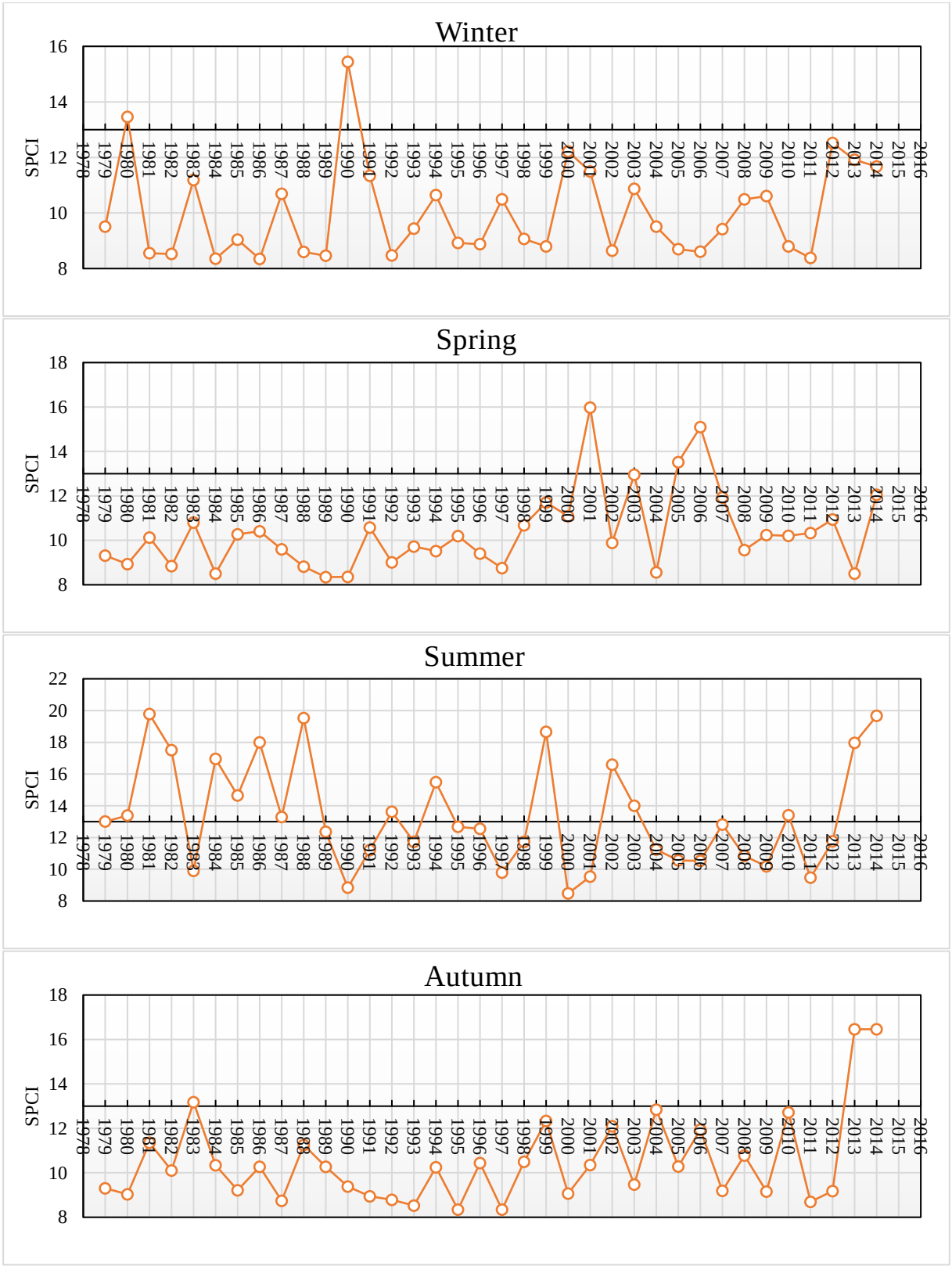


Figure V-18 Seasonal PCI of the study area between 1979 and 2014

# Data Input Acquisition, Preparation and Analysis

# VI Data Input Acquisition, Preparation and Analysis

## VI.1 Introduction

Information about water resources and the environment is inherently geographic. Maps, whether on paper or in digital GIS formats, continue to be the medium for expression of engineering plans and designs. We are concerned about the spatial distribution and character of the land and its waters. Weather patterns, rainfall and other precipitation, and resultant water runoff are primary driving forces for land development, water supplies, and environmental impacts and pollution (Wang & Yang, 2014). GIS are databases that usually have a spatial component to the storage and processing of the data. Hence, they have the potential to both store and create map products. They also offer the potential for performing multiple analyses or evaluations of scenarios such as model simulations. Data are stored in multiple files. Each file contains data in a coordinate system that identifies a position for each data point or entry. Characteristics of the data point are stored as "attributes." A database of individual files is developed and the combined files may contain characteristics or attributes such as stream locations, topography, water or soil chemical sampling, management practices, ownership, biota, point sources, and any other data that can be collected and have meaning for the analysis (Lyon, 2002). Planning and design in water resources engineering typically involve the use of maps at various scales and the development of documents in map formats. For example, in a river basin study, the map scale often covers a portion of a state and includes several counties and other jurisdictions. The river drains a certain geography having topographic, geologic and soil, vegetation, and hydrological characteristics. Cities and human-built facilities are located along the river and across the basin, and transportation and pipeline networks link these together. It is required that all of these datasets be established in a common geo-reference framework so that overlays of themes can be made and the coincidence of features identified in the planning and design phase (Wang & Yang, 2014).

Satellite remote sensing can provide various sources of data for water resources applications ranging from basic land use characteristics (and changes over time) to terrain and to meteorological event tracking. Satellites using the visible and near-infrared regions of the spectrum can provide detailed information of the land characteristics, topographic information,

Image processing functions have been developed to extract information from satellite imagery, although many of the procedures may be applied to other grid datasets as well.

Jensen (1986) describes image processing functions and techniques in some detail. Image classification is accomplished using multispectral classification methods that transform raw reflectivity data into information on land cover classes. There are a variety of classification algorithms including (1) hard classification using supervised or unsupervised approaches, classification using fuzzy logic, and/or (2) hybrid approaches using ancillary (collateral) information. Supervised classification involves a priori identification and location of land cover types, such as urban, agriculture, or wetland, through a combination of field work, aerial photography, and other mapping. Specific sites, called training sites, having known spectral characteristics are located in the image and are used to train the classification algorithm for application to the remainder of the image. This is a hard classification scheme since each pixel is assigned to only one class. In unsupervised classification, the identities of land cover types are not known a priori, and training site data are not collected or are unavailable.

The association of Algeria to the international project DMC (Digital Monitoring Constellation) which implies 8 observation satellites shows that the identification of the causes and the forecast of flood formation in several Algerian cities became one of the dominating concerns of public authorities. The interest of Algerians is to supervise the phenomena called «dynamic changes », as the disaster, which occurred in Bab El – Oued (Algiers) on November 10 2001, when a 24 hours flood (110 mm of rain) had caused a national disaster. Today the modeling in hydrology has reached a mature stage. The benefits that remote sensing holds for hydrology are always apparent and the use of the distributed models became more convenient. Remote sensing can be incorporated into the system in a variety of ways: as a measure of land use and for impervious surfaces, for providing initial conditions for flood forecasting, and for monitoring flooded areas (Schultz & Engman, 2012)

The integration of a GIS and Remote Sensing has been widely used and is recognized as a useful and effective tool in locating urban expansion. Remote sensing has multi-resolution, multispectral and multi-temporal data, transforming them into information valuable for understanding the processes and monitoring of land use/land cover changes. GIS technology includes an array of powerful tools for entering, analyzing and displaying digital data from the various sources necessary to detect urban phenomena changes, identification and dataset development as well as an important tool in the analysis of parameters such as land cover, land use, soils, topographical and hydrological conditions. The use of GIS is inevitable in water resource

studies, planning, and system management, where it offers the data in the form of maps and tables expressed by feature classes and their attributes, which containing all things required for land management and decision support (Wang & Yang, 2014).

River basin management poses big challenges especially in developing countries because of lack of continuous data particularly streamflow data that require automatic recording instruments to acquire. As an alternative to observed data, rainfall-runoff models can be used, such models are distributed, semi-distributed or lumped. The distributed models have more parameters and therefore they are used in catchments with good data records. The less complex lumped models have fewer parameters and are commonly used in catchments with poor data. The rainfall-runoff models used in simulating runoff data are made of physical and conceptual parameters, which need to be estimated before the models can be used to improve data in gauged catchments or be extrapolated in ungauged catchments. Simulation of streamflow data in ungauged catchments is complicated by lack of observed data for model calibration.

Remote sensing technology can augment the conventional methods to a great extent in rainfall-runoff studies. The role of remote sensing in runoff calculation is generally to provide a source of input data or it is used as an aid for estimating equation coefficients and model parameters. One of the first applications of remote sensing data in hydrologic models used satellite data to determine both urban and rural land use for estimating runoff coefficients. The runoff coefficient, which is influenced by not only climatic effects but also human impacts, is a fundamental indicator used in flood control.

The models based purely physical or conceptual, facing the problem of calibrating the large number of parameters that they contain, which are not almost available (Rezaeianzadeh et al., 2013; Shamseldin & O'Connor, 2001; Valizadeh et al., 2017) . Remote Sensing RS and GIS has been available as an alternative in recent years, for the extraction, manipulation and treatment of digital information. Although the great help that offers the GIS to hydrologists modelers, the high-quality resolution data is not freely accessible. The inferior data resolution negatively impacts the hydrological model, besides the extended time taken in downloading and preprocessing the required data.

This chapter demonstrate the procedures to collect and prepare the data input including rainfall events, and their statistical description, on the other side preparation of thematic maps by downloading from the USGS the Landsat maps that used afterward to construct the land use maps,

we also demonstrate how these images are rectified, processed and classified, and how we evaluate this classification if that is in correct way or not by using a widely used criteria. The soil map also digitized from a national soil map of Algeria using GIS software, that used later to drawn the hydrological soil group HSG maps. The combination of these two maps enabled us to extract and estimate the CN values for various years ago from 1984 to this day. Where its importance lies in simulation the runoff in ungagged watershed using only one parameter (the CN value).

Table VI-1 Statistical description of rainfall and runoff time series events used in this study.

| | **Rainfall intensity** | | | | | **Observed runoff** | | | | |
|---|---|---|---|---|---|---|---|---|---|---|
| **Event** | **Min** | **Max** | **Mean** | **Median** | **Cv** | **Min** | **Max** | **Mean** | **Median** | **Cv** |
| EV $_1$ | 0 | 8.00 | 4.50 | 5.00 | 0.92 | 0.10 | 4.30 | 1.31 | 0.75 | 0.96 |
| EV $_2$ | 0 | 7.00 | 1.83 | 2.00 | 1.08 | 0.15 | 2.29 | 0.78 | 0.50 | 0.84 |
| EV $_3$ | 0 | 5.00 | 2.00 | 1.50 | 1.04 | 0.40 | 2.89 | 1.31 | 1.03 | 0.59 |
| EV $_4$ | 0 | 0.85 | 0.63 | 0.30 | 0.72 | 0.00 | 1.15 | 0.40 | 0.23 | 0.86 |
| EV $_5$ | 0 | 4.00 | 2.00 | 0.00 | 0.87 | 0.10 | 1.81 | 1.06 | 1.43 | 0.57 |
| EV $_6$ | 0 | 6.00 | 1.25 | 0.00 | 1.55 | 0.10 | 1.70 | 0.74 | 0.73 | 0.59 |
| EV $_7$ | 0 | 3.50 | 0.96 | 0.60 | 1.11 | 0.01 | 2.56 | 1.12 | 1.05 | 0.64 |
| EV $_8$ | 0 | 4.00 | 2.00 | 1.00 | 0.91 | 0.04 | 2.41 | 0.66 | 0.34 | 1.20 |
| EV $_9$ | 1 | 6.00 | 2.75 | 2.00 | 0.80 | 0.20 | 2.50 | 0.95 | 0.80 | 0.81 |
| EV $_{10}$ | 0 | 4.00 | 1.20 | 2.00 | 1.49 | 0.44 | 2.70 | 1.04 | 0.77 | 0.65 |
| EV $_{11}$ | 0 | 17.00 | 5.50 | 3.50 | 1.21 | 0.00 | 6.56 | 2.71 | 2.02 | 0.83 |
| EV $_{12}$ | 1 | 6.00 | 2.75 | 2.00 | 0.81 | 0.10 | 2.65 | 1.11 | 0.90 | 0.73 |
| EV $_{13}$ | 0 | 0.60 | 0.26 | 0.20 | 0.81 | 0.00 | 0.50 | 0.18 | 0.13 | 0.81 |
| EV $_{14}$ | 0 | 1.00 | 0.17 | 0.10 | 1.42 | 0.01 | 0.41 | 0.15 | 0.15 | 0.77 |

Note: Cv = Coefficient of variation; Max = Maximum; Min = Minimum.

## VI.2 Rainfall Data

In this work fourteen single storm events of hourly time step are used. They were recorded during a study conducted by order of the National Office of Sanitation (NOS). **Table.VI.1** illustrates statistical description of storm events. They are chosen randomly and given by 14 events. The coefficient of variation ($C_v$) shows that rainfall intensity and runoff series are distributed according to an interval of variation of [0.72, 1.49] and [0.57, 1.20]. The results indicate that the event 9 and 12 have a similar value, given by an average of 2.75, for the Min of 1 and

the Max of 6. On the other hand, the discharges have a more variation in event 9 than of event 12, given by a $C_v$ with value of 0.81 and 0.73 respectively. The events 12, 13 and 14 are chosen variously for the test part that it was used as a comparative study. Moreover, the **Table.VI.1** shows that the Min, Max and Mean of series of these events are different.

## VI.3 Thematic data

Land Use (LU) change detection becomes a key research priority with their continued impacts on natural and human systems (Ishtiaque et al., 2017). Many techniques of change detection are available, but remote sensing is the most commonly used technique because of its cost-effectiveness and timesaving characteristics (Lambin et al., 2003). Remote sensing data are primary sources extensively used for change detection in recent decades (Lu et al., 2004).

To obtain thematic information from multi-spectral imagery, multi-dimensional, continuous reflection measurements from remote sensing images have to be transformed into discrete objects, which are distinguished from each other by a discrete thematic classification (Schultz & Engman, 2012). Lu et al. (2004) mentioned the mainline classification methods, they divided into 6 major models such as: (1) Algebra, (2) Transformation, (3) Classification, (4) Advanced models, (5) GIS, (6) Visual Analysis. The author provided an exhaustive list of pixel-based change detection methods. Of all these methods pre- and post-classification comparisons have widely been used owing to their comparative advantages. A variety of classifications methods exists. A first distinction is between unsupervised and supervised classification. The first one is a classification can be obtained by plotting all feature vectors of the image in a feature space, and then analyzing the feature space to group the feature vectors into clusters (classes) (Schultz & Engman, 2012). Unlike computer-controlled unsupervised classification, the supervised classification process gives a much better control. In this process, patterns of pixels can be selected such that they recognizable by us. the later which is used in this study.

### *VI.3.1 Landsat imagery acquisition*

Nowadays remote sensing technologies combined with GIS technics provide Physical characteristics of the watershed such as soil information (infiltration rates, soil moisture, interception), surface characteristics (land use information, imperviousness, geometry of basins) and plains channels (slopes, lengths, surfaces, perimeters). Several studies integrate GIS and RS in hydrological modeling to extract input data for simulation of the basin response, the physical parameters extracted over remote sensing depends on the measurements of the emitted and reflected

electromagnetic energy from and to the earth surface by calculating this energy at different wavelengths (Jacobs et al., 2003; Li et al., 2018; Schmugge et al., 2002).

a

b

Figure VI-1 Satellite image from Landsat 8-collection 2-Level 2 of Bejaia region for December ,18, 2020. (a) RGB false colors 5.3.1 and (b) RGB 7.4.1

Since 1972, the two joint companies National Aeronautics and Space Administration NASA and the United States Geological Survey USGS provides the service of land surveying of the Earth's land surface, it makes available continuously data for earth's research, the data are useful for a number of scientific researches in relation to the earth including environmental research, forestry, agriculture, geology, water resources, and urban studies, etc.

In this study, Satellite Images derived from the American geological survey USGS (USGS 2016), including images from Landsat 5 TM (Thematic Mapper) ,Landsat 7 ETM+ (Enhanced Thematic Mapper plus) and Landsat 8 OLI/TIRS The Operational Land Imager (OLI) and

Thermal Infrared Sensor (TIRS), The images have a resolution cell size of 15 m and 30 m. All images were first projected to The World Geodetic System (WGS84). The images used in this study are showed in **Fig.VI.2**. the satellite images downloaded from the website https://earthexplorer.usgs.gov.

**Table.VI.2** show the image date of the satellite image and their corresponding sensor version, all of image's date were chosen in the spring season considering that land cover differs from season to season, because of atmospheric condition changed, In addition to land surface temperature and cultivation and harvest seasons.

Table VI-2 Landsat images downloaded from the website Earth Explorer (usgs.gov) used for Land use classification

| ***Image date*** | ***Sensor*** |
|---|---|
| 29/05/1984 | Landsat 5 TM |
| 15/05/1991 | |
| 28/04/2002 | Landsat 7 ETM+ |
| 23/05/2014 | Landsat 8 OLI/TIRS |
| 11/05/2018 | |

### *VI.3.2 What is the supervised classification?*

The supervised classification is that classification applied by the machine according to chosen algorithm and controlled by the user, it is based on the external knowledge of the area of interest, that must be inputted to the model, this input may be derived from fieldwork, air photo analysis, reports or from the study of appropriate maps of the area of interest. Supervised methods are implemented using either statistical or non-statistical algorithms.

Statistical algorithms use parameters derived from sample data in the form of training classes, such as the minimum and maximum values on the features, or the mean values of the individual clusters, or the mean and variance-covariance matrices for each of the classes. Non-statistical methods such as ANNs do not rely on statistical information derived from the sample data but

are trained on the sample data directly and do not rely on assumptions about the frequency distributions of the image bands. In contrast, statistical methods such as the maximum likelihood procedure is based on the assumption that the frequency distribution for each class

is multivariate normal in form. Thus, statistical methods are said to be parametric (because they use estimates of statistical parameters derived from training data) whereas neural methods are non-parametric.

*VI.3.2.A Conducting supervised classification*

The classification purpose is to translate spectral information into thermal classes. Unlike computer-controlled unsupervised classification, the supervised classification process gives a much better control. In this process, patterns of pixels can be selected such that they recognizable by us. Knowledge of the data, the classes desired, and the algorithm to be used is required before beginning the selection of training samples (Kadam et al., 2012) patterns of Images can be recognized by the help of the terrain visualization or by the help of remote sensing of vegetation NDVI and water NDW indices. By identifying patterns in the imagery, we can "train" the computer system to identify pixels with similar characteristics. By setting priorities for these classes, we supervise the classification of pixels as they are assigned to class values. If the classification is accurate, then each resulting class corresponds to a pattern that has been originally identified.

The treatments of satellite images carried out with the help of ARC GIS software from ESRI. The study watershed extracted from each satellite image and then classified according to the maximum likelihood supervised classification method which is the most common supervised classification method used in image processing.

The first step consists of opening the Image/map in Arc GIS; combine all bands of satellite Image from "Arc Toolbox", then they were clipped according to the shape of the study area from the "extract by mask" tool ; subsequently, creating training samples by identifying areas for each individual class and save the "signature file" under the ".sgs" extension witch used later to performing a supervised classification by click on "Maximum Likelihood Classification" in "image classification" toolbar.

*VI.3.2.B Assessing the accuracy of the classified images*

The classified image must be assessed, this will allow a degree of confidence and indicate if the objectives of analysis have been achieved (Richards & Richards, 1999).we define two accuracy assessment approaches:

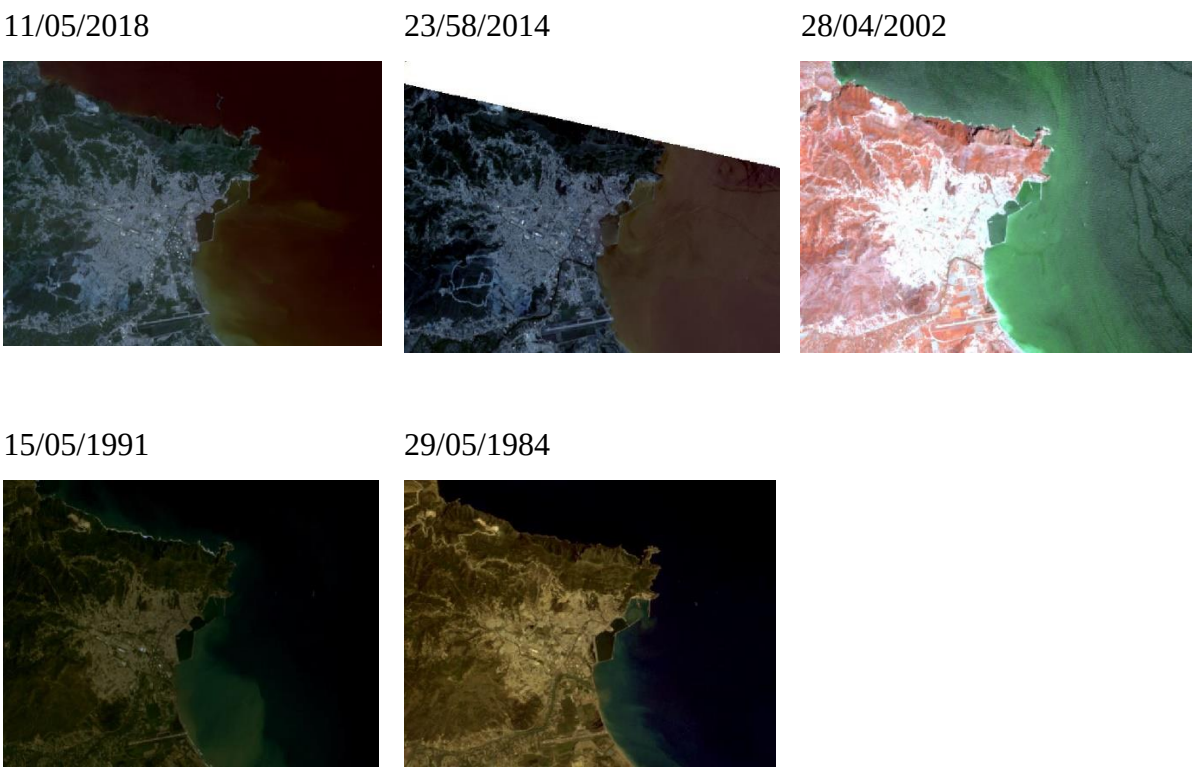


Figure VI-2 Satellite images used in this study to classify the Land Use, the Table.VI.2 showed the images information.

*VI.3.2.B.1 Positional accuracy assessment*

In 1849, the first appearance of the photogrammetry Science (Congalton & Green, 2019)which is the Science interested in measuring from photos. Photogrammetry provides information on the quantitative data contained in the photo (Linder, 2013) these photos must be assessed in terms of position. Positional accuracy is to compare the coordinates at least of three samples points on a map with the coordinates of the same pointes derived from the earth or other sources judged to be more accurate or already corrected (Congalton & Green, 2019)

*VI.3.2.B.2 Thematic accuracy assessment*

Evaluation the extent of compatibility has gone through stages, the first one known as visual interpretation. (Spurr, 1948) mentioned that the check restricted only to certain parts suspicious. After it has become necessary to evaluate quantitatively the photos, from here it seemed to think about statistical method (Young & Stoeckeler, 1956). the history of evaluating maps begins with the launch of remote sensing and satellites Images, this was a big challenge for researchers at the time and from here began the veritable map accuracy (Congalton & Green, 2019) . (Hord

& Brooner, 1976) suggest a statistical technic to assess each cover separately, boundary lines and control point placement on classified land use map (Congalton et al., 1983) assess the accuracy of Landsat Imagery using three statistical technics in the form of error matrices and they found a very helpful results.

*VI.3.2.B.3 Error Matrix and Kappa coefficient*

The accuracy of classification is generally found out by generating an error matrix. Assessment accuracy provide the user about where the errors are occurring. An error matrix compares pixels in a classified map with the information in the reference data supplied .Accuracy of the classified image is determined empirically by selecting a sample of pixels (ground truth point) from the thematic map (from google earth) against classes determined from reference data (Foody, 2010), then it is easy to estimate a number of pixels labelled correctly by the classifier together with the proportions of pixels in each class wrongly labelled. The test pixels should be evenly distributed across the image, and they also should be distinct pixels from the training areas used for supervised classification.

The confusion/error matrix approach is the one most widely and accepted method for determining the accuracy of classification. but it is important to remember that the biases that are present in their test pixels will also bias the accuracy of the confusion matrix. For good classification results the number of test pixels should be ten times the number of classes, but it remains depend on the surface of each class, it would make sense to have test pixels as evenly as possible distributed.

In order to properly generate an error matrix, one must consider the following factors: (1) reference data collection, (2) classification scheme, (3) sampling scheme, (4) spatial autocorrelation, and (5) sample size and sample unit (Congalton et al., 2002)

The generation of the error matrix enabling to measure other important accuracy assessment elements such as: the overall accuracy and the KAPPA coefficient which are used for assessing all the classified image, the user's accuracy, producers' accuracy, omission and commission intended for assessing each class separately. The Overall accuracy defined by the sum of the major diagonal (i.e., the correctly classified sample units) divided by the total number of sample unit in the error matrix. This value is the most commonly reported accuracy assessment statistic and was part of the older, site-specific assessment. Producer's and user's accuracies are ways of representing individual category accuracies instead of just the overall classification accuracy.

Sometimes a distinction is made between errors of omission and errors of commission, particularly when only a small number of cover types is of interest, such as in the estimation of the area of a single crop in agricultural applications. Errors of omission correspond to those pixels belonging to the class of interest that the classifier has failed to recognize whereas errors of commission are those that correspond to pixels from other classes that the classifier has labelled as belonging to the class of interest. Omission error occurs when an area is omitted from the correct category. Commission error occurs when an area is placed in the wrong category.

The **Tables VI.3,4,5,6,7** show the assessment accuracy results where the diagonal elements represent the number of correctly classified pixels of each class while the off-diagonal values represent wrongly classified pixels. The producer's and user's accuracy are associated with the error of omission and commission respectively. As shown in the tables, there are four classes chosen according to visual and field investigation and through google earth images. The class of 2018 shown a very satisfactory results by 0.94 of Kappa coefficient and 0.96 of overall accuracy, in the first columns in the confusion matrix which corresponds to forest class, all the individual cells are classified as forest, in other words omission is zero indicate that there is not any of the remaining classes categorized with the forest class, this is confirmed by the producer's accuracy criterion which equal 100% , which means that this class (forest) is correctly classified as 100% i.e., all samples data are correctly labeled. A quick calculation of the "user's accuracy" computed by dividing the total number of correct sample units in the Forest class (i.e., 30) by the total number of sample units classified as forest (i.e., 31 or the row total) reveals a value of 96.77%. In this study we are interested much more with the urban class, whereas it gave for the producer's accuracy 96.97%, 95%, 100%, 93.33%, and 86.67% respectively for 2018, 2014, 2002, 1991, and 1984 which is quite good. Kappa coefficient are 96%, 79%, 91%, 90%, and 89% respectively for 2018, 2014, 2002, 1991, and 1984.

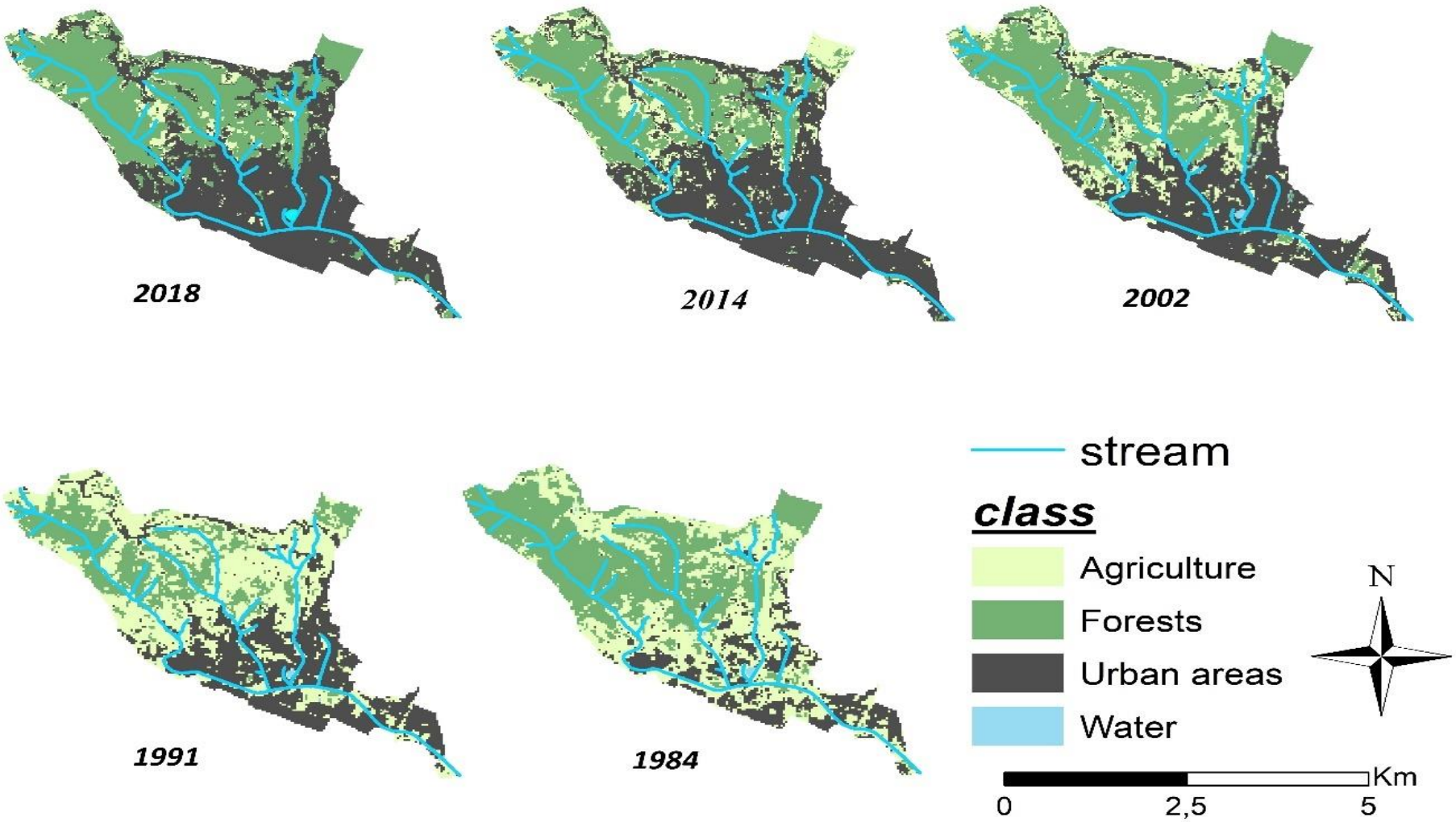


Figure VI-3 Cartography of land use changes in Oued Seghir catchment, given in 1984, 2002, 2014 and 2018

The result of classification map is shown in the **Fig.VI.3** The changes in land use are derived and are summarized in **Fig.VI.4 a, b.** The later illustrates the huge increase in urban areas including roads, industrial surfaces and the built up by the order of 70% in the period between 1984 to 2018.The ratio of the urban area is about 15.7% in 1984 and became more than half in 2018. The agriculture has a dramatically decline. But it is not necessarily by the effect of urbanization, apparently by the reason of drought impact, the urbanization expansion was in detriment of forests areas.

### *VI.3.3 Soil Map*

Soil map derived from geographical service of defense in 1949 drawn by R. JASEIX BETTON, study area georeferenced and digitized using Arc GIS software, then the according information added to the attribute table.

Digitizing in GIS is the process of "tracing", in a geographically correct way, information from images/maps. The process of georeferencing relies on the coordination of points on the scanned image (data to be georeferenced) with points on a geographically referenced data (data to which the image will be georeferenced). By "linking" points on the image with those same locations in the geographically referenced data we will create a polynomial transformation that converts the location of the entire image to the correct geographic location.

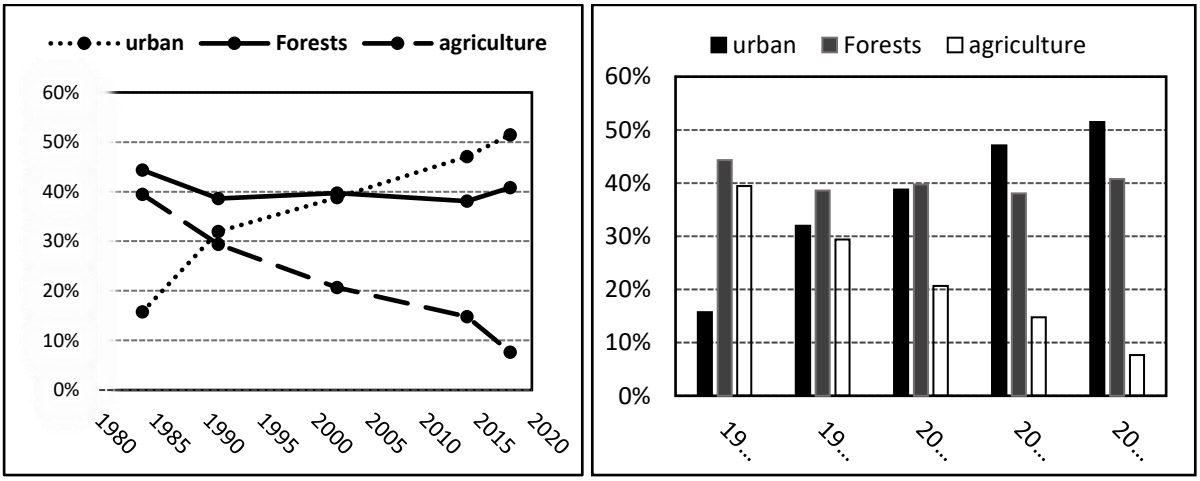


**(a)** **(b)**

Figure VI-4 change in Land Use of each component of the study area

Table VI-3 Error matrix of classified Landsat satellite map for the year 2018 classified according to maximum likelihood supervised classification method

| *Class 2018* | | reference data | | | | | | |
|---|---|---|---|---|---|---|---|---|
| | | Forest | Urban | Agriculture | Water | *Total* | **User's Accuracy** | **Commission** |
| **classified map** | Forest | **30** | 0 | 1 | 0 | *31* | **96.77** | **3.23** |
| | Urban | 0 | **29** | 0 | 3 | *32* | **90.63** | **9.38** |
| | Agriculture | 0 | 1 | **29** | 0 | *30* | **96.67** | **3.33** |
| | water | 0 | 0 | 0 | **23** | *23* | **100.00** | **0.00** |
| | Total | 30 | 30 | 30 | 26 | | | |
| | **producers' accuracy** | **100** | **96.67** | **96.67** | **88.46** | | | |
| | **Omission** | **0** | **3.33** | **3.33** | **11.54** | | | |
| | ***overall accuracy*** | ***0.96*** | | | | | | |
| | ***kappa*** | ***0.94*** | | | | | | |

Table VI-4 Error matrix of classified Landsat satellite map for the year 2014 classified according to maximum likelihood supervised classification method

| *Class 2014* | | reference data | | | | | | |
|---|---|---|---|---|---|---|---|---|
| | | Forest | Urban | Agriculture | Water | *Total* | **User's Accuracy** | **Commission** |
| **classified map** | Forest | **36** | 1 | 4 | 5 | 46 | **78.26** | **21.74** |
| | Urban | 0 | **38** | 0 | 16 | 54 | **70.37** | **29.63** |
| | Agriculture | 0 | 0 | **24** | 0 | 24 | **100** | **0** |
| | water | 4 | 1 | 0 | **18** | 23 | **78.26** | **21.74** |
| | *Total* | 40 | 40 | 28 | 39 | | | |
| | **producers' accuracy** | **90** | **95** | **85.71** | **46.15** | | | |
| | **Omission** | **10** | **5** | **14.29** | **53.85** | | | |
| | ***overall accuracy*** | ***0.79*** | | | | | | |
| | ***kappa*** | ***0.72*** | | | | | | |

Table VI-5 Error matrix of classified Landsat satellite map for the year 2002 classified according to maximum likelihood supervised classification method

| *Class 2002* | | reference data | | | | | | |
|---|---|---|---|---|---|---|---|---|
| | | Forest | Urban | Agriculture | Water | *Total* | **User's Accuracy** | **Commission** |
| **classified map** | Forest | **30** | 0 | 5 | 0 | *35* | **85.71** | **14.29** |
| | Urban | 0 | **30** | 5 | 0 | *35* | **85.71** | **14.29** |
| | Agriculture | 0 | 0 | **19** | 0 | *19* | **100** | **0** |
| | water | 0 | 0 | 0 | **26** | *26* | **100.00** | **0.00** |
| | *Total* | *30* | *30* | *29* | *26* | | | |
| | **producers' accuracy** | **100** | **100** | **65.52** | **100** | | | |
| | **Omission** | **0** | **0** | **34.48** | **0** | | | |
| | ***overall accuracy*** | ***0.91*** | | | | | | |
| | ***kappa*** | ***0.88*** | | | | | | |

Table VI-6 Error matrix of classified Landsat satellite map for the year 1991 classified according to maximum likelihood supervised classification method

| *Class 1991* | | reference data | | | | | | |
|---|---|---|---|---|---|---|---|---|
| | | Forest | Urban | Agriculture | Water | *Total* | **User's Accuracy** | **Commission** |
| **classified map** | Forest | **26** | 0 | 0 | 0 | *26* | **100.00** | **0.00** |
| | Urban | 0 | **28** | 1 | 0 | *29* | **96.55** | **3.45** |
| | Agriculture | 4 | 2 | **27** | 3 | *36* | **75** | **25** |
| | water | 0 | 0 | 0 | **14** | *14* | **100.00** | **0.00** |
| | *Total* | *40* | *40* | *28* | *39* | | | |
| | **producers' accuracy** | **86.67** | **93.33** | **96.4** | **82.4** | | | |
| | **Omission** | **13.33** | **6.67** | **3.57** | **17.65** | | | |
| | ***overall accuracy*** | ***0.90*** | | | | | | |
| | ***kappa*** | ***0.87*** | | | | | | |

Table VI-7 Error matrix of classified Landsat satellite map for the year 1984 classified according to maximum likelihood supervised classification method

| *Class 1984* | | reference data | | | | | | |
|---|---|---|---|---|---|---|---|---|
| | | Forest | Urban | Agriculture | Water | *Total* | **User's Accuracy** | **Commission** |
| **classified map** | Forest | **29** | 0 | 4 | 0 | *33* | 87.88 | **12.12** |
| | Urban | 0 | **26** | 3 | 0 | *29* | 89.66 | **10.34** |
| | Agriculture | 1 | 4 | **23** | 0 | *28* | 82.14 | **17.86** |
| | water | 0 | 0 | 0 | **21** | *21* | 100.00 | **0.00** |
| | *Total* | *30* | *30* | *30* | *21* | | | |
| | **producers' accuracy** | **96.67** | **86.67** | **76.67** | **100** | | | |
| | **Omission** | **3.33** | **13.33** | **23.33** | **0** | | | |
| | ***overall accuracy*** | ***0.89*** | | | | | | |
| | ***kappa*** | ***0.85*** | | | | | | |

### *VI.3.4 Hydrological Soil Group HSG map*

The hydrological soil group related by the rate of infiltration who distinguishes each soil category according to rate of infiltration, here soils are classified into four classes A, B, C, D based on the infiltration and other characteristics. The important soil characteristics the influence the hydrological classification of soils is effective depth of soil, average clay content, infiltration characteristics and the permeability.

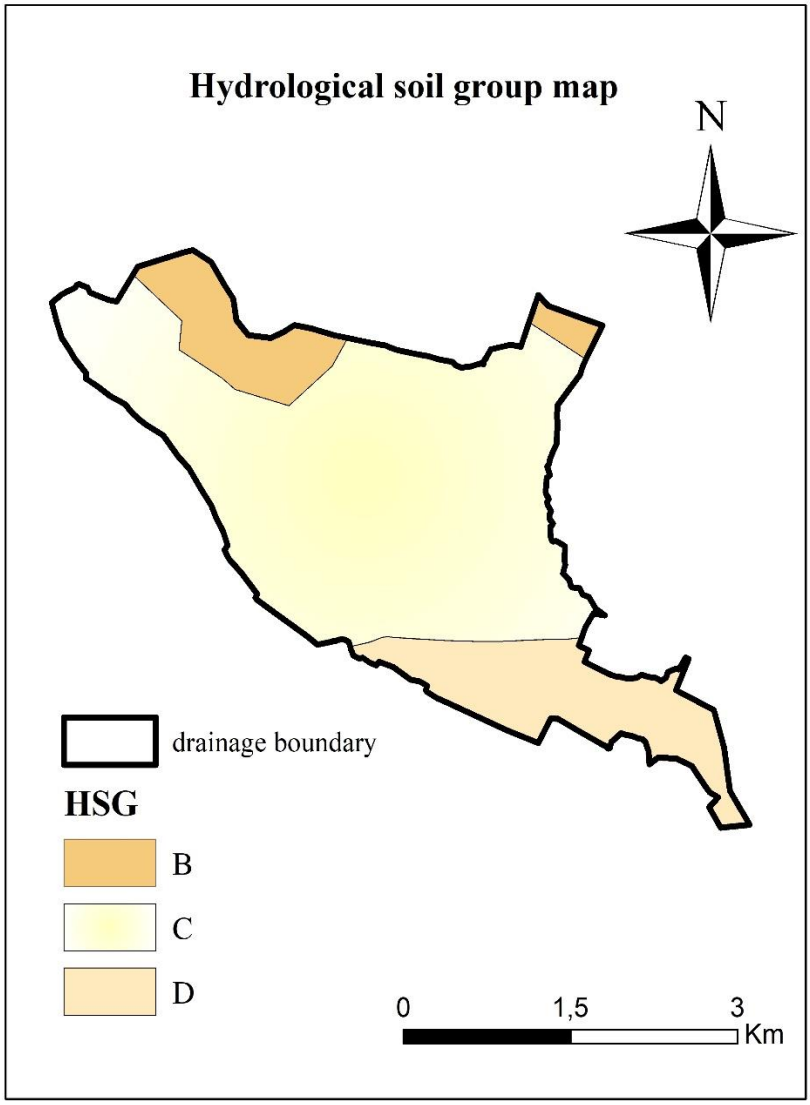


Figure VI-5 Hydrological soil group HSG map

The group "A" the lowest runoff potential characterized by high infiltration capacity, even when thoroughly wetted (Deep sand, deep loess, aggregated silts); group "B" the moderately low runoff potential characterized by moderate infiltration rate when thoroughly wetted, moderately

deep to deep and moderately well to well drained with moderately fine to moderately coarse texture (Shallow loess, sandy loam); group "C" the moderately high runoff potential, soil with slow infiltration rate when thoroughly wetted, usually have a layer that impedes vertical drainage or have a moderately fine to fine texture (Clay loams, shallow sandy loam, soils low in organic content, and soils usually high in clay); finally, group "D" with high runoff potential, Soil with slow infiltration rate when thoroughly wetted, chiefly clay with a high swelling potential, soil with a high permanent water table, soil with a clay layer or near the surface (Soils that swell significantly when wet, heavy plastic clays, and certain saline soils) (USDA 2009). The result is shown in **Fig.VI.5**

### VI.4 Estimation of CN value

The SCS-CN method was developed by the United States Department of Agriculture- Soil Conservation Service ) USDA-SCS in 1954 (Satheeshkumar et al., 2017). The SCS model uses the CN value as an input parameter for the calculation of runoff depth. The SCS curve number is a purpose of the ability of soils to allow infiltration of water with respect to land use/ land cover and antecedent soil moisture condition (AMC) **TableVI.8**. Based on USDA-SCS soils are distributed into four hydrologic soil groups such as group A, B, C & D with respect to rate of runoff probable and final infiltration. The selection of curve number is based on the Land Use and the Hydrological soil group HSG information using Geographic Information system GIS technics, the ARC-GIS software from ESRI is used to prepare the Land Use map, and soil map as explained above in **sectionVI.3.2**, The CN is estimated for a drainage basin from the combination of HSG and Land Use maps. The determination of the CN is done automatically through the WMS platform where the hydrological soil group HSG and the land use LU maps used as a vector layer, each polygon in each map contained an attribute describe the soil group A, B, C or D for the soil map and the LU of the corresponding HSG , this step is done through the "Hydrologic modelling module" toolbar by clicking on the "calculators" then "compute GIS attribute", the inputs are the HSG map, the LU map and a table contain the values of CN selected by the NRCS group (USDA 2009). **TableVI.9** summarized the obtained CN-values and the change of the impervious area for the corresponding year, and the classification procedures are showed in **Fig.VI.6.**

Table VI-8 Antecedent moisture conditions (AMC) for determining the value of CN

| AMC TYPE | Dormant season (Total rain in previous 5 days) | Growing season (Total rain in previous 5 days) |
|---|---|---|
| **I** | Less than 13 mm | Less than 36 mm |
| **II** | 13 to 28 mm | 36 to 53 mm |
| **III** | Greater than 28 mm | More than 53 mm |

The CN for a watershed can be estimated as a function of land use, soil type, and antecedent watershed moisture, using tables published by the SCS. With these tables and knowledge of the soil type and land use, the single-valued CN can be found. For a watershed that consists of several soil types and land uses, a composite CN is calculated as:

$$CN_{composite} = \frac{\sum A_i CN_i}{\sum A_i} \qquad (11)$$

In which:

$CN_{composite}$ = the composite CN used for runoff volume computations;

i = an index of watershed subdivisions of uniform land use and soil type;

$CN_i$ = the CN for subdivision i;

$A_i$ = the drainage area of subdivision i.

Table VI-9 results of CN values and imperviousness for the wadi Sghir catchment from 1984 to 2018

| Year | CN | impervious area % |
|---|---|---|
| **2018** | 76,8 | 51,5 |
| **2014** | 77,3 | 47,0 |
| **2002** | 77,4 | 38,8 |
| **1991** | 77,6 | 32,0 |
| **1984** | 77,2 | 15,7 |

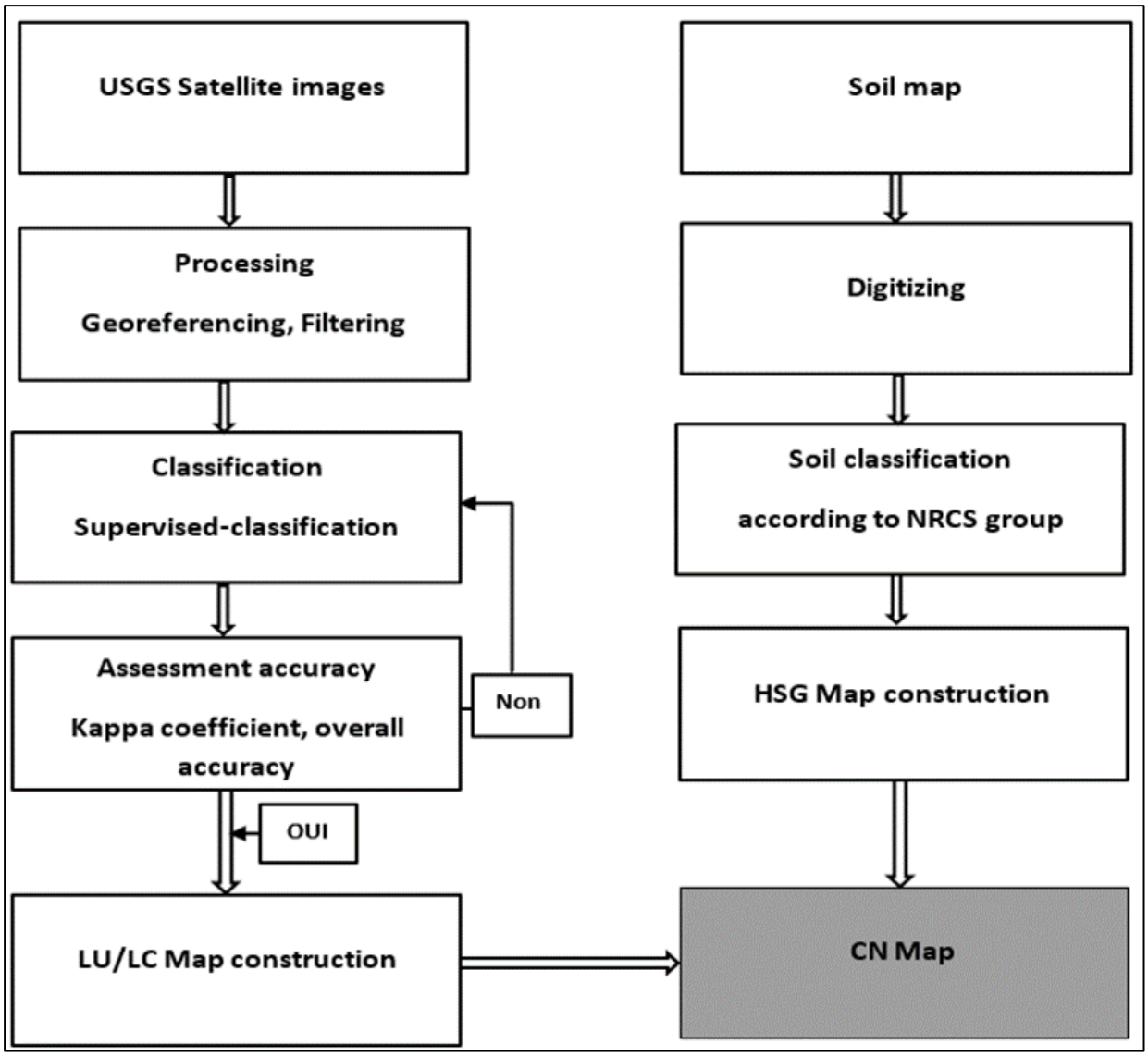


Figure VI-6 procedures followed to estimate CN values

## VI.5 Conclusion

Estimation of different component of rainfall runoff model is a big challenge occupied the researchers for a long period of time. Rainfall runoff model accuracy depend essentially by the model input parameters required to construct a given hydrological model. In this work we focus on estimating the SCS-CN parameter, The Soil Conservation Service Curve Number (SCS-CN) is a method widely applied for estimating the rainfall excess by eliminating the initial losses from a given rainfall event. the selection of curve number is based on the Land Use LU and Hydrological soil group HSG information using Geographic Information system GIS and Remote sensing RS technics, the LU maps extracted from Landsat satellite images derived from the American geological survey USGS classified as groups of each land cover combined by the

HSG divided into A, B, C and D groups related by the rate of infiltration who distinguishes each soil category , the combination of the LU and HSG with help of RS and GIS of the study watershed allowed us to calculate the weighted value of CN in large case studies easy and fast with high accuracy.

For the ungauged watersheds the SCS based GIS and RS method has been among the best solutions for rainfall-runoff modelling. GIS and RS have a great importance in constructing the model and collect and organize the data; develop the watershed model drainage boundary and streams; Preparing thematic maps and feature symbols and is integrated with databases containing attribute data on the features; Extract basin characteristics Surfaces, length, slop, etc.

remote sensing provides spatial and temporal information from long periods. In our case satellite images derived from Landsat sensor classified and assessed integrating the soil type to calculate the CN from 1984 to 2018.

# NARX-NN and HEC-HMS Models for Modelling Wadi Seghir Urban Runoff

# VII NARX-NN and HEC-HMS Models for Modelling Wadi Seghir Urban Runoff

## VII.1 Introduction

The primary characteristic known about the relationship between rainfall and runoff is the high nonlinearity. The challenge that usually faces the hydrologists is the reproduction of watershed response regarding to the changes taking places in the basin unit, the spatiotemporal scales, and the objective of the modelling. For that; a great effort has been made to accurately simulate watersheds response through large types and numbers of rainfall-runoff (RR) models. According to Refsgaard (1997), the hydrological models are classified into physical or conceptual, based on the manner where the description of the relationship between the inputs and the outputs is presented. The black-box models express the relationship between inputs and outputs of a given hydro-system. It provides the quantification of adjusting parameters, excluding the physical properties or any hydro-system description. This latter includes the linear or the nonlinear patterns, such as the AR-X and the N-AR-X models, (AR :Auto Regressive, N :Nonlinear, X :eXogenous) (Samarasinghe, 2007; Suykens et al., 1996).The nonlinear term refers to the mapping function of the ANN. The models that are based purely physical or conceptual, facing the problem of calibrating the large number of parameters that they contain, which are not available often times (Paik et al., 2005; Rezaeianzadeh et al., 2013; Shamseldin & O'Connor, 2001; Valizadeh et al., 2017).

Remote Sensing (RS) and Geographic Information system (GIS) have been available as an alternative solution in the recent years, for the extraction, the manipulation and the treatment of the digital information. Although the great help that offers the GIS to hydrologist's modelers, the data of high-quality resolution is not freely available. On the other hand, the lower data resolution can negatively impact the hydrological models, besides that; the long time that is taken for downloading and pre-processing the required data. For this, it was clear that the ANN models seem a promising alternative. The use of ANN technics in R-R modelling, enabling overcome the internal processes, thereby deleting the empiricism that may not offer the value in some cases (Anthony W & Michael J, 2004). In the static network, the input data must be lagged to provide a consistent and robust resilience against the highly non-linear behavior of the hydrological system. In such studies the modelers looking for a causal relationship between a set of input data and lagged time and network response (Christian W, 2004). They attained this goal through the use of analytical technics or selecting appropriate inputs based on

modeler's expertise (Ali, 2009; Dawson & Wilby, 1998; Dehghani et al., 2014; Maier & Dandy, 2000; Roadknight et al., 1997; Talei et al., 2010). The choice of optimal rainfall lag is a crucial task in static NN modelling, as it can affect the outflow's prediction accuracy. The short lag conductive to insufficient information to cover the whole process. In contrast, too long rainfall lag provides a rainfall that did not actually participate in surface flow. According to Maier et al. (2010), the selection of data input configuration based upon the hydrologist's skill leads to the loss of certain elements that might be needed for the network to capture the dynamism. In contrast, the dynamic models have the advantage that it can commensurate with the non-stationary behavior of different hydrological systems and R-R transformation modelling (Bhattacharjee & Tollner, 2016; F.-J. Chang et al., 2014; Chang et al., 2015; L.-C. Chang et al., 2014; Coulibaly et al., 2001; Coulibaly & Baldwin, 2005; Ghose et al., 2018; Sahoo et al., 2019; Wang et al., 2020).The dynamic NARX Neural Network models were classified under this category. The use of single storm events to design the R-R process in urban areas is scarcely reported in the literature. Shen and Chang (2013)used a single storm event to investigate three NARX-NN configurations to simulate online flood inundation depth, they concluded that the NARX-NN had a great ability to inhibit the error growth even though the use of outputs from the model instead of real data, but only if consistent input-output data is used in both training and testing.

The present study aims to investigate the ability of the NARX-NN black-box model to simulate surface runoff of a small urban watershed resulting from real storm events. Hence, to explore their applicability to simulate single storm events, fourteen hourly storms used to estimate the basin discharge in the outlet. The NARX-NN model is compared to the conceptual HEC-HMS model. The two models are extremely different in terms of data requirements. The drainage area is a small urban basin, which the percentage of impervious area is about 51.5%. The percentage of the impervious area in addition to watershed physical characteristics and CN values for the years 1984, 1991, 2014 and 2018 were determined by the help of GIS and satellite images.

## VII.2 Study Area and Data Collection

The wadi Seghir is a small urban watershed, which is located in north-eastern of Algeria (**Fig.VII.1)** It extends over an area of 11.84 $Km^2$. It is located in the coastal part of the country, characterized by a Mediterranean climate, where the climate regime there depends on meteoric precipitation and temperature. The summer of this region is driest, which have an annual

average of 10 mm However; the winter season is wettest, given by a mean value of 109 mm. The percentage of impervious area was around 15.7% in 1984, however in 2018; it was more remarkable, where it reached the proportions of 51.5 % of the total area.

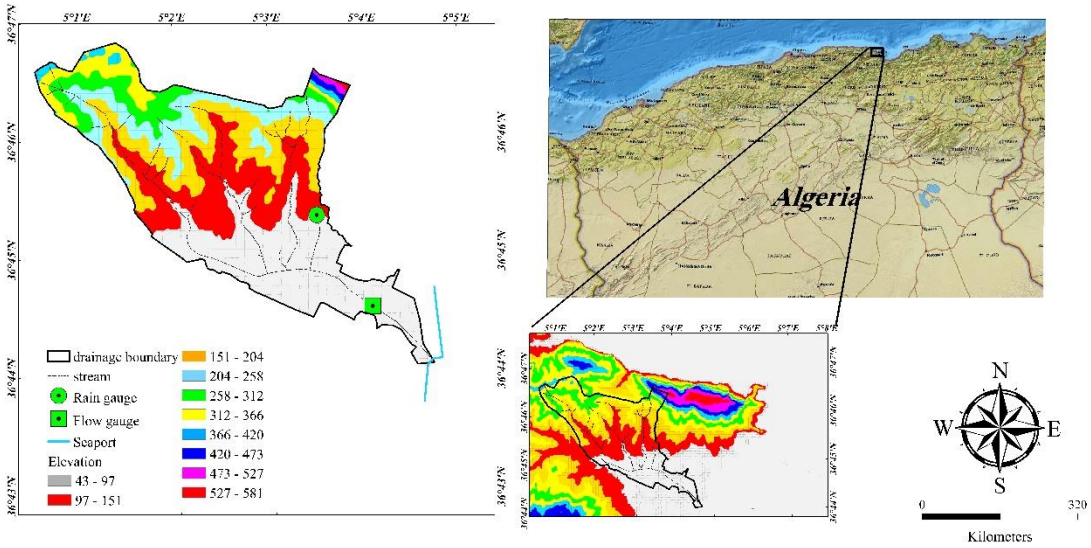


Figure VII-1 Map of study watershed location, rainfall gauge and flow gauge locations.

In this work fourteen single storm events of hourly time step are used. They were recorded during a study conducted by order of the National Office of Sanitation (NOS). The Landsat 8 OLI/TIRS Operational Land Imager (OLI) and Thermal Infrared Sensor (TIRS) satellite images of the land surface derived from the United States Geological Survey USGS database, used to extract the Land- Use (LU) maps, the satellite images downloaded from the website https://earthexplorer.usgs.gov. In addition, the soil information is derived from the soil map of geographical service of defense.

## VII.3 Materials and Methods

### *VII.3.1.A NARX-NN Model*

NARX is a nonlinear system identification extended from the linear ARX model to simulate complex and dynamic processes. It is defined by the following equation:

$$y_t = f\left(y_{t-1}, y_{t-2} \ldots\ldots y_{t-n_y}, u_{t-1}, \ldots\ldots u_{t-n_u}\right) + e_t \qquad (12)$$

Where $y_t$ is the output vector; $u_t$ is the input vector; $e_t$ is the exogenous inputs, $n_y$ *and* $n_u$ are the lags of outputs and inputs, and $f$ is the Nonlinear function (Suykens et al., 1996) .

The NARX-NN model is a part of recurrent dynamic neural network with global feedback, which composed of input, output and hidden layer, used to simulate time varying systems. A tapped Delay unit (ID) is applied on the input to which is considered as exogenous, due to its originating. On the other hand, The delayed outputs are backward by Feedback Delay unit (FD) which is regressed on the model outputs (Haykin, 2010).

The NARX-NN model is highly flexible, where the network converted between open and closed mode easily which allow training the model by the measured targets instead of estimated outputs. It is also important to indicate that the output values produced by the model can be regressed in both training and testing phases. In the ideal case, when the model could be as a reference model., it can be trained and tested in open loop configuration (Shen & Chang, 2013).

The structure of the network can be characterized by the ID and the FD, where its determination is not an obvious task (Lee et al., 2017).The structure of the network can be characterized by the ID and the FD, where its determination is not an obvious task(Maier & Dandy, 2000; Maier et al., 2010). In fact, the Number of Weights (NW)should not exceed the quantity, expressed by equation (13):

$$NW = (ID + FD + 2) \times NH \qquad (13)$$

Where $NH$is the number of hidden nodes (Diaconescu, 2008).The Levenberg-Marquardt (LM) algorithm showed a better convergence when the $NW$has a few hundred, increasing number of weight, hence; the model complexity leads to decrease algorithm performance(Diaconescu, 2008; Hagan & Menhaj, 1994).

*VII.3.1.B NARX-NN Implementation*

The NARX-NN model was developed to simulate the basin response to event-based R-R using the precipitation values and the regressed discharge as input within the model (**Fig.VII.2**). The approach of entering data into the model has always been the focus of a permanent and renewed researches (Bowden et al., 2005; He et al., 2011). Many modelers have taken a great interest to this fundamental step, because of its significant effect on the output. Anthony and Michael (2004) found through the literature, two commonly data entered methods for the R-R neural networks models. The first method based on the entering the successive ordinates of the hyetograph and their corresponding ordinates of the hydrograph. The second is called dynamic approach, in which the concurrent inputs from record stations in the same catchment with the

corresponding parallel outputs are chosen. The dynamic approach of inputs data can be decomposed into three types. The simplest one uses only the rainfall ordinates as input. However, the second one a is rainfall-runoff simulation model that used in addition to rainfall ordinates, the previous ordinates of runoff data. The last one is the purely autoregressive approach, which uses only the antecedent runoff values to predict the concurrent outflow. The present model is generally considered as a combination of the first approach and the dynamic regressive approach. It should be noted that the inputs are to be pre-processed before entering them into the network.

#### *VII.3.1.B.1 Data Preprocessing Step*

The inputs are pre-processed before entering them into the network. The linear normalization function was applied to scale the data into the range of [-1; 1]. Additional pre-process setting could undergo by removing rows with constant values. Post-process data is done before the last layer of the network after finding the final result.

#### *VII.3.1.B.2 Training Algorithm*

The LM back-propagation algorithm (Hagan & Menhaj, 1994) was used for optimization in the training process. It is considered the fastest for feed-forward networks. This algorithm is successfully used in several studies in training the NARX model (Chang et al., 2015; Guzman et al., 2017; Lee & Sheridan, 2018; Lee et al., 2017; Wunsch et al., 2018). The model benefits from the availability of the truly observed runoff that used to train the network in series-parallel configuration (**Fig.VII.2. A**). However, the network tested in parallel mode where the estimated outputs produced by the system fed back into the input layer (**Fig.VII.2. B**). The training with the real data gives more accurate results (Beal et al., 2017). The randomly chosen weights are calibrated during the model iteration. Each time the learning is repeated, the model gave different results due to weights and biases reinitializing, running is continuing until the best performance is achieved

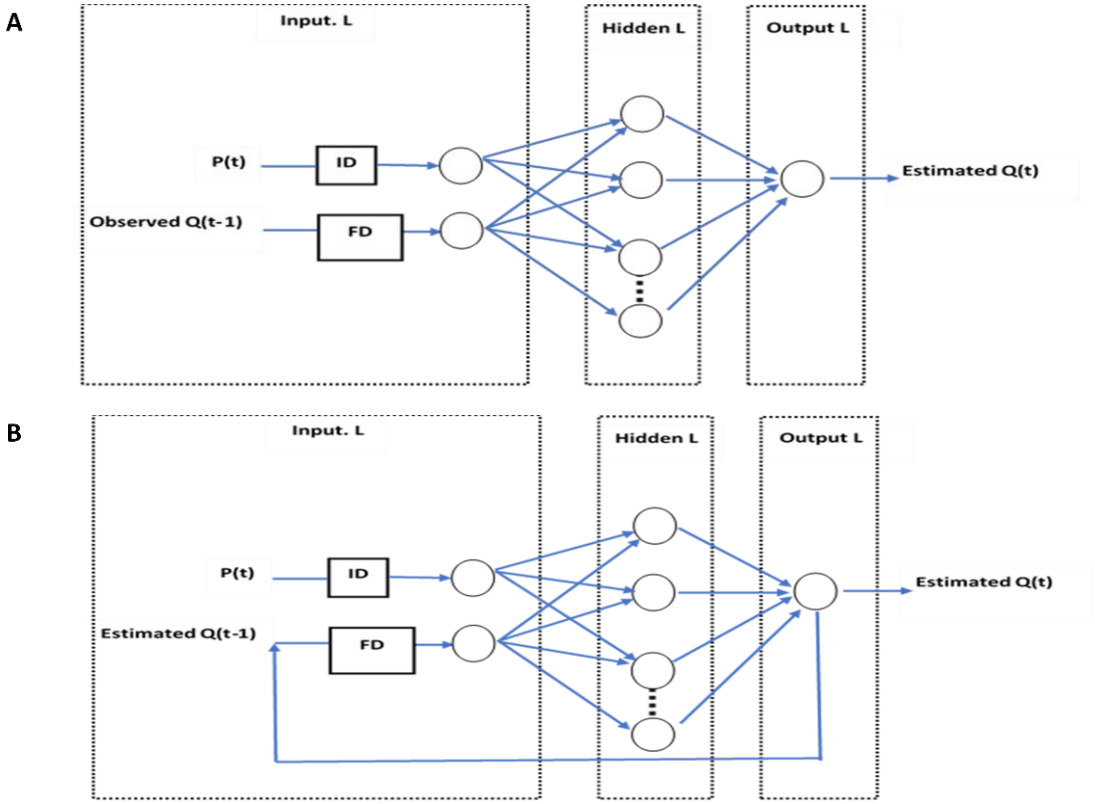


Figure VII-2 NARX-NN model architecture, used to estimate the runoff Q(t). Rainfall P(t) and observed runoff Q(t) are the input data of this model. The Parallel configuration (A)used to train the network, while; the Series-parallel configuration (B) used for the test. Input time delay (ID), feedback time delay (FD).

#### *VII.3.1.B.3 Dividing Dataset*

The data divided randomly into three sets. The first set that gets the most significant part of data for the learning, in this step the adjusting parameters (weights and biases) were fitted gradually to improve the objective function, here; the Mean Squared Error (MSE) is used for evaluation. The second represent the validation dataset, which used the weights updated from the training step to verify the decreasing of MSE. In validation step, the NARX-NN model keeps looking for the weights and bias levels that give the smallest MSE, until it fails to improve. The latest represents the dataset, which used for testing the model. The test evaluated the generalization of model. The test used the set of parameters (without a change in weights or biases), obtained from the validation dataset to construct the model.

### *VII.3.2 HEC-HMS Model*

The Hydrologic Engineering Centre Hydrologic Modelling System (HEC-HMS) is a conceptual R-R model developed by the United States Army Corps of Engineers (USACE). HEC-HMS support both event-based and continues simulation processes (Scharffenberg et al.,

2018).As reported in the literature, the HEC-HMS is widely used for event-based rainfall-runoff modelling (Abushandi & Merkel, 2013; Chu & Steinman, 2009; De Silva et al., 2014; Rahman et al., 2017; Yang et al., 2017)

### *VII.3.2.A HEC-HMS Implementation*

Four necessary components were used construct the HEC-HMS model. The basin model component permits the physical description of the watershed which contains the sub-basin and the outlet elements, the sub-basin elements grant the design of the rainfall excess and the transform function. The meteorological component calculates the liquid or frozen precipitation input, the control specification element for monitoring date and time step of the event. Finally, the time series component permit of entering real storm events (real precipitation and their corresponding discharge. Only the loss function and the transfer function were considered in this study to simulate the rainfall runoff process, evaporation considered not influential to short storm events (Abushandi & Merkel, 2013; Nandalal & Ratmayake, 2010), therefore, it has been eliminated. It was considered that the interception by vegetation and storage by depressions have non-significant effect on flow generation in urban areas. Here, just infiltration has been modelled using the soil conservation service (SCS-CN) method. However; The Snyder transfer function is used to model the direct runoff.

#### *VII.3.2.A.1 Inputs Data Preparation*

The study watershed witnessed tremendous urban development in the last two decades. Hydrologically, this development has been translated through the Curve Number (CN) calculation. A diachronic cartography of land use (LU) of 1984, 1991, 2014 and 2018 is done to demonstrate changes in land use due to anthropic activities see **Fig.VII.4**. The LU map of the last year (2018) was used to extract Curve Number (CN) value of the SCS-CN method, which is exploits later to calculate the loss function.

Two parameters are required for the SCS-CN method, which are the CN and the Imperviousness. The selection of curve number is based on the LU and Hydrological Soil Group (HSG) information using the GIS technics. The treatments of satellite images are carried out with the help of Arc-GIS software. The LU of the study watershed extracted from the satellite image, which was classified according to the maximum likelihood supervised classification method. The classified image must be assessed, this would give more confidence and indicate if the objective of analysis was achieved (Richards & Jia, 1999). Accuracy of the classified images is

determined empirically by selecting a sample of pixels (ground truth point) from the thematic map (from google earth) against classes determined from reference data (Congalton & Green, 2019). In general, the accuracy of classification can be obtained by generating an error matrix, through which, two important coefficients can be calculated, which are the Kappa coefficient and the overall accuracy that equal 94% and 96% in 2018; respectively.

The HSG map has been established based on soil map. The study area georeferenced and digitized using Arc-GIS software, and then the according information added to the attribute table. The CN was estimated from the combination of HSG and LU maps. The Snyder model parameters that must be entered into HEC-HMS model are the standard lag HR and the peaking coefficient Cp, calculated using the physical characteristics of the study watershed. The HR can be obtained by applying the following expression:

$$HR = 0.75 \times Ct \times (L \times Lc)^{0.3} \qquad (14)$$

Where L is the longest flow path (m); Lc is the length along the main stream from outlet to a point nearest the centroid of watershed (m); and Ct is the basin coefficient. Since the CP and Ct coefficients are not physical parameters, however, they are best adjusting during the calibration process (Feldman, 2000).

*VII.3.2.A.2 Calibration and Testing*

Calibration process is carried out to estimate model parameters using observed data, some of these parameters can be obtained from measured data or from thematic maps for the drainage basin (Musy et al., 2014). The HEC-HMS model was calibrated using Nelder and Mead algorithm (Nelder & Mead, 1965). In order to adjust the model parameters, the combination of automatic calibration with manual modifications are used to ensure that parameters adjusted in realistic intervals. The sum of squared residuals (SSR) objective function used to minimize the error between the observed and computed hydrographs. This function computes the squared difference as measure of fit. The HR which is function of Ct, and Cp for the Snyder transform's function, and the initial abstraction Ia for SCS-CN loss method adjusted via calibration for all the storm events. The choice of parameters based on manual sensitivity analysis is performed to find to the most sensitive inputs. The test of the HEC-HMS model performed by inserting the calibrated parameters as input for simulation of new storm events in order to evaluate the model generalization. KlemeŠ (1986) has reported that in case if the available data are long enough, the observed data should be divided into two halves, where, the first used for calibration

and the second used for the test. Otherwise, the appropriate calibration should take the biggest part, while; the rest of the data was served for the test (70% of data for calibration and 30% of data for testing).

### VII.4 Results and Discussion

This section will focus on the descriptive analysis to show the performance of the models used to estimate R-R compared to real data. A set of qualitative and quantitative tests were used in order to obtain the best parameters of the HEC-HMS and also to designate the stop condition of NARX-NN model iteration step. The trends of each model were analyzed by residual analysis curve, followed by a set of statistical parameters to compare between the performances of the two models. Where, NSE, $R^2$, $R^2_{Adj}$, PEP (Percent Error in peak), MAE (Mean Absolute Error) and RMSE (Root Mean Square Error) performance criteria are used to compare between the two models. NSE criterion (Nash & Sutcliffe, 1970)has the ability to assess the model in terms of the correlation between estimated and observed values (Gupta et al., 2009), which makes it more appropriate and meaningful to evaluate R-R models, Green and Stephenson (1986)proposed the use of PEP criterion to assess the peak flow of the single event models. MAE and RMSE compute all deviation regardless the outliers and quantify the error abandoned of negative values. Unlike the absolute errors, the measure of relative errors such as NSE and $R^2$, $R^2_{Adj}$ provides only a sensitivity to extreme values but not in the unit range of variables(Cheng et al., 2017; Christian W & Robert L, 2004; Legates & McCabe Jr, 1999; Singh & Chakrapani, 2015; Srivastava et al., 1995). All the used criteria are defined by the equations shown in the **Table.VII.1**.

Table VII-1 Statistical criteria used to evaluate the performance of HECH-HMS and NARX-NN models.

| Criteria | Equation unit | Reference |
|---|---|---|
| Mean Squared Error (MSE) | $MSE = \frac{1}{N}\sum_{i=1}^{N}(Qsi - Qoi)^2$ | (Hsu et al., 1995) |
| Nash-Sutcliffe Efficiency (NSE) | $NSE = 1 - \frac{\sum_{i=1}^{N}(Qsi - Qoi)^2}{\sum_{i=1}^{N}\left(Qoi - \overline{Qo}\right)^2}$ | (Nash & Sutcliffe, 1970) |

| | | |
|---|---|---|
| Percent Bias (PB) | $PB = \frac{\sum_{i=1}^{N}(Qoi - Qsi)}{\sum_{i=1}^{N} Qoi} \times 100$ | (N. Moriasi et al., 2007) |
| Ratio of the root mean square error to the standard deviation of measured data (RSR) | $RSR = \frac{\sqrt{\sum_{i=1}^{N}(Qoi - Qsi)^2}}{\sqrt{\sum_{i=1}^{N}\left(Qoi - \overline{Qo}\right)^2}}$ | (N. Moriasi et al., 2007; Singh & Chakrapani, 2015) |
| sum of squared residuals (SSR) | $SSR = \sum_{i=1}^{N}(Qoi - Qsi)^2$ | (Green & Stephenson, 1986) |
| Percent Error in Peak (PEP) | $PEP = \frac{Qpo - Qps}{Qpo} \times 100$ | (Cheng et al., 2017; Green & Stephenson, 1986) |
| Mean Absolute Error (MAE) | $MAE = \frac{\sum_{i=1}^{N}\lvert Qoi - Qsi\rvert}{N}$ | (Cheng et al., 2017) |
| Coefficient of determination ($R^2$) | $R^2 = \frac{\sum_{i=1}^{N}\left(Qoi - \overline{Qo}\right) \times \left(Qsi - \overline{Qs}\right)}{\left[\sum_{i=1}^{N}\left(Qoi - \overline{Qo}\right)^2\right]^{0.5}\left[\sum_{i=1}^{N}\left(Qsi - \overline{Qs}\right)^2\right]^{0.5}}$ | (Legates & McCabe Jr, 1999) |
| Adjusted coefficient of determination ($R^2_{Adj}$) | $R^2_{adj} = 1 - \frac{(1 - R^2)(N - 1)}{N - K - 1}$ | (Srivastava et al., 1995) |
| Root Mean Square Error (RMSE) | $RMSE = \sqrt{\frac{\sum_{i=1}^{N}(Q_{si} - Q_{oi})^2}{N}}$ | (Green & Stephenson, 1986) |

Note: Qs = Estimated runoff ($m^3/s$); Qo = Observed runoff ($m^3/s$); Qps = Peak simulated runoff ($m^3/s$); Qpo = Peak observed runoff ($m^3/s$); N = Total number of ordinates; K = Number of independent variables.

### *VII.4.1HEC-HMS Results*

Eleven events were calibrated by using SSR objective function, in order to get the best runoff results of each event. The stop condition will be provided when the SSR error shows the minimum value. In this part, the performance analysis of the HEC-HMS model was classified into

two phases. Starting by a comparison study between calibration results of 11 events, using the NSE, PB and RSR parameters. The objective of this step is to show the event that gives the optimum parameters of HR, TP and Ia (**Table.VII.2**). In the second step, two other computation forms are shown, which are given by equations (15) and (16), for estimating parameters of this model.

$$ACp = \frac{\sum_{i=1}^{i=n} Cp_i}{n} \quad (15)$$

$$WACp = \frac{\sum_{i=1}^{i=n} Cp_i * NSE_i}{\sum_{i=1}^{i=n} NSE_i} \quad (16)$$

Where $Cpi$ is the calibration parameters of each event, $ACp$ and WACP are the estimated parameters, which obtained by average and weighted average functions, respectively. Based statistically on the same criteria, the results of the proposed methods of three events were compared (**Table.VII.3**).

Table VII-2 Statistical comparison of estimated runoff performance used different calibrated parameters (HR, Tp, Ia) in 11 events.

| Event | calibrated parameters | | | Performances | | |
|---|---|---|---|---|---|---|
| | **HR (m*m)** | **Tp** | **Ia (mm)** | **NSE** | **PB %** | **RSR** |
| EV $_1$ | 5.10 | 0.61 | 17.05 | 0.80 | 20.17 | 0.45 |
| EV $_2$ | 4.50 | 0.75 | 17.60 | 0.87 | -9.47 | 0.40 |
| EV $_3$ | 4.43 | 0.66 | 17.45 | 0.82 | -0.46 | 0.42 |
| EV $_4$ | 3.96 | 0.48 | 12.4 | 0.81 | 18.36 | 0.48 |
| EV $_5$ | 4.67 | 0.76 | 17.38 | 0.94 | 8.77 | 0.25 |
| EV $_6$ | 4.96 | 0.69 | 17.33 | 0.76 | -1.31 | 0.50 |
| EV $_7$ | 4.86 | 0.75 | 15.34 | 0.85 | 6.59 | 0.39 |
| EV $_8$ | 4.69 | 0.75 | 13.66 | 0.82 | 17.29 | 0.43 |
| EV $_9$ | 4.18 | 0.59 | 17.83 | 0.87 | -7.36 | 0.36 |
| EV $_{10}$ | 4.90 | 0.67 | 15.34 | 0.77 | -4.13 | 0.475 |
| EV $_{11}$ | 5.64 | 0.87 | 17.97 | 0.96 | -9.10 | 0.19 |

Note: NSE = Nash-Sutcliffe; PB = Percent Bias; RSR = Ratio of the root mean square error to the standard deviation of measured data.

Table VII-3 Performance results of HEC-HMS testing phase, given by three events ($EV_{12}$, $EV_{13}$ and $EV_{14}$), using different methods

| Method | C.P | | | $EV_{12}$ | | | $EV_{13}$ | | | $EV_{14}$ | | |
|---|---|---|---|---|---|---|---|---|---|---|---|---|
| | **HR (m*m)** | **Tp** | **Ia (mm)** | **NSE** | **PB %** | **RSR** | **NSE** | **PB %** | **RSR** | **NSE** | **PB %** | **RSR** |
| Cp-$EV_{11}$ | 5.64 | 0.87 | 17.97 | 0.80 | 0.00 | 0.45 | 0.82 | 2.43 | 0.42 | 0.77 | -27.57 | 0.48 |
| Cp-AV | 4.72 | 0.69 | 16.30 | 0.88 | -0.14 | 0.35 | 0.91 | 2.24 | 0.30 | 0.75 | -27.66 | 0.50 |
| Cp-WAV | 4.72 | 0.69 | 16.36 | 0.87 | -1.20 | 0.45 | 0.91 | 2.29 | 0.30 | 0.83 | -27.59 | 0.50 |

Note: Cp-EV11, Cp-AV and Cp-WAV = methods used to obtain calibrated parameters (C.P); NSE = Nash-Sutcliffe; PB = Percent Bias; RSR = Ratio of the root mean square error to the standard deviation of measured data; Event= EV.

The NSE was used to show the degree of reliability, where the best results could be achieved close to 1. However, The PB and RSR parameters were used to study the trend of simulated data compared to the observed one. The Positive values of PB indicate that the model underestimated. However; the negative values indicate the overestimation of the model. Whereas, the best adjustment corresponding to the null value. **Table.VII.2** shows that during calibration step, NSE gave values between 0.76 and 0.96, where the model providing the best performance. In addition, PB parameter indicates that the HEC-HMS model had remarkable trend compared to the actual values, which varied between a minimum of 0.46% and maximum of 20.17%. From the results given by $EV_2$, $EV_3$, $EV_6$, $EV_9$, $EV_{10}$ and $EV_{11}$, this model shows an overestimation, compared to the actual data. Whereas, in $EV_1$, $EV_4$, $EV_5$, $EV_7$ and $EV_8$, the model had an under estimation. **Table.VII.2** shows that the best calibration parameters (HR, TP and Ia) were given by event $EV_{11}$, where the NSE represent the best performance and the RSR shows the minimum of errors, given by 0.96 and 0.196; respectively. In this regard, **Table.VII.3** shows the comparison results between HEC-HMS and real discharge, given by three events ($EV_{12}$, $EV_{13}$ and $EV_{14}$), using three different forms of calibrating parameters, noted by Cp-$Ev_{11}$, Cp-AV and Cp - WAV; respectively. During the testing phase, the results shows that when the Cp-AV and Cp-WAV parameters are used, the model performs very well, compared to Cp-$EV_{11}$. In $EV_{14}$, the model shows a good performance with Cp-WA compared to Cp-$EV_{11}$ and Cp-AV. Generally, the model has the best results with the Cp-WA parameter, where the NSE proved values more than 0.8 in all events. In addition, PB and RSR do not give a significant trend of errors when we use Cp-WAV parameters. In this case HR, Tp and Ia are given by 4.72, 0.69 and 16.36; respectively.

### *VII.4.2 NARX-NN Results*

The input and target data arranged side by side in a continuous-time series to provide the widest time series of data. Several experiments have been conducted focusing on NARX-NN characteristics to get the most efficient scenario in order to represent the R-R relationship. An analysis of ID and FD under change of DD and NH is realized, these parameters had chosen to investigate their strong influence on the network and for better understanding the functioning system.

The best performance in terms of MSE objective function, Error Auto-Correlation EAC, and Input Error Cross-Correlation IECC was selected. The most efficient configuration can be obtained with:

- ID=FD=2;
- NH=10;
- DD (training=65%, validation=15%, test=20%).

In addition to the sigmoid transfer function in the hidden layer and the linear transfer function in the output layer. The best obtained scenario was compared by the conceptual HEC-HMS model.

The **Fig.VII.3. B.** presents the EAC function. It displays the autocorrelation of the lagged MSE. The Perfect model provides null values in all lags, except the zero-lag should be greater than zero. Approximately lagged errors fall within the 95% confidence interval and the value of zero lag is not zero. The IECC (**Fig.VII.3. A**). measures the correlation between the inputs and the difference of observed and estimated values. It illustrates the relation of the errors by the input sequences. For typical model prediction all values must be zero, or at least within the confidence interval. However, there are just a few values outside the limits, herein the inputs are correlated with the error.

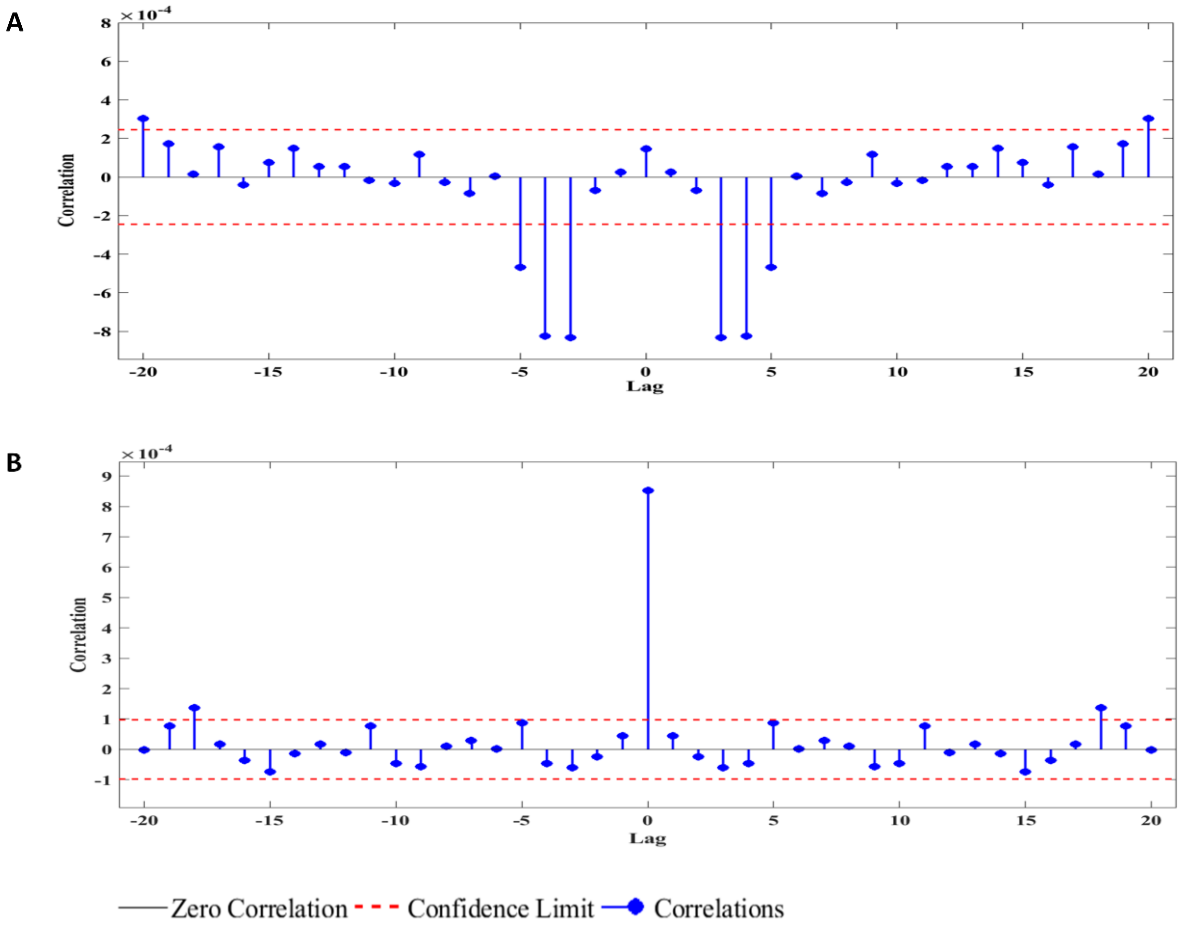


Figure VII-3 Auto correlation of mean squared error function (A), followed by cross correlation of inputs and the difference of observed and estimated values (B).

### *VII.4.3 Statistical Comparison*

Two different models were used to simulate the watershed response for single storm events. The two models are completely different in terms of data entry and the type of data. The HEC-HMS model requires several sorts of data (planimetric data, thematic maps) and many steps. However, the R-R process in HEC-HMS disjointed into several components implies simulation of each component alone that is the reason to ignore one of them. The NARX-NN requires only the measured rainfall and runoff as input; it needs the control of some parameters that play a vital role in prediction performance, including time delays, NH, and DD. The two models were previously evaluated distinctly. Furthermore, statistical and visual interpretation are essential for both models. The performance of the NARX-NN model was compared with HEC-HMS statistically using NSE, PEP, and MAE. These indexes were chosen according to reasons mentioned above. The appropriate peak flow estimating is crucial for event-based storm modelling, since it is one of the key parameters in single event hydrograph. The PEP performance criterion

is used to evaluate the capability of models to estimate the peak flow. The negative values of PEP indicate that the peaks are under estimated.

The summary statistics for calibration of the two models are presented in **Fig.VII.4**. Therefore, no significant disparities between the models. The both models were judged to be successfully reflected the basin response. The results show that among 11 events, there are 7 events in which the NARX-NN model performs better. However, in the rest of the 4 events, the HEC-HMS model shows its performance. The PEP graph shows that the first model has very weak trends of estimation errors, where throughout the calibration, the model gives results which are distributed homogeneously between underestimated and overestimated compared to real data. On the other hand, the HEC-HMS shows 8 events out of 11 are overestimated. These results are more significant in the MAE graph, where in the majority of cases, the NARX-NN model shows less errors compared to those given by the HEC-HMS model.

Table VII-4 Results of statistical parameters used to compare between NARX-NN and HEC-HMS performance during the testing phase.

| Performance | NAX-NN | | | HEC-HMS | | |
|---|---|---|---|---|---|---|
| | **$EV_{12}$** | **$EV_{13}$** | **$EV_{14}$** | **$EV_{12}$** | **$EV_{13}$** | **$EV_{14}$** |
| $R^2$ | 0.97 | 0.98 | 0.98 | 0.87 | 0.88 | 0.85 |
| $R^2_{Adj}$ | 0.97 | 0.98 | 0.98 | 0.88 | 0.88 | 0.85 |
| NSE | 0.92 | 0.96 | 0.96 | 0.75 | 0.88 | 0.91 |
| PEP (%) | 0.68 | -7.56 | -1.98 | 5.31 | -3.6 | -0.24 |
| RMSE | 0.15 | 0.03 | 0.02 | 0.43 | 0.07 | 0.05 |
| MAE | 0.110 | 0.026 | 0.019 | 0.320 | 0.058 | 0.022 |

Note: $R^2$= Coefficient of determination; $R^2_{Adj}$ =Adjusted coefficient of determination; NSE = Nash-Sutcliffe; PEP = Percent Error in Peak; RMSE = Root Mean Square Error; MAE = Mean Absolute Error.

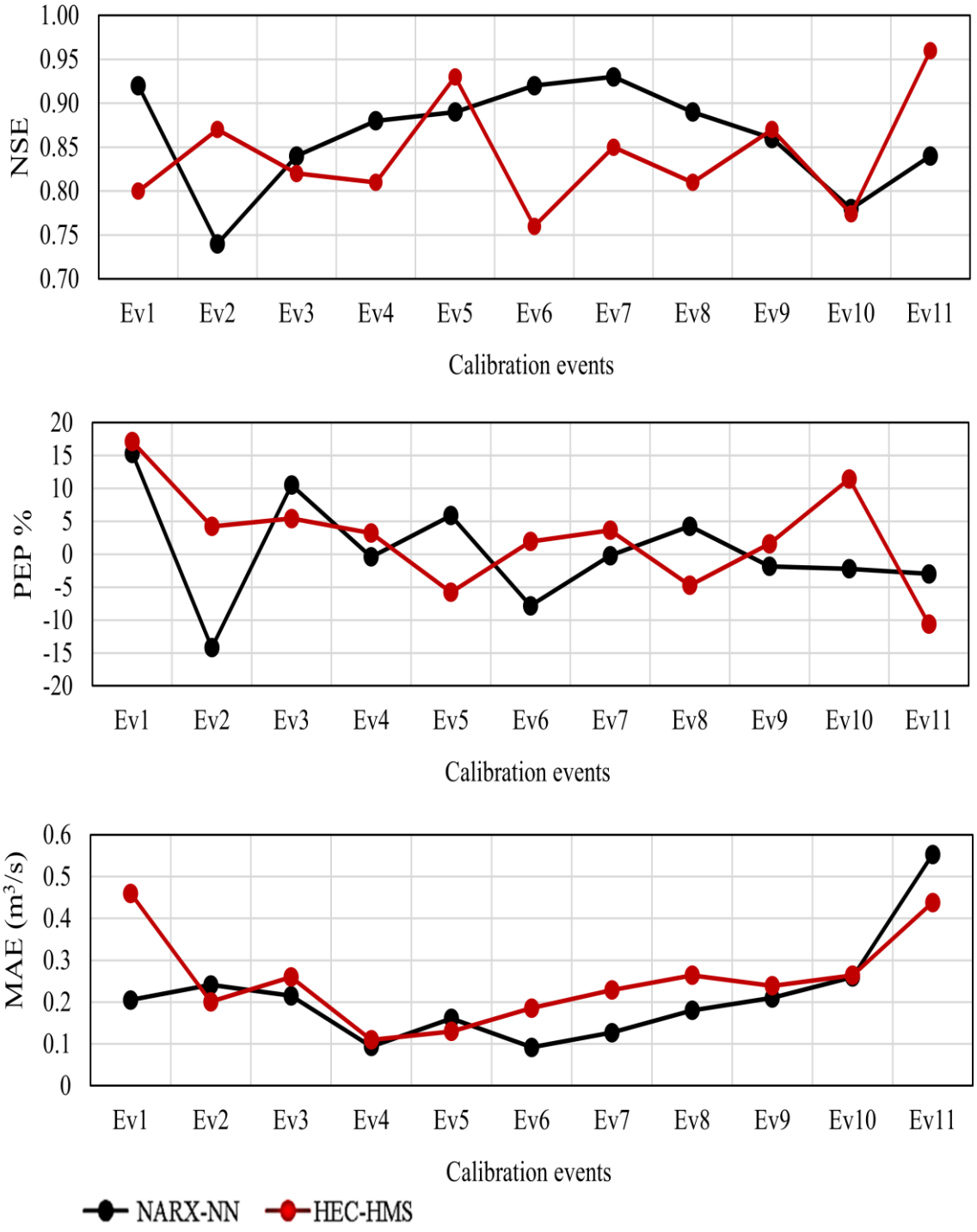


Figure VII-4 Curves show Nash-Sutcliffe efficiency (NSE), Percent Error in Peak (PEP) and Mean Absolute Error (MAE) criteria for calibration evaluation of NARX-NN and HEC-HMS models.

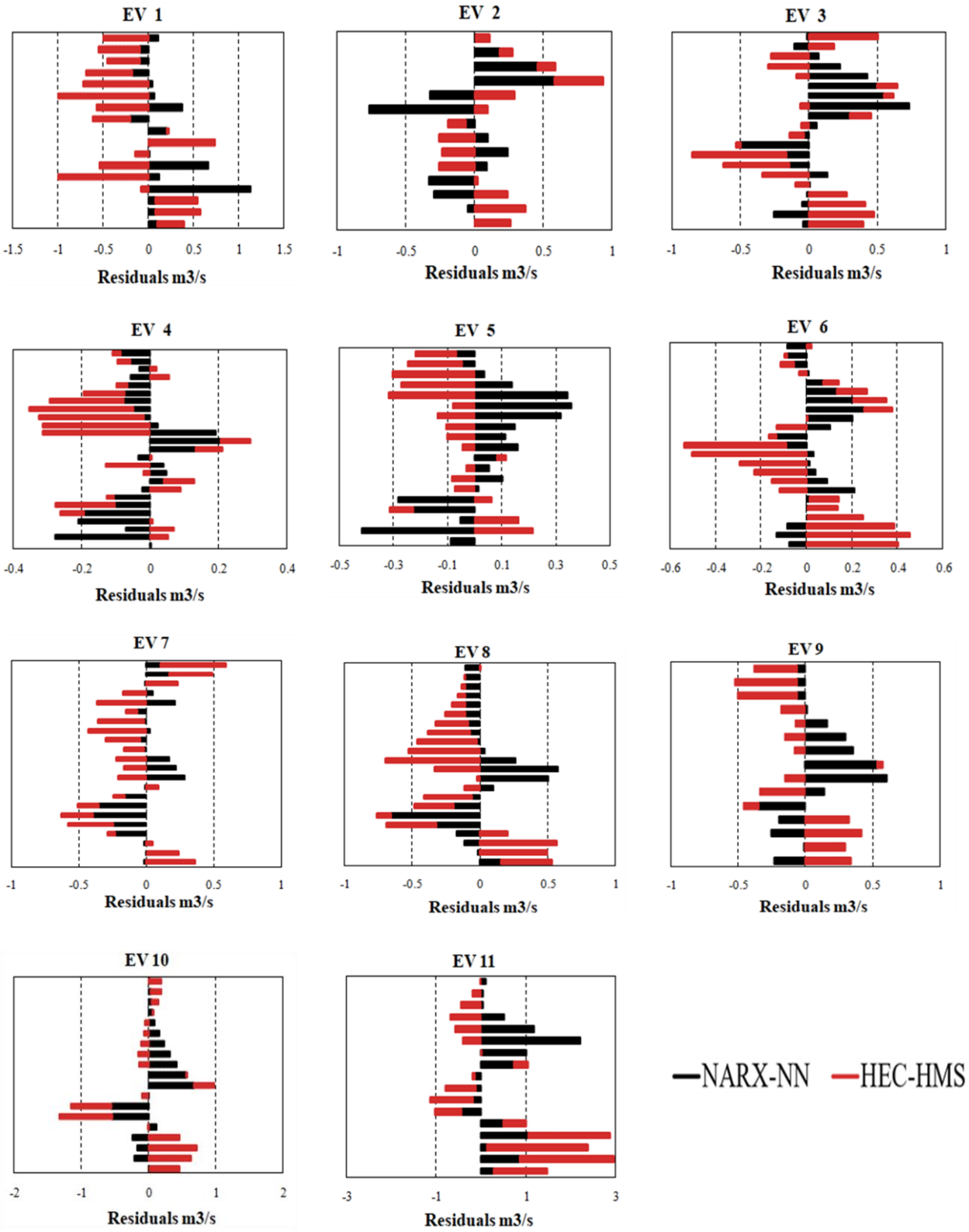


Figure VII-5 Residuals curves of runoff results, obtained from NARX-NN and HEC-HMS models in calibration phase.

The difference between observed and predicted runoff for the calibration phase is shown in **Fig.VII.5**. It compares localized residuals in each point of HEC-HMS and NARX-NN models; it is clear that residuals in HEC-HMS exceed than that in the NARX-NN model. The results strongly support the high capability of NARX-NN to mapping the R-R relationship, which needs to model several components in the conceptual model to achieve it. **Fig.VII.6. A** display the graphical representation of the testing period of NARX-NN and HEC-HMS compared to the measured one, which expresses optimally the outcomes. The **Fig.VII.6** shows hydrographs of the testing period, in the bottom of each one of them its residuals histogram. The residuals are a good indicator to analyze trends of results which were given by the model. In all testing events, the range of the residuals for the NARX-NN model is much less than from those in the conceptual. The NARX-NN model has more strength to produce the shape bending of the hydrograph. Whereas, in the HEC-HMS model, the rising and falling limb represents a straight curvature. These curvatures are the result of local peaks of rainfall, which better highlighted by the NARX-NN model. These results confirm that the NARX-NN model has a high capability to produce the nonlinearities, although the short time-series data used in training and testing.

**Fig.VII.7** shows a graphical representation of real and estimated outflow, which were obtained by NARX-NN and HEC-HMS models. This analysis was done by a Box plot in order to compare between the performances of the two models according to the data distribution, using a set of descriptive statistical parameters. The graph shows that the NARX-NN model has the best performance, where the obtained values by this model show a similarity of data distribution with the actual observation. On the other hand, HEC-HMS gave an underestimation, where the Min, 1st quantile, Median, 3rd quantile and Max are less than those of observed runoff. Moreover, **Table.VII.4** gives a trend analysis of this comparison using three different testing events ($EV_{12}$, $EV_{13}$ and $EV_{14}$). In this table, $R^2$, $R^2_{adj}$ and NSE show that the maximum values were given with NARX-NN model, where the performance of the model varies between a min value of 0.92 and a max value of 0.98. Whereas, HEC-HMS model shows an R2, R2adj and NSE between 0.75 and 0.91. PEP%, MAE and RMSE show also that NARX-NN model has a weak trend of residues compared to HEC-HMS.

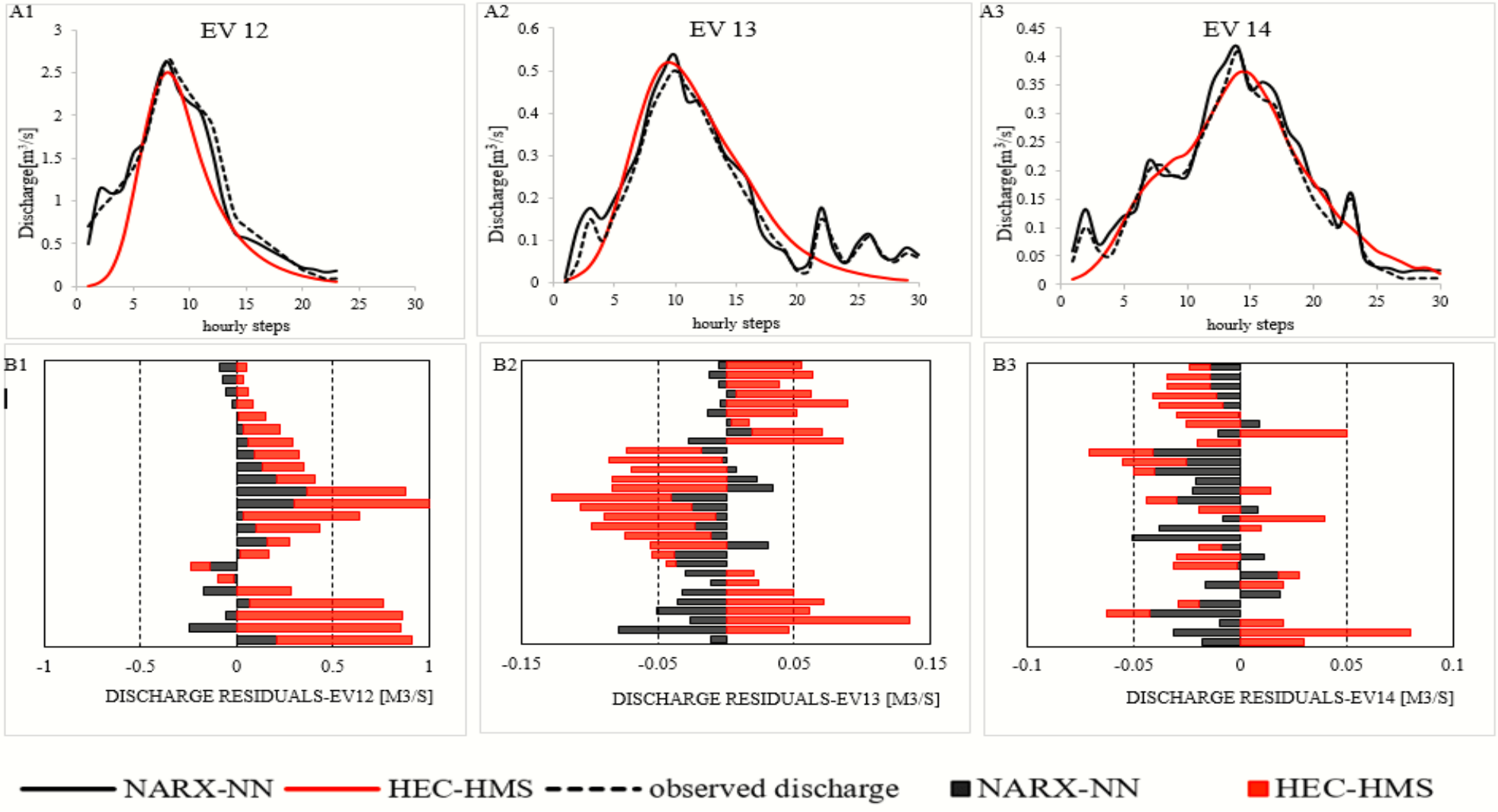


Figure VII-6 Hydrographs of observed versus simulated runoff, modeled by NARX-NN and HEC-HMS models (A) and their corresponding residuals (B). Event (EV).

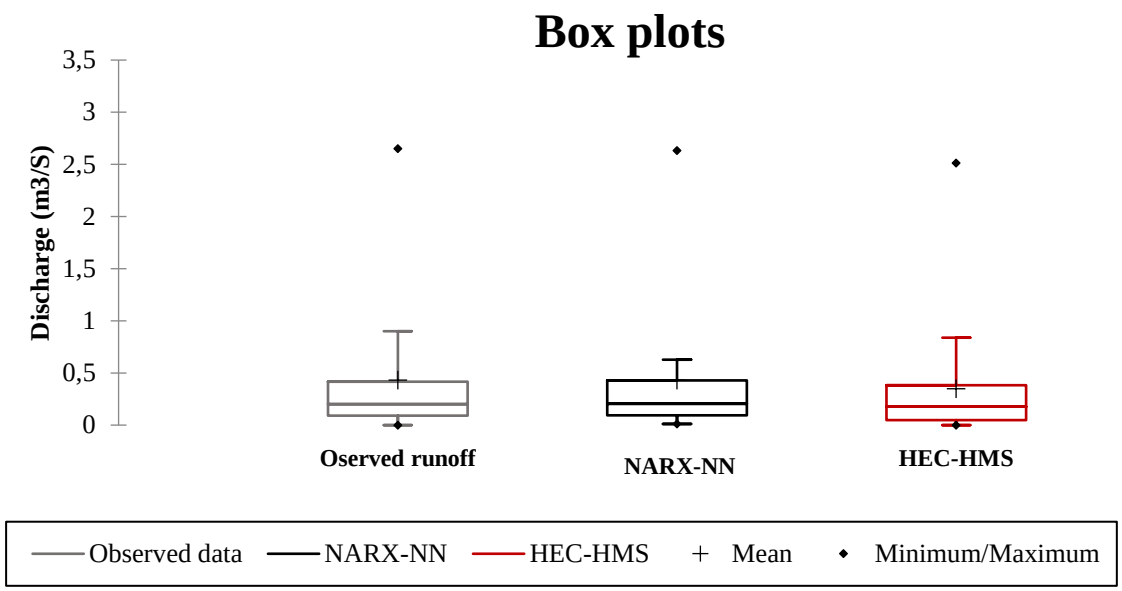


Figure VII-7 Box Plots of observed runoff and estimated runoff, which obtained by NARX-NN and HEC-HMS mode ls during the validation phase.

## VII.5 Conclusion

In the conceptual HEC-HMS model, the GIS has great importance in constructing the model, collecting and organizing the data. The conceptual model needs several steps to achieve direct runoff. Moreover, the model contains an important number of parameters compared with the black-box model; its calibration is relatively complicated, impose the choice of the most sensitive parameters that affect the hydrograph. In the testing phase, the HEC-HMS proved its best performance when it applied the weighted average on the calibrating parameters of all events.

For the black-box NARX-NN model, the selection of the network parameters such as ID, FD, NH, and DD are a crucial task to optimize the network performance. They are determined by the trial-and-error manner. It can be concluded that ID and FD have strong effects on the network performance, it replaces the lag of inputs in the static networks. This characteristic is integrated into the NARX-NN dynamic network. Giving more incentive to use the dynamic models as an alternative means to simulate time series dynamic systems, instead of searching the optimal lag by the traditional tools in the static networks. Also, it can be concluded that the NARX-NN gave the best results when the ID is equal to the FD.

The statistical assessment shows that during calibration, the two models are closely the same in terms of NSE and MAE with a slight superiority of NARX-NN. Except for PEP benchmark which indicates the supremacy of the NARX-NN over HEC-HMS to mapping the peak of the hydrograph, which agreed as one of the most important elements in the short storm events. In the testing phase, statistical parameters indicate that the NARX-NN outperforms to model the basin response.

The findings drawn from the results demonstrate the high capability of the NARX-NN model to capture the R-R process, although the short time-series data used in training and testing phases. Moreover, the result of testing is more accurate than that of the training phase, which demonstrates the strength of the generalization feature of NARX-NN. It has more strength to produce the shape bending of the hydrograph; in contrast, the rising and falling limb in the HEC-HMS model presents straight curvature. Consequently, the NARX-NN model is better to highlight the curvatures resulted from the local peaks of rainfall.

# VIII General conclusion

The high nonlinearity and the dynamism are the major distinctions in the relationship between precipitation and runoff. Rainfall transformation into the surface runoff is an essential hydrological process. As it is required in water relates problem solution for the engineers and decision-makers. Modeling this relationship is an essential hydrological process task, needed for many purposes, to solve the engineering problems and to deeply analyze and understand the watershed compartment. The challenge that usually faces the hydrologists is reflecting the basin response, having regard to changes that occurred in the basin unit; the spatial and the temporal scales; and the objective of the modeling.

This study is undergone to simulate the runoff in the ungagged basin with considering impervious surfaces. The focus was on the short storm events of hourly steps that occurred in a Mediterranean urban basin. In addition to their geographical location, since it inflowing directly into the Mediterranean Sea. A very ragged relief characterizes the Wadi Seghir basin, the basin's upper boundaries are covered totally with forests while the lower boundaries near the basin outlet are covered with an extensive urban area, knowing that this area is entirely flat. This would cause disaster flooding due to acceleration of runoff after a short period of rain (short time of concentration). The geographical location of Wadi Seghir is between the Highlands in the East and the Sommam Valley in the West; this location and the proximity of the urban areas to the basin outlet make the area of particular interest and fertile for research and exploration. In particular, this area was the subject of a previous public contract conducted by the National office of Sanitation (ONA). Therefore, the hydrological and meteorological measures were obtained. This data is used for calibration and validation purposes.

The existed hydrological models that were used to describe the hydrological processes varied between the pure mathematic analysis and equations toward the relations that describe the process empirically based on the physics of the watershed, another recent approach that took a great interest and gave a very good performance is the black-box models. They express the relationship between inputs and outputs of a given hydro system by providing the quantification of adjusting parameters, excluding the physical properties or any hydro-system description. We need a further understanding and manipulation of these kinds of rainfall-runoff models, and to discover the difference between the Data-Driven and the traditional models, in this context we proposed this study, we choose different models from both conceptual and Data-driven to analyze the first is the black box Nonlinear Auto-Regressive with eXogenous inputs-Neural

Network (NARX-NN), and the second is conceptual Hydrologic Engineering Center-Hydrologic Modeling System (HEC-HMS) models. The study area was selected in order to verify the applicability of the NARX-NN model in small drainage areas, containing the conditions of the Semi-urbanism and the low intensity of rainfall, and then it will be compared to the conceptual HEC-HMS model.

In the conceptual HEC-HMS model the GIS and RS have great importance in constructing the model, collecting and organizing the data; developing the watershed drainage boundary and streams; preparing thematic maps and feature symbols, and are integrated with databases containing attribute data on the features; and extract basin characteristics such as surfaces, length, and slop, etc. the conceptual model needs several steps to achieve the direct runoff, the use of diverse data, tools, and software programs, Moreover, the conceptual model contains an important number of parameters compared to the black-box model; its calibration is relatively complicated, and imposes the choice of the most sensitive parameters that affect the hydrograph. the percentage of the impervious area determined by the help of satellite images, and extracted by the GIS technic, as well as watershed physical characteristics, and CN values for the years 1984, 1991, 2002, 2014, and 2018. Fourteen hourly storm events were used to simulate and calibrate the basin discharge at the outlet.

This thesis uses benchmarks to validate the results of land-use change models. These benchmarks can be applied in the assessment of the predictive accuracy and the process accuracy and serve as an indication of the minimum accuracy that a model requires in order to pass the validation. The accuracy of classification is generally found by generating an error matrix. Assessment accuracy provides the user about where the errors are occurring. The generation of the error matrix enables to the measurement of other important accuracy assessment elements such as the overall accuracy and the KAPPA coefficient which are used for assessing all the classified images, the user's accuracy, producers' accuracy, omission, and commission intended for assessing each class separately.

The evaluation of the Rainfall-runoff models is based on a set of qualitative and quantitative tests used to obtain the best parameters of the HEC-HMS and to designate the stop condition of the NARX-NN model iteration step. The trends of each model were analyzed by a residual analysis curve, followed by a set of statistical parameters to compare the performances of the two models. Where NSE, $R^2$, $R^2_{Adj}$, PEP (Percent Error in peak), MAE (Mean Absolute Error), and RMSE (Root Mean Square Error) performance criteria are used to compare the two models.

For the black-box NARX-NN model the selection of the network parameters such as ID and FD, NH and DD is a crucial task to optimize the network performance, and they are determined by the trial and error manner, we concluded that ID and FD have strong effects on the network performance, it replaces the lag of inputs in the static networks, this characteristic is integrated into the NARX-NN dynamic network, This gives more incentive to use the dynamic models as an alternative means to simulate time series dynamic systems instead of searching the optimal lag by the traditional tools in the static, the NARX-NN gave best results when the ID is equal the FD; therefore the performance deteriorates other than that. The statistical assessment shows that the average values for the events of calibration in the two models are closely the same in terms of NSE and MAE with a slight superiority of NARX-NN, except for the PEP benchmark which indicates the supremacy of the NARX-NN over HEC-HMS to mapping the pick of the hydrograph, which agreed as one of the most important elements in the short storm events. In the testing phase, the NAR-NN outperforms overwhelmingly to model the basin response.

The findings drawn from the results demonstrate:

1. The HEC-HMS proved its best performance in the testing phase when it applied the weighted average on the calibrating parameters of all events.
2. The high capability of the NARX-NN model to capture the R-R process, although the short time-series data is used in the training and testing phases;
3. The result of testing is more accurate than that of the training phase, which demonstrates the strength of the generalization feature of the NARX-NN network;
4. the NARX-NN and HEC-HMS gave a close result in the calibration phase and judged it falls in the acceptable range;
5. The NARX-NN model has more strength to produce the shape bending of the hydrograph; in contrast, the rising and falling limb in the HEC-HMS model presents straight curvature;
6. The NARX-NN model is better to highlight the curvatures resulted from the local picks of rainfall.

# IX Refrences


Abushandi, E., & Merkel, B. (2013). Modelling Rainfall Runoff Relations Using HEC-HMS and IHACRES for a Single Rain Event in an Arid Region of Jordan. *Water Resources Management*, *27*(7), 2391-2409. https://doi.org/10.1007/s11269-013-0293-4

Al-Hashimi, M. A., & Mohsin, A. N. (2008). Remote Sensing and GIS Techniques for Monitoring Industrial Wastes for Baghdad City. *Al-Nahrain Journal for Engineering Sciences*, *11*(3), 357-365.

Ali, A. (2009). Nonlinear multivariate rainfall–stage model for large wetland systems. *Journal of Hydrology*, *374*(3), 338-350. https://doi.org/https://doi.org/10.1016/j.jhydrol.2009.06.033

Ali, E. (2020). Geographic Information System (GIS): Definition, Development, Applications & Components. *Department of Geography, Ananda Chandra College. India*.

Ali, M., Khan, S. J., Aslam, I., & Khan, Z. (2011). Simulation of the impacts of land-use change on surface runoff of Lai Nullah Basin in Islamabad, Pakistan. *Landscape and Urban Planning*, *102*(4), 271-279.

Alley, W. M., & Veenhuis, J. E. (1983). Effective impervious area in urban runoff modeling. *Journal of Hydraulic Engineering*, *109*(2), 313-319.

Allison, H. R., & William, D. S. (2009). ASSESSING IMPERVIOUS SURFACE CONNECTIVITY AND APPLICATIONS FOR WATERSHED MANAGEMENT. *Journal of The American Water Resources Association*. https://doi.org/10.1111/j.1752-1688.2008.00271.x

Almousawi, D., Almedeij, J., & Alsumaiei, A. A. (2020). Impact of urbanization on desert flash flood generation. *Arabian Journal of Geosciences*, *13*(12), 441. https://doi.org/10.1007/s12517-020-05446-z

Amisigo, B. A. (2005). *Modelling riverflow in the Volta Basin of West Africa: A data-driven framework*. Cuvillier Verlag.

Anne, C. (2006). Urban transformation of river landscapes in a global context. *Geomorphology*. https://doi.org/10.1016/j.geomorph.2006.06.033

Anthony W, M., & Michael J, H. (2004). Rainfall-runoff modelling. In A. Robert J, K. Pauline E, & S. Linda (Eds.), *Neural networks for hydrological modelling* (1st ed., pp. 158-178). CRC Press.

Antonius, L. (1983). Storm runoff as related to urbanization based on data collected in Salem and Portland, and generalized for the Willamette Valley, Oregon. *Water-Resources Investigations Report*. https://doi.org/10.3133/wri834143

Arnell, V. (1982). ESTIMATING RUNOFF VOLUMES FROM URBAN AREAS 1. *JAWRA Journal of the American Water Resources Association*, *18*(3), 383-387.

Arora, V. K. (2002). The use of the aridity index to assess climate change effect on annual runoff. *Journal of Hydrology*, *265*(1), 164-177. https://doi.org/https://doi.org/10.1016/S0022-1694(02)00101-4

Atasoy, M., Karslı, F., Bıyık, C., & Demir, O. (2006). Determining land use changes with digital photogrammetric techniques. *Environmental Engineering Science*, *23*(4), 712-721.

Baig, M. F., Mustafa, M. R. U., Baig, I., Takaijudin, H. B., & Zeshan, M. T. (2022). Assessment of Land Use Land Cover Changes and Future Predictions Using CA-ANN Simulation for Selangor, Malaysia. *Water*, *14*(3), 402.

Barnes, K. B., Morgan, J., & Roberge, M. (2001). Impervious surfaces and the quality of natural and built environments. *Baltimore: Department of Geography and Environmental Planning, Towson University*.

Barnsley, M. J., Moller-Jensen, L., & Barr, S. L. (2000). Inferring urban land use by spatial and structural pattern recognition. *Remote sensing and image analysis, Routledge*, 115-144.

Bawahidi, K. S. Y. (2005). Integrated land use change analysis for soil erosion study in ulu kinta catchment. *Universiti Sains Malaysia*.

Beal, M. H., Hagan, M. T., & Demuth, H. B. (2017). Neural Network Toolbox™ User's Guide R2017b. *The MathWorks*.

Beven, J. K. (2000). Rainfall-Runoff Modelling The Primer, John Willey & Sons Ltd, New York.

Beven, K. J. (2011). *Rainfall-runoff modelling: the primer*. John Wiley & Sons.

Beven, K. J., & Cloke, H. L. (2012). Comment on: Hyperresolution global land surface modeling: Meeting a grand challenge for monitoring Earth's terrestrial water by Eric F Wood et al. *Water Resources Research*, *48*(1).

Bhadra, A., Bandyopadhyay, A., Singh, R., & Raghuwanshi, N. S. (2010). Rainfall-Runoff Modeling: Comparison of Two Approaches with Different Data Requirements. *Water Resources Management*, *24*(1), 37-62. https://doi.org/10.1007/s11269-009-9436-z

Bhattacharjee, N. V., & Tollner, E. W. (2016). Improving management of windrow composting systems by modeling runoff water quality dynamics using recurrent neural network. *Ecological Modelling*, *339*, 68-76.

Boggs, J., & Sun, G. (2011). Urbanization alters watershed hydrology in the Piedmont of North Carolina. *Ecohydrology*, *4*(2), 256-264.

Booth, D. B., & Jackson, C. R. (1997). URBANIZATION OF AQUATIC SYSTEMS: DEGRADATION THRESHOLDS, STORMWATER DETECTION, AND THE LIMITS OF MITIGATION1. *JAWRA Journal of the American Water Resources Association*, *33*(5), 1077-1090. https://doi.org/https://doi.org/10.1111/j.1752-1688.1997.tb04126.x

Booth, D. B., & Jackson, C. R. (1997). Urbanization of aquatic systems: degradation thresholds, stormwater detection, and the limits of mitigation 1. *JAWRA Journal of the American Water Resources Association*, *33*(5), 1077-1090.

Bormann, H., & Elfert, S. (2010). Application of WaSiM-ETH model to Northern German lowland catchments: model performance in relation to catchment characteristics and sensitivity to land use change. *Advances in Geosciences*, *27*, 1-10.

Boutaghane, H., Boulmaiz, T., Lameche, E. K., Lefkir, A., Hasbaia, M., Abdelbaki, C., Moulahoum, A. W., Keblouti, M., & Bermad, A. (2022). Flood Analysis and Mitigation Strategies in Algeria. In *Wadi Flash Floods* (pp. 95-118). Springer, Singapore.

Bowden, G. J., Dandy, G. C., & Maier, H. R. (2005). Input determination for neural network models in water resources applications. Part 1—background and methodology. *Journal of Hydrology*, *301*(1), 75-92. https://doi.org/https://doi.org/10.1016/j.jhydrol.2004.06.021

Boyd, M. J., Bufill, M. C., & Knee, R. M. (1993). Pervious and impervious runoff in urban catchments. *Hydrological Sciences Journal*, *38*(6), 463-478. https://doi.org/10.1080/02626669309492699

Britannica. (1 May 2017). *condensation nucleus*. Encyclopedia Britannica. https://www.britannica.com/science/condensation-nucleus

Budyko, M. I. (1974). *Climate and life*. Academic Press, Inc.

Burak, S., & Margat, J. (2016). Water management in the Mediterranean region: concepts and policies. *Water Resources Management*, *30*(15), 5779-5797.

Chahine, M. T., Pagano, T. S., Aumann, H. H., Atlas, R., Barnet, C., Blaisdell, J., Chen, L., FETZER, E. J., GOLDBERG, M., & GAUTIER, C. (2006). AIRS: Improving weather forecasting and providing new data on greenhouse gases. *Bulletin of the American Meteorological Society*, *87*(7), 911-926.

Chang, F.-J., Chen, P.-A., Lu, Y.-R., Huang, E., & Chang, K.-Y. (2014). Real-time multi-step-ahead water level forecasting by recurrent neural networks for urban flood control. *Journal of Hydrology*, *517*, 836-846. https://doi.org/https://doi.org/10.1016/j.jhydrol.2014.06.013

Chang, F.-J., Tsai, Y.-H., Chen, P.-A., Coynel, A., & Vachaud, G. (2015). Modeling water quality in an urban river using hydrological factors – Data driven approaches. *Journal of Environmental Management*, *151*, 87-96. https://doi.org/https://doi.org/10.1016/j.jenvman.2014.12.014

Chang, L.-C., Shen, H.-Y., & Chang, F.-J. (2014). Regional flood inundation nowcast using hybrid SOM and dynamic neural networks. *Journal of Hydrology*, *519*, 476-489. https://doi.org/https://doi.org/10.1016/j.jhydrol.2014.07.036

Cheng, K.-S., Lien, Y.-T., Wu, Y.-C., & Su, Y.-F. (2017). On the criteria of model performance evaluation for real-time flood forecasting. *Stochastic Environmental Research and Risk Assessment*, *31*(5), 1123-1146. https://doi.org/10.1007/s00477-016-1322-7

Chow Ven Te , D. R. M., & Larry, W. Mays (1998), Applied Hydrology. In: McGraw-Hill, Inc.

Chow, V. T. (1964). Handbook of applied hydrology: a compendium of water-resources technology.

Christian W, D., & Robert L, W. (2004). Single network modelling solutions. In A. Robert J, K. Pauline E, & S. Linda (Eds.), *Neural networks for hydrological modelling* (1st ed., pp. 38-58). CRC Press.

Christian W, D. R. L., Wilby. (2004). Single network modelling solutions. In A. Robert J, K. Pauline E, & S. Linda (Eds.), *Neural networks for hydrological modelling* (1st ed., pp. 38-58). CRC Press.

Christopher, P. K., & Derek, B. B. (2002). Hydrologic trends associated with urban development for selected streams in the Puget Sound basin, western Washington. *Water-Resources Investigations Report*. https://doi.org/10.3133/wri024040

Christopher, P. K., Derek, B. B., & Stephen, J. B. (2005). Effects of urban development in the Puget Lowland, Washington, on interannual streamflow patterns: Consequences for channel form and streambed disturbance. *Water Resources Research*. https://doi.org/10.1029/2005wr004097

Chu, X., & Steinman, A. (2009). Event and continuous hydrologic modeling with HEC-HMS. *Journal of Irrigation and Drainage Engineering*, *135*(1), 119-124.

Congalton, R. G., & Green, K. (2019). *Assessing the accuracy of remotely sensed data: principles and practices*. CRC press.

Congalton, R. G., Oderwald, R. G., & Mead, R. A. (1983). Assessing Landsat classification accuracy using discrete multivariate analysis statistical techniques. *Photogrammetric Engineering and Remote Sensing*, *49*(12), 1671-1678.

Congalton, R. G., Plourde, L., & Bossler, J. (2002). Quality assurance and accuracy assessment of information derived from remotely sensed data. *Manual of geospatial science and technology*, 349-361.

Cornelissen, T., Diekkrüger, B., & Giertz, S. (2013). A comparison of hydrological models for assessing the impact of land use and climate change on discharge in a tropical catchment. *Journal of Hydrology*, *498*, 221-236. https://doi.org/https://doi.org/10.1016/j.jhydrol.2013.06.016

Coulibaly, P., Anctil, F., Aravena, R., & Bobée, B. (2001). Artificial neural network modeling of water table depth fluctuations. *Water Resources Research*, *37*(4), 885-896. https://doi.org/10.1029/2000wr900368

Coulibaly, P., & Baldwin, C. K. (2005). Nonstationary hydrological time series forecasting using nonlinear dynamic methods. *Journal of Hydrology*, *307*(1), 164-174. https://doi.org/https://doi.org/10.1016/j.jhydrol.2004.10.008

Cuo, L., Lettenmaier, D. P., Mattheussen, B. V., Storck, P., & Wiley, M. (2008). Hydrologic prediction for urban watersheds with the Distributed Hydrology–Soil–Vegetation Model. *Hydrological Processes*, *22*(21), 4205-4213.

Dale, L. S., & Richard, J. R. (1982). Effects of Urbanization on Base Flow of Selected South-Shore Streams, Long Island, New York. *Journal of The American Water Resources Association*. https://doi.org/10.1111/j.1752-1688.1982.tb00075.x

Dawson, C. W., & Wilby, R. (1998). An artificial neural network approach to rainfall-runoff modelling. *Hydrological Sciences Journal*, *43*(1), 47-66. https://doi.org/10.1080/02626669809492102

Dayaratne, S. T. (2001). *Modelling of urban stormwater drainage systems using ILSAX* Victoria University].

De Martonne, E. (1926). *Aréisme et indice d'aridité*. Gauthier-Villars.

De Silva, M., Weerakoon, S., & Herath, S. (2014). Modeling of event and continuous flow hydrographs with HEC–HMS: case study in the Kelani River Basin, Sri Lanka. *Journal of Hydrologic Engineering*, *19*(4), 800-806.

Dehghani, M., Saghafian, B., Nasiri Saleh, F., Farokhnia, A., & Noori, R. (2014). Uncertainty analysis of streamflow drought forecast using artificial neural networks and Monte-Carlo simulation. *International Journal of Climatology*, *34*(4), 1169-1180. https://doi.org/10.1002/joc.3754

Deng, S., Chen, T., Yang, N., Qu, L., Li, M., & Chen, D. (2018). Spatial and temporal distribution of rainfall and drought characteristics across the Pearl River basin. *Science of The Total Environment*, *619*, 28-41.

Derek, B. B., David, M. H., & Rhett, J. (2002). Forest cover, impervious-surface area, and the mitigation of stormwater impacts. *Journal of The American Water Resources Association*. https://doi.org/10.1111/j.1752-1688.2002.tb01000.x

DESA, U. (2019). World Population Prospects 2019. United Nations. Department of Economic and Social Affairs. *World Population Prospects 2019*.

Desmond, E. W., Des, E. W., & Gregory, K. J. (1970). The measurement of the effects of building construction on drainage basin dynamics. *Journal of Hydrology*. https://doi.org/10.1016/0022-1694(70)90099-5

Dhawale, A. W. (2013). Runoff estimation for Darewadi watershed using RS and GIS. *International Journal of Recent Technology and Engineering*, *1*(6), 46-50.

Diaconescu, E. (2008). The use of NARX neural networks to predict chaotic time series. *WSEAS Transactions on Computers archive*, *3*, 182-191.

Dibike, Y. B., Velickov, S., Solomatine, D., & Abbott, M. B. (2001). Model induction with support vector machines: introduction and applications. *Journal of Computing in Civil Engineering*, *15*(3), 208-216.

Douglas, I. (1983). The urban environment.

Dow, C. L., & DeWalle, D. R. (2000). Trends in evaporation and Bowen ratio on urbanizing watersheds in eastern United States. *Water Resources Research*, *36*(7), 1835-1843.

Du, J., Qian, L., Rui, H., Zuo, T., Zheng, D., Xu, Y., & Xu, C.-Y. (2012). Assessing the effects of urbanization on annual runoff and flood events using an integrated hydrological modeling system for Qinhuai River basin, China. *Journal of Hydrology*, *464*, 127-139.

Dube, K., Nhamo, G., & Chikodzi, D. (2021). Flooding trends and their impacts on coastal communities of Western Cape Province, South Africa. *GeoJournal*, 1-16.

Dunne, T., Zhang, W., & Aubry, B. F. (1991). Effects of Rainfall, Vegetation, and Microtopography on Infiltration and Runoff. *Water Resources Research*, *27*(9), 2271-2285. https://doi.org/https://doi.org/10.1029/91WR01585

Dwarakish, G. S., & Ganasri, B. P. (2015). Impact of land use change on hydrological systems: A review of current modeling approaches. *Cogent Geoscience*, *1*(1), 1115691. https://doi.org/10.1080/23312041.2015.1115691

Džubáková, K. (2010). Rainfall-Runoff Modelling: Its development, classification and possible applications. *ACTA Geographica universitatis comenianae*, *54*(2), 173-181.

Elaji, A., & Ji, W. (2020). Urban Runoff Simulation: How Do Land Use/Cover Change Patterning and Geospatial Data Quality Impact Model Outcome? *Water*, *12*(10), 2715.

Erena, S. H., & Worku, H. (2018). Flood risk analysis: causes and landscape based mitigation strategies in Dire Dawa city, Ethiopia. *Geoenvironmental Disasters*, *5*(1), 1-19.

Fan, F., Deng, Y., Hu, X., Weng, Q., & Change, E. Systems E, Haute T. 2013. *Estimating composite curve number using an improved SCS-CN method with remotely sensed variables in*, 1425-1438.

Fankhauser, R. (1999). Automatic determination of imperviousness in urban areas from digital orthophotos. *Water Science and Technology*, *39*(9), 81-86.

Faruq, A., Abdullah, S. S., Marto, A., Abu Bakar, M. A., Mohd Hussein, S. F., & Che Razali, C. M. (2019). The use of radial basis function and non-linear autoregressive exogenous neural networks to forecast multi-step ahead of time flood water level. *International Journal of Advances in Intelligent Informatics; Vol 5, No 1 (2019): March 2019DO - 10.26555/ijain.v5i1.280*. http://ijain.org/index.php/IJAIN/article/view/280%7Cto_array%3A0

Federal Interagency Stream Restoration Working, G. (1998). *Stream corridor restoration: Principles, processes, and practices*. National Technical Info Svc.

Feldman, A. D. (2000). *Hydrologic modeling system (HEC-HMS) :Technical Refrence Manual* (F. Arlen D, Ed.).

Feng, B., Zhang, Y., & Bourke, R. (2021). Urbanization impacts on flood risks based on urban growth data and coupled flood models. *Natural Hazards*, *106*(1), 613-627.

Finkenbine, J. K., Atwater, J., & Mavinic, D. (2000). Stream health after urbanization 1. *JAWRA Journal of the American Water Resources Association*, *36*(5), 1149-1160.

Fletcher, T. D., Andrieu, H., & Hamel, P. (2013). Understanding, management and modelling of urban hydrology and its consequences for receiving waters: A state of the art. *Advances in Water Resources*, *51*, 261-279. https://doi.org/https://doi.org/10.1016/j.advwatres.2012.09.001

Fola, S. E. (1989). Patterns of stream channel response to urbanization in the humid tropics and their implications for urban land use planning: a case study from southwestern Nigeria. *Applied Geography*. https://doi.org/10.1016/0143-6228(89)90028-3

Foody, G. (2010). Assessing the accuracy of remotely sensed data: principles and practices. *The Photogrammetric Record*, *130*(25), 204-205.

Fox, D., Bryan, R., & Price, A. (1997). The influence of slope angle on final infiltration rate for interrill conditions. *Geoderma*, *80*(1-2), 181-194.

Freire Diogo, A., & Antunes do Carmo, J. (2019). Peak flows and stormwater networks design—current and future management of urban surface watersheds. *Water*, *11*(4), 759.

Geiger, W., Marsalek, J., Rawls, W., & Zuidema, F. (1987). Manual on drainage in urban areas. Volume I–Planning and design of drainage systems. *Studies and reports in hydrology*(43).

Ghonchepour, D., Sadoddin, A., Bahremand, A., Croke, B., Jakeman, A., & Salmanmahiny, A. (2021). A methodological framework for the hydrological model selection process in water resource management projects. *Natural Resource Modeling*, *34*(3), e12326.

Ghose, D., Das, U., & Roy, P. (2018). Modeling response of runoff and evapotranspiration for predicting water table depth in arid region using dynamic recurrent neural network. *Groundwater for Sustainable Development*, *6*, 263-269. https://doi.org/https://doi.org/10.1016/j.gsd.2018.01.007

Giorgi, F. (2006). Climate change hot-spots. *Geophysical Research Letters*, *33*(8). https://doi.org/https://doi.org/10.1029/2006GL025734

Green, I. R. A., & Stephenson, D. (1986). Criteria for comparison of single event models. *Hydrological Sciences Journal*, *31*(3), 395-411. https://doi.org/10.1080/02626668609491056

Gregory, J. H., Dukes, M. D., Jones, P. H., & Miller, G. L. (2006). Effect of urban soil compaction on infiltration rate. *Journal of soil and water conservation*, *61*(3), 117-124.

Grove, M., Harbor, J., & Engel, B. (1998). COMPOSITE VS. DISTRIBUTED CURVE NUMBERS: EFFECTS ON ESTIMATES OF STORM RUNOFF DEPTHS 1. *JAWRA Journal of the American Water Resources Association*, *34*(5), 1015-1023.

Gupta, A. (1982). Observations on the effects of urbanization on runoff and sediment production in Singapore. *Singapore Journal of Tropical Geography*, *3*(2), 137-146.

Gupta, H. V., Kling, H., Yilmaz, K. K., & Martinez, G. F. (2009). Decomposition of the mean squared error and NSE performance criteria: Implications for improving hydrological modelling. *Journal of Hydrology*, *377*(1), 80-91. https://doi.org/https://doi.org/10.1016/j.jhydrol.2009.08.003

Gupta, P., Das, T., & Raghuwansh, N. (1999). Hydrological modeling of canal command using Remote sensing and GIS. *Gisdevelopment. net*.

Guzman, S. M., Paz, J. O., & Tagert, M. L. M. (2017). The Use of NARX Neural Networks to Forecast Daily Groundwater Levels. *Water Resources Management*, *31*(5), 1591-1603. https://doi.org/10.1007/s11269-017-1598-5

Hagan, M. T., & Menhaj, M. B. (1994). Training feedforward networks with the Marquardt algorithm. *IEEE Transactions on Neural Networks*, *5*(6), 989-993.

Hammer, T. R. (1972). Stream channel enlargement due to urbanization. *Water Resources Research*, *8*(6), 1530-1540.

Han, W. S., & Burian, S. J. (2009). Determining effective impervious area for urban hydrologic modeling. *Journal of Hydrologic Engineering*, *14*(2), 111-120.

Harris, E. E., & Rantz, S. E. (1964). Effect of urban growth on streamflow regimen of Permanente Creek, Santa Clara County, California. https://doi.org/10.3133/wsp1591b

Hasda, R., Rahaman, M. F., Jahan, C. S., Molla, K. I., & Mazumder, Q. H. (2020). Climatic data analysis for groundwater level simulation in drought prone Barind Tract, Bangladesh: Modelling approach using artificial neural network. *Groundwater for Sustainable Development*, *10*, 100361. https://doi.org/https://doi.org/10.1016/j.gsd.2020.100361

Haykin, S. (2010). *Neural Networks and Learning Machines* (3 ed.). Pearson Education India.

He, J., Valeo, C., Chu, A., & Neumann, N. F. (2011). Prediction of event-based stormwater runoff quantity and quality by ANNs developed using PMI-based input selection. *Journal of Hydrology*, *400*(1), 10-23. https://doi.org/https://doi.org/10.1016/j.jhydrol.2011.01.024

Heaney, J. P., Huber, W. C., & Nix, S. J. (1976). *Storm Water Management Model: Level I, Preliminary Screening Procedures* (Vol. 1). US Environmental Protection Agency, Office of Research and Development ….

Hellweger, F. L., & Maidment, D. R. (1999). Definition and connection of hydrologic elements using geographic data. *Journal of Hydrologic Engineering*, *4*(1), 10-18.

Hemmati, M., Ellingwood, B. R., & Mahmoud, H. N. (2020). The role of urban growth in resilience of communities under flood risk. *Earth's future*, *8*(3), e2019EF001382.

Hord, R. M., & Brooner, W. G. (1976). LAND-USE MAP ACCURACY CRITERIA. *Photogrammetric Engineering and Remote Sensing*, *42*.

Hsu, K.-l., Gupta, H. V., & Sorooshian, S. (1995). Artificial Neural Network Modeling of the Rainfall-Runoff Process. *Water Resources Research*, *31*(10), 2517-2530. https://doi.org/10.1029/95WR01955

Huang, H.-j., Cheng, S.-j., Wen, J.-c., & Lee, J.-h. (2008). Effect of growing watershed imperviousness on hydrograph parameters and peak discharge. *Hydrological Processes*, *22*(13), 2075-2085. https://doi.org/https://doi.org/10.1002/hyp.6807

Huang, S.-y., Cheng, S.-j., Wen, J.-c., & Lee, J.-h. (2008). Identifying peak-imperviousness-recurrence relationships on a growing-impervious watershed, Taiwan. *Journal of Hydrology*, *362*(3), 320-336. https://doi.org/https://doi.org/10.1016/j.jhydrol.2008.09.002

Huang, S.-Y., Cheng, S.-J., Wen, J.-C., & Lee, J.-H. (2012). Identifying hydrograph parameters and their relationships to urbanization variables. *Hydrological Sciences Journal*, *57*(1), 144-161. https://doi.org/10.1080/02626667.2011.637044

In Shik, K., Jun Il, P., & Vijay, P. S. (1998). Effect of urbanization on runoff characteristics of the On-Cheon Stream watershed in Pusan, Korea. *Hydrological Processes*. https://doi.org/10.1002/(sici)1099-1085(199802)12:2<351::aid-hyp569>3.0.co;2-o

INSPIRE, T. W. G. L. C. (2013). *D2.8.II.2 INSPIRE Data Specification on Land Cover – Technical Guideline*. E. C. J. R. Centre.

Ishtiaque, A., Shrestha, M., & Chhetri, N. (2017). Rapid urban growth in the Kathmandu Valley, Nepal: Monitoring land use land cover dynamics of a himalayan city with landsat imageries. *Environments*, *4*(4), 72.

Izady, A., Davary, K., Alizadeh, A., Moghaddam Nia, A., Ziaei, A. N., & Hasheminia, S. M. (2013). Application of NN-ARX Model to Predict Groundwater Levels in the Neishaboor Plain, Iran. *Water Resources Management*, *27*(14), 4773-4794. https://doi.org/10.1007/s11269-013-0432-y

Jacobs, J. M., Myers, D. A., & Whitfield, B. M. (2003). Improved rainfall/runoff estimates using remotely sensed soil moisture 1. *JAWRA Journal of the American Water Resources Association*, *39*(2), 313-324.

Jacobson, C. R. (2011). Identification and quantification of the hydrological impacts of imperviousness in urban catchments: A review. *Journal of Environmental Management*, *92*(6), 1438-1448.

Jain, A., Sudheer, K., & Srinivasulu, S. (2004). Identification of physical processes inherent in artificial neural network rainfall runoff models. *Hydrological Processes*, *18*(3), 571-581.

Jensen, J. R. (1986). *Introductory digital image processing: a remote sensing perspective*.

Kadam, A. K., Kale, S. S., Pande, N. N., Pawar, N., & Sankhua, R. (2012). Identifying potential rainwater harvesting sites of a semi-arid, basaltic region of Western India, using SCS-CN method. *Water Resources Management*, *26*(9), 2537-2554.

Kenneth, G., Davis, R. J., & Downs, P. W. (1992). Identification of river channel change to due to urbanization. *Applied Geography*. https://doi.org/10.1016/0143-6228(92)90011-b

Khan, M. T., Shoaib, M., Hammad, M., Salahudin, H., Ahmad, F., & Ahmad, S. (2021). Application of Machine Learning Techniques in Rainfall–Runoff Modelling of the Soan River Basin, Pakistan. *Water*, *13*(24), 3528.

Kibaroğlu, A. (2017). Water challenges in the Mediterranean. *IEMed Mediterranean Yearbook 2017*.

Kleemann, J., Baysal, G., Bulley, H. N., & Fürst, C. (2017). Assessing driving forces of land use and land cover change by a mixed-method approach in north-eastern Ghana, West Africa. *Journal of Environmental Management*, *196*, 411-442.

KlemeŠ, V. (1986). Operational testing of hydrological simulation models. *Hydrological Sciences Journal*, *31*(1), 13-24. https://doi.org/10.1080/02626668609491024

Kuichling, E. (1889). The Relation Between the Rainfall and the Discharge of Sewers in Populous Districts. *Transactions of the American Society of Civil Engineers*, *20*(1), 1-56. https://doi.org/doi:10.1061/TACEAT.0000694

Ladson, A. R., Walsh, C. J., & Fletcher, T. D. (2006). Improving stream health in urban areas by reducing runoff frequency from impervious surfaces. *Australasian Journal of Water Resources*, *10*(1), 23-33.

Lambin, E. F., Geist, H. J., & Lepers, E. (2003). Dynamics of Land-Use and Land-Cover Change in Tropical Regions. *Annual Review of Environment and Resources*, *28*(1), 205-241. https://doi.org/10.1146/annurev.energy.28.050302.105459

Lazaro, T. R. (1990). *Urban Hydrology (revised edition)*. CRC Press.

Lee, C. C., & Sheridan, S. C. (2018). A new approach to modeling temperature-related mortality: Non-linear autoregressive models with exogenous input. *Environmental Research*, *164*, 53-64. https://doi.org/https://doi.org/10.1016/j.envres.2018.02.020

Lee, C. C., Sheridan, S. C., Barnes, B. B., Hu, C., Pirhalla, D. E., Ransibrahmanakul, V., & Shein, K. (2017). The development of a non-linear autoregressive model with exogenous input (NARX) to model climate-water clarity relationships: reconstructing a historical water clarity index for the coastal waters of the southeastern USA. *Theoretical and Applied Climatology*, *130*(1), 557-569. https://doi.org/10.1007/s00704-016-1906-7

Lee, J. G., & Heaney, J. P. (2003). Estimation of urban imperviousness and its impacts on storm water systems. *Journal of Water Resources Planning and Management*, *129*(5), 419-426.

Legates, D. R., & McCabe Jr, G. J. (1999). Evaluating the use of "goodness-of-fit" Measures in hydrologic and hydroclimatic model validation. *Water Resources Research*, *35*(1), 233-241. https://doi.org/10.1029/1998WR900018

Leopold, L. B. (1991). Lag times for small drainage basins. *Catena*, *18*(2), 157-171. https://doi.org/https://doi.org/10.1016/0341-8162(91)90014-O

Li, Y., Grimaldi, S., Pauwels, V. R., & Walker, J. P. (2018). Hydrologic model calibration using remotely sensed soil moisture and discharge measurements: The impact on predictions at gauged and ungauged locations. *Journal of Hydrology*, *557*, 897-909.

Lillesand, T., Kiefer, R. W., & Chipman, J. (2015). *Remote sensing and image interpretation*. John Wiley & Sons.

Linder, W. (2013). *Digital photogrammetry: theory and applications*. Springer Science & Business Media.

Lloyd-Davies, D. E. (1906). THE ELIMINATION OF STORM WATER FROM SEWERAGE SYSTEMS.(INCLUDING APPENDIX AND PLATE). Minutes of the Proceedings of the Institution of Civil Engineers,

Lu, D., Mausel, P., Brondízio, E., & Moran, E. (2004). Change detection techniques. *International journal of remote sensing*, *25*(12), 2365-2401. https://doi.org/10.1080/0143116031000139863

Luk, K., Ball, J. E., & Sharma, A. (2000). A study of optimal model lag and spatial inputs to artificial neural network for rainfall forecasting. *Journal of Hydrology*, *227*(1-4), 56-65.

Luk, K. C., Ball, J. E., & Sharma, A. (2001). An application of artificial neural networks for rainfall forecasting. *Mathematical and Computer Modelling*, *33*(6), 683-693. https://doi.org/https://doi.org/10.1016/S0895-7177(00)00272-7

Lyon, J. G. (2002). *GIS for water resource and watershed management*. CRC Press.

Maidment, D. R. (1993). *Handbook of hydrology*. McGraw-Hill.

Maier, H. R., & Dandy, G. C. (2000). Neural networks for the prediction and forecasting of water resources variables: a review of modelling issues and applications. *Environmental Modelling & Software*, *15*(1), 101-124. https://doi.org/https://doi.org/10.1016/S1364-8152(99)00007-9

Maier, H. R., Jain, A., Dandy, G. C., & Sudheer, K. P. (2010). Methods used for the development of neural networks for the prediction of water resource variables in river systems: Current status

and future directions. *Environmental Modelling & Software*, *25*(8), 891-909. https://doi.org/https://doi.org/10.1016/j.envsoft.2010.02.003

Mao, D., & Cherkauer, K. A. (2009). Impacts of land-use change on hydrologic responses in the Great Lakes region. *Journal of Hydrology*, *374*(1-2), 71-82.

Maria, S., & Moshe, I. (1992). Some hydrologic effects of urbanization in Catalan rivers. *Catena*. https://doi.org/10.1016/0341-8162(92)90009-z

Marsalek, J., Cisneros, B. J., Karamouz, M., Malmquist, P.-A., Goldenfum, J. A., & Chocat, B. (2008). *Urban water cycle processes and interactions: Urban Water Series-UNESCO-IHP* (Vol. 2). CRC press.

Mays, L. W. (2012). *Ground and surface water hydrology*. Wiley.

Meierdiercks, K. L., Kolozsvary, M. B., Rhoads, K. P., Golden, M., & McCloskey, N. F. (2017). The role of land surface versus drainage network characteristics in controlling water quality and quantity in a small urban watershed. *Hydrological Processes*, *31*(24), 4384-4397.

Meierdiercks, K. L., Smith, J. A., Baeck, M. L., & Miller, A. J. (2010). Analyses of Urban Drainage Network Structure and its Impact on Hydrologic Response1. *JAWRA Journal of the American Water Resources Association*, *46*(5), 932-943. https://doi.org/https://doi.org/10.1111/j.1752-1688.2010.00465.x

Meierdiercks, K. L., Smith, J. A., Baeck, M. L., & Miller, A. J. (2010). Analyses of Urban Drainage Network Structure and its Impact on Hydrologic Response 1. *JAWRA Journal of the American Water Resources Association*, *46*(5), 932-943.

Miller, R. A. (1979). *Characteristics of four urbanized basins in South Florida* (2331-1258).

Moretti, G., & Montanari, A. (2008). Inferring the flood frequency distribution for an ungauged basin using a spatially distributed rainfall-runoff model. *Hydrology and Earth System Sciences*, *12*(4), 1141-1152.

Mulvaney, T. J. (1851). On the use of self-registering rain and flood gauges in making observations of the relations of rainfall and flood discharges in a given catchment. *Proceedings of the institution of Civil Engineers of Ireland*, *4*, 19-31.

Musy, A., Hingray, B., & Picouet, C. (2014). *Hydrology: a science for engineers*. CRC press.

N. Moriasi, D., G. Arnold, J., W. Van Liew, M., L. Bingner, R., D. Harmel, R., & L. Veith, T. (2007). Model Evaluation Guidelines for Systematic Quantification of Accuracy in Watershed Simulations. *Transactions of the ASABE*, *50*(3), 885-900. https://doi.org/https://doi.org/10.13031/2013.23153

Naidu, D. S. (2015). Use of GIS in Hydrological Investigations. *Pdf). International Journal of Interdisciplinary Advanced Research Trends. Ii (2)*.

Nanda, T., Sahoo, B., Beria, H., & Chatterjee, C. (2016). A wavelet-based non-linear autoregressive with exogenous inputs (WNARX) dynamic neural network model for real-time flood forecasting using satellite-based rainfall products. *Journal of Hydrology*, *539*, 57-73. https://doi.org/https://doi.org/10.1016/j.jhydrol.2016.05.014

Nandalal, H., & Ratmayake, U. (2010). Event based modeling of a watershed using HEC-HMS. *Engineer: Journal of the Institution of Engineers, Sri Lanka*, *43*(2).

Nash, J. E., & Sutcliffe, J. V. (1970). River flow forecasting through conceptual models part I — A discussion of principles. *Journal of Hydrology*, *10*(3), 282-290. https://doi.org/https://doi.org/10.1016/0022-1694(70)90255-6

Nelder, J. A., & Mead, R. (1965). A simplex method for function minimization. *The computer journal*, *7*(4), 308-313.

Ngigi, S. N., Savenije, H. H., & Gichuki, F. N. (2007). Land use changes and hydrological impacts related to up-scaling of rainwater harvesting and management in upper Ewaso Ng'iro river basin, Kenya. *Land Use Policy*, *24*(1), 129-140.

Nie, W., Yuan, Y., Kepner, W., Nash, M. S., Jackson, M., & Erickson, C. (2011). Assessing impacts of Landuse and Landcover changes on hydrology for the upper San Pedro watershed. *Journal of Hydrology*, *407*(1-4), 105-114.

Nigussie, T. A., & Altunkaynak, A. (2016). Assessing the Hydrological Response of Ayamama Watershed from Urbanization Predicted under Various Landuse Policy Scenarios. *Water Resources Management*, *30*(10), 3427-3441. https://doi.org/10.1007/s11269-016-1360-4

Oke, T. R., Mills, G., Christen, A., & Voogt, J. A. (2017). *Urban climates*. Cambridge University Press.

Oliver, J. E. (1980). MONTHLY PRECIPITATION DISTRIBUTION: A COMPARATIVE INDEX. *The Professional Geographer*, *32*(3), 300-309. https://doi.org/10.1111/j.0033-0124.1980.00300.x

Öztürk, M., Copty, N. K., & Saysel, A. K. (2013). Modeling the impact of land use change on the hydrology of a rural watershed. *Journal of Hydrology*, *497*, 97-109.

Pabi, O., Egyir, S., & Attua, E. M. (2021). Flood hazard response to scenarios of rainfall dynamics and land use and land cover change in an urbanized river basin in Accra, Ghana. *City and Environment Interactions*, *12*, 100075. https://doi.org/https://doi.org/10.1016/j.cacint.2021.100075

Paik, K., Kim, J. H., Kim, H. S., & Lee, D. R. (2005). A conceptual rainfall-runoff model considering seasonal variation. *Hydrological Processes*, *19*(19), 3837-3850. https://doi.org/https://doi.org/10.1002/hyp.5984

Pizzuto, J., Hession, W., & McBride, M. (2000). Comparing gravel-bed rivers in paired urban and rural catchments of southeastern Pennsylvania. *Geology*, *28*(1), 79-82.

Preetha, P., & Al-Hamdan, A. (2022). A Union of Dynamic Hydrological Modeling and Satellite Remotely-Sensed Data for Spatiotemporal Assessment of Sediment Yields. *Remote Sensing*, *14*(2), 400.

Rafael, L. B., & Frank, E. P. (1975). Effects of Urbanization on Catchment Response. *Journal of Hydraulic Engineering*. https://scholar.google.com/scholar?q=Effects of Urbanization on Catchment Response

Ragan, R. M., & Jackson, T. J. (1975). Use of satellite data in urban hydrologic models. *Journal of the Hydraulics Division*, *101*(12), 1469-1475.

Rahman, K. U., Balkhair, K. S., Almazroui, M., & Masood, A. (2017). Sub-catchments flow losses computation using Muskingum–Cunge routing method and HEC-HMS GIS based techniques, case study of Wadi Al-Lith, Saudi Arabia. *Modeling Earth Systems and Environment*, *3*(1), 4.

Ramachandra, T., & Mujumdar, P. P. (2009). Urban floods: Case study of Bangalore. *Disaster Dev*, *3*(2), 1-98.

Ravagnani, F., Pellegrinelli, A., & Franchini, M. (2009). Estimation of Urban Impervious Fraction from Satellite Images and Its Impact on Peak Discharge Entering a Storm Sewer System. *Water Resources Management*, *23*(10), 1893-1915. https://doi.org/10.1007/s11269-008-9359-0

Refsgaard, J. C. (1997). Parameterisation, calibration and validation of distributed hydrological models. *Journal of Hydrology*, *198*(1), 69-97. https://doi.org/https://doi.org/10.1016/S0022-1694(96)03329-X

Refsgaard, J. C., & Henriksen, H. J. (2004). Modelling guidelines—terminology and guiding principles. *Advances in Water Resources*, *27*(1), 71-82.

Remesan, R., Shamim, M. A., Han, D., & Mathew, J. (2008, 12-15 Oct. 2008). ANFIS and NNARX based rainfall-runoff modeling. 2008 IEEE International Conference on Systems, Man and Cybernetics,

Rezaei, A. R., Ismail, Z. B., Niksokhan, M. H., Ramli, A. H., Sidek, L. M., & Dayarian, M. A. (2019). Investigating the effective factors influencing surface runoff generation in urban catchments–A review. *Desalination Water Treat, 164*, 276-292.

Rezaeianzadeh, M., Stein, A., Tabari, H., Abghari, H., Jalalkamali, N., Hosseinipour, E. Z., & Singh, V. P. (2013). Assessment of a conceptual hydrological model and artificial neural networks for daily outflows forecasting. *International Journal of Environmental Science and Technology*, *10*(6), 1181-1192. https://doi.org/10.1007/s13762-013-0209-0

Rezaul, M., Roger, A. P., Kenneth, G. H., Dev, N., Gordon, B. B., Peter, J. L., Richard, T. M., Clive, M., Andrés, E., Samuel, G., Budong, Q., Andrew, M. C., Adriana, B. P., Thomas, N. C., Arturo, I. Q., Jimmy, A., Sajith, V., Glen, C., Salvi, A., . . . Jozef, S. (2010). Impacts of land use/land cover change on climate and future research priorities. *Bulletin of the American Meteorological Society*. https://doi.org/10.1175/2009bams2769.1

Richard, D. K. (1979). URBANIZATION AND STREAM QUALITY IMPAIRMENT. *Journal of The American Water Resources Association*. https://doi.org/10.1111/j.1752-1688.1979.tb01074.x

Richards, J. A., & Jia, X. (1999). *Remote sensing digital image analysis: An Introduction* (3 ed., Vol. 3). Springer Berlin Heidelberg.

Richards, J. A., & Richards, J. (1999). *Remote sensing digital image analysis* (Vol. 3). Springer.

Richards, K. S. (1980). Book reviews : Dunne, T. and Leopold, L .B. 1978: Water in environmental planning. San Francisco: W. H.| Freeman. xxvii + 818 pp. £17.40. *Progress in Physical Geography: Earth and Environment*, *4*(2), 301-304. https://doi.org/10.1177/030913338000400216

Ridd, M. K. (1995). Exploring a VIS (vegetation-impervious surface-soil) model for urban ecosystem analysis through remote sensing: comparative anatomy for cities. *International journal of remote sensing*, *16*(12), 2165-2185.

Ridwansyah, I. (2010). Applying SWAT and GIS to Predict impact of Landuse Change to Water Yield and Optimizing Landuse in Upper Cimanuk Catchment Area.

Rinsema, J. G. (2014). *Comparison of rainfall runoff models for the Florentine Catchment* University of Twente].

Ripley, B. D. (2007). *Pattern recognition and neural networks*. Cambridge university press.

Ritchie, J., & Rango, A. (1996). Remote sensing applications to hydrology: introduction. *Hydrological Sciences Journal*, *41*(4), 429-431.

Roadknight, C. M., Balls, G. R., Mills, G. E., & Palmer-Brown, D. (1997). Modeling complex environmental data. *IEEE Transactions on Neural Networks*, *8*(4), 852-862.

Sahoo, A., Samantaray, S., & Ghose, D. K. (2019). Stream Flow Forecasting in Mahanadi River Basin using Artificial Neural Networks. *Procedia Computer Science*, *157*, 168-174. https://doi.org/https://doi.org/10.1016/j.procs.2019.08.154

Sahour, H., Gholami, V., & Vazifedan, M. (2020). A comparative analysis of statistical and machine learning techniques for mapping the spatial distribution of groundwater salinity in a coastal aquifer. *Journal of Hydrology*, *591*, 125321.

Salvadore, E., Bronders, J., & Batelaan, O. (2015). Hydrological modelling of urbanized catchments: A review and future directions. *Journal of Hydrology*, *529*, 62-81.

Samarasinghe, S. (2007). *Neural Networks for Applied Sciences and Engineering* (1st ed ed.). Auerbach Publications. https://doi.org/10.1201/9780849333750

Sandau, R. (2006). *International study on cost-effective earth observation missions*. CRC Press.

Satheeshkumar, S., Venkateswaran, S., & Kannan, R. (2017). Rainfall–runoff estimation using SCS–CN and GIS approach in the Pappiredipatti watershed of the Vaniyar sub basin, South India. *Modeling Earth Systems and Environment*, *3*(1), 1-8.

Scharffenberg, B., Bartles, M., Brauer, T., Fleming, M., & Karlovits, G. (2018). *Hydrologic modeling system (HEC-HMS) User's Manual: version 4.3. 0*.

Schmugge, T. J., Kustas, W. P., Ritchie, J. C., Jackson, T. J., & Rango, A. (2002). Remote sensing in hydrology. *Advances in Water Resources*, *25*(8), 1367-1385. https://doi.org/https://doi.org/10.1016/S0309-1708(02)00065-9

Scholten, H., Kassahun, A., Refsgaard, J. C., Kargas, T., Gavardinas, C., & Beulens, A. J. (2007). A methodology to support multidisciplinary model-based water management. *Environmental Modelling & Software*, *22*(5), 743-759.

Schultz, G. A., & Engman, E. T. (2012). *Remote sensing in hydrology and water management*. Springer Science & Business Media.

SCS. (1986). *Urban hydrology for small watersheds*. Engineering Division, Soil Conservation Service, US Department of Agriculture.

Senthil Kumar, A. R., Sudheer, K. P., Jain, S. K., & Agarwal, P. K. (2005). Rainfall-runoff modelling using artificial neural networks: comparison of network types. *Hydrological Processes*, *19*(6), 1277-1291. https://doi.org/10.1002/hyp.5581

Shamseldin, A. Y. (2009). Artificial neural network model for river flow forecasting in a developing country. *Journal of Hydroinformatics*, *12*(1), 22-35. https://doi.org/10.2166/hydro.2010.027

Shamseldin, A. Y., & O'Connor, K. M. (2001). A non-linear neural network technique for updating of river flow forecasts. *Hydrol. Earth Syst. Sci.*, *5*(4), 577-598. https://doi.org/10.5194/hess-5-577-2001

Shanableh, A., Al-Ruzouq, R., Yilmaz, A. G., Siddique, M., Merabtene, T., & Imteaz, M. A. (2018). Effects of land cover change on urban floods and rainwater harvesting: a case study in Sharjah, UAE. *Water*, *10*(5), 631.

Sheeder, S. A., Ross, J. D., & Carlson, T. N. (2002). Dual urban and rural hydrograph signals in three small watersheds 1. *JAWRA Journal of the American Water Resources Association*, *38*(4), 1027-1040.

Shen, C., & Phanikumar, M. S. (2010). A process-based, distributed hydrologic model based on a large-scale method for surface–subsurface coupling. *Advances in Water Resources*, *33*(12), 1524-1541.

Shen, H. Y., & Chang, L. C. (2013). Online multistep-ahead inundation depth forecasts by recurrent NARX networks. *Hydrol. Earth Syst. Sci.*, *17*(3), 935-945. https://doi.org/10.5194/hess-17-935-2013

Shuster, W. D., Bonta, J., Thurston, H., Warnemuende, E., & Smith, D. (2005). Impacts of impervious surface on watershed hydrology: A review. *Urban Water Journal*, *2*(4), 263-275.

Simmons, D. L., & Reynolds, R. J. (1982). EFFECTS OF URBANIZATION ON BASE FLOW OF SELECTED SOUTH-SHORE STREAMS, LONG ISLAND, NEW YORK 1. *JAWRA Journal of the American Water Resources Association*, *18*(5), 797-805.

Singh, N., & Chakrapani, G. J. (2015). ANN modelling of sediment concentration in the dynamic glacial environment of Gangotri in Himalaya. *Environmental Monitoring and Assessment*, *187*(8), 494. https://doi.org/10.1007/s10661-015-4672-6

Singh, V. P. (1995). *Computer models of watershed hydrology*. Water Resources Publications.

Singh, V. P., Frevert, D. K., Rieker, J. D., Leverson, V., Meyer, S., & Meyer, S. (2006). Hydrologic modeling inventory: Cooperative research effort. *Journal of Irrigation and Drainage Engineering*, *132*(2), 98-103.

Sitterson, J., Knightes, C., Parmar, R., Wolfe, K., Avant, B., & Muche, M. (2018). An overview of rainfall-runoff model types.

Solomatine, D., & Wagener, T. (2011). Hydrological modeling.

Song, Z., & James, L. D. (1992). AN OBJECTWE TEST FOR HYDROLOGIC SCALE 1. *JAWRA Journal of the American Water Resources Association*, *28*(5), 833-844.

Spurr, S. H. (1948). Aerial photographs in forestry. *Aerial photographs in forestry.*

Srivastava, A. K., Srivastava, V. K., & Ullah, A. (1995). The coefficient of determination and its adjusted version in linear regression models. *Econometric Reviews*, *14*(2), 229-240. https://doi.org/10.1080/07474939508800317

Subramanya, K. (2008). Engineering Hydrology. 7 West Patal Nagar. *New delhi*, *110*(008).

Suykens, J. A. K., Vandewalle, J. P. L., & De Moor, B. L. R. (1996). Nonlinear system identification using neural networks. In *Artificial Neural Networks for Modelling and Control of Non-Linear Systems* (pp. 37-82). Springer US. https://doi.org/10.1007/978-1-4757-2493-6_3

Talei, A., Chua, L. H. C., & Wong, T. S. W. (2010). Evaluation of rainfall and discharge inputs used by Adaptive Network-based Fuzzy Inference Systems (ANFIS) in rainfall–runoff modeling. *Journal of Hydrology*, *391*(3), 248-262. https://doi.org/https://doi.org/10.1016/j.jhydrol.2010.07.023

Te Chow, V. (2010). *Applied hydrology*. Tata McGraw-Hill Education.

Teegavarapu, R. S. (2019). Methods for Analysis of Trends and Changes in Hydroclimatological Time-Series. In *Trends and Changes in Hydroclimatic Variables* (pp. 1-89). Elsevier.

Thanapakpawin, P., Richey, J., Thomas, D., Rodda, S., Campbell, B., & Logsdon, M. (2007). Effects of landuse change on the hydrologic regime of the Mae Chaem river basin, NW Thailand. *Journal of Hydrology*, *334*(1-2), 215-230.

Treitz, P., & Rogan, J. (2004). Remote sensing for mapping and monitoring land-cover and land-use change-an introduction. *Progress in planning*, *61*(4), 269-279.

Tsihrintzis, V. A., & Hamid, R. (1998). Runoff quality prediction from small urban catchments using SWMM. *Hydrological Processes*, *12*(2), 311-329.

United Nations, D. o. E. a. S. A., Population Division (2019). *World Urbanization Prospects: The 2018 Revision (ST/ESA/SER.A/420)*.

Valizadeh, N., Mirzaei, M., Allawi, M. F., Afan, H. A., Mohd, N. S., Hussain, A., & El-Shafie, A. (2017). Artificial intelligence and geo-statistical models for stream-flow forecasting in ungauged stations: state of the art. *Natural Hazards*, *86*(3), 1377-1392. https://doi.org/10.1007/s11069-017-2740-7

Varvani, J., & Khaleghi, M. (2019). A performance evaluation of neuro-fuzzy and regression methods in estimation of sediment load of selective rivers. *Acta Geophysica*, *67*(1), 205-214.

Varvani, J., Khaleghi, M. R., & Gholami, V. (2019). Investigation of the relationship between sediment graph and hydrograph of flood events (case study: Gharachay River Tributaries, Arak, Iran). *Water Resources*, *46*(6), 883-893.

Vaze, J., Jordan, P., Beecham, R., Frost, A., & Summerell, G. (2011). Guidelines for rainfall-runoff modelling: towards best practice model application.

Verma, A. K., Jha, M. K., & Mahana, R. K. (2010). Evaluation of HEC-HMS and WEPP for simulating watershed runoff using remote sensing and geographical information system. *Paddy and Water Environment*, *8*(2), 131-144.

Vladimir, N., & Gordon, C. (1981). Handbook of nonpoint pollution: sources and management. *Van Nostrand Reinhold environmental engineering series (USA)*.

Wagener, T., Wheater, H., & Gupta, H. V. (2004). *Rainfall-runoff modelling in gauged and ungauged catchments*. World Scientific.

Walsh, C., Sim, P., & Yoo, J. (2002). Methods for the determination of catchment imperviousness and drainage connection. *Project D210. Cooperative Research Centre for Freshwater Ecology, Melbourne, Australia*.

Wang, L. K., & Yang, C. T. (2014). *Modern water resources engineering*. Springer.

Wang, Q., Huang, J., Liu, R., Men, C., Guo, L., Miao, Y., Jiao, L., Wang, Y., Shoaib, M., & Xia, X. (2020). Sequence-based statistical downscaling and its application to hydrologic simulations based on machine learning and big data. *Journal of Hydrology*, 124875.

Wang, S., Wang, Y., Ran, L., & Su, T. (2015). Climatic and anthropogenic impacts on runoff changes in the Songhua River basin over the last 56 years (1955–2010), Northeastern China. *Catena*, *127*, 258-269.

Ward, H., & Grimmond, C. (2017). Assessing the impact of changes in surface cover, human behaviour and climate on energy partitioning across Greater London. *Landscape and Urban Planning*, *165*, 142-161.

Wei, Y., Yuanxi, L., Yu, L., Mingxiang, X., Liping, Z., & Qiuliang, D. (2020). Impacts of rainfall intensity and urbanization on water environment of urban lakes. *Ecohydrology & Hydrobiology*, *20*(4), 513-524. https://doi.org/https://doi.org/10.1016/j.ecohyd.2020.06.006

Weng, Q. (2019). *Techniques and Methods in Urban Remote Sensing*. John Wiley & Sons.

Wenger, S. J., Peterson, J. T., Freeman, M. C., Freeman, B. J., & Homans, D. D. (2008). Stream fish occurrence in response to impervious cover, historic land use, and hydrogeomorphic factors. *Canadian Journal of Fisheries and Aquatic Sciences*, *65*(7), 1250-1264.

Wheater, H., Jakeman, A., & Beven, K. (1993). Progress and directions in rainfall-runoff modelling.

Wheater, H., Sorooshian, S., & Sharma, K. D. (2007). *Hydrological modelling in arid and semi-arid areas*. Cambridge University Press.

Wijesekara, G., & Marceau, D. (2012). Elbow River Watershed MIKE-SHE model: enhancement and scenario modelling project. *Report submitted to Dr. Anil Gupta, Alberta Environment, Calgary, AB, Canada*.

Wu, K., & Johnston, C. A. (2007). Hydrologic response to climatic variability in a Great Lakes Watershed: A case study with the SWAT model. *Journal of Hydrology*, *337*(1-2), 187-199.

Wunsch, A., Liesch, T., & Broda, S. (2018). Forecasting groundwater levels using nonlinear autoregressive networks with exogenous input (NARX). *Journal of Hydrology*, *567*, 743-758. https://doi.org/https://doi.org/10.1016/j.jhydrol.2018.01.045

Yang, S., Yang, D., Chen, J., & Zhao, B. (2019). Real-time reservoir operation using recurrent neural networks and inflow forecast from a distributed hydrological model. *Journal of Hydrology*, *579*, 124229. https://doi.org/https://doi.org/10.1016/j.jhydrol.2019.124229

Yang, Y., Du, J., Cheng, L., & Xu, W. (2017). Applicability of TRMM satellite precipitation in driving hydrological model for identifying flood events: a case study in the Xiangjiang River Basin, China. *Natural Hazards*, *87*(3), 1489-1505.

Yao, L., Chen, L., & Wei, W. (2016). Assessing the effectiveness of imperviousness on stormwater runoff in micro urban catchments by model simulation. *Hydrological Processes*, *30*(12), 1836-1848. https://doi.org/https://doi.org/10.1002/hyp.10758

Young, H. E., & Stoeckeler, E. G. (1956). Quantitative evaluation of photo interpretation mapping. *Photogrammetric Engineering*, *22*(1), 137-143.

Zhang, L., Hickel, K., Dawes, W. R., Chiew, F. H. S., Western, A. W., & Briggs, P. R. (2004). A rational function approach for estimating mean annual evapotranspiration. *Water Resources Research*, *40*(2). https://doi.org/https://doi.org/10.1029/2003WR002710

Zhang, L., Potter, N., Hickel, K., Zhang, Y., & Shao, Q. (2008). Water balance modeling over variable time scales based on the Budyko framework – Model development and testing. *Journal of Hydrology*, *360*(1), 117-131. https://doi.org/https://doi.org/10.1016/j.jhydrol.2008.07.021

Zhou, Y., Wang, Y., Gold, A. J., & August, P. V. (2010). Modeling watershed rainfall–runoff relations using impervious surface-area data with high spatial resolution. *Hydrogeology Journal*, *18*(6), 1413-1423. https://doi.org/10.1007/s10040-010-0618-9